

**Preventieve conservatie van kunstwerken in historische gebouwen:
beoordeling en modelleren**

**Preventive Conservation of Works of Art in Historic Buildings:
Assessment and Modelling**

Lien De Backer

**Promotoren: prof. dr. ir. -architect A. Janssens, prof. dr. ir. M. De Paepe
Proefschrift ingediend tot het behalen van de graad van
Doctor in de ingenieurswetenschappen: architectuur**



**Vakgroep Architectuur en Stedenbouw
Voorzitter: prof. dr. ir.-architect A. Janssens
Faculteit Ingenieurswetenschappen en Architectuur
Academiejaar 2017 - 2018**

ISBN 978-94-6355-098-7
NUR 950
Wettelijk depot: D/2018/10.500/16



Universiteit Gent
Faculteit Ingenieurswetenschappen en Architectuur
Vakgroep Architectuur en Stedenbouw

Promotoren: prof. dr. ir. arch. Arnold Janssens
prof. dr. Ir. Michel De Paepe

Universiteit Gent
Faculteit Ingenieurswetenschappen en Architectuur
Vakgroep Architectuur en Stedenbouw
Jozef Plateastraat 22, B-9000 Gent, België
Tel.: +32(9)264 37 42
Fax.: +32(9)264 41 85

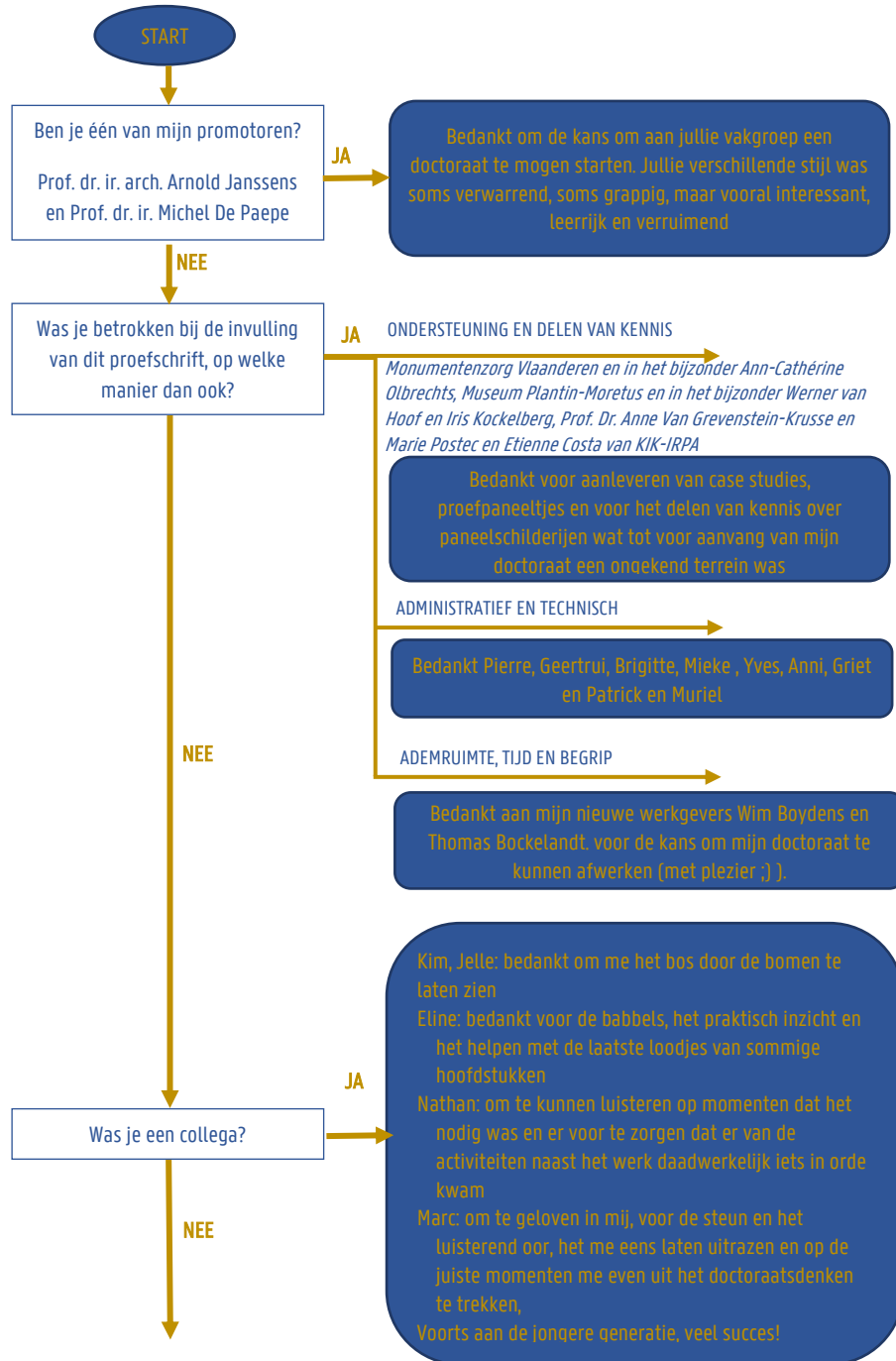
Dit werk werd grotendeels ondersteund door een FWO-project G.0448.10 (Fonds Wetenschappelijk Onderzoek – Vlaanderen)

Examencommissie:

Prof. dr.ir. Gert De Cooman (Universiteit Gent, voorzitter)
Prof. dr. ir. arch. Arnold Janssens (Universiteit Gent, promotor)
Prof. dr. ir. Michel De Paepe (Universiteit Gent, promotor)
Prof. dr. ir. arch Jelle Laverge (Universiteit Gent, secretaris)
Prof. dr. ir. arch Marijke Steeman (Universiteit Gent)
Prof. dr. ir. arch Gustaaf Roels (Universiteit Leuven)
Prof. dr. ir. Henk L. Schellen (Eindhoven University of Technology, Netherlands)
Dr.ir Hendrik-Jan Steeman (Arcadis Belgium)
Prof. dr. ir. Jan Pieters (Universiteit Gent)

Proefschrift tot het bekomen van de graad van
Doctor in de ingenieurswetenschappen: architectuur
Academiejaar 2017-2018

Function Thanks(string relation)



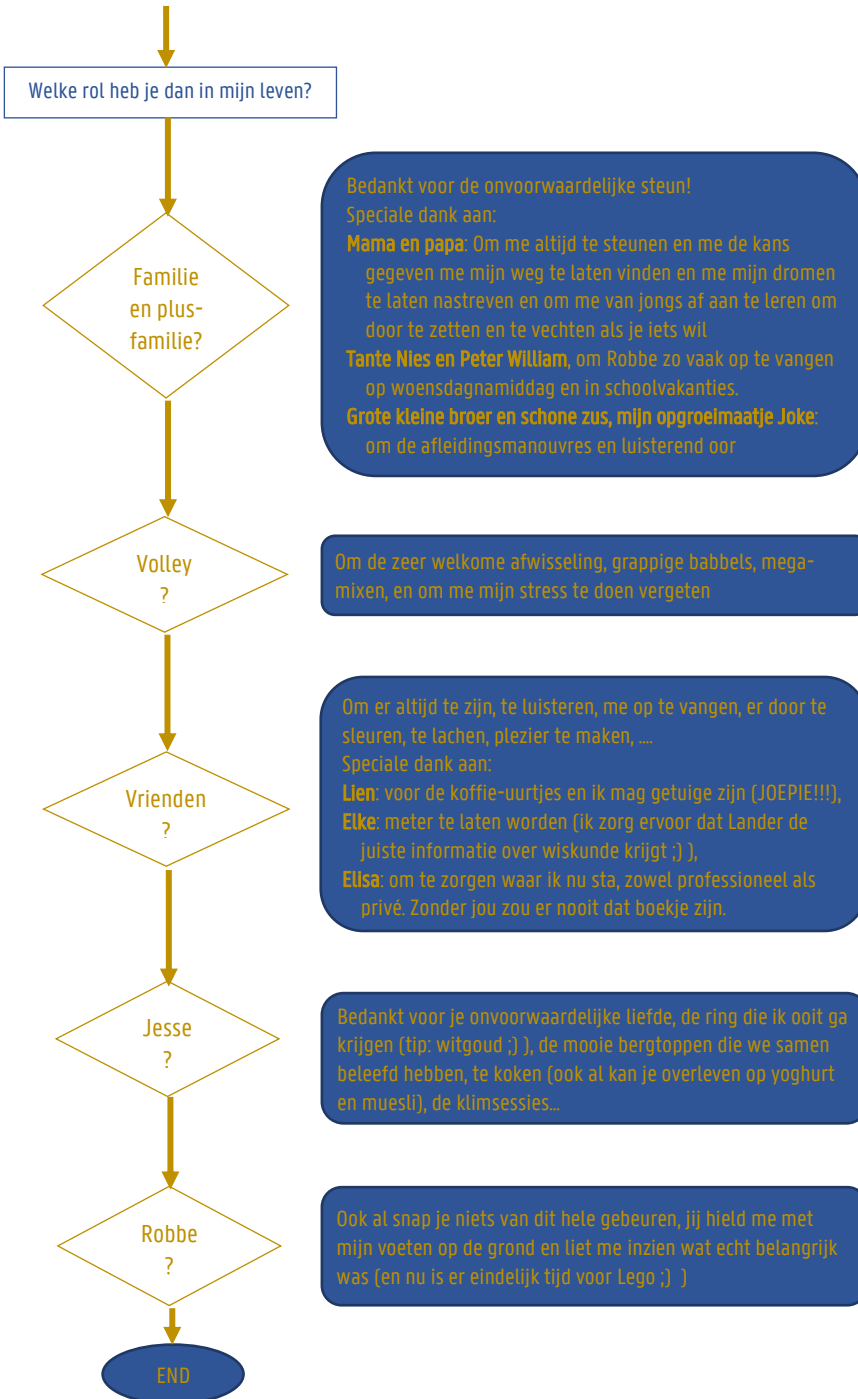


Table of contents

Nomenclature	i
Greek symbols.....	iii
Subscripts and superscripts.....	iii
Acronyms	iv
Nederlandstalige Samenvatting	vii
Summary	xi
1. Objective and Outline	1
1.1 Background: Preventive Conservation of Works of Art.....	2
1.2 Building (Energy) Simulation.....	4
1.2.1 Simulations as an Analysis Tool.....	4
1.2.2 Simulation Tools for the Building and its System.....	4
1.2.3 Used BES-software.....	8
1.3 Outline.....	10
1.3.1 Assessment.....	10
1.3.2 Modelling.....	11
1.3.3 Application.....	12
2. Predicting Damage Risk of Works of Art: Guidelines and Damage Functions	14
2.1 Development of Climate Standards.....	15
2.1.1 Search for the Optimal Climate Numbers.....	15
2.1.2 Is a Broader Range of Optimal Climate Numbers Acceptable?.....	17
2.1.3 A More Realistic, Risk-Management Based Approach.....	18
2.1.4 Focus on Object: The Three Types of Degradation Principle.....	25
2.2 Selected Evaluation Methods.....	34
2.2.1 ASHRAE Method.....	35
2.2.2 Object Oriented Method.....	37
3. Predicting Preservation Conditions for Panel Paintings	39
3.1 Object Behaviour of Panel Paintings.....	40
3.1.1 Panel Painting: Composition & Characteristics.....	40
3.1.2 Mechanical Degradation of Panel Paintings.....	43

3.1.3	Estimating Risk of Mechanical Damage for Panel Paintings by Modelling Moisture Transport.....	50
3.2	Evaluation of the Diffusion coefficient and Sorption Isotherm of the Different Layers of Early-Netherlandish Wooden Panel Paintings	55
3.2.1	Practical Implications	55
3.2.2	Materials and Measurement Methods	56
3.3	Case Study of a Panel Painting: "The Mystic Lamb"	66
3.3.1	Description of the Case Study.....	66
3.3.2	Measurement Campaign	68
3.3.3	Evaluation of the Preservation Conditions for the Panel Painting	69
3.4	Conclusion	79
4.	Sub-Modelling Approaches to Predict Dynamic Moisture Response in Historic Buildings ..	83
4.1	Model Calibration and Model Uncertainties.....	84
4.2	Calibration of a BES-Model.....	85
4.2.1	Development model	86
4.2.2	Model Calibration.....	86
4.2.3	Simulation Based Forecasting.....	88
4.3	Uncertainties Related to the Simulation Model: Sub-Models for Moisture Buffering of the Building Envelope.....	90
4.3.1	Sub-models in a BES-simulation software.....	90
4.3.2	Conductive Heat Transfer	91
4.3.3	Moisture Buffering.....	94
4.4	Uncertainty Analysis	100
4.4.1	Description Case Study.....	100
4.4.2	The Building Simulation Model.....	100
4.4.3	Model Calibration.....	105
4.4.4	Uncertainty Related to Time-Base	108
4.4.5	Uncertainty Related to the Choice of Moisture Model: EC, EMPD-model and HAM-model.....	108
4.5	Conclusion	112
5.	Modelling Indoor Climate in Large Enclosures.....	113
5.1	Tall Historic Buildings.....	114
5.1.1	Damage to works of art Related to Stratification.....	114

5.1.2	BES as an Analysis Tool.....	114
5.1.3	Airflow Modelling in a Building.....	116
5.1.4	Intermediate Approach: Simplified Modelling Methods for Temperature and Humidity Distribution.....	117
5.1.5	The Thermal-Zonal Model.....	122
5.2	Mathematical Description of the Thermal-Zonal Model.....	127
5.2.1	The Original Model of Togari et al.....	127
5.2.2	Addition of Equations for Infiltration.....	134
5.2.3	Addition of a Jet Flow model for Non-Isothermal Free turbulent Jets.....	134
5.2.4	Addition of Moisture Transport Equations.....	142
5.3	Coupling of the Thermal-zonal Model with TRNSYS.....	145
5.3.1	Possibilities of the BES-tool TRNSYS v17.....	145
5.3.2	Implementation of the Thermal-Zonal Model.....	146
5.3.3	Detailed Representation of the Coupling Strategy.....	148
5.4	Verification Studies.....	151
5.4.1	Case Description.....	151
5.4.2	The TRNSYS model.....	152
5.4.3	Cases without Moisture Source.....	153
5.4.4	Issues Using the Coupled Zonal Model Starting from Outside Boundary Conditions.....	157
5.4.5	Cases with Moisture Source.....	162
5.5	Discussion and Conclusion.....	171
6.	Preventive Conservation of a Panel Painting in Historic Buildings: A Simulation Study.....	173
6.1	Background of the Church Building.....	174
6.2	Two Causes of a Non-optimal Indoor Climate.....	177
6.3	Method of the Simulation Study.....	180
6.3.1	The Building Model.....	181
6.3.2	The HAM-model for the Panel Painting.....	188
6.3.3	Evaluation of preservation Conditions.....	189
6.4	Results found by the Simulation Study.....	191
6.4.1	Jet: Actual Situation.....	191
6.4.2	Temporary solution - Jet: Raising Minimum temperature to 11°C.....	195
6.4.3	Variant 1 -Jet: Warming up time of 2°C per hour.....	199
6.4.4	Variant 2 - Underfloor Heating.....	203

6.5	Conclusion.....	208
7.	Conclusion and Perspectives.....	209
7.1	Conclusions.....	209
7.2	Perspectives.....	213
-	Publications.....	215
	Journal publications as first author.....	215
	Publications in proceedings of conferences as first author.....	215
-	References.....	217
	ANNEXES.....	241
	Annex H2.....	243
	ANNEX 2.A: Standard EN16883:2017.....	243
	ANNEX 2.B: Chemical Degradation of Objects.....	244
	Arrhenius Equation.....	244
	Arrhenius Equation applied for Works of Arts.....	244
	Light guidelines.....	247
	ANNEX 2.C: The Sedlbauer model - A possible model to predict mould growth.....	248
	ANNEX 2.D: Rainflow Counting Method & Palmgren-Miner Rule.....	251
	Rainflow Counting Method.....	251
	Palmgren-Miner Rule.....	251
	Annex H3.....	253
	ANNEX 3A. Additional Data Case Study Mystic Lamb.....	253
	Chemical Decay.....	253
	Dimensions of all Panel of the Mystic Lamb.....	254
	Annex H4.....	255
	ANNEX 4.A: Non-Isothermal Simplified Moisture Model (EMPD).....	255
	Annex H5.....	257
	ANNEX 5.A: Temperature of Boundary Layer.....	257
	ANNEX 5.B: Infiltration equations in the thermal-zonal model.....	259
	ANNEX 5.C: Radiation.....	261
	Radiation Properties.....	261
	Heat exchange between bodies.....	261
	ANNEX 5.D: Convective Heat Transfer Coefficients.....	265

Natural Convection	265
Mixed Convection.....	265

Nomenclature

A	Surface area	m^2
A_0	Effective area of jet outlet	m^2
Ar	Archimedes number	[-]
a_w	Water activity	[-]
b	Thermal effusivity	$[\text{J}/(\text{m}^2\text{Ks}^{1/2})]$
c	Moisture content	$\text{kg}_{\text{moist}}/\text{m}^3_{\text{drymat}}$
c_p	Specific heat capacity	$\text{J}/(\text{kgK})$
C_d	Discharge coefficient	[-]
d	Thickness	m
d_0	Effective diameter	m
D_c	Diffusion coefficient	
E	Moisture content in terms of a dimensionless concentration change / fractional weight change	[-]
E_a	Activation energy	$\text{J}/(\text{K.mol})$
G	Vapour flow	kg/s
g	Vapour flux	$\text{kg}/(\text{m}^2.\text{s})$
H	Flux history term	W/m^2
h	Height	m
h_p	Convective vapour mass transfer coefficient for wall (vapour mass as driving potential)	$\text{kg}/(\text{Pa.m}^2.\text{s})$
K_1	Throw constant of the jet	[-]
K_2	A constant for the temperature of the jet	[-]

k	Chemical decay rate	[-]
m	mass	kg
n	Air change rate	1/h
n	Number of data points	[-]
n_{rad}	Capacity exponent for the unit	[-]
n_x, n_y, n_z	Number of exterior, cross and interior CTF terms	[-]
n_ϕ	Number of flux history terms	[-]
p	Pressure	Pa
p_v	Partial vapour pressure	Pa
Pr	Prandtl number	[-]
q	Heat flow rate	W/m ²
r	Radial coordinate	m
R	Universal gas constant	J/(K.mol)
R	Heat resistance	m ² K/W
R_v	Gas constant of water vapour	462 J/(kgK)
T	Temperature	°C/K
t	Time	s
u	Moisture content of the material	kg _{moist} /kg _{drymat}
V	Volume	m ³
v	Velocity	m/s
x	Horizontal distance	m
y	Vertical distance	m
Y	Mass fraction of water vapour	kg _{vap} /kg _{air}
Z	Moisture transfer resistance for diffusion	Pa.m ² .s/kg

Greek symbols

α	Thermal diffusivity	m^2/s
	Surface coefficient for heat transfer	$\text{W}/(\text{m}^2\cdot\text{K})$
β	Surface coefficient for vapour transfer	$\text{kg}/(\text{Pa}\cdot\text{m}^2\cdot\text{s})$
δ	Water vapour permeability	$\text{kg}/(\text{Pa}\cdot\text{m}\cdot\text{s})$
	Distance to the jet boundary which is related to the spread of the profile across the centreline	m
ε	Emissivity	-
λ	Thermal conductivity	$\text{W}/(\text{m}\cdot\text{K})$
μ	Water vapour resistance	-
ρ	Density	kg/m^3
ξ	Moisture capacity	kg/m^3
σ	Stefan-Boltzmann constant	$5.67\times 10^{-8} \text{ W}/\text{m}^2\text{K}^4$
φ	Relative humidity	%
Φ	Flux coefficient	[-]

Subscripts and superscripts

a	Air
app	Apparent
e	Exterior
i	Interior
i	Number of layer in the temperature zonal model
K	Number of wall in the temperature zonal model

max	Maximum
meas	Measured
ref	Reference
s	Surface
sat	Saturation
sim	Simulated
surf	Surface
t	Current time
w	Wall

Acronyms

BES	Building Energy Simulation <i>Numerical modelling of energy related processes in buildings</i>
CCI	Canadian Conservation Institute <i>Canadian research organization belonging to the federal Department of Canadian Heritage</i>
CFD	Computational Fluid Dynamics <i>Numerical modelling of fluid mechanics</i>
CTF	Conduction Transfer Function (X, Y, Z) <i>Numerical method to solve the partial differential equation of conductive heat transfer without discretization</i>
CV(RMSE)	Coefficient of Variation of Root Mean Square Error <i>Allows one to determine how well a model fits the data</i>
DLL	Dynamic-link library
EC	Effective moisture Capacitance <i>Simplified model to incorporate the moisture exchange between the air and the materials</i>

EMPD	Effective Moisture Penetration Depth <i>Simplified model to incorporate the moisture exchange between the air and the materials</i>
HAM	Heat Air and Moisture <i>Hygrothermal model for porous materials</i>
HVAC	Heating Ventilation and Air Conditioning <i>Mechanical system for climate control in buildings</i>
HIR	Hygric inertia of the room [kg/m ³ .%RH]
ICC	International Institute for Conservation of historic and artistic works <i>An independent international organisation supported by individual and institutional members which aims at bringing together likeminded specialists, to summarise and debate the latest progress and practice, and to present recent advances and research [1].</i>
ICOM-CC	International Council of Museums – Committee for Conservation <i>Part of ICOM, which is an international organisation of museums and museum professionals which is committed to the conservation, continuation and communication to society [2].</i>
LIM	Lowest Isopleth of Mould <i>The lowest boundary lines of possible fungus activity</i>
MBE	Mean Bias Error [%] <i>Non-dimensional bias measure between measured and simulated data</i>
MBV	Moisture buffering value [kg/m ² .%RH]
RMSE	Root Mean Squared Error

Samenvatting -Summary in Dutch-

Binnenklimaatcondities zijn vaak de oorzaak van degradatie van kunstwerken in een historisch gebouw. De belangrijkste kunstwerken worden gerestaureerd, wat ook welk benoemd wordt als een de zogenaamde 'directe actie'. Echter, dergelijke ingrijpende invasieve behandeling is zeer duur. Om deze kost te kunnen vermijden en er voor te zorgen dat het kunstwerk zo min mogelijk zal degraderen, is het aangewezen het verouderingsproces te vertragen door gebruik te maken van zogenaamde 'indirecte acties'. Dit houdt in dat er gestreefd wordt om zo goed als mogelijk optimale binnenklimaatcondities te creëren, voor zover dit compatibel is met het gebruik van het gebouw. Om de binnenklimaatcondities van het historisch gebouw te verbeteren, zijn er vaak aanpassingen aan het gebouw of diens systemen nodig. Simulatietools die het verloop van het binnenklimaat modelleren, zijn geschikt voor het voorspellen van de invloed van diverse retrofittingopties. In een vorig project (FWO G.0420.05), werd een gekoppeld 3D-HAM-CFD model ontwikkeld welke de lokale temperatuur- en vochtigheidsvariëaties van het binnenklimaat voorspelt in combinatie met het hygro-thermisch gedrag van hygroscopische materialen, zoals houten sculpturen, paneelschilderijen, boeken,... Hoewel de resultaten bruikbaar zijn voor het evalueren van lokale effecten en vochtgerelateerde schade, is de koppeling niet bruikbaar voor het evalueren van het binnenklimaat van het hele gebouw voor een lange tijdsperiode (vb. één jaar). De reden hiervoor is dat dergelijke studie een lange rekentijd nodig heeft. In dat geval zijn GebouwEnergieSimulatietools (BES) nuttiger omdat ze in staat zijn met een relatief korte rekentijd het binnenklimaat van het hele gebouw voor een langer tijdsverloop te simuleren. Dit laat toe om verschillende retrofittingopties te simuleren, te analyseren en te vergelijken en zo op zoek te gaan naar de meest optimale oplossing. Voor historische gebouwen waarbij een ongeschikt binnenklimaat kan leiden tot het verlies van onvervangbare kunstwerken, is dergelijke simulatiestudie dus zeer waardevol.

Om een correcte inschatting te kunnen maken van de preservatiecondities van het binnenklimaat, is het van belang om typische condities van historische gebouwen in acht te nemen in de simulatiestudie. In dit proefschrift wordt er dieper ingegaan op de aanwezigheid van vocht in de massieve muren, de aanwezigheid van hygro-thermische gradiënten (stratificatie) in hoge volumes veroorzaakt door het verwarmingsregime met vaak verouderde en/of beperkte installaties. Dit werk, onderdeel van FWO-project G.0448.10, streeft naar het vinden van een benaderingswijze om risico's op schade aan kunstwerken in historische gebouwen in te schatten door gebruik te maken van een simulatiestudie waarbij deze typische randcondities in opgenomen zijn. De nadruk van de studie ligt op een snelle rekentijd en op een praktisch bruikbare tool. Dit houdt in dat er vertrokken wordt van een 'klassieke' BES-tool en er bestudeerd wordt welke aanpassingen nodig zijn om deze randvoorwaarden in acht te nemen. Aangezien de resultaten van de simulatiestudie gebruikt worden om verschillende retrofittingsstrategieën te evalueren, wordt er ook gekeken naar geschikte evaluatietools om het risico op schade aan kunstwerken in te schatten. Dit leidt tot de volgende structuur:

Hoofdstuk 2 doorgrondt aan de hand van een literatuurstudie de evolutie van de klimaatstandaarden en methoden om het binnenklimaat in historische gebouwen te evalueren. Grofweg kan men de methoden in twee groepen opdelen: deze welke algemene voorschriften geven voor het binnenklimaat en deze die zich focussen op het gedrag van een specifiek object. Van beide groepen zal er in dit werk één methodiek gebruikt worden. Om het binnenklimaat algemeen te beoordelen zal de ASHRAE –methode gebruikt worden. Deze methode is wijdverspreid en eerder eenvoudig in gebruik, omdat enkel temperatuur en relatieve vochtigheid van de binnenruimte gekend moeten zijn. Voor de methode die focust op een specifiek object, wordt de zogenaamde 'drie-schade-functies'-methodiek gebruikt, namelijk het beoordelen van chemische, biologische en mechanische schade.

Hoofdstuk 3, 4 en 5 behandelen ieder een specifiek thema gerelateerd aan de voorgestelde simulatiestrategie. De gebruikte software in het werk is TRNSYS 17.

Hoofdstuk 3 onderzoekt de toegevoegde waarde van het co-simuleren van individueel objectgedrag van een kunstwerk in een BES-simulatie. Het risico op schade voor het desbetreffend kunstwerk werd geëvalueerd met behulp van de methodes besproken in hoofdstuk 2: nl. ASHRAE en 'drie-schade-functies'-methodiek. Daar deze benadering zeer objectspecifiek is, werd als voorbeeld een houten paneelschilderij, meer bepaald uit de 15e-16e eeuw, geselecteerd om in detail te bestuderen. Dergelijke paneelschilderijen zijn een belangrijk onderdeel van ons cultureel erfgoed en worden in het algemeen beschouwd als 'zeer gevoelig' voor schade door een binnenklimaat. Voor het gebruiken van de objectgerichte methode werd het vochttransport in het paneelschilderij gesimuleerd met een 1D-HAM model. Materiaalkarakteristieken nodig voor het modelleren van het vochttransport, werden experimenteel bepaald. Wanneer het object zich in de midden-zone van relatieve vochtigheid bevindt (40-60%RV), zal de algemene methode veilig genoeg zijn. In de hogere en lagere vochtigheidszones zal de objectgerichte methode een nauwkeurigere en genuanceerdere analyse toelaten daar het verschil in dimensionele reactie van de verschillende materiaallagen van het paneelschilderij sterk beginnen differentiëren en bijgevolg minder grote fluctuaties toelaatbaar zijn dan genoemd in de algemene methode. Voorts zal het co-modelleren van het 1D-vochttransport met een BES-model geen significante invloed hebben op de rekentijd.

Hoofdstuk 4 focust zich op het in rekening brengen van de thermische en hygrische buffering door de massieve wanden van historische gebouwen. Immers, omwille van de thermische en hygrische capaciteit kent het verloop van de binnentemperatuur en relatieve vochtigheid een demping en vertraging. Aangezien de amplitude van de schommelingen een belangrijke oorzaak is voor schade aan kunstwerken, is het belangrijk de amplitude juist in te schatten en bijgevolg de bufferende eigenschap correct te modelleren. Om het verloop van het binnenklimaat gedurende een jaar te simuleren met een korte rekentijd, wordt in de BES-software gebruik gemaakt van vereenvoudigingen om het tijdsafhankelijk massa- en warmte transport op te lossen. Dit hoofdstuk gaat dieper in op de wiskundige achtergrond van de sub-modellen voor thermisch transport en vochttransport van een wand. Aan de hand van een gevalideerde case studie werden verschillende sub-modellen voor vochttransport gesimuleerd om te bestuderen hoe de keuze van het sub-model, en de graad van vereenvoudiging, invloed heeft op het resultaat en de praktische bruikbaarheid van de tool. Volgende drie vochtmodellen werden vergeleken, gaande van eenvoudig naar gedetailleerd: het vochtcapaciteitsmodel, het EMPD-model en 1D-

HAM-model. Er werd geconstateerd dat het gebruik van de zeer gedetailleerde modellering van de vochtbuffering niet tot een significant accuratere oplossing leidt in vergelijking met het vereenvoudigde EMPD-model. Dit was te wijten aan andere vochtwinsten of -verliezen (bezoekers, infiltratie) die bij een lek gebouw meer significant waren.

Hoofdstuk 5 beschrijft de mogelijkheid om een BES-tool te koppelen met een zonaal model om op deze wijze de tijdsafhankelijke hygrothermische respons en stratificatie in hoge gebouwen te voorspellen. Het voordeel van deze koppeling is dat de rekentijd nog steeds voldoende kort is terwijl er nog steeds een langere tijdsperiode gesimuleerd wordt. Op basis van een literatuurstudie werd gekozen voor een zonaal model gedreven door temperatuurs-verschillen. Eerst werd het gekoppeld thermisch zonaal-BES-model gevalideerd om de correctheid van de koppeling na te gaan waarbij de case studies voor het oorspronkelijke thermisch-zonaal model werden gebruikt. Hierbij zijn er twee belangrijke opmerkingen:

- Het gebruik van tijdsafhankelijke waarden voor de convectieve overdrachts-coëfficiënten in plaats van constante waarden, verbeterde de overeenkomst tussen de gemeten en gesimuleerde resultaten.
- Het berekenen van lang golf straling en diffuse korte golf straling met behulp van zogenaamde Gebhart-factoren verhoogt de rekentijd, maar leidt tot een significante betere overeenkomst tussen gemeten en gesimuleerde temperatuur.

Omdat voor het schatten van de conservatiecondities ook de variatie in relatieve luchtvochtigheid gekend moet zijn, werden aan het oorspronkelijke model vergelijkingen toegevoegd voor het berekenen van vochtverdeling in de zone en voor het berekenen van de vochtflux afkomstig van de muren. Om de vochtvergelijkingen te analyseren, werd het effect van de toevoeging van vochtbronnen numeriek onderzocht. De gesimuleerde cases waren varianten op de cases gevalideerd voor temperatuur. De resultaten voor de vochtverdeling waren logisch en kunnen verklaard worden door de luchtstroom in de zone te analyseren.

Hoofdstuk 6 brengt de proposities voortvloeiend uit hoofdstuk 3, hoofdstuk 4 en hoofdstuk 5 bij elkaar door middel van een case studie van een historisch kerkgebouw waarin een belangrijk paneelschilderij tentoongesteld wordt. Hoofdstuk 7 bevat algemene conclusies over het praktisch opbouwen van een simulatiemodel in het kader van preventief behoud van kunstwerken, meer bepaald paneelschilderijen, en de ideeën van de auteur voor verder onderzoek.

Summary

Most of the degradation at works of art in historic buildings is caused by unfavourable indoor climate conditions. The most important works of art receive invasive conservation treatment, called direct action, but this treatment is very expensive. To avoid invasive conservation treatments and ensure that works of art are protected for now and for the future, indirect action to mitigate the deterioration process is strongly advised. This holds that exposure to unfavourable indoor climate conditions should be avoided, as far as is compatible with its social use.

To improve the indoor climate of the historic building, adaptations to the building or its systems are often necessary. Building performance simulation may be used in predicting the effect of a retrofitting strategy on the indoor climate, and in designing the adaptations to the building. In a previous project (FWO G.0420.05), a coupled 3D-HAM-CFD-model has been developed which predicts the local temperature and relative humidity variations of the indoor air as well as the hygrothermal interaction with hygroscopic materials like sculpture, panel paintings, books,... Although these results are useful to evaluate the risk of moisture related damage, evaluating the indoor climate of an entire building with CFD is very time-consuming because of the computational cost, certainly if a long time period has to be analysed. Furthermore, besides evaluating preservation conditions, also other criteria, like annual energy use and comfort criteria are of interest. In this case Building Energy Simulation (BES) methods are more appropriate as they are able to simulate the indoor climate dynamics of the whole building for a long time span relatively fast. This allows to simulate, analyse and compare multiple retrofitting strategies and define the most 'optimal' solution.

To assess the preservation conditions properly, it is necessary to take typical conditions in monumental historical buildings into account in the simulation study. In this work, the main focus is placed on the presence of moisture in heavy building walls and the occurrence of hygrothermal gradients (stratification) in the often very large interior volumes due to the limited control by (older) climate installation system. This PhD-dissertation, part of FWO-project G.0448.10, aims at developing a simulation strategy to estimate the predicted risk for works of art, taking into account these typical boundary conditions of an historical building. The emphasis lies on developing a fast calculating modelling approach intended for practical use. This holds that there was started from a 'classical' BES tool, where further studied indicates which adjustments are required to contain the boundary conditions.

Since the results of the simulation studies are used to assess the outcome of different retrofitting measures on the indoor climate, there is first studied which assessment tool is suitable. Therefore, this dissertation reviews in Chapter 2 the origin and the present situation of climate standards in detail, while Chapter 3 investigates the added value of simulating individual object behaviour in the BES-model. Chapter 4 and 5 examine to which extent the expansion of a BES tool with simplified moisture buffer models and simplified stratification models allows to

improve the simulation of the indoor climate in historic buildings. Chapter 6 brings the different solutions found in Chapter 3, 4 and 5 together in a case study.

The literature review in Chapter 2 shows different methods to evaluate the preservation conditions for works of art in historic buildings. Roughly speaking, the methods could be divided into two groups: those who focus on prescriptions for the whole indoor climate, and those focus on the climate-induced dimensional changes of an individual object. In this work, both approaches will be used next to each other to evaluate the indoor climate. To evaluate the indoor climate in general the ASHRAE preservation classes will be used. This method is widely known and rather easy in use, because only temperature and relative humidity of the indoor environment have to be provided. For the approach focussing on the individual object behaviour, three damage functions will be applied, respectively for chemical, biological and mechanical damage.

In this context, Chapter 3 investigates to which extend HAM-models allow to assess the damage risks to panel paintings more sophisticated compared to the assessment based on the indoor climate guidelines. As an illustration, a wooden panel painting, and more particular a wooden panel painting from the 15th-16th century, was selected to study in detail. This type of work of art is generally regarded as the most sensitive type of object requiring a particularly tight indoor climate control. The damage risk of the particular object was estimated, once by evaluating the indoor climate (T and RH) using a general approach (ASHRAE) and once by evaluating the biological, chemical and mechanical damage, for which the moisture distribution in the panel was needed. To simulate the moisture distribution in the panel painting, a 1D-HAM-model was used. The model is an adapted version of the former model developed by M. Steeman. Necessary material characteristics related to moisture transfer were determined experimentally. Comparing the outcome of both evaluation methods, shows that three-type-degradation principle allows to assess more precisely the damage risks of a certain object and look closer at causes of failure. A significant difference is that in case of a high relative humidity smaller fluctuations are allowed than in the mid-region, due to the mismatch in dimensional behaviour of the different material layers. This implies that in case the relative humidity is in the mid-range (40-60%RH), the ASHRAE class is save to use, while in case of a high relative humidity this is not always the case. A common criticism on using a more individual approach is that it is related to one particular object. Determining these characteristics is time demanding. As a consequence, the simulation study with a coupled BES-HAM model is not time demanding, but the determination of the material characteristics is. So, more material research leading to a material database would be beneficial.

Chapter 4 focusses on the modelling of hygric and thermal buffering capacity in historical buildings with heavy building walls. Because of the high thermal and hygric capacity of the building envelope, the indoor temperature and humidity of historic buildings is attenuated. As the amplitude of the fluctuations is an essential cause of damage to works of art, it is important to estimate the amplitude correctly. Therefore, buffering characteristics must be taken into account in simulating the indoor climate. To solve in a BES-software the transient behaviour for a longer time period relative fast, the buffering behaviour is solved in a simplified way. Looking closer on how the heat and moisture balance of the building space is solved, one can notice that the balances are subdivided into separate sub-models. This chapter goes deeper into detail in the

mathematical background of the sub-model which solves the wall heat conduction process, responsible for the thermal capacity of the wall and the sub-model which calculates the moisture buffering of the envelope. Using a case study, different options of sub-models for moisture transport were compared to show how the choice of sub-model (equalling grade of simplification), will affect the results and practical use for a historic building under limited conditioned conditions. The most simple model was the moisture capacitance model available in TRNSYS. For the detailed modelling of moisture flux, a slightly adapted moisture transport model intended to use in the BES software TRNSYS, was used (former model developed by M. Steeman). In between the very simplified and detailed approach, the EMPD model of TRNSYS was used. There was found that the very detailed modelling of the moisture buffering by the building envelope had no significant improvement in the prediction of the relative humidity course compared to the more simplified EMPD-model. This was due to other moisture gains or losses (visitors, infiltration) which were more relevant in case of a leaky building.

Chapter 5 describes the possibility of coupling of a zonal model with a BES-software (in this case TRNSYS) in order to predict the transient hygrothermal response of tall historical buildings while taking into account the vertical hygrothermal gradients in one zone. The advantage of this coupling is that it has a short calculation time and can predict longer time periods (minimum one year). Based on a literature review, there was opted for a temperature-based zonal model. A validation is performed to check the correctness of the coupled thermal-zonal-BES model using the same cases used for the original model. There are two important comments :

- Using unsteady values for of the convection transfer coefficients calculated by algorithms suggested in former studies instead of using constant values improved the agreement between the measured and simulated results.
- Calculating longwave radiation and shortwave diffuse radiation using so-called Gebhart factors increases computing time, but has an significant improvement on the agreement between measured and simulated temperature.

Because to estimate the preservation conditions also the variation in relative humidity in the space have to be known, equations for calculating moisture distribution in the zone were added to the original model as the original model only calculated temperature distribution. To analyse the moisture equations, the effect of the addition of a moisture sources was examined numerically. The studied cases were variants on the validated cases for temperature distribution. The results found for the moisture distribution were logical and could be explained by analysing the air flow in the zone.

1

Objective and Outline

"The cultural heritage sector is an ever expanding and diverse sector with a variety of organizations. But some key words can be found in each sector, including: professionalism, conservation and management, preventive conservation, collections care, ... In both museums and heritage libraries as repositories and archives, the call for qualitative preventive conservation becomes louder [3]."

1.1 Background: Preventive Conservation of Works of Art

It is unavoidable that works of art degrade. Different possible causes for the deterioration of a work of art were summarized by UNESCO [4]. These are: mechanical forces, theft and vandalism, fire, water, biological agents, air pollution and dust, light, infrared and ultraviolet radiation, and the indoor climate conditions; temperature and relative humidity. Although, the impact of incorrect climate values on an object appears negligibly small compared to fire, water or physical forces, **most of the degradation to works of art in historic buildings are caused by unfavourable indoor climate conditions** [5,6]. This is because of the higher frequency of the risk and because a large part of the collection is exposed at the same time to incorrect climate values. Degradation caused by exposure to an indoor climate, is called natural deterioration and this degradation process is unavoidable (e.g. Figure 1.1).

The most important works of art get invasive conservation treatment, called direct action, but this treatment is very expensive. An example is the restoration of the polyptych 'The adoration of the mystic lamb' for which the restoration cost is projected to be 1.4 million euro [7].

Another solution is to slow down the ageing process and to avoid damage and therefore avoiding the need for invasive conservation treatment. This is called preventive conservation [8]. In preventive conservation those environmental factors that cause deterioration to works of art are determined, like too large humidity fluctuations. Once the cause is identified, action can be taken to improve the indoor climate. Contrary to a treatment, preventive conservation consists of indirect action [9,10]. As a consequence, damage can be mitigated and in some cases prevented [11]. Therefore, applying preventive conservation reduces or even eliminates the need for future treatment and provides a cost-effective method for the preservation of works of art [12].



Figure 1.1: Natural deterioration of a panel painting: yellowing of the varnish. Detail of the Ghent Altarpiece before (left) and after (right) restoration. Composition: KIKIRPA/Lukas Art [13].

In recent years not only from scientific angle, but also in the museum world [14], politics, etc. awareness of the importance of the conditions of conservation of works of art has increased and preventive conservation has become a popular topic. To that end, a legal framework to protect and safeguard the cultural heritage in Flanders was drawn up, defined as the masterpieces decree. The decree holds: "*the timely adoption of measures to ensure an appropriate and stable storage environment for the protected objects, such as by appropriate climate control, by avoiding water and light damage and resisting dust, pests and fungi*" [15].

In case the indoor climate is not sufficient, an obvious solution to preserve these objects seems to move the works of art to a building with a more favourable climate. However, in many cases the owner tries to keep the works of art within the building because of historical, cultural or economic value. One possibility to preserve works of art within an unfavourable climate is creating a stable microclimate within the building by a so-called climate box or vitrine like is shown in Figure 1.2. The PROPAIN project [16] devoted an entire study to the use of microclimate boxes and vitrines and explains which box fits in which occasion.

In some cases, however, a microclimate box is not an option because of aesthetical reasons (most people prefer being close to the work of art [17]), weight, difficulty of handling, risk of breakage, trapping of internally generated pollutants¹ and cost [16–20]. In case a climate box is not an option, the other possibility is to improve the indoor climate until it is as stable as possible. To improve the indoor climate, often adaptations to the building or its systems are necessary. To choose which adaptation is sufficient, simulation tools are helpful.



Figure 1.2: Panel painting preserved in a climate box [17,21].

¹ In the PROPAIN-project it was found that many different volatile organic compounds (VOCs) were detected inside the microclimate frames, many in high concentrations. However, little is known about the degradation effects of the VOCs on cultural heritage objects made from organic materials, such as panel paintings. For this reason, in the PROPAIN-project is mentioned that more research needs to be performed to establish which degradation effects organic acids and other VOCs have on diverse organic materials in cultural heritage objects. They suggest that this research should include continued investigation of effects on varnishes and paintings generally and that more study of especially acetic acid effects on varnishes and paintings, including old varnish and paint layers, should be performed.[16].

1.2 Building (Energy) Simulation

1.2.1 Simulations as an Analysis Tool

As described in the first paragraph, preventive conservation highlights the following: “The work of art must be conserved as well as possible by an indirect action, such as environmental management [10]”. However, different causes of failure of works of art exist related to inadequate indoor climate conditions. Some common causes are listed.

- One possibility is that the unconditioned indoor climate is not sufficient to preserve the work of art. Although the historic building attenuates the outdoor climate because of their hygrothermal inertia [22–25], daily and seasonal amplitudes can become too large. In other cases, the average relative humidity can be too high leading to mould growth, deformation, ...
- A different possibility is that damage can occur in case the historic building changes function, imposing new boundary conditions to the works of art. For example, a historic building is converted into a museum, resulting in another heating regime, another visitor load, ...
- Another possibility, which is quite common, is related to the installation of a HVAC system as an answer to the increased thermal comfort demand. Although the (intermittent) use of the system improves the thermal comfort, it could cause large temperature and relative humidity fluctuations and a too low relative humidity during heating season.

Dependent on the cause, adaptations to the building or its systems are generally necessary to improve the indoor climate of the historic building. Building performance simulation may be used in designing the adaptations to the building and in predicting the effect of retrofitting strategies on the indoor climate. Because there are different retrofitting options and many unknown building characteristics and boundary conditions, simulation tools are powerful tools as they allow to vary these parameters without performing physical tests. For these reasons, it is customary to use a simulation tool to analyse the effect of interventions on the indoor climate [26].

1.2.2 Simulation Tools for the Building and its System

Simulation involves the creation of numerical models of a building and is thereby a process of simplifying the complex physical reality to a computable set of equations [27,28]. In other words, the purpose of modelling is to create a mathematical model from a physical system [29]. In the past few decades, the development and professional use of simulation tools has been strongly evolved. To predict the unsteady indoor conditions in a building, many simulation tools are available. Underwood and Yik categorized these tools into three groups [30]. A fourth group was added in this dissertation to incorporate the software focussing on modelling of the building envelope. The four groups are:

- Group 1: Building energy and environment. Part of this group of simulation tools are building energy simulation (BES) software. They are widely used for the evaluation or comparison of different heating systems to meet sizing and energy operating cost

requirements [31]. In the work of Harish and Kumar [32] a review can be read of all noteworthy modelling methodologies which have been developed and adopted to model the energy systems of buildings.

- Group 2: Plant and control: This group consists of models which focusses on the modelling of systems, plants and control. Some programs belonging to the first group also provide a full treatment of the plants and controls [30].
- Group 3: Zonal ventilation modelling and computational fluid dynamics: This group consists of models which focus on the airflow in a space.
- Group 4: Building envelope: In this group detailed transient tools have been developed (e.g. in the context of IEA Annex 24 [33]) for combined heat, air and moisture transfer (HAM) within individual building components [34].

In the scope of this work, following criteria were considered in selecting the simulation tool:

- The model of the building contains the room or whole building and its systems (not modelling microclimate).
- The modelling tool has to estimate long-term fluctuations, as well as short-term fluctuations. In other words, a non-steady calculation of the building and its system for at least a year.
- The simulation tool has to be fast so the calculation of one retrofitting option for a case study will be performed in maximum one hour.
- The calculations can be performed by a 'standard' laptop (8GB RAM –CPU 2 cores- 2.67 GHz).

Based on these criteria, the preferred tool to estimate the indoor climate in a historic building is the tool which is also used for the modelling of building energy use (group 1). These tools are most suitable because they calculate the desired parameters over the course of a full year relatively fast, which is needed to be able to evaluate the indoor climate for the long term seasonal changes [35–37]. Thereby, a fast calculation allows to simulate, analyse and compare multiple retrofitting strategies and define the 'optimal' solution. Concerning historical buildings, where an insufficient climate could cause the loss of irreplaceable valuable works of art, this makes those simulation tools indispensable [22]. Damage to works of art can also be studied with computational fluid dynamics (CFD – group 3) [38–40]. For example, in a previous project (FWO G.0420.05) a coupled 3D-HAM-CFD-model² has been developed which predicts the local temperature and relative humidity variations of the indoor air together with the hygrothermal interaction with hygroscopic materials like sculpture, panel paintings, books,... [41,42]. However, CFD is not in the scope of this work since this tool is too computationally demanding and too time-consuming.

Simulation Tools for the Building (group 1)

According to ASHRAE handbook [43], modelling of building energy use can be classified into two different approaches: forward and inverse approach.

² link between Building envelope and CFD

The forward modelling approach, also called the law-driven approach, is the classical approach. The objective of this approach is to predict the output (e.g. the temperature course) based on input of the physical system (e.g. weather, occupancy, ...). This approach includes Building Energy Simulation (BES) models where TRNSYS, ESP-r, BLAST, DOE-2, and Energy Plus are the most widespread simulation codes [37]. In the forward approach, the goal is to build a model of the building and its boundary conditions as detailed as necessary. To do so, information is needed about the building geometry, material properties, user behaviour, internal gains, ... For old historic buildings, however, this information is often lacking. Furthermore, destructive methods to obtain building material properties are often not allowed because the building is protected [44].

Therefore, some researchers prefer the second approach, the inverse or data-driven approach. Inverse approach refers to modelling methods which determine model parameters by matching the output of the model as close as possible to measurement data [44,45]. The data-driven approach has a higher accuracy than the forward modelling approach, but suffers from generalization beyond the existing situation and is therefore more useful for the evaluation of as-built system performance [37,46] [47]. In other words, the forward modelling approach is satisfactory and allows more accurate prediction of future system performance under specific, real boundary conditions..

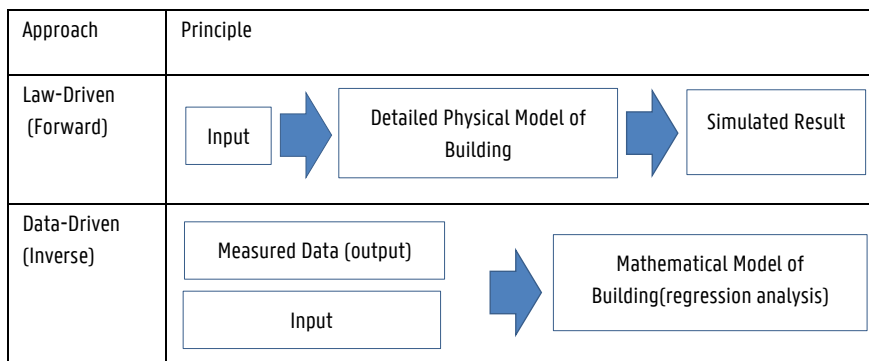


Figure 1.3: Law-driven (forward) models vs. data-driven (inverse) models

In this dissertation, it is preferred to work with the forward modelling approach. Although more assumptions are necessary, the classical approach is more appropriate to design a new system or to improve the existing system. To deal with the lack of some detailed information, on required input parameters, in this work the BES models were calibrated using measured data, which is called grey box modelling approach [47–49].

Other tools necessary?

To assess the preservation conditions properly, it is important to take typical conditions in monumental historical buildings into account in the simulation study which are calculated by

tools from another group. For example; the presence of moisture in heavy building walls (group 4: HAM) and the occurrence of hygrothermal gradients in the often very large interior volumes (group 3: zonal airflow model).

Though fully integrated programs encompassing all groups are possible, as shown in Figure 1.4, the current state-of-the-art remains somewhat fragmented and a single program code that treats all areas in an integrated manner is still under development [30].

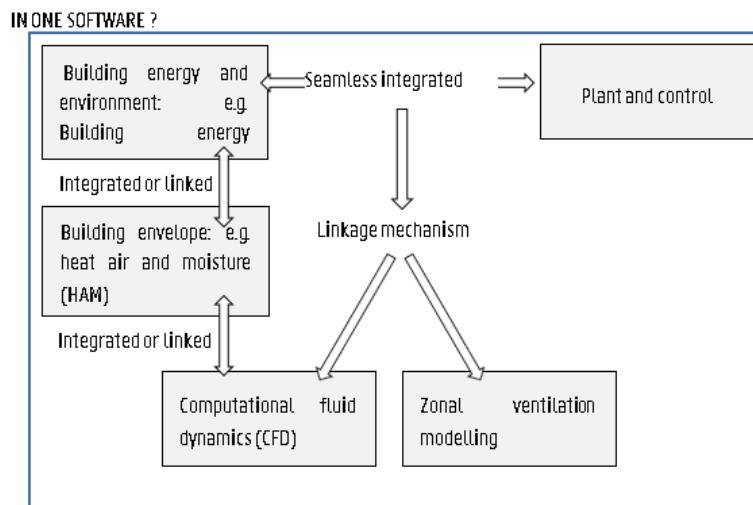


Figure 1.4: Relationships between available program codes. Based on Underwood and Yik [30].

This PhD-dissertation aims at developing a simulation strategy to assess the damage risk for works of art, taking into account the presence of moisture in heavy building walls and the occurrence of hygrothermal gradients (stratification) in the often very large interior volumes due to the limited control by (older) climate installation system. The emphasis lies on developing a fast calculating modelling approach intended for practical use which predicts if the preservation measures lead to the desired improvement concerning preservation conditions. This holds that there was started from a 'classical' BES tool and it has been studied which adjustments to the tool are required to contain the mentioned boundary conditions. This means that the necessary adjustments are integrated in the BES-tool and not linked to another software tool. Because the results of the simulation study are used to assess and to compare the outcome on the indoor climate of different retro-fitting measures, there is also looked which assessment tool is suitable.

1.2.3 Used BES-software

In this dissertation, the software tool TRNSYS is used. TRNSYS is an abbreviation of Transient System Simulation program and is a simulation environment for the transient simulation of systems, including multi-zone buildings [50]. The version used in this research to perform building energy simulations is TRNSYS v17. TRNSYS is a well-known and oft-used computer simulation tool for building energy performance assessment [51]. However, the method suggested in this work can also be performed by other simulation tools that have been developed over the last few decades (e.g. Energyplus³, ESP-r⁴, ...).

Principle of TRNSYS

Each physical part in the system, such as the building, the heat source (e.g a heat pump) and the HVAC system is represented by a so-called component which is equal to a FORTRAN subroutine. Each component models the performance of one part of the simulated system [52]. The subroutines are combined into an input file which describes what physical parts are involved in the system and how they are connected [53]. Figure 1.5 shows schematically how the different parts of the software are connected.

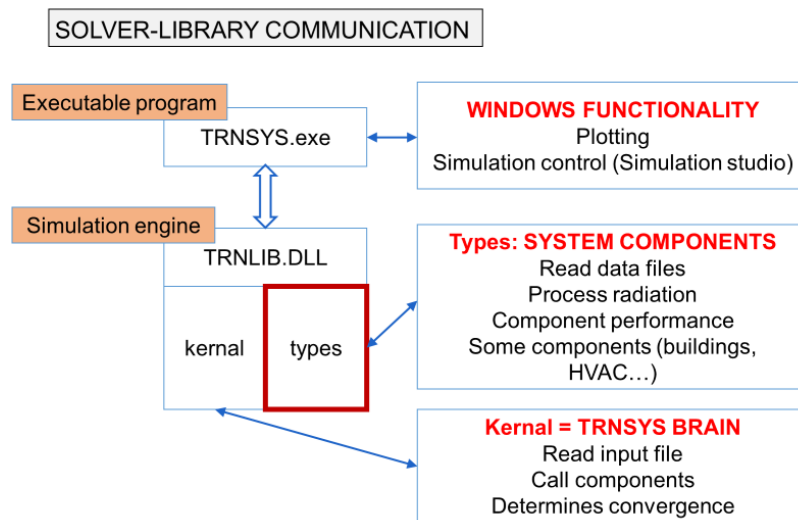


Figure 1.5: TRNSYS: different parts of the software program [54].

³ <https://energyplus.net/> (EnergyPlus is developed in collaboration with NREL, various DOE National Laboratories, academic institutions, and private firms.)

⁴ <http://www.esru.strath.ac.uk/Programs/ESP-r.htm>

The executable (TRNSYS.exe) holds the visual part that most user are familiar with, such as the simulation studio. The simulation engine of TRNSYS (TRNLIB.dll), which is called by the executable program (TRNSYS.exe), consists of two parts. The first part is the kernel that reads and processes input files, iteratively solves the system, The second part, essential for this dissertation, is a library of the FORTRAN subroutines. Next to the default library of components, the software allows for implementing own user defined components. New components can be developed in any programming language [51]. Codes developed in this dissertation are available on request.

1.3 Outline

In case the indoor climate is insufficient, the general approach for a simulation study stated in literature is:

- Develop a model of the actual situation
- Test different adaptations to the building or its system
- Analyse outcome of the different adaptations

Following this approach, the following two topics were examined more into detail: “How to assess risk of damage?” and “What has to be taken into account in the simulation model?”.

1.3.1 Assessment

As shown in Figure 1.6, different criteria play a role in the decision-making process of adaptations to the building or its systems. One of the criteria, the major criterion, is the conservation condition for the works of art in the historic building. To be able to analyse and compare different simulated options, the following questions should be answered:

- “Which indoor climate conditions are necessary for preserving a work of art?”
- “How can we assess the risk of damage to a work of art, which is related to the indoor climate?”.

For this reason, a review of the climate standards was performed (**Chapter 2**). From the literature review of chapter 2 was noticed that roughly two approaches are frequently used: general evaluation of the indoor climate and a more individualised approach focussing on the individual work of art.

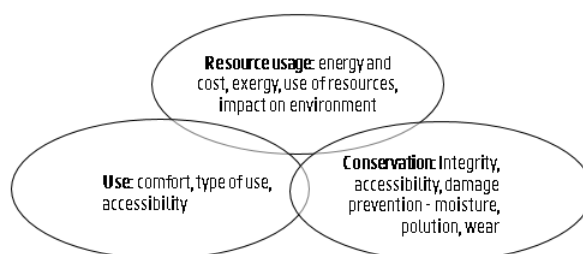


Figure 1.6: Needs taking into account in historical buildings [55].

By evaluating the indoor preservation conditions, indoor temperature and relative humidity is used to analyse the risk of damage to works of art. AIC [56], however, states that a more individualised approach of the work of art is required to ensure safety of the most sensitive objects. Furthermore, a more individualised approach would offer broader settings for climate control than the strict control classes “20°C and 40-60% relative humidity”, leading to lower energy use or even fewer second order damage mechanisms like wood rot due to condensation

at single-glazed windows [57]. On the contrary, a more individualised approach focussing on the work of art itself, requires detailed information of the material characteristics of the work of art.

As this work deals with damage to works of art in historic buildings, the first research objective is to evaluate in which case the simulated indoor temperature and relative humidity directly can be used to assess damage risk and in which case it is beneficial to model the relation between indoor climate and the work of art. In addition to Chapter 2, it is investigated to which extent HAM-models allow to assess the damage risks in panel paintings on a more reliable way compared to the assessment based on the indoor climate guidelines. This is done in Chapter 3.

Chapter 3 applies both methods to evaluate the preservation conditions of a real case. Many types of works of art exist, but because a wooden panel painting is generally regarded as the most sensitive type of object requiring particularly tight indoor climate control [58], this work of art was selected to study in detail. Based on the literature review of Chapter 2, next to the ASHRAE preservation classes, a risk assessment based on the three-types of degradation were chosen as a principle for evaluating indoor climate in this work. In case of the more individualised approach, the effect of (simulated) indoor climate on moisture behaviour of the object is examined, using a Heat, Air and Moisture (HAM) model. To this end, material characteristics of the panel painting were determined.

1.3.2 Modelling

In case it is desired to improve the existing indoor climate or to change the indoor climate by installing a new HVAC system, best practice dictates to use a simulation model to analyse the response of the modelled system and then improve, adjust or revise the system [26]. As the indoor climate in monumental historic buildings is influenced by typical conditions, the approach of how the historical building is simulated is important to find an optimal solution. Therefore, following points were studied in depth:

- To which extent is the expansion of a BES tool with (simplified) moisture buffer models sufficient to assess damage risk?
- What if the volume of the historic building is quite large and stratification occurs, for example in a church building?

Modelling of the buffering capacity in BES-tools

Historic buildings are characterised by thick walls made of brick masonry which have a high thermal and hygric capacity [59]. Furthermore, also the moisture buffering capacity of objects inside the building, like furniture, works of art, books, ... will affect the indoor climate. Due to the buffering capacity, the daily and seasonal temperature and humidity variations of the indoor environment will be moderated. To make a correct assessment of the preservation conditions, the buffering has to be taken into account in the BES-model. **Chapter 4** deals with how the (thermal) and hygric behaviour is modelled in a BES-tool.

What if the volume of the historic building is quite large?

In the past, church buildings often lacked heating systems. Due to the thick high stone walls, fluctuations of the ambient air temperature and relative humidity were attenuated and the indoor climate in church buildings was quite stable [22]. After the Second World War the living standard of the people increased and the increased prosperity lead to higher comfort demands [60], not only in residential dwellings, but also in churches. Consequently, heating systems were installed which heat the whole indoor air volume of the church. The current heating system in most churches is central heating such as air heating [61]. In cold seasons, most of these churches are heated very quickly before services in order to obtain an acceptable comfort level for the churchgoer. Consequently, next to larger temperature and humidity fluctuations in time, also temperature and humidity differences in space occur. In literature [39,62,63] several cases are described where these comfort requirements had dramatic effects on the works of art. Likewise, the Flemish Monumental Building Guard observed increased damage over the last 30 years due to uncontrolled installations of hot air systems, compared to the previous 150 years [64].

For the evaluation of different heating techniques to meet settings, sizing and energy operating cost requirements, the use of building energy simulation (BES) software is widespread used. These simulation tools have been focused on the simulation of building services systems rather than on the air flow and temperature variation in the space. In these models, each zone represents an air volume with uniform properties. In doing so, the simulation time and computational costs are kept low, at the expense of accuracy in the determination of air flow and temperature in the building [65]. The assumption of a fully homogeneous volume, however, does not allow to incorporate the stratification during heating. Damage to work of art and objects, however, is not only related due to humidity fluctuations in time, but also to humidity variation in space. As a consequence, the occurring stratification should also be taken into account when estimating damage risk of object and works of art. To this end a zonal model based on the block-model proposed by Togari [66], was implemented in the BES-software TRNSYS. **Chapter 5** describes the extensions of the original model and the implementation in TRNSYS.

1.3.3 Application

In Chapter 2, assessment tools for preventive conservation conditions were reviewed and in Chapter 3, 4 and 5 a simulation strategy was developed. Chapter 6 brings the ideas of Chapter 3, Chapter 4 and Chapter 5 together in a case study. Chapters 3, 4 and 6 each describe a part of the research question and illustrate it on a case study. Table 1.1 summarizes the theme and the case study:

- In Chapter 3 a case of a panel painting in a small enclosure was used to investigate to witch extent a HAM-model is an added-value to assess damage risk of a work of art.
- Chapter 4 used a room in a historic building to study how detailed moisture buffering has to be modelled using a BES-model.
- Chapter 6 dealt about modelling temperature and relative humidity of a whole church building while taking into account the stratification that occurred by intermittent heating.

Table 1.1: Overview of the studied cases in this dissertation.

Topic	Models	Case Study
Indoor climate vs. object behaviour Added value of simulating object	BES + HAM	
Buffering	BES + Moisture buffering models	
Hygrothermal stratification	BES+ Hygrothermal-zonal model	

Chapter 7 contains general conclusions regarding best practises for building simulation in the context of preventive conservation and the author's ideas for further research.

2

Predicting Damage Risk of Works of Art: Guidelines and Damage Functions

The preventive conservation of works of art in historical buildings requires that an appropriate indoor climate is maintained. In this chapter, climate standards are reviewed in order to identify (1) which indoor climate conditions are necessary for preserving a work of art and (2) how the damage risk due to indoor climate conditions can be assessed.

2.1 Development of Climate Standards

2.1.1 Search for the Optimal Climate Numbers

For the preservation of works of art and objects sensitive to moisture-induced damage, indoor climate recommendations have been formulated, adapted and reformulated over time. The first recommendations were mainly based on experience. The central concern of these recommendations is that humidity should not fluctuate too much, not decrease to a level which causes brittle failure of organic artefacts, nor rise to a point where mould growth can occur [67]. These recommendations thus prescribe allowable ranges for the temperature and relative humidity of the indoor climate.

The awareness that some deterioration processes are determined by the indoor climate goes back to the 19th century [68]. For example, the paint chemist Church [69] stated that "*If a stream of warm and dry air enters a gallery,...., the canvases, frames, and panels become altered in shape and size each day*". Furthermore, problems regarding the conservation of works of art were observed soon after industrial heating technologies got adopted in buildings. The concern to do something about the problem systematized in the 20th century into terms of good housekeeping, leading to reliance on active mechanical systems [68]. To avoid damage caused by the HVAC system, conservators searched for the most optimal system settings. From their experiences, the first climate specifications have emerged [70]. In literature several examples are described where climate systems were introduced to control the relative humidity in public buildings. For example, the Boston Museum of Fine Arts installed a central heating, air washing, and humidification system in 1908. After two years of observation they found that the humidity levels best adapted for paintings and other works of art range from 55 to 60 %RH. Consequently, these values became the set points of the system [71,72].

Throughout the 1930's, a spirited discussion evolved about the optimal temperature and relative humidity and the effects of their extremes on works of art and artefacts [56]. Meanwhile, the introduction of scientific methods did speed up and different museums and institutions established their own scientific laboratories⁵ where they performed experiments on works of art in order to find the 'optimal' conditions [73]. The numbers, 60% RH and 60°F (15°C) were cited by various authors as optimal conditions for preserving collections [56,67,74].

A significant experience in defining the 'optimal' climate occurred in the period during and after the Second World War. In the early years of the Second World War repositories to store the valuable collections were needed and often abandoned quarries and mines were chosen. Because these spaces had very stable climates, it was easy to obtain a stable climate with the aid of calcium chloride and a simple heating system to drop the high relative humidity, which was naturally in the range of 95%RH [73]. For example, for Manod quarry the conditions were 17°C with 58%RH and for Westwood Quarry the indoor conditions were 15.5°C–23.8°C with 60%–65% RH [75,76]. After the war, the successful recovery of the collections became a reference for

⁵ For example, in 1934 Paul Coremans founded the Physics and Chemistry Research Laboratory in Brussels (Belgium), which evolved later into KIK-IRPA [9].

conservators. In the following decades the successful preservation in mines was quoted several times as evidence of the effectiveness of the specified hygrothermal values and to confirm the absolute need of air conditioning in major museums [73,77].

Meanwhile, also thermal comfort of the visitors gained more importance. New works appeared with new 'ideal' numbers or confirming the old numbers. Among them were the works of Plenderleith [78] and Buck[79]. Plenderleith, full-time chemist of the British Museum [75], defined for temperature a range of 16-25°C and for the relative humidity a range of 50%RH - 65%RH [78]. These values were chosen because below 50% RH damage to organic materials was observed and above 65%RH there was risk for mould growth. In 1964 Buck [79] was the first to suggest ranges for relative humidity for different materials. This mental legacy culminated in the publication of "The Museum Environment" in 1978 by Garry Thomson [80]. This book was also called the 'bible of conservation' and contains formulations of indoor climate recommendations for the preservation of works of art on building level. It promoted the idea that the control of environmental conditions could minimize damage to artefacts and slow their deterioration, which would later be developed in the theory known as preventive conservation [73]. To reduce the risk of damage, the author looked at previous cases where the collection was well-preserved and to the control range of an air-conditioning system [71]. Based on these findings, he suggested average values of 20°C and 55 %RH and an amplitude of $\pm 4^\circ\text{C}$ and 5%RH for allowable fluctuations. However, he remained critical about his suggested numbers⁶. The method followed by Thomson for determining the best range for relative humidity was very simple. An upper limit at 65/70% was taken to avoid mould growth and a lower limit at 40/45% was taken to avoid embrittlement. The value of 55%RH was most likely chosen because it corresponded to the yearly average relative humidity of most heated spaces in Europe [70,72] [73]. In 1986, a second edition of the book appeared which made a subdivision into two classes related to the building environment [81]:

- Class 1: appropriate for major national museums, old or new, and all important new museum buildings (19/24 \pm 1°C (winter/summer) - 50 or 55 \pm 5%RH)
- Class 2: aims at avoiding major dangers while keeping cost and alteration to a minimum. E.g. most important historic houses and churches (temperature reasonable to stabilise RH - 40-70%RH using room (de)humidifiers)

Over time these guidelines became a convenient standard to which museums and borrowers were held for collecting institutions across the globe [56,67]. However, the problem was that Thomson's criticism about the numbers was often neglected and class 1 was definitely seen as 'better', whereas class 2 became synonymous with 'second class' [67,82]. Because class 1 conditions often preserve historic material very well, this specification became the norm for

⁶ Thomson literally writes: "There is impressive general evidence, for example in the records of the National Gallery, London, that transferring paintings to an air conditioned environment very greatly reduced the need for treatment of detached paint... But the question of how constant RH needs to be to be to ensure that no physical deterioration will occur remains at present unanswered. The standard specification of ± 4 or $\pm 5\%$ RH control is based more on what we can reasonably expect the [air conditioning] equipment to do than on any deep knowledge of the effect of small variations on the exhibit..."

museums, and little research has been performed to determine if historical material can survive in different environmental conditions [83].

2.1.2 Is a Broader Range of Optimal Climate Numbers Acceptable?

A new transition in the view on preservation conditions started in the early 1990's. With the growing understanding of the effects of climate conditions on materials and objects, the requirements of Thomson were criticized [83,84].

A first criticism was that allowing a broader range of temperature and relative humidity averages and amplitudes would allow a wider choice of climate management systems and settings which are less expensive to design, install and operate. This is illustrated in Figure 2.1 which shows how the energy cost per Square Foot is related to the allowable fluctuation for relative humidity around a setpoint of 50%RH for different case-studies [85]. For example, allowing a fluctuation of $\pm 10\%RH$ instead of $\pm 5\%RH$, decreases the cost from 2.6 to 1.3.

Another criticism on the former defined "ideal numbers" was that historical buildings were not designed to comply with these stringent guidelines and when following the recommendations, damage could even become worse [86,87]. For example, in re-using historical buildings heating and people can cause condensation on the stained glass leading to corrosion [88].

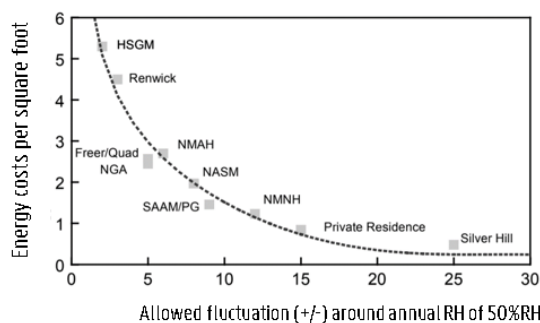


Figure 2.1: Energy cost per Square Foot related to the allowable RH-fluctuation around a setpoint of 50%RH [85].

Consequently, to succeed in managing the indoor museum environments in an efficient manner, as well as in satisfying the high standards of collection care, more and more object based research was performed, for example on the modelling of wood behaviour. The goal of these research projects was to understand the influence of the indoor climate on the object of art, and to investigate the loosening of the indoor climate boundaries without causing deterioration. Object based research led to new general climate guidelines and specific damage functions specific for a certain object [76]. They generally contain recommendations on three principal

components by which the indoor climate is statistically represented: long-term average levels (usually over one year), seasonal cycles and short-term fluctuations [58].

2.1.3 A More Realistic, Risk-Management Based Approach

General Climate Assessment by ASHRAE

An innovation in the new way of thinking were the guidelines published in 1999 by the American Society of Heating, Refrigerating and Air-Conditioning Engineers (ASHRAE [89]) in collaboration with the Canadian Conservation Institute (CCI [90]). In these guidelines, five preservation classes were defined, expressing the concept of different “qualities” of climate control [91]. As presented in Table 2.1, classes range from AA, corresponding to the highest possible control with a minor risk of damage to most artefacts, to D, with a minimized control in which only the risk of mould growth is avoided.

To overcome the problem that historical buildings were never designed for the ideal numbers: “21°C and 50%RH with minimal fluctuations”, ASHRAE suggested the following set points: the historic annual average relative humidity for a permanent collection and an average annual temperature between 15°C and 25°C. This specification recognises that a collection can acclimatise to an average annual relative humidity and that the temperature set point can to be dictated by human comfort [91]. Although class A is the optimum for most museums, class B and C are often the best that can be achieved in historical buildings. Hence, when implementing an HVAC system in historical buildings to achieve a “good” climate for comfort and preservation, the risk to the structure and the building envelope is often overlooked [89,92]. Therefore Conrad[93] grouped buildings in terms of the capability to control the indoor climate and linked these types to the achievable ASHRAE level (Table 2.2).

in Canada, where CCI actively promoted its use, the ASHRAE class of control nomenclature was quickly adopted by museum consultants and conservators. In the United States and elsewhere, it was also adopted by engineers but not the conservation community, except for those who worked with historical houses, who were happy to see the compromises between collections and the building given formal definitions [68].

USA: Smithsonian Institute

Similar advice was developed at the Smithsonian institute in the USA [68]. For decades the guidelines of the Smithsonian Institute were 21°C±2°C and 50%±5% RH. In 2004, broader guidelines were suggested; a relative humidity of 45%RH ±8% RH and a temperature of 21°C±2°C. These recommendations allow, without restriction, any point within the environmental box formed between 37% RH and 53% RH and from 19°C to 23°C for the vast majority of the collections [92].

Europe: Bizot group

In Europe guidelines were written by the Bizot group. This group was established in 1992 and is a group of museum directors from European Institutions, who initially aimed at facilitating and intensifying exchanges between their institutions [94]. Therefore, they wrote guidelines which specified the conditions in which the artwork should be contained temporary during an exchange. In 2004, ICOM-CC and ICC noted that these guidelines for international loan exhibitions implies that specifications for permanent collections remain up to individual users [68]. Therefore they agreed that the existing interim guidelines, should become general guidelines and not interim guidelines [95].

The Bizot Group defined for most classes of objects containing hygroscopic material (such as canvas paintings, textiles, ethnographic objects or animal glue) a stable relative humidity range, namely between 40–60%RH, and a stable temperature in the range of 16–25°C. Fluctuations in relative humidity may be no more than $\pm 10\%$ RH per 24 hours within the specified range.

General Climate Assessment by the Standard EN15757:2010

In 2010, the European Standard EN15757:2010, "Conservation of Cultural Property - Specifications for temperature and relative humidity to limit climate-induced mechanical damage in organic hygroscopic materials" [96], was published. Contrary to the other methods no limiting values or ranges are provided, but the existing climate is evaluated as harmful or not. This standard starts from the "*historical climate*", defined as "*Climatic conditions in a micro-environment where a cultural heritage object has always been kept, or has been kept for a long period of time (at least one year) and to which it has become acclimatised*". In case this microclimate has been proved to be not harmful, the standard recommends to maintain the historical climate, especially as far as relative humidity is concerned. The stability of the indoor climate, and especially the relative humidity, is evaluated based on statistical values.

General Climate Assessment by the Standard EN16883:2017

In 2017, the European Standard EN16883, "Conservation of cultural heritage — Guidelines for improving the energy performance of historic buildings" [96], was published.

This European Standard provides guidelines for sustainably improving the energy performance of historic buildings, e.g. historically, architecturally or culturally valuable buildings, while respecting their heritage significance. Thereby, it provides a systematic procedure to facilitate the best decision in each individual case. It proposes to assess different categories, in which damage risk for works of art is one of the many. Other categories are economic viability, heritage significance, energy... An example of the assessment table is shown in Annex 2.A. The standard is interesting to compare different buildings and assess the building on different topics. It is however not a tool to assess the preservation conditions.

Table 2.1: ASHRAE preservation classes for general museums, art galleries, libraries and archives.

Class	Short Fluctuations & Space Gradients		Seasonal Adjustments		Collection Risks
	T	RH	T	RH	
AA	±2°C	±5%	±5°C	No change	No risk of mechanical damage to most artefacts and paintings. Some metals and minerals may degrade if 50% RH exceeds a critical relative humidity.
A	As	±5%	+5°C -10°C	±10%	Small risk of mechanical damage to high-vulnerability artefacts; no mechanical risk to most artefacts, paintings, photographs and books. Chemically unstable objects unusable within decades.
	A	±10%	+5°C -10°C	No change	
B	±5°C	±10%	+10°C (max 30°C) Down: as low as necessary to maintain RH control	±10%	Moderate risk of mechanical damage to high-vulnerability artefacts; tiny risk to most paintings, most photographs, some artefacts, some books; no risk to many artefacts and most books. Chemically unstable objects unusable within decades, less if routinely at 30°C, but cold winter periods double life.
C	25-75% RH, <25°C (rarely over 30°C)				High risk of mechanical damage to high-vulnerability artefacts; moderate risk to most paintings, most photographs, some artefacts, some books; tiny risk to many artefacts and most books. Chemically unstable objects unusable within decades, less if routinely at 30°C, but cold winter periods double life.
D	<75% RH				High risk of sudden or cumulative mechanical damage to most artefacts and paintings because of low-humidity fracture; but avoids high-humidity delamination and deformations, especially in veneers, paintings, paper and photographs. Mould growth and rapid corrosion avoided. Chemically unstable objects unusable within decades, less if routinely at 30°C, but cold winter periods double life.

Table 2.2: Classification of climate control in potential related to the building type concerning ASHRAE [97].

Category of control	Building Class	Typical Building construction	Typical Type of Building	Typical Building use	System used	Practical limit of Climate Control	Class of Control Possible
Uncontrolled	I	Open Structure	Privy, stocks, bridge, sawmill, well	No occupancy, open to viewers all year.	No system.	None	D (if benign climate)
	II	Sheathed post and beam	Cabins, barns, sheds, silos, icehouse	No occupancy, Special event access.	Exhaust fans, open windows, supply fans, attic venting. No heat.	Ventilation	C (if benign climate) D (unless damp climate)
Partial controlled	III	Uninsulated masonry, framed and sided walls, single-glazed windows	Boat, train, lighthouse, rough frame house, forge	Summer tour use. Closed to public in winter. No occupancy.	Low-level heat, summer exhaust ventilation, humidistatic heating for winter control	Heating, ventilation	C (if benign climate) D (unless hot, damp climate)
	IV	Heavy masonry or composite walls with plaster. Tight construction; storm windows	Finished house, church, meeting house, store, inn, some office building	Staff in isolated rooms, gift shop. Walk-through visitors only. Limited occupancy. No winter use.	Ducted low-level heat. Summer cooling, on/off control, DX cooling, some humidification. Reheat capability	Basis HVAC	B (if benign climate) C (if mild winter) D
Climate controlled	V	Insulated structures, double glazing, vapour retardant, double doors	Purpose-built museums, research libraries, galleries, exhibits, storage rooms	Education groups, Good open public facility. Unlimited occupancy.	Ducted heat, cooling, reheat, and humidification with control dead band.	Climate control, often with seasonal drift	AA (if mild winter) A B

Specific Prescriptions Applied on Historical Church Buildings

To evaluate the indoor climate, the prescriptions described above could be applied. Besides, recommendations and standards specific for the historical church buildings can be found. These are largely related to the heating regime, as the heating regime is one of the main reasons of the large humidity fluctuations causing damage.

Important Researches

In 2002, H. Schellen investigated important parameters concerning conservation of monumental churches and their interiors related to heating [22]. As a result, he listed recommendations found in literature. These recommendations were adopted and complemented by Troi in 2010, who investigated the balance between level of comfort for visitors, energy costs and damage when heating historic churches [98]. An overview of these recommendations are listed in Table 2.3.

Table 2.3: Comparison of recommendations in literature for indoor climate in heated churches, according to Schellen [22] and Troi [98].

Author	Year	T _i *	T _{primary} **	ΔT/Δt	φ***	Δφ
Badertscher	1965	<15	8-10	-	45-65	-
Hennings	1966	15	8	-	55-75	-
Supper	1967	17-19	5-7	-	<60	-
Schlieder	1967	<15	7-10	<2	50-70	-
Knol	1971	≤15	-	1.5	<75	-
Stadtmüller	1972	-	-	-	60-70	-
Gossens	1972	12-15	8-10	1.5-2	50-60	-
Schmidt-Thomsen	1973	12-15	8	<1.5	-	-
Mainz	1973	12-15	8	<1.5	-	-
Pfeil	1975	12-16	-	-	Constant	±5%
Mayer	1981	-	-	-	40-60	-
Beck & Koller	1981	10	-	-	50-60	-
Dulosy	1981	8-10	-	-	>50	-
Arendt	1986	10	8	0.5-1.5	-	--
Künzel & Holz	1991	12-16	5-8	fast	50-80	Δφ _{day} ≤10% Δφ _{year} ≤30%
Bordass	1993	-	-	-	-	-
Schellen	2002	15-20 ≤15 FH	5-10 ≥8 GH	2	45-75 40-90	Δφ _{day} ≤10% Δφ _{year} ≤30%

* Indoor temperature while heating

** Minimum temperature in the church

*** Recommendations based on damage of an organ

The Friendly Heating Project

From 2002 till 2005, the EU funded the project called "*Friendly heating Project*". The goal was to preserve works of art in their natural, historical climate and, at the same time, to warm people at the highest thermal comfort compatible with conservation [60]. In the classical heating strategy heat is accumulated in the upper part of the building (Figure 2.2). Instead, local heating systems were investigated aiming to produce the best radiant temperature within the occupied area of the church only, with some local increase in air temperature and minimum draughts, while the rest of the building remains almost unaffected and preserves or remains close to its historical climate [61].

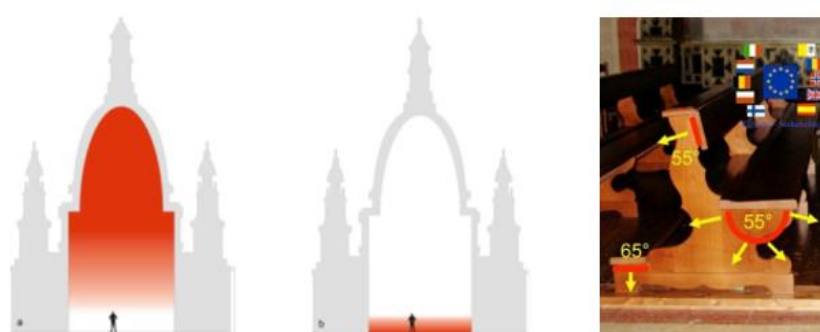


Figure 2.2: (a) Concept of heating strategy in the "Friendly Heating Project": only local heating for people instead of heating the whole church with warm air [61]. (b) Outcome of the "Friendly Heating Project": Location and temperature of the heaters fixed to pews in the EU Friendly-Heating project[99].

European Standards

The basic concepts from the Friendly Heating project have inspired the standard: EN 15759 (2011) "*Conservation of Cultural Property - Indoor Climate - Part 1: Heating Churches, Chapels and other Places of Worship*" [100]. This standard provides guidelines for the selection of heating strategies and heating systems in churches, chapels and other places of worship. The standard doesn't describe preservation guidelines for the climate, but helps in the decision-making processes. The steps given in the standard are:

- establish the historic indoor climate;
- determine an indoor climate specification for conservation;
- determine an indoor climate specification for thermal comfort;
- if needed, find a compromise between b) and c).

Once this is done, a heating strategy and a heating system can be determined. Then, the new heating system can be implemented. Finally, any changes regarding indoor climate, heating strategy or heating systems shall be evaluated to ensure that the objectives, with respect to conservation and comfort, have been met.

The Belgian Situation

Due to the many cases in Belgium where damage occurred at objects of art (paintings, organs, textiles...) in churches, guidelines for heating parameters were also given in the circular ML/11 [64], written in 2011 by the department of Urban Planning of the Flemish government. These guidelines are summarized below.

- When heating during the service, the temperature must be limited to 15°C, and this limitation holds not only at the place where visitors are located, but also at the organ.
- The temperature of the space may not be increased more than 2°C per hour.
- The minimum temperature in the church must be between 10 to 12°C, regarding permanent heating in colder periods. Better would be to keep the temperature all the time at 13-14°C, without heating during services.
- The supply temperature of the heating must be between 40°C to 45°C.
- The relative humidity in the bulk air of the church must be kept, if possible, between 55% and 70%.

2.1.4 Focus on Object: The Three Types of Degradation Principle

Other researchers thought/found it necessary to analyse the response of individual materials and objects to changes in temperature and relative humidity. When assessing the degradation risk, three types of degradation are commonly mentioned: chemical, biological and mechanical degradation. The risk on damage for the object is then assessed for each type of degradation.

The risk for each type of degradation can be related to temperature and relative humidity [70]. Two values are of importance: the average value and the value of the amplitude of the fluctuations. The scheme below points out how the deterioration types are related to these (Figure 2.3). If the average value of the temperature or relative humidity is too high, biological, and/or chemical degradation may occur, whereas fluctuations in temperature and relative humidity mainly lead to mechanical degradation. However, it must be pointed out that mechanical degradation is also indirectly related to the average temperature and the relative humidity.

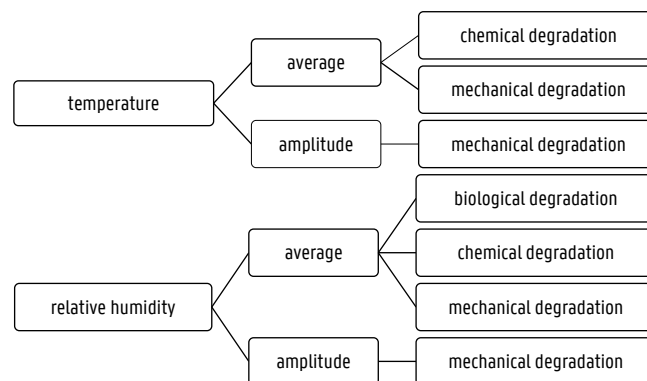
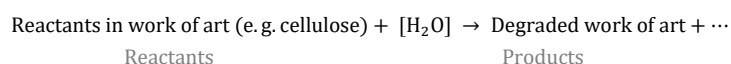


Figure 2.3: Schematic overview of the three types of degradation related to temperature and relative humidity.

Chemical Degradation

The cause of chemical degradation is a chemical modification of the work of art because of chemical reactions taking place within the organic material under certain temperature and humidity conditions. The two environmental parameters, temperature and relative humidity, have a different role in the chemical reaction. It must be mentioned that next to temperature and relative humidity, daylight and electrical light sources also cause chemical changes in various works of art. Degradation by light, however, is out of the scope of this work.

The humidity, which is the presence of water molecules in the object, is necessary to cause a chemical reaction because it serves as reactant. Examples of chemical reactions related to moisture⁷ are hydrolysis and corrosion. The water molecules react with the material of the object, among others with cellulose, which is found throughout museum collections in the form of fibres, papers, woods and textiles [101]. Schematically the chemical reaction can be expressed as:



The higher the concentration of water molecules, the more chemical reactions can occur. Commonly the relative humidity is used instead of the moisture content of the object, to express the relation between the environment and the chemical damage. However, one should be aware that the relative humidity is a parameter related indirectly.

Temperature determines the speed of the chemical reaction. It is commonly known that a chemical reaction occurs faster at higher temperatures. Since temperature presents the amount of energy contained within an object, at a higher temperature atoms and molecules move faster. Consequently, chemical reactions occur more quickly, resulting in an increase of the decay rate of an object.

Different formulas were developed to assess the chemical degradation risk related to humidity and temperature. All these are based on the so-called Arrhenius equation, which is commonly used to calculate the rate of decay in function of the temperature. Using this chemical background, in conservation science the concept of relative lifetime expectancy was developed. This holds that the relative change in the deterioration rate is calculated as the ratio of the two decay rates: the existing environmental conditions with rate k_1 , and the new condition or a default condition with rate k_2 . Different definitions to calculate the relative lifetime of a work of art exist. These are summarized in Annex 2.B.

Biological Degradation

Biological degradation can be defined as “any undesirable change in the properties of a material caused by the vital activities of organisms” [102]. Bacteria, archaea, fungi and lichens as well as insect pests are constantly causing problems in the conservation of cultural heritage [103]. In museums and historical buildings biological degradation is common, because environmental conditions are suitable for the growth of these organisms, either due to building problems, malfunctioning of HVAC (heating, ventilation, and air conditioning), or accidents [104,105]. The most important role in biological degradation in museums and in libraries is played by fungi and mould [103,106].

⁷ It is important to note that the ambient environment has many mechanisms for degradation besides temperature and moisture; for example, light degradation (UV) [101]. However, this study is limited to temperature and relative humidity.

Fungi and mould

There are many species of fungi and simply put, mould is a subdivision of the kingdom 'fungi'. Numerous fungal spores are constantly present in the surrounding air. However, specific environmental and nutritional conditions must be met for them to grow and to cause biological degradation. In all situations, moisture is an important factor for germination and for successful colonization of the substrate by the fungus [107]. Other factors are temperature, nutrients, spores oxygen, light and pH-value of the substrate [108]. According to Sedlbauer [109] humidity, temperature and the substrate type are most important boundary conditions and they must exist simultaneously over a certain period of time.

The water requirement for mould growth is usually expressed as water activity (a_w). The water activity is defined by the accessible water in the material, expressed as the relative humidity in equilibrium (when the relative humidity is equal between the material and the surrounding air) [110]. It is calculated as:

$$a_w = \frac{\varphi}{100} \quad (2.1)$$

Three critical temperatures for fungi are the temperature below which no growth occurs, the temperature above which no growth occurs, and the optimum temperature, at which the most rapid growth takes place [111]. Most microbial forms found in collections will grow in temperatures ranging from 15 to 25°C [111].

Organic collection materials, especially textiles, paper, wood, leather and other animal products, serve as nutrient source [104].

Prediction of mould growth⁸

To prevent mould growth, two approaches 'exist': a general approach and a more complex approach.

The general approach only defines a critical water activity or a critical relative humidity as a limit to prevent mould growth. Below 0.55 all metabolic activity ceases and DNA is denatured. Therefore, a water activity of 0.60 is considered the lower limit for microbial growth [97,112]. This is for example visible on the graph presented by Michalski [113]. The graph (Figure 2.4) presents the time before mould growth becomes visible for a certain relative humidity.

Using the value of 0.60 is safe, but rather conservative [97]. Therefore, a common limit given in literature, is a water activity of 0.75 or a RH of 75%(e.g. [112,114],...). On Figure 2.4 it can be observed that at 75%RH, growth is noticeable after two to three months and that mould growth increases exponentially with increasing relative humidity. At 80-100%RH growth is noticeable between 1 and 10 days.

⁸ Boundary conditions to avoid fungal growth are commonly linked to mould growth as many mould fungi start to develop at a lower relative humidity than other fungi species.

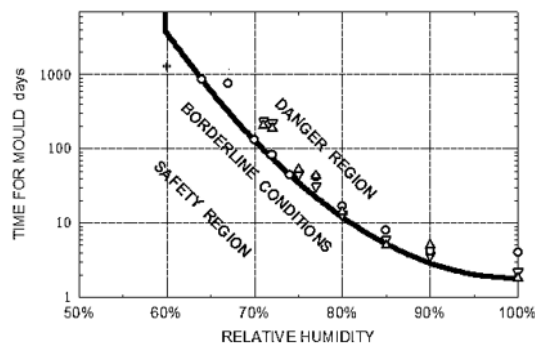


Figure 2.4: Time required for visible mould growth, assuming highly susceptible material at about 25°C and a relative humidity that has climbed (not fallen) to these values. [113].

A critical humidity alone, however, could overestimate potential mould growth as other factors such as time and temperature are not taken into account [115]. Therefore, more sophisticated mould growth models consider also other factors in their damage function. Vereecken [116] provides an extensive overview of the different existing models. Since the temperature and relative humidity are the main influencing factors for mould growth, several models are based on isopleth systems which indicate the mould potential in function of the temperature and relative humidity combination [116]. Examples are VTT, Sedlbauer,....

Isopleth curves express the relation between mould risk and main mould inducing factors; i.e. relative humidity (or water activity), temperature and the exposure time [116].

Mechanical Degradation

Physical mechanical processes are caused by the changes in humidity and temperature. A change in humidity or temperature leads to dimensional changes of the object. These dimensional changes result in stress in the material. If stresses are larger than the yield point of the material, irreversible deformation occurs. Hence, to avoid mechanical degradation, fluctuations in temperature and humidity must be limited. The following situations must be avoided:

- Too large fluctuations causing stress/strain which leads to instant mechanical damage like deformation or failure. (mechanical damage)
- Loads that are repeated many times, causing damage to stress levels which are lower than the limits. (fatigue damage)

Instant Mechanical damage

All materials considered can reversibly sustain some stress and strain. However, when certain limits are exceeded, permanent change or damage such as warping or cracking occurs [71]. Mecklenburg, Erhardt, Tumosa and McCormick-Goodhart, researchers from the Smithsonian

Museum Conservation Institute, stated that limits for relative humidity can be found by measuring the yield point of the material, which is a material characteristic that can be determined in a laboratory. They defined stress-strain curves for many hygroscopic materials found in a collection (e.g. hide glue Figure 2.5). Combining all the collected data, the overall conclusion was that in the range of 30% to 60%RH the climate is safe for general collections, but that exceptions exist which should be kept in more stable environments [71,101,118,119].

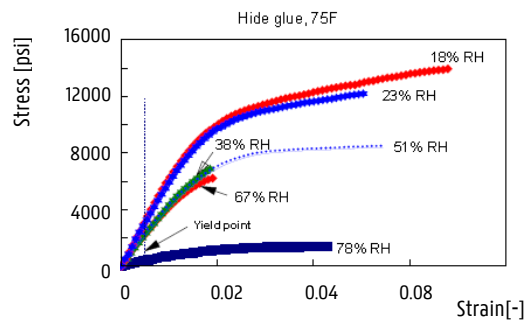


Figure 2.5: The tensile stress-strain tests for hide glue⁹ at different RH levels.

Michalski criticized the lack of information for this "category of exceptions", which is according to him precisely what is of importance when estimating object damage. As long as there is a lack of data to develop a general model valid for all objects, or to start modelling of individual objects, another approach is needed [68,120]. Although the situation is recently changing by research of a group of researchers in Cracow¹⁰ who perform research in modelling of panel paintings, Michalski suggests to use the so called 'proofed fluctuation' of the objects. This method is based on historical data of the indoor climate and not on a scientific analysis, which is not usable because of its complexity. The idea is that the largest fluctuation experienced by the object in the past has caused all the mechanical damage possible by that size of fluctuation and therefore future fluctuations equal to, or smaller than the proofed fluctuation will not cause further mechanical damage, unless the collection has aged chemically, has been damaged or has been consolidated [84,121]. This concept of maintaining the historic environment because it has not been too harmful in the past is incorporated in the European standard EN 15757:2010 (paragraph 2.1.3) [122].

⁹ Hide glue is present in nearly all cultural collections. It is found as the adhesive for bonding parts and veneers in wood furniture, it is used as the size in traditional canvas paintings and some watercolour papers, and it is used to make gesso. When refined into gelatine, it is used as the image emulsion in photographic materials.

¹⁰ i.e. Kozłowski, Bratasz, Lukomski and Rachwał

Fatigue damage

If the limit of the yield point of the material is not exceeded, the object returns to its initial condition when the load is removed. In theory, this process may be repeated infinite times. However, in reality it is noticed that if the loads are repeated many times, damage will occur at stress levels which are lower than the limits. This type of mechanical damage is called fatigue damage.

Figure 2.6 explains the path to estimate the fatigue life for an object. Starting from real life conditions, first a stress strain cycle analysis must be performed. Next, these results are analysed if there is a risk of damage, to come finally to a fatigue life estimate.

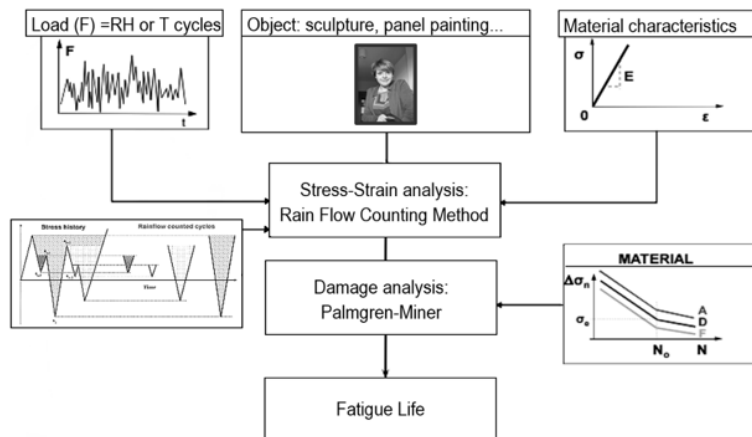


Figure 2.6: Information path for fatigue life estimation based on the strain-cycle method [123].

In the first step, the stress-cycle or strain-cycle applied to an object has to be determined. In this field - damage to works of art caused by indoor climate conditions - the stress-cycles are the changes in temperature and in relative humidity¹¹. To study the relation between the amplitude of a cycle and the amount of cycles that may occur before failure of the object is noticed, a fully reversed load with a constant amplitude is imposed to a material in a laboratory. Therefore, the load cycles are represented by a sine wave. As a result of this test, a stress-cycle (S-N) or strain-cycle (ϵ -N) curve is defined for a material in which the number of cycles to failure is related to stress. In reality, however, objects prone to fatigue will experience stresses that vary with time as a result of an irregular load history. Therefore, things are much more complicated and the direct use of S-N curves is not applicable because these curves are developed and presented for constant stress amplitude operation [124]. To analyse the stress-cycle or strain-cycle, some type of cycle counting scheme must be employed. The counting method allows to reduce a complex

¹¹ Expressed as relative humidity. In the experimental conditions temperature is kept constant, so in fact it is the absolute humidity which determines the relative humidity

irregular loading history into a series of constant amplitude events [125]. There are six main methods: peak counting, time counting, simple range counting, range pair counting, level crossing counting and rain-flow counting [124]. The most widely used method to analyse estimate fatigue life is the rain flow counting method[124,126].

The rain flow counting method is a way to separate small, non-destructive oscillations from the large harmful ones, without affecting turning points. Especially, in fatigue damage calculations, small amplitude ranges can often be neglected because they do not cause the cracks to grow. The rain flow cycle counting method was originally defined by M. Matsuishi and T. Endo as an algorithm [127] where they describe the process in terms of rain falling off a Japanese pagoda style roof. However, an equivalent algorithm that is easier to implement, is generally recommended by ASTM E 1049-85 [128]. The last one will be used in this work. Counting is carried out on the basis of the stress-strain behaviour of the material and as a result a number of cycles to failure for each different amplitude interval is found. The amplitude of the cycles and their corresponding frequency results from the counting method. The method is explained more into detail in Annex A.

The second step to estimate the fatigue life is to predict if there will be failure by cumulative damage. For this, a linear or a non-linear cumulative damage rule can be used. In a linear rule, like the commonly used Palmgren-Miner rule[129], fatigue damage is simply calculated by adding the damage for each measured cycle. For Palmgren-Miner this holds that the resulting fatigue damage is given by adding the corresponding damage ratio's N/N_i . The amount of cycles N at level i is given by the counting method, and the cycle life N_i is obtained from S-N data tests. The sum of these ratio's leads to the estimation of the fatigue life. A value larger than one results in damage and a value lower than one, does not. As a consequence of this linear rule, the order of application of the various loadings should not play any role. This is rarely the case in reality. Notwithstanding the inadequacy of the Miner rule, which has no real physical basis, it is much used because of its simplicity [124].

Michalski [130] suggested to measure the fatigue damage based on the S-N-curve (or ϵ -N-curve) of a material and the theory of proofed fluctuation. He states that an object will have a negligible likelihood of further fracture damage as long as the combination of stress and number of cycles does not exceed the S-N curve. For example, as plotted in Figure 2.9., one cycle at the proofed fluctuation, 30 cycles at 0.9 of the proofed fluctuation, or for the most brittle materials, 10k cycles at 0.45 of the proofed fluctuation.

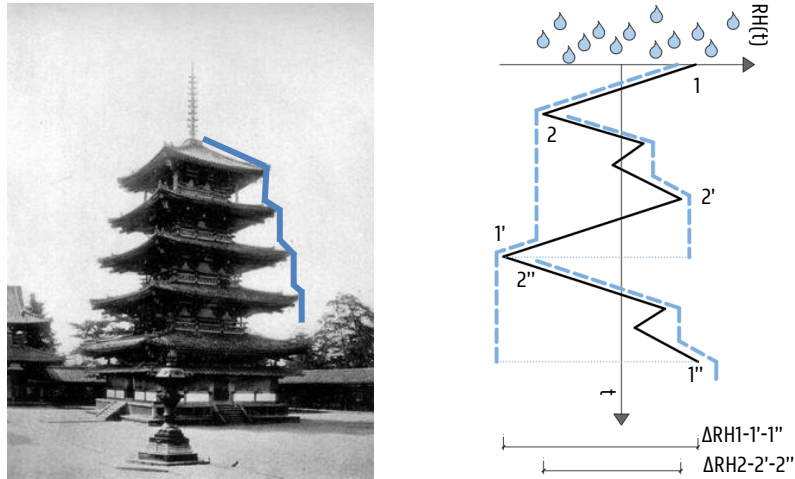


Figure 2.7: The rain flow cycle counting method was originally defined by M. Matsuishi and T. Endo as an algorithm [127] where they describe the process in terms of rain falling off a Japanese pagoda style roof (figure left: [131], figure right [132]).

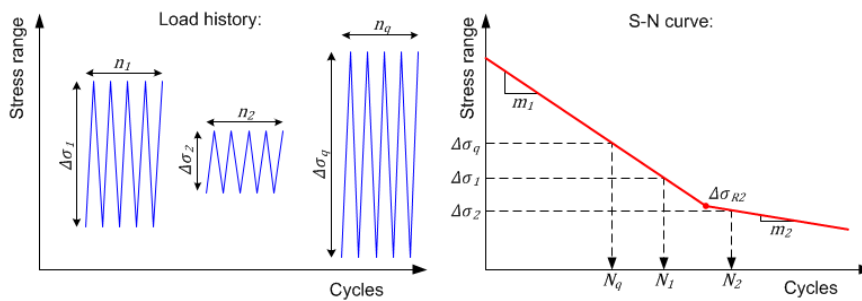


Figure 2.8 [133]: Principle of Palmgren-Miner damage accumulation. [Left] The load history split up by the counting method into several cycles with the same amplitude. [Right] The S-N curve corresponding from experiments. This graph gives the maximum amount of cycles N_i necessary to calculate the ratio D .

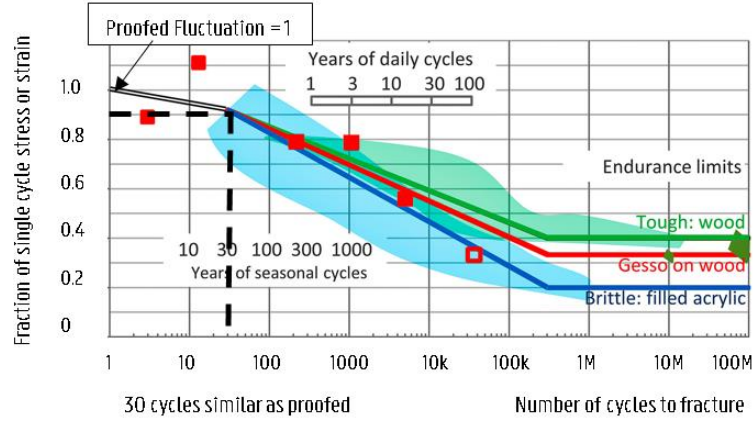


Figure 2.9: Picture presented by Michalski [130]. Summary of fatigue data (S-N plots). Green: stress for wood (spruce and Douglas fir in bending) pale green area for scatter in the 70 samples that broke; dark green patches: scatter in the 10 samples that did not break even at 10–100 million cycles [134]. Blue: stress for acrylic plus filler; pale blue area for scatter of 173 samples from a set of 180 [135]. Red: strain in gesso on wood, six samples, red solid squares for cracks initiated, open red square for no crack at 36500 cycles [136,137].

2.2 Selected Evaluation Methods

The literature review showed different methods to evaluate the preservation conditions for a work of art in a historic building. Roughly, these recommendations can be divided into two groups (Figure 2.10):

- those who focus on general prescriptions for the indoor climate
- those who focus on the behaviour of a particular art object

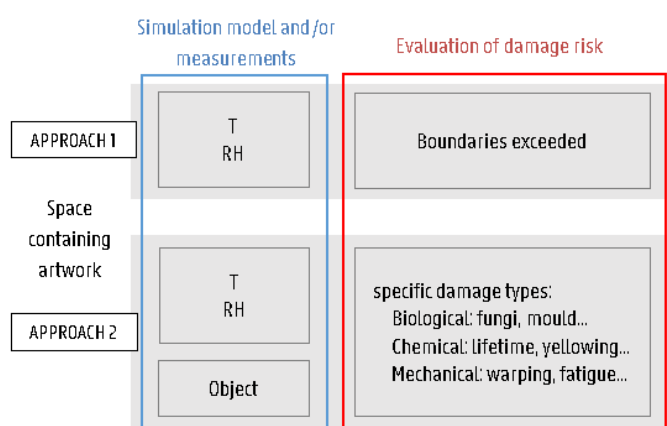


Figure 2.10: Approach studied in this work to estimate damage risk.

Methods belonging to the first group look whether the simulated temperature and relative humidity fall between allowed boundaries. If they do not, it is concluded that there is a risk of damage. These methods are rather easy to use because only temperature and relative humidity of the indoor environment have to be known to evaluate the preservation conditions. For defining the allowed boundaries, different guidelines to evaluate the indoor climate (see paragraph 2.1.3). When generalizing the guidelines found in literature, it seems as if every single organisation strives to find its own guidelines or recommendations, although these are all quite similar. Table 2.4 summarises the recommendations from major organisations. Concerning the relative humidity, the guidelines include an average value with allowable fluctuations or an allowable range. These values are mostly centred in the mid-range of 40-60%RH. In this dissertation, the ASHRAE method to evaluate the preservation conditions is used, and more specifically class B. The reason is that this method is widely used and incorporates short-term and seasonal fluctuations providing flexibility for historical buildings. Because, a criticism on these methods is that they are too rigorous, compared to the observed damage of the object and therefore leading to too stringent climate conditions, the method that focuses on object behaviour is also used.

Table 2.4: Comparison of the boundary values for the indoor air temperature and relative humidity given by the ASHRAE, the Smithsonian institute and the Bizot group. For ASHRAE class B was selected as this is what can be achieved in a historical building (based on [68,138]).

Parameter	ASHRAE (class B)	Smithsonian Institute	Bizot Group	
T [°C]	Setpoint	15-25	21	
	Minimum		19	15
	Maximum		23	25
	Daily fluctuation	±5		
	Seasonal fluctuation	±10		
RH [%]	Setpoint	50 or annual average	45	
	Minimum		37 (30)	40
	Maximum	75	53 (60)	60
	Daily fluctuation	±10		±10
	Seasonal fluctuation	±10		

2.2.1 ASHRAE Method

ASHRAE does not provide a clear description of how short-term and seasonal fluctuations should be used. Several authors use different methods [139–141], that can lead to different results. In this work, the method to evaluate the indoor climate as described by Martens [141,142] is used. This method is a so-called reverse method because ASHRAE classes are normally used as design parameters and not as an evaluation tool. The principle of the ASHRAE method is to define a bandwidth which the short-term (daily) fluctuations may not exceed. This bandwidth is derived from the average course over the year, including long-term (seasonal) variations.

To define the bandwidth, first the seasonal variation is calculated. To calculate the allowed seasonal variation the yearly average or control set point can be used. Since the work of art has been in the historic building for decades, the target values will be based on the yearly average which is more representative than the control set-point. The long-time variation defined in the ASHREA-class (*Table 2.1*) is added or subtracted to the yearly average to set the boundaries for the allowable seasonal fluctuation (Figure 2.11a).

Next, the moving average used to express the average course, is calculated for the temperature and relative humidity fluctuations of the space (eq.(2.2)). By using the moving average, short-term fluctuations are smoothed out and long-term variations are highlighted. The period for calculating the moving average covers three months and is centred¹². Furthermore, the restriction that the temperature should be between 15°C and 25°C [143] is not taken into account. This is because this guideline is beneficial for human comfort, but not for the preservation conditions since for a work of art a lower temperature results in a lower chemical degradation. Because the course of the moving average for an entire year is needed, the sampling period needs to be

¹² This guarantees that variations in the average temperature and relative humidity are not being shifted in time.

extended by one and a half month before and after. When the moving average exceeds the boundaries set by the seasonal yearly average, the moving average is truncated by these boundaries (Figure 2.11b).

$$\bar{x}_{\text{moving}} = \frac{X_{i-1.5 \text{ month}} + \dots + X_i + \dots + X_{i+1.5 \text{ month}}}{n} \quad (2.2)$$

Then the allowable short-time variation defined by the chosen ASHRAE class is added to or subtracted from the average course to set the boundaries for the allowable short-term fluctuations (Figure 2.11c).

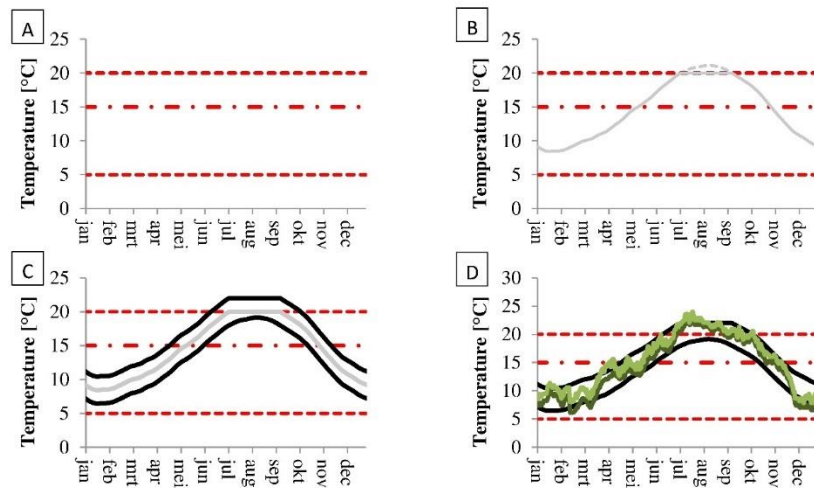


Figure 2.11: Reversed ASHRAE method used in characterising the preservation conditions.

To evaluate if the measured or simulated indoor temperature or relative humidity satisfies the conditions of the desired ASHRAE class, it should be checked whether the daily minimum and maximum lie between the boundaries (Figure 2.11d). Results are expressed as the percentage of time that target values for temperature, relative humidity or humidity were met during the the combination of temperature and relative humidity were met during the monitoring campaign or simulation period. **These percentages give an indication of how far the conditions for the indoor climate deviate from the conditions required to achieve a certain preservation class. It is important to remark that once the conditions for a certain class are not continuously fulfilled, there is risk of damage,** no matter whether the preservation conditions are within the specified class for 99% of the time or for only 10% of the time.

2.2.2 Object Oriented Method

The methods from the second group also take object-related characteristics into account in addition to temperature and relative humidity. An example is the three-types of degradation principle, including damage functions for chemical, biological and mechanical deterioration. Martens [141] used such a method to assess the preservation conditions of an indoor environment by linking temperature, relative humidity and an object type to the three-types of object degradation (Figure 2.12). Four types of objects were defined: paper, panel painting, wooden sculpture and furniture. The damage risk assessment for each type of degradation is based on methods described in literature. For example, to assess the risk of mechanical damage for a panel painting, the study of Mecklenburg [144] and Bratasz [145] was used.

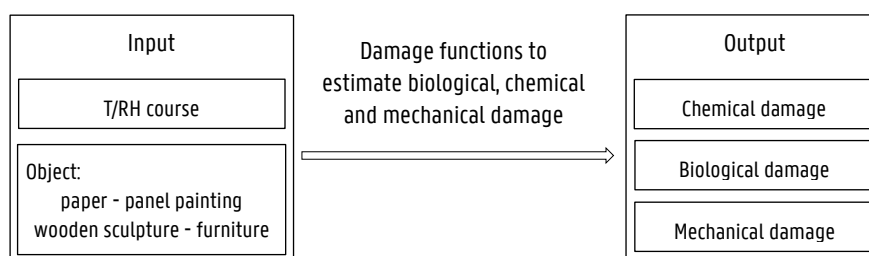


Figure 2.12: Approach developed by Martens [141].

In this work, a similar approach as the approach from Martens [141] is used, meaning that the climate assessment will be made for the three degradation types. In contrast with the work of Martens, the mechanical damage risk will not be estimated by using temperature and relative humidity directly, and linking them to previous defined boundaries. Instead temperature and relative humidity will serve as input for the estimation of the moisture content in the object. To do so, the moisture transport of the work of art will be modelled using a coupled BES-HAM model (Chapter 3).

This approach can itself be used for different kinds of objects. However, to estimate the mechanical damage risk, a proper evaluation of the moisture content of an object is necessary as the moisture content is directly related to shrink and expansion of materials. To calculate the changes in moisture content of the object, material characteristics related to the object are required [56]. Therefore in this work, one type of work of art object was chosen as case study, that is wooden panel paintings, from the 15th -16th century, which are part of the Early-Netherlandish paintings¹³. This type of panel paintings was selected for two reasons. On the one

¹³'Early Netherlandish paintings' refers to a style developed in the 15th and 16th century Northern Renaissance and the painters are known as the so-called 'Primitifs flamands'. During this period, Flanders was the centre of the Northern Renaissance. Next to the many artworks that were made for the Burgundian court, paintings were also made to be hung in churches.

hand, wooden panels are an important category of organic works of art and are representative models of inhomogeneous organic constructions [146]. On the other hand, the Early-Netherlandish panel paintings are very important to preserve, including many famous pieces that are protected by the government. [15].

The three types of damage will be assessed. The focus in this work lies on the mechanical degradation. To have a thorough comparison with the general method, chemical and biological degradation were also measured, either to a limited extent. However, in reality it is up to the user to decide what to take into account and what not.

- Chemical damage risk: 'Lifetime multiplier' [112] and Equivalent lifetime multiplier [147] to assess improvement of the relative lifetime.
- Biological damage risk: Only mould risk is assessed which is mainly related to a too high relative humidity. Other kinds of biological degradation like insects, are not taken into account. In this work, the hygro-thermal model of Sedlbauer is used to assess the mould risk [148]. This model is available through the freeware WUFI-Bio [149] and a theoretical background of this model is described in Annex 2C. The discussion whether which mould model should be used, is outside the scope of this work.
- Mechanical damage risk: Numerical simulation to predict the moisture response of the object (HAM). Although experimental studies of dimensional changes of works of art are also possible and interesting, they are time consuming and expensive and they are not always sufficient [150]. Furthermore, experiments with objects of cultural heritage are often not possible since the objects are unique, and possible damages cannot be accepted. In this study, based on the results of a numerical simulation, mechanical damage and fatigue damage will be assessed.
 - Yield: Related to material characteristics. Object specific research necessary.
 - Fatigue Damage: A similar approach as suggested by Bratasz [136] will be used. The method of 'proofed fluctuation' of Michalski [130] seems less usable for the purposes of this dissertation. This is because in case the proofed fluctuation causes undesirable damage, necessitating a restoration of the work of art, one would like to avoid this fluctuation at all costs. It is thus known that the proofed fluctuation was a too large fluctuation. However, predicting an allowed threshold based on this value, becomes a difficult objective exercise. For this purpose, experiments and results are useful.

The results of both methods will be compared. In case a discrepancy is noticed in the results, the discussion will focus on finding out in which case a more individualized approach (from the second group of methods (§2.2.2)) is required and in which case a more general approach (according to the first group of methods §2.2.1) is sufficient.

3

Predicting Preservation Conditions for Panel Paintings

This chapter studies the assessment of the preservation conditions of a panel painting. A major concern in the conservation of panel paintings is mechanical damage, which is related to the structural movement of the panel painting due to fluctuations in temperature and relative humidity [146].

Because mechanical damage is related to the composition of the panel painting and the material characteristics of each layer, an understanding of the panel composition is needed. Therefore the first section of this chapter describes the structure of the panel painting, how it is related to mechanical damage and how it can be analysed using a numerical simulation.

To perform reliable simulations, material characteristics of panel paintings are required model inputs. The second section describes the measurements performed to obtain the values of the material characteristics that are necessary for the third section, a case study of an Early-Netherlandish panel painting.

3.1 Object Behaviour of Panel Paintings

3.1.1 Panel Painting: Composition & Characteristics

A characteristic feature of panel paintings is their multi-layered structure (Figure 3.1). A typical build-up consists of a wooden support with a glue sizing¹⁴, several ground layers and a number of layers of paint. To protect the paint from dirt, dust and pollution in the environment, the paint layers are covered with varnish [152]. Sometimes the back side of the panel is impregnated with bee wax to retard the rate of moisture transfer to and from the wooden panel [153] and to prevent it from warping.

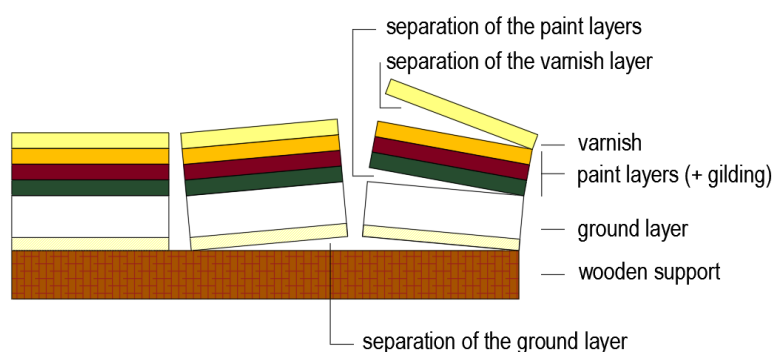


Figure 3.1: Schematic cross-section of a panel painting and types of separation [152].

Because the material layers behave differently, stresses are created between the interface of the material layers: shear stresses arise between the wood fibres and tensile stresses develop perpendicular to the grain in the wood and the coatings on the front [source]. These stresses cause differences in dimensional changes that can weaken the adhesion between the paint layers and/or ground layers and the wooden support. This results in the occurrence of cracks in the paint layers or in paint loss [152,154]. To prevent this from happening, it is necessary to understand how each of the different layers of the panel painting reacts to changes in the environment.

The wooden support

The wooden panel which serves as support [155] usually consists of one piece of wood or of different panels joined with dowels, animal hide glue or cheese glue [80,156]. A wide variety of species are possible, but artists typically used wood from their region. For example, Albrecht Dürer (1471–1528) painted on poplar when he was in Venice and on oak when he was in the

¹⁴ Sizing is the application of a substance, such as hide glue, to a support to reduce the absorbency of the support and to keep the paint from coming in direct contact with the fibres that make up the support. In the past, animal hide glues, such as rabbit-skin glue, were used as substance [151].

Flanders, Netherlands or southern Germany [69,157]. In the 15th and 16th century, in the Southern Netherlands Baltic oak was common for wooden panel paintings [158].

The dimensional changes in wood are due to the hygroscopic and porous character of wood. Being a hygroscopic material, the panel painting adsorbs or desorbs vapour to attain equilibrium with the relative humidity present in the indoor air. This leads to swelling or shrinking. The amount of moisture in the panel at this state of equilibrium is named the equilibrium moisture content. Moisture in wood may exist in two forms, as free water or as bound water [159].

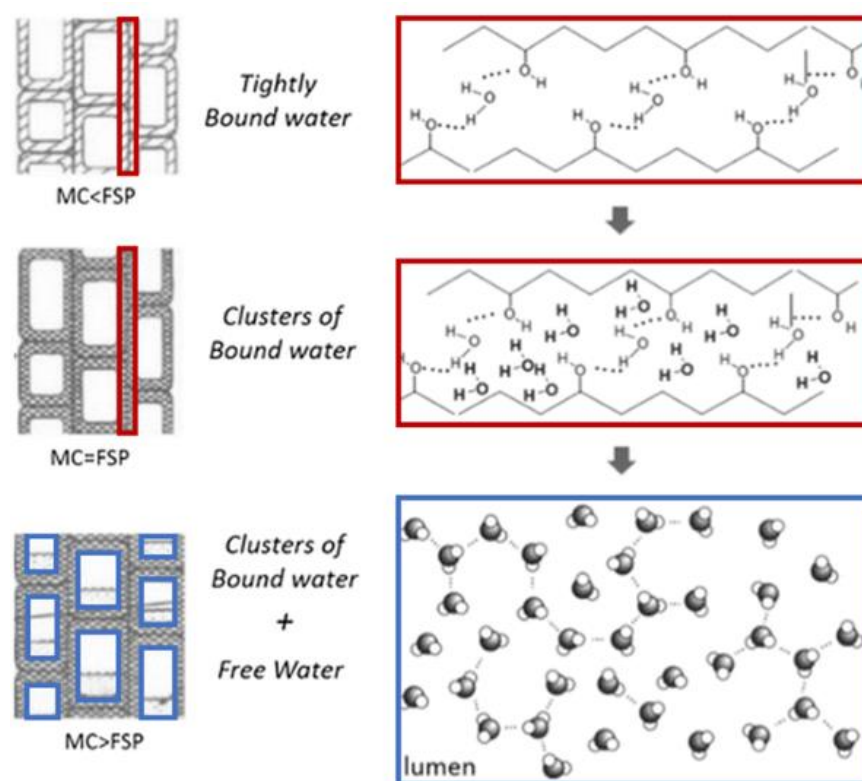


Figure 3.2: The schematic presentation of different states of water present in the cell wall and the lumen, the interactions (hydrogen bonds) between water and the hydroxyl groups of cellulose, and the relaxation time distributions, when a $MC < FSP$, b $MC = FSP$, and c $MC > FSP$ [159].

Each of these forms of water has very different characteristics. Bound water, also called hygroscopic water, is part of the cell wall and affects the physical and mechanical properties of the wood. Free water on the other hand, exists in the cell cavity (lumina) and other capillaries and is therefore also called capillary water (Figure 3.2) [160,161]. Based on these two forms, the wood-water system can be divided into the following states:

1. Absolute dry or oven dry: The wood moisture content is 0%.
2. Below fibre saturation point (FSP)
3. Above fibre saturation point

The fibre saturation point is a theoretical concept, that was first described by Tiemann [162]. Since the fibres have only a limited capacity to hold moisture, above some point liquid water will appear within the wood cells and capillaries [163]. The fibre saturation point indicates the transition between the presence of bound water and the presence of bound water and free water. In the hygroscopic moisture range (i.e. below the FSP) the bound water is present only as vapour in the porous system of wood [164]. The panel paintings in this work are assumed to be in the hygroscopic region (below FSP), where changes in moisture content of wood are related to dimensional changes.

For both the dimensional and mechanical response, wood is highly anisotropic. In other words, the moisture related dimensional changes are different in each of the three primary directions; the longitudinal direction (the direction parallel to the grain of the wood), the radial direction (perpendicular to the concentric rings of wood), and the tangential direction (tangent to the concentric rings in wood). As W. Simpson [165] showed, the relative change in length of wood for each direction is directly proportional to the moisture content. In a study performed by Leenaars J. and Schellen H.[166] the hygric expansion coefficient for Baltic oak is measured. Results are shown in Table 3.1.

On Figure 3.3 the different possibilities of saw-cuts for the planks of the wooden sub-board are shown. Because the dimensional changes due to moisture fluctuations of the environment are the smallest for radially cut wood, this woodcut is preferred for the construction of the wooden sub-board of panel paintings [118,156,167,168].

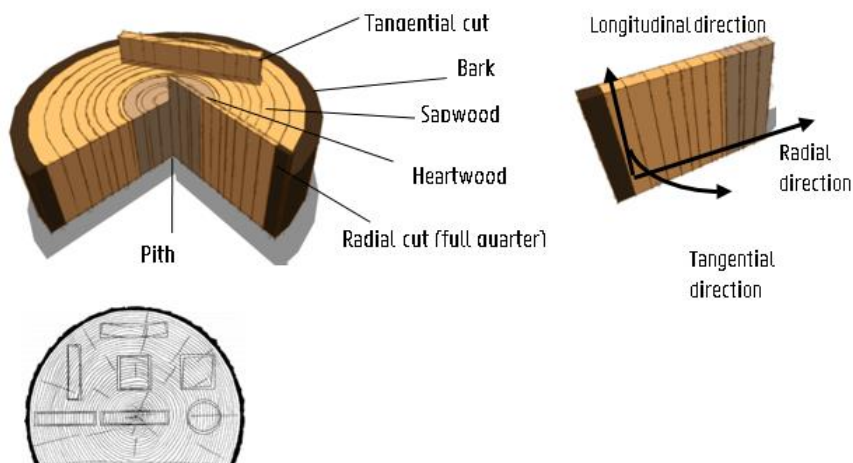


Figure 3.3: (a) Scheme of the transversal section of an oak trunk: the different parts of the tree; the succession of annual growth rings; the different orientations for splitting planks. (b) Characteristic shrinkage and distortion of wooden pieces dependent on the saw cut [167].

Table 3.1: Hygric expansion coefficient for Baltic Oak (often used in Flemish panel paintings) [166].

direction	Hygric expansion coefficient [m ³ /kg]	
	adsorption	desorption
longitudinal	negligible	negligible
radial	0,23	0,27
tangential	0,32	0,26

The applied layers

Because the untreated surface of wood is not ideal for applying the ground and paint layers, a sizing layer of animal glue was typically applied to create a smooth surface and as an aid in binding the ground layer to the wooden support [168]. This is called glue size. After the sizing had dried, the ground layer was applied to the support. The ground layer was usually gesso. This is a mixture consisting of water, a binder and some filler. The most used binder for gesso applied on a Flemish wooden panel was rabbit skin glue and for the filler a chalk was used [168,169]. After the chalky layers were dry, they were sanded and a first draft was drawn on it. Before applying the paint layers, often an invisible priming layer was applied. The principal function of the priming was probably to isolate the ground, preventing it from absorbing medium from the layers of oil paint above and thus causing them to become lean and matt in appearance [155].

3.1.2 Mechanical Degradation of Panel Paintings

Mechanical degradation may result in different sorts of damage. Sometimes deformation of the wooden support is observed, which is called warping. However, most often the outcome of mechanical deterioration is observed on the surface of the panel painting where a network of cracks in the paint develops [170]. Further, also mechanical damage due to the fatigue of a panel painting is discussed.

Warping

As described above, wood is a material that reacts to moisture changes by shrinking when it loses moisture or by swelling when it gains moisture. If wood is painted and varnished, it can show an asymmetric moisture uptake or release due to the lower vapour permeability of the painted face [170,171]. The internal stress induced by the mechanical response will manifest itself by cupping concave to the drier face. As the moisture content becomes uniform across the panel, the panel painting will become flat again, unless the stress has gone beyond the critical level which causes permanent deformation [172,173]. Figure 3.4 shows the asymmetric behaviour of the panel painting while drying, while in hygroscopic equilibrium with the ambient and while wetting [174].

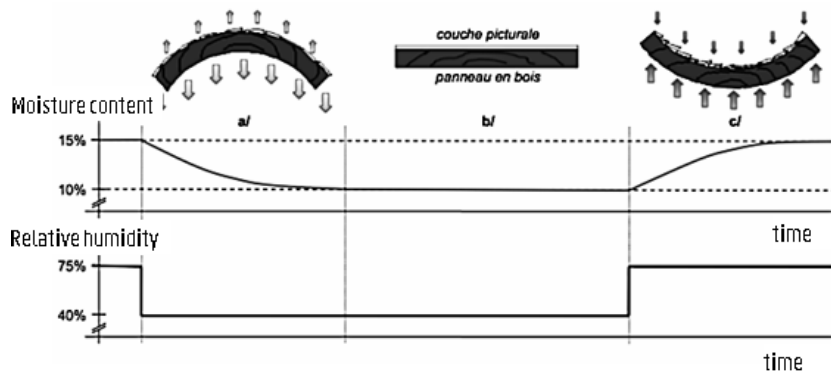


Figure 3.4: Scheme of the asymmetric behaviour of the panel painting while drying (a), while in hygroscopic equilibrium with the ambient (b) and while wetting (c) [174].

Cracking of top layers

Cracking is a consequence of the different material layers reacting differently to changes in ambient temperature and relative humidity. Namely, the material layers do not expand and contract at the same rate. As a result of the developed stresses the material layer breaks [175]. Two kinds of cracks caused by mechanical stresses exist: mechanical cracks and age related cracks¹⁵. While mechanical cracks are caused by temporary external stress, age cracks are due to stresses caused by repeated climate changes such as variations in temperature and relative humidity [168,176].

Because the wood panel is relatively thick compared to the other layers, its response determines the dimensional change, or the lack of it, in the other layers [57]. Contrary to the wood's response, which is anisotropic, the response of the paint layer, ground layer and glue size is isotropic; they swell and shrink equally in all directions [18]. Therefore, one would suspect that the predominant direction of the cracks will be perpendicular to the grain, as shrinkage of wood is larger and therefore more stress will occur in the direction parallel to the grain. Bucklow, however, showed that the cracks may be 'parallel' or 'perpendicular' to the grain and that specific kinds of crackle patterns are correlated to the methods and materials used by the artist [95,96].

To gain a more technical insight in the interaction between the wooden support and the other layers, several studies were performed on the material characteristics aiming to understand the mathematical background of the behaviour. A study in this field, which served and nowadays still serves as a basis for many other studies, is the work of Mecklenburg and Tumosa [144,179,180],

¹⁵ Mechanical cracks or age related cracks may not be confused with premature cracks or varnish cracks. Mechanical cracks and age cracks are caused by mechanical stresses, whereas premature cracks are due to a defective technical execution and varnish cracks are due to oxidation (chemical damage) [176]. Drying cracks usually confine themselves to the layer or layers so stressed and do not, like age cracks, penetrate the entire structure from the support to the surface.

who used a finite element analysis approach to predict the stresses in a painting when subjected to changes in temperature and relative humidity. They found that in the longitudinal dimension (parallel-to-grain) the wood acts as a restraint for the paint layers, ground layers and glue size, because the longitudinal dimension of the wood remains essentially unchanged. In the direction across the grain, however, moisture movement of the wood may override the less responsive layers [144]. This is illustrated in Figure 3.5.

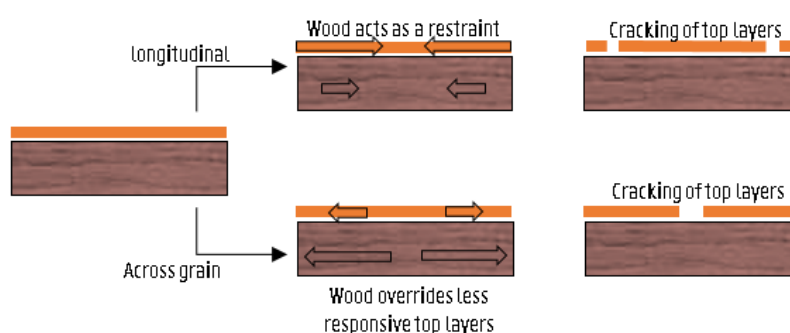


Figure 3.5: Cracking of the top layer(s) caused by temperature and humidity changes. (a) In the longitudinal dimension (parallel-to-grain) the wood acts as a restraint for paint, ground and glue hide, because wood's longitudinal dimension remains essentially unchanged. (b) In the direction across the grain, however, moisture movement of the wood may override the less responsive paint layers [106].

The question now is: "What is the weak link that leads to cracking?". Mecklenburg, Erhardt, Tumosa and McCormick-Goodhart¹⁶ investigated the mechanical characteristics for a whole range of material layers of a panel painting by experiments [71,101,118,119]. In order to study when damage occurs, the dimensional changes of the different material layers, expressed by the moisture coefficient of expansion, were related to strains expected in the panel painting.

Figure 3.6 shows the moisture expansion coefficient related to relative humidity. Between 40 and 60%RH, the differences in swelling coefficients between the wooden panel and the other layers-gesso, hide glue and oil paint - are very low [181]. Outside this zone however, the gesso, wood and hide glue will experience a swelling mismatch [144]. Hide glue, used to join the components, to size the surface prior to the other layers or as an ingredient in gesso, is the most dimensionally responsive to moisture [144,168]. Till 70 %RH, hide glue attempts to swell or shrink at a slightly higher rate than wood in the direction across the grain, which reduces stresses. The glue strengths, however, are quite high and its failure will be extremely rare at room temperatures and at relative humidity levels above 75%. Gesso's response to relative humidity is similar to that of hide glue and oil paint. The difference with hide glue is that the total length change of gesso is considerably less at comparable ranges of relative humidity, and that 80% RH (not 70% RH) seems to mark the point of demarcation between the different swelling rates [168].

¹⁶ Smithsonian Museum Conservation Institute

The selected criterion for the material damage is that strain of the different material layers should not exceed their yield points (i.e., non-recoverable deformation) both in tension (swelling) as in compression (shrinking). The yield point for the different materials was also found by experiments. For paint, a yield point of 0.004 was used as boundary, for gesso a yield point of 0.002 [144]. Using these boundary values, the value for the maximum allowable relative humidity amplitude were calculated according to equation 3.1 by [181]:

$$\Delta\varepsilon = \int_{RH1}^{RH2} \kappa dRH \quad (3.1)$$

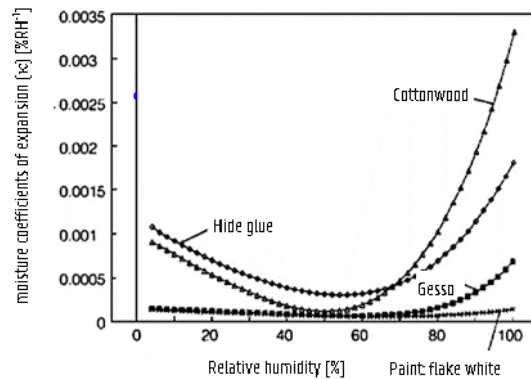


Figure 3.6: A comparison of the moisture coefficients of expansion (κ) for hide glue, gesso and cottonwood. [181].

Based on these results, Mecklenburg et al. [118] stated that the gesso layer of the panel painting limits the allowable fluctuations in the ambient relative humidity. This was confirmed by De Willigen [168] who stated that the ground is the most mechanically vulnerable material and that ground layers are the first to crack and cracking may not penetrate the paint layer until years later.

Grounded on the newly found results of the yield point analyses, Mecklenburg proposed to use the former guidelines for relative humidity boundaries of the Smithsonian as safe zone (37%-53%) and the region between 30% and 37% RH and 53% and 60%RH as cautionary zone [118]. Outside these boundaries, there is a high risk for damage. As shown in Figure 3.7 the generally defined zone in the mid-region almost matches the elastic region of a material.

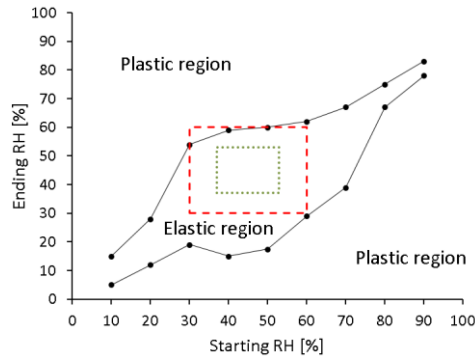


Figure 3.7: Comparison between the elastic region for an oak panel found by experiments and the general defined zones: safety zone (green dotted) and cautionary zone (red striped) [118].

Lukomski [171,182], Rachwal [136] and Bratasz [137] tried to expand the definition of the safe strain level suggested by Mecklenburg, and Tumosa. Lukomski [171,182] and Rachwal [136] measured the strain-cycle (ϵ -N) curve of the gesso layer by subjecting specimens to stretching and compressing at constant amplitudes with a frequency of approximately 0.3Hz. The relative humidity remained constant at 50%RH while strain was varied between 0.15% and 0.5%. Using the moisture expansion coefficient of the gesso and the swelling isotherm of the wood, the relationship found between on one hand the strain causing damage in the design layer and the corresponding amplitude of the relative humidity variation the number of cycles is illustrated in Figure 3.8. It can be noticed that the earlier defined yield point of 0.002 was in case off an average relative humidity of 50% equivalent to an amplitude of 6%RH and equals a lifetime of 100 years.

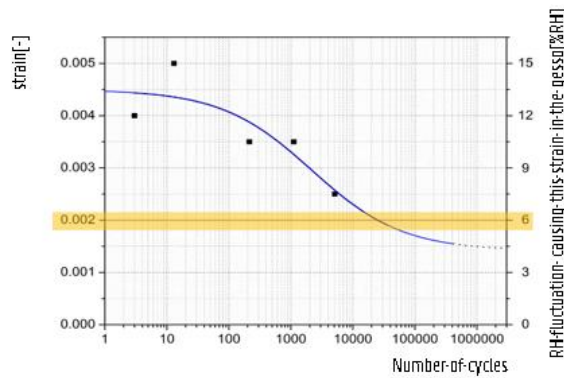


Figure 3.8: Strain, and corresponding amplitude of RH variation, leading to fracture in gesso versus number of cycles to cause fracture at that strain [171].

Using the results of the tests in gesso coated wood in combination with the expansion related to the moisture content in wood, Lukomski [171,182] determined by using numerical simulations the most critical cycle duration and the acceptable relative humidity amplitude for a given panel thickness to avoid initiation of fracture to the gesso layer within a time span of 100 years cycle exposure. Results of the maximum allowable amplitude and the cycle duration for a certain thickness are given in Table 3.2 and Figure 3.9. Figure 3.9 shows the relationships between the allowable amplitude of a RH cycle and the cycle duration for panel thicknesses of 10 mm and for the moisture flow through one or both faces. The panel responds less and less significantly when the duration of the fluctuations decreases, which is expressed in an increase of the allowable amplitude of the fluctuations. Table 3.2 tabulates the most critical allowable amplitude for a given cycle and thickness of unrestrained single panels coated with a 0.5 mm thick gesso layer, and free moisture flow through both faces. Notice that for 10mm thick panels a sinusoidal relative humidity cycle with an amplitude of 15%RH and duration of 14 days represents the most critical duration, whereas for 30mm thick panels a cycle with an amplitude of 13%RH and a duration of 90 days is the most critical. It is important to mention that the experiments were conducted under a constant relative humidity of 50%RH.

Table 3.2: Most critical allowable amplitude for a given cycle and thickness of unrestrained, single panels coated with a 0.5 mm thick gesso layer, and free moisture flow through both faces [171,182].

Panel thickness [mm]	Allowable amplitude [%]	Cycle duration [day]
2	15.26	3
5	15.31	7
10	14.87	14
30	13.19	90
40	13.41	365 ^a

^a40 mm thick panel does not fully respond to a sinusoidal RH variation with period of 365 days.

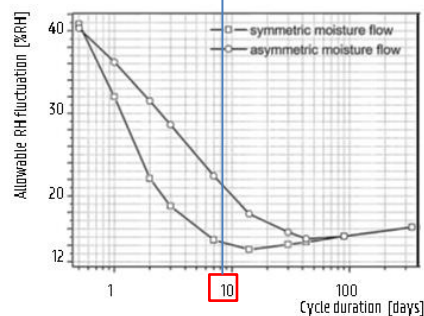


Figure 3.9: Relationships between the allowable amplitude of an RH cycle and the cycle duration for panel thicknesses of 10 mm and the moisture flow through one or both faces.

Using the stress-strain cycle (Figure 3.8) on real situations, Bratasz et al. [137,183] applied the popular rain flow counting method [128] and the Palmgren-Miner linear damage hypothesis to calculate a climatological damage risk index for panel paintings [184]. To measure the effect of repeated cycles for painted wood he induced a risk index 'C', instead of the risk index 'D', defined as:

$$C = \frac{1}{a} \left(\sum_{i=1}^k \frac{n_i}{N_i} + \sum_{j=1}^l n_j \frac{A_j}{A_0} \right) \quad (3.2)$$

Where: k number of RH ranges smaller than $A_0 = 12\%$ RH (a threshold range for fracture of the design layer in a single cycle) - each contributing n_i cycles and N_i being number of cycles to failure for a given RH range;
 j number of RH ranges greater than $A_0 = 12\%$ RH - each contributing n_j cycles of range A_j
 a number of years over which the RH cycles are counted

3.1.3 Estimating Risk of Mechanical Damage for Panel Paintings by Modelling Moisture Transport

Simulations as an Analysis Tool

In the previous section it was explained how cracking of the top layers and warping of the panel occur. To estimate the effect of the simulated or measured climate on panel paintings, the hygrothermal response of the wooden panel is modelled. A simulation study for the hygrothermal response of the wooden panel is useful to complement empirical and experience-based knowledge of mechanical damage of an object of cultural heritage.

To estimate the time-dependent object based moisture-originated deterioration process, Carmeliet [185] describes two modelling options that could also be used to analyse the deterioration of a work of art. One option is to directly model the moisture-originated damage process. For instance, in Poland and in France models are used [58,172,186,187] which calculate the stress related to the dimensional response caused by changing boundary conditions in a wooden panel. The yield point, indicating plastic deformation and fracture, is used as damage criterion. Since it is difficult to explicitly model the time-dependent deterioration, the second option is that the analysis is limited to modelling the hygro-thermal response by a Heat, Air and Moisture (HAM) model. This type of model calculates the coupled heat and mass transfer and predicts the local moisture content in the object. The calculated moisture response is then compared with a pre-defined critical level [185]. This is the approach used in this work since the modelling of the time-dependent dimensional response of panel paintings is going too far for the scope in this work.

Moisture Transport in Panel Paintings

Vapour transport inside the panel painting

For a panel painting consisting of radial-sawn cut wood, the moisture transport within the range of hygroscopic moisture, is mostly treated as a mass diffusion process in one dimension perpendicular to the painted surface [172,186,188,189]. As a result, the transient moisture transport in the material can be mathematically described by the law of mass transfer, also called Fick's second law, which expresses the relation between the vapour flux and the concentration gradient responsible for this mass transfer [190]. In most research in the field of wood science, the driving force is the moisture content in the wood c [kg/m³], resulting in eq.(3.3). In the field of building simulation however, it is common practice to use the vapour pressure p_v [Pa] as driving force, resulting in eq.(3.4).

$$\frac{\partial c}{\partial t} = \frac{\partial}{\partial x} \left(D_c(c, T) \frac{\partial c}{\partial x} \right) \text{ for } 0 < x < d \quad (3.3)$$

Where: $\partial c / \partial x$ the space gradient of the moisture content
 $\partial c / \partial t$ the time gradient, which equals the space gradient of the moisture flux $\partial g_v / \partial x$.
 D_c the diffusion coefficient [m²/s].

$$\frac{\partial C}{\partial \phi} \frac{\partial p_v}{\partial t} = \frac{\partial}{\partial x} \left(\delta \frac{\partial p_v}{\partial x} \right) \quad (3.4)$$

Where: $p_{v,sat}$ saturated vapour pressure at temperature T[°C],
 $\frac{\partial C}{\partial \phi}$ derivative of the sorption isotherm and expresses the moisture capacity ξ [kg/m³].
 δ Vapour permeability, equal to $\frac{D_c}{\frac{\partial C}{\partial \phi} \cdot p_{v,sat}}$.

For solving this equation two material properties are needed: the vapour permeability of the different panel painting materials and the moisture sorption isotherm of the material which expresses the moisture content at position x within the material.

Vapour transport between the panel painting and the environment

While the diffusion process governs the moisture transfer inside the painted panel, the mass transfer between the surface of the painted panel and the moving air is called external moisture transport or convective mass transfer. In models using the moisture content of wood as driving potential, the external mass transfer between the specimen and the environment is expressed by a so-called "surface emission coefficient h_c [m/s]" (e.g.[187–189,191–193]) relating the moisture content at the wooden surface [kg/m³] to C_e the moisture content in wood in equilibrium with the air [kg/m³] (eq.(3.5)). For models using vapour pressure as driving potential, the external mass transfer is expressed by a mass transfer coefficient h_p [kg/(Pa.m².s)], relating the vapour pressure at the wooden surface [Pa] to the vapour pressure in the air [kg/m³] (eq. (3.6)).

$$g = h_c \cdot (C_{surf} - c_e) \quad (3.5)$$

Where: C_{surf} the moisture content at the surface [kg/m³]
 c_e the moisture content in wood in equilibrium with the air [kg/m³].

For models using a material independent driving potential, like vapour pressure, the external mass transfer is expressed by a vapour mass transfer coefficient h_p [kg/(Pa.m².s)].

$$g = h_p \cdot (p_{v,surf} - p_{v,e}) \quad (3.6)$$

Where: $p_{v,surf}$ the vapour pressure at the surface [Pa]
 $p_{v,e}$ the vapour pressure of the air [Pa].

Hygric material characteristics necessary to model vapour transport

Moisture content

The moisture content is a function of the relative humidity and can be derived from the sorption isotherm. This is a mathematical expression for the equilibrium moisture content in the material as a function of the relative humidity. Most often, the moisture content is determined for different levels of relative humidity at constant temperature by measuring the weight of a sample with a balance when equilibrium is reached. This method is called the gravimetric method [194]. For organic materials, Brunauer et al. [195] classified the sorption isotherms into five different types according to the shape of the curve. The type II sorption isotherm, a sigmoidal shaped curve, is typical for wood [196]. Coatings (polymers) show a widely varying appearance of sorption isotherms [197]: linear, type II and type III.

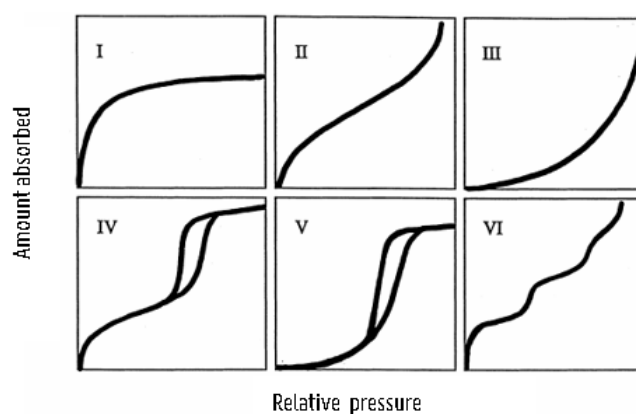


Figure 3.10: Types of sorption isotherms [196,198].

Afterwards a moisture sorption isotherm is fitted to the measured results. Different mathematical models have been proposed for describing this sorption isotherm. They can be divided into three categories: theoretical, empirical and semi-empirical models [199]. Two theoretical models are frequently used in wood science: the Hailwood and Horrobin-model and the Guggenheim Anderson and Boer-Dent (GAB) model [200]. Numerous studies are presented in literature in which sorption isotherms of wood have been reported. In this work, results for oak are presented, as oak was a typical material for the support of Early-Netherlandish wooden panel paintings from the 15th-16th century (Figure 3.11). The results found in the literature will be used to compare with own measurements to see whether realistic results were obtained. In the field of building physics, the empirical equation given by Hansen [201] is often used for building materials, including wood. Carmeliet [202], Hansen [203] and Leenaars [166] used the empirical equation to model the sorption isotherm for oak. Bratasz et al. [204] used earlier measurements performed by Grosser et al. [205,206] to model the sorption curve by the GAB-method for 21 wood species, including oak, which were used for panel paintings and woodcarving.

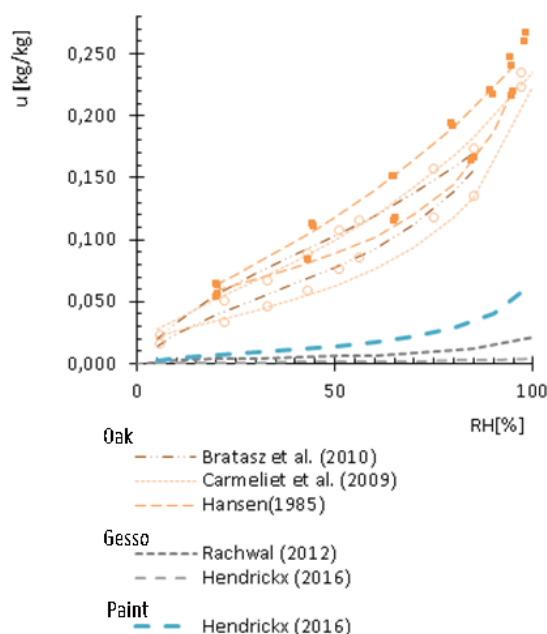


Figure 3.11: Sorption isotherm for oak (orange), gesso (grey) and paint (blue).

Diffusion coefficient and vapour permeability

The issue of the determination of moisture diffusion coefficients in wood is widely discussed in the literature [207]. Two methods are commonly used to evaluate the diffusion coefficient D_c or the vapour permeability δ . The first method determines D_c or δ based on a steady-state diffusion process, also called the cup method. The principle of the test is to create a constant moisture flux g [$\text{kg}/(\text{m}^2 \cdot \text{s})$] through a sample by imposing a different but constant moisture concentration (usually expressed as vapour pressure) in the air at each side of the sample. The second experimental method determines the coefficient by a 'non-steady state' method. This situation is obtained by exposing the samples to a stepwise humidity change in the environment, as done in the experiments performed to measure the sorption curves. To obtain the diffusion coefficient or vapour permeability, the partial derivative equation of Fick's second law Eqs. (eq.3.3) must be solved. The calculated value is then referred to as 'apparent'.

In comparison to the wooden support, the top layers are very thin and the amount of moisture added by paint, varnish and wax is very small [194,203,208]. This is illustrated in Figure 3.11, in which the comparison of the different sorption isotherms for oak, for gesso and for paint are shown. A recent study of Boon et al. [208] in which the water uptake in painting canvases and preparation layers was studied using neutron radiography, confirmed the low moisture uptake by the chalk-glue ground. For this reason, moisture sorption in the top layers is usually neglected. This implies that their presence is expressed as a reduced external moisture transport to the

environment and not as a separate material layer on the wooden support. The reduced external moisture transport is taken into account by adding an extra term S_d to the original mass transfer coefficient h_p . The S_d -value represents the thickness of an air layer with the same vapour resistance as the coating.

$$h_{p, \text{restr}} = \frac{1}{\frac{1}{h_p} + \frac{S_d}{\delta_a(T)}} \quad (3.7)$$

Where: h_p the original convective vapour mass transfer coefficient [kg/(Pa.m².s)],
 $h_{p, \text{restr}}$ the convective vapour mass transfer coefficient taken into account the diffusion resistance of the coating [kg/(Pa.m².s)],
 δ_a the vapour permeability of air calculated by the equation of Schirmer [kg/(Pa.m.s)].
 S_d -value the thickness of an air layer with the same vapour resistance as the coating [m].

Rachwal et al. [136] measured the vapour resistance of the ground layer (gesso) and found no measurable barrier effect. Hendrickx et al.[209] found a very low resistance for gesso (Table 3.3). Although early research on paint films [210,211] exists, specific data for panel paintings and the different material layers is rare. Two recent works which tie in closely with panel paintings are these of Ruus et al.[212] and Hendrickx et al.[209]. Ruus et al.[212] examined the water vapour permeability of some natural paints using the cup method. Linseed oil paint and egg tempera approximate the paint used for panel paintings. Hendrickx et al.[209] investigated the permeability of canvas paintings¹⁷ and their components, among which oil paint, using the cup method. Results obtained by both authors are listed in Table 3.3. Allegretti [213] measured the mass transfer coefficient of wood covered with varnishes and resins commonly used for the restoration of panel paintings. As discussed further in the section 'Testing method', these values cannot be used in the current case and are therefore not presented in this section.

Table 3.3: S_d-values [m] found for similar materials in literature measured by the cup method.

Author	Material	S _d [m]
Ruus, 2001 [212]	linseed oil paint	0.21-0.25
	egg tempera	0.04-0.06
Hendricxk, 2016 [209]	gesso dry cup	0.02
	gesso wet cup	0.00
	paint dry cup	0.25
	paint wet cup	0.11

¹⁷ The building-up of the canvas painting was typical for the early work of the Swiss painter Cuno Amiet (1868–1961).

3.2 Evaluation of the Diffusion coefficient and Sorption Isotherm of the Different Layers of Early-Netherlandish Wooden Panel Paintings

3.2.1 Practical Implications

In this work, moisture transport in the work of art is modelled in relation to a (simulated) indoor climate. A HAM-model which uses vapour pressure as driving potential is more appropriate for this than a model that uses the material's moisture content. The reason is that vapour pressure as driving potential is material independent and moisture content of wood is not. As a consequence, it is easier to apply the HAM model to multi-layered objects. Additionally, the coupling of a HAM model with other simulation models, such as BES-models (and CFD-models¹⁸), is more straightforward if one unique driving potential is used in both tools.

Up till now, studies on moisture transport and moisture induced damage in panel paintings are mainly based on wood mechanics using the moisture content in wood as driving potential. When using the material properties found in the literature, which are derived based on the moisture content in wood, some difficulties arise.

Firstly, as a consequence of using moisture concentration in wood as driving potential, the diffusion coefficient D_c is measured and not the vapour permeability δ . To convert the diffusion coefficient D_c to the vapour permeability δ , the vapour saturation pressure, the density of the material (to convert kg/kg to kg/m³) and the moisture capacity $\partial c / \partial \varphi$ are required. The last value can be derived in case the sorption isotherm is provided. However, even if all these parameters are known, the question arises at which relative humidity this moisture capacity has to be derived.

Secondly, the presence of a vapour resistance such as paint and varnish is expressed as an additional surface resistance for external mass transfer. In literature, several values of reduced mass transfer coefficient values are presented. However, the quantity h_c often used in wood science, for example by Allegretti and Raffaell [213], is not useful. A first comment is that ' $c_{e,wood}$ ' is not physically correct [214,215]. Though several authors suggested a conversion method [216,217], too few parameters are known to convert values presented in literature to a reduced external mass coefficient $h_{p,restricted}$ based on a vapour pressure potential.

Therefore, the main goal of the performed experiments in this work is to measure the sorption isotherm and the vapour barrier effect of some common finishing layers of an early Netherlandish panel painting of the 15th and 16th century which can be used in a HAM model with vapour pressure as driving potential.

¹⁸ This is not part of this work, but from a in a previous FWO-project (FWO G.0420.05) by H.-J. Steeman [41,42].

3.2.2 Materials and Measurement Methods

Sample build-up

In this study, 80 samples were prepared by Marie Postec and Etienne Costa from KIK-IRPA¹⁹. They are experienced restaurateurs who participated in the restoration of different historical panel paintings. The samples were prepared following the historic artistic techniques applied in restoration projects of Early-Netherlandish panel paintings. Figure 3.12 depicts the samples and the way they have been composed.

Two types of wood support were used for the samples. The first wooden support was made of radially sawn oak board. This type of wood was selected because oak was a common support of panel paintings in Flanders and the Netherlands and radially sawn boards were generally used for panel paintings as they were the most stable [155,158]. However, because oak has a high vapour resistance, it was also decided to make the same samples with particle board as support, to obtain an independent set of results for the diffusion resistance of the top layers. The samples measured ± 120 mm (tangential and longitudinal) x ± 10 mm (radial). The last dimension corresponds to the thickness of the sample.



Figure 3.12: The building-up of the samples, representing old panel paintings.

The ground layer was made of one layer of animal glue and four layers of gesso, a mixture of animal glue and ground chalk. The animal glue consisted of water mixed in a ratio of 8g of glue to 100g of water. For the paint layer, two different oil paints were used (referred to as green and red paint). The stratigraphy of the paint layers was similar to that of a painting of the 15th -16th century. Because the pictorial layer of a Flemish painting has no uniform thickness over the painting surface, three layers were applied on the samples, representing an average between the thinner and the thicker paint layers. These are:

¹⁹ The KIK-IRPA is a federal scientific institute responsible for the documentation, study and conservation-restoration of the cultural and artistic heritage of our country (www.kikirpa.be)

For the red oil paint layers:

- one sublayer consisting of vermilion pigment (Kremer) and flake white pigment (Old Holland) with boiled linseed oil as binder
- two layers consisting of orange madder pigment (Kremer) ground in boiled linseed oil and resin (10%)

For the green paint layers:

- one sublayer consisting of verdigris, lead-tin yellow (Kremer) and flake white pigment (Old Holland) in boiled linseed oil as binder
- two layers of verdigris ground in boiled linseed oil and resin (10%). The pigment was made by first treating copper sheets with vapours of vinegar and afterwards scraping the corroded crust.

Before the paint was put on the ground layer, a priming layer of line seed oil was applied. On top of the paint layers, two layers of varnish were applied. The varnish was a Damar varnish with white spirit as thinner (20%). It is a more recently used varnish and different from the historically used varnishes, which were based on oil. However, a more recent type of varnish is more representative because the original varnish layer is usually removed due to restoration effort. A wax layer was put on the back of the panel painting and was made of a mixture of beeswax, paraffin (ratio of 1:2) and mineral turpentine, commonly used in the field of restoration for the protection of wood.

To allow defining the moisture properties of each layer, the samples were built up gradually; five samples only consist of a wooden support, five samples consist of a wooden support and one face coated with gesso layer Table 3.4. The moisture properties from multi-layered samples were measured, and not from each layer separately to account for the interaction between the wood support and the layers [218]. Because the top layers are expected to reduce the amount of vapour sorption of the wood [197,219], it would not be correct to measure the sorption of each material layer separately and add them together. Hulden and Hansen [210] reported several additional reasons for measuring an inaccurate permeability when measuring each material layer separately. They state that the effective thickness of the wooden panel will be less because some of the coatings may penetrate in the wood pores. This will cause the interface between the coating and the wood to be larger than its geometrical surface, thus influencing the moisture flux and thereby the results.

Table 3.4: Composition of the wooden samples.

wooden support	gesso	paint layer	varnish	wax
particle board (5)/oak(5)				
particle board (5)/oak(5)	x			
particle board (5)/oak(5)		green		
particle board (5)/oak(5)		red		
particle board (5)/oak(5)		green	x	
particle board (5)/oak(5)		red	x	
particle board (5)/oak(5)		green	x	x
particle board (5)/oak(5)		red	x	x

Testing method

Dry density

The oven-dry density ρ_0 of the samples was determined in accordance with the standard EN ISO 12570:2000 [220]. Oven drying was used instead of desiccant drying because according to Feng et al. [221] the desiccant drying method takes a very long time. For the samples only consisting of oak or particle board the drying temperature in the oven was 70°C. The other samples were dried at 40°C. The samples were dried until the weight change was less than 0.1% of the total mass in 3 days. The measurement error on the dimensions of the samples was $\pm 0.05\text{mm}$ for the length and width, $\pm 0.005\text{mm}$ for the thickness and $\pm 0.1\text{g}$ for weight.

Sorption isotherm

The isothermal adsorption and desorption curve was determined according to the European standard EN ISO 12571:2000 [222]. The moisture content was determined for different relative humidity levels and at a constant temperature of 23° C until constant mass was reached. The constant temperature and relative humidity were created in a climate chamber which is capable of maintaining the temperature within a 0.5° C and the relative humidity within a 3% RH interval. Once the samples were at equilibrium, the relative humidity in the climate chamber was rapidly changed to a new relative humidity. Two measurement series were performed. In the first set-up, first the relative humidity increased up to 93% (adsorption). Afterwards the relative humidity decreased to 50% (desorption). The second set-up was performed to minimize the experimental error on the sorption isotherm.

First set-up:

- from 50% to 60% RH
- from 60% to 93% RH
- from 93% to 85% RH
- from 85% to 50% RH

Second set-up:

- from oven dry (6 %) to 37% RH
- from 37% to 79% RH
- from 79% to 93% RH

The sorption isotherms were fitted using a three-parameter equation model, in which the three constants A_{HH} , B_{HH} and C_{HH} were calculated using the experimental data. After transforming the data points by dividing the moisture content by the relative humidity, the quadratic curve was obtained by minimizing the least square error. The adsorption curve was fitted through five points: 37%, 50%, 60% and 79% and 93%.

$$C(\varphi) = \frac{\varphi}{A_H + B_H\varphi - C_H\varphi^2} \quad (3.8)$$

Moisture Diffusion

Apparent vapour permeability of the wooden panels

First, the vapour permeability for wood was determined from the consecutive mass measurements which were performed to define the moisture content at a certain relative humidity and not from the cup method. This so-called unsteady sorption method is favoured because the same measurement can be used to determine the moisture content at a certain relative humidity as well as the vapour permeability. This makes the measurement campaign less time-consuming. Moreover, the sorption method often has lower experimental error [223,224]. Two methods to determine the apparent vapour permeability of wood were used and compared: a traditional analytical method and a so-called inverse approach. For both methods, test data of isothermal moisture adsorption and desorption experiments were used.

The first method is the analytical method described by Crank [225]. Using the moisture content in wood as driving potential, the global diffusion coefficient D_c was estimated. Therefore, he proposed a general solution for a plane sheet with uniform initial moisture distribution and a constant diffusion coefficient by using the analytical technique of separation of variables. The solution of the transient form of Fick's second law (eq.(3.9)) for a plane sheet with uniform initial moisture distribution and a constant diffusion coefficient solved by using the analytical technique of separation of variables is:

$$D_{c,app} = \frac{\pi}{4} \left(\frac{d\overline{E}(t)}{d\sqrt{\left(\frac{t}{l^2}\right)}} \right)^2 \quad (3.9)$$

Where: $\overline{E}(t)$ fractional weight change of the whole sample, calculated by

$$\overline{E}(t) = \frac{m(t) - m_0}{m_\infty - m_0}$$

 l half the thickness of the sheet [m]
 m_0 initial weight in the sheet [kg]
 m_∞ final uniform weight in equilibrium state [kg]
 $m(t)$ weight of the sample at time t [s].

The diffusion coefficient $D_{c,app}$ was calculated by plotting the results of the normalized mass change $\overline{E}(t)$ against $\sqrt{\left(\frac{t}{l^2}\right)}$. The slope of this curve was calculated by linear regression. Afterwards the diffusion coefficient $D_{c,app}$ was converted to the vapour permeability δ by the coefficient $\frac{p_{sat}}{\frac{\partial c}{\partial \varphi}}$.

The second method is numerically and makes use of a 1D-HAM model. In the inverse method the diffusion process during the sorption experiment is calculated, in this case using the finite element method, and afterwards compared with the measurements. By using an iteration procedure, the most feasible solution for the vapour permeability can be found. Olek and Weres [192] extended the inverse method by assuming a linear or exponential relation between the moisture content and the diffusion coefficient. The vapour permeability was determined by

finding the best fit between the calculated diffusion process and the measurements. To do so, the least square difference between the slope of the measured and calculated normalized mass change against time was determined for all measuring points at time t (s) by:

$$\varepsilon = \sqrt{\sum_{i=1}^n \left[\left(\frac{d\overline{E}(t)}{d\sqrt{\left(\frac{t}{\tau^2}\right)}} \right)_{n,\text{measured}} - \left(\frac{d\overline{E}(t)}{d\sqrt{\left(\frac{t}{\tau^2}\right)}} \right)_{n,\text{calculated}} \right]^2} \quad (3.10)$$

The moisture transport in the material itself was calculated by a slightly adapted 1D-HAM calculation based on a code developed by Steeman [226] using the following discretisation scheme:

$$\begin{aligned} \left(\rho_m \xi_{\varphi}^{t+\Delta t} \frac{\left(\frac{P_v}{P_{\text{sat}_i}} \right)^{t,m} - \left(\frac{P_v}{P_{\text{sat}_i}} \right)^{t,m-1}}{\Delta t} + \frac{c_i^{t,m} - c_i^{t-+\Delta t}}{\Delta t} \right) \Delta x_P \\ = \frac{p_{v,E}^{t,m}}{Z_{PE}} - \left(\frac{1}{Z_{PE}} + \frac{1}{Z_{WP}} \right) p_{v,P}^{t,m} + \frac{p_{v,W}^{t,m}}{Z_{WP}} \end{aligned} \quad (3.11)$$

Where: P, W, E spatial indexes and refer to the central node (P), the node to the left (W) and the node to the right (E).
 Δx_{ew} equals the length of the discretization cell.
 Z the vapour resistance between the two referred nodes.
 Δt timestep

In case of internal diffusive flow, Z_{PE} is calculated by $\frac{\Delta x_P/2}{\delta_P} + \frac{\Delta x_E/2}{\delta_E}$. If P refers to the first or to the last node, an extra term is added to the vapour resistance to account for the external mass transfer between the surface of the object and the indoor air. In that case Z_{PE} is calculated by $\frac{\Delta x_P/2}{\delta_P} + \frac{1}{h_p}$. The superscripts m and t refer to previous and current iteration step and the time step.

S_d value for the other layers (gesso, paint, varnish and wax)

Once the vapour permeability of all the wooden samples had been determined, the barrier effect of the top layers was calculated. Since the build-up of the samples was not symmetric, and since the analytical solution becomes too complicated [225], only the inverse method was used. Using the vapour permeability of the wooden panel, the S_d value for the other layers (gesso, paint, varnish and wax) was estimated by finding the best fit for a fixed δ -value and a variable mass transfer coefficient $h_{p,\text{restricted}}$ calculated by eq. (3.7).

Results

Dry density

Figure 3.13 displays the dry density of all the samples. The dry density of the oak panels varied between 595.3 ± 0.4 and 703.5 ± 0.5 kg/m³. For particle board, the dry density varied between 653.0 ± 0.5 and 717.6 ± 0.5 kg/m³. Samples with a density that diverged more than twice the standard deviation (outside error bars) were excluded from the sorption and diffusion measurement.

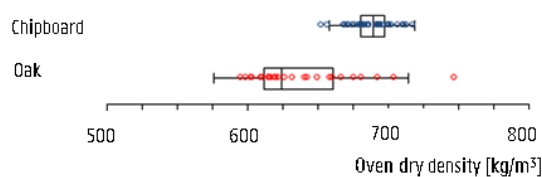


Figure 3.13: Dry density of the samples.

Sorption isotherms

Adsorption isotherms obtained from the samples of oak and particle board are shown in Figure 3.14. Each result (point in graph) represents the average value of minimum 3 and maximum 5 samples. The averaged coefficients for the Hailwood and Horrobin-sorption curve are presented in Table 3.5.

Taking into account the measurements, no effect on the moisture sorption could be noticed for both types of wooden supports if they were covered with gesso. Consequently, the gesso layer has no effect on the moisture content of the samples. In case the samples were covered with paint or with paint and varnish, a reduction in the adsorption curve was observed. In case the back of the samples was impregnated with wax, a further reduction was observed. According to Van Meel [218], the reduced sorption can be ascribed to the clogging of part of the pits near the surface.

Table 3.5: Coefficients for the HH-sorption curve for the different types of samples [kg/m³] and the standard error of the estimate.

Adsorption	A _{HH}	B _{HH}	C _{HH}	Standard Error of the estimate [kg/m ³]	Goodness of fit R ²
Oak	-0.0293	0.0352	0.0000	3.70	0.990
+paint / varnish	-0.0437	0.0482	0.0001	3.33	0.992
+wax	-0.0554	0.0591	0.0001	5.61	0.978
Particle board	-0.0406	0.0460	0.0000	2.64	0.994
+paint / varnish	-0.0452	0.0506	0.0001	1.84	0.997
+wax	-0.0622	0.0666	-0.0003	4.10	0.984

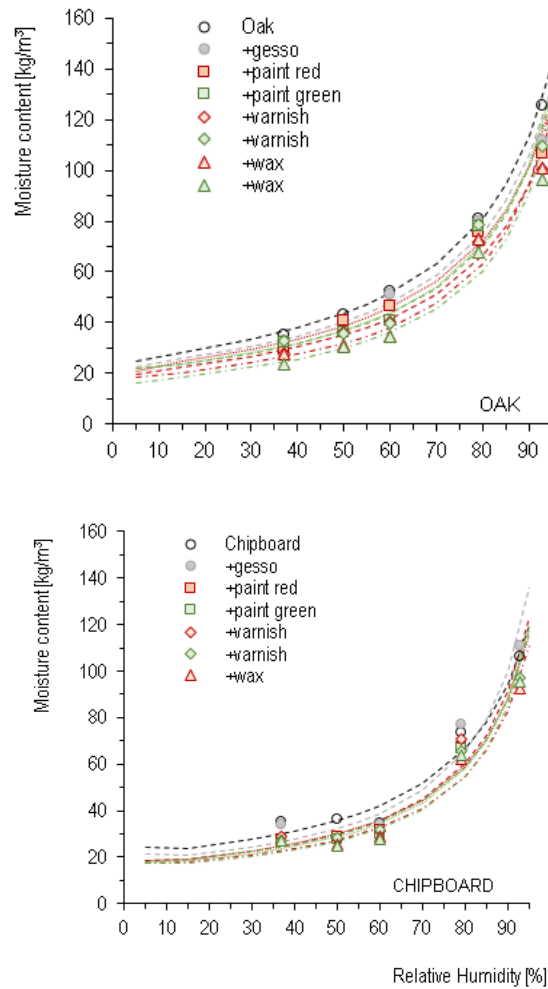


Figure 3.14: Adsorption isotherm of oak, particle board and of its different compositions (Symbols: Measurements - Lines: Theoretical sorption curves).

Moisture diffusion

The vapour permeability during adsorption and desorption was only determined for the measurement from 37% to 79%RH, from 60% to 93%RH and from 85% to 50%RH. This was due to experimental limitations:

- On the normalized sorption from 50% to 60% RH and from 93% to 85%RH the relative error became too large. This large error was due to the small differences in mass change between the first and last measurement (m_{∞} and m_0).
- For the measurement from oven dry (6%RH) to 37% RH the moisture capacity, dependent on the relative humidity, varied too much to obtain reliable results. This is illustrated in Figure 3.15.

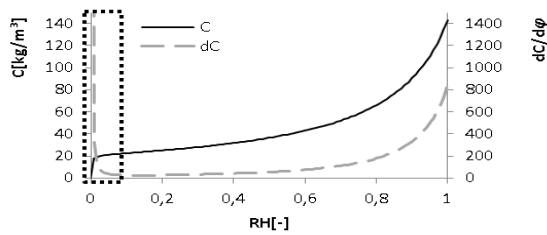


Figure 3.15: Sorption and moisture capacity of particle board.

To convert the value D_c to δ , the conversion factor $\partial C / \partial \phi$ has to be known. Therefore, the relative humidity at half sorption time was used ($E= 0.5$). Results are displayed on Table 3.6. The results found by the equation of Crank were close to the values derived by the inverse method, except for the range 60-93%.

Table 3.6: Comparison of the value for the vapour permeability [$kg/(m.s.Pa)$] of particle board and oak calculated by the formula of Crank and by the inverse method.

		by Crank	RH for conversion from D_c to δ	by inverse method	RH for conversion from δ to calculated D_c
Particle board	37 - 79% RH	$2.0 E^{-12}$	67	$2.7E^{-12}$	73
	60 - 93% RH ¹	$2.4 E^{-12}$	79	$4.2 E^{-12}$	88
	85 - 50% RH	$3.0 E^{-12}$	72	$2.9 E^{-12}$	71
Oak	37 - 79% RH	$1.2 E^{-12}$	67	$1.5 E^{-12}$ ²	71
	60 - 93% RH	$3.8 E^{-12}$	85	$1.5 E^{-11}$	92
	85 - 50% RH	$1.4 E^{-12}$	73	$1.6 E^{-12}$	76

¹ Gives incorrect result when reproducing the sorption process from 60 to 93%RH, due to the late measurement (first point at \sqrt{t}/l^2).

² Measurement not reliable because equilibrium was not reached and too many points were known at the first half of the sorption isotherm.

To calculate the S_d -value for the coatings, the asymmetric panel was simulated. Figure 3.16a shows an example of the best fit found between the slope of the measured and calculated normalized mass change against time. Each point equals a certain asymmetric moisture distribution in the panel (Figure 3.16b).

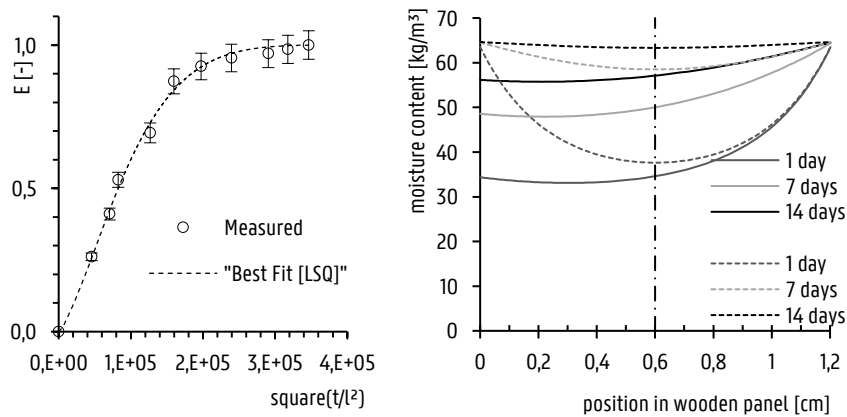


Figure 3.16: (a) best fit and measured values for the normalized mass change against time. (b) Asymmetric moisture content in the wooden panel found for the best fit. (in dotted lines the symmetric profile (only a wooden panel)).

The S_d -value $[\text{m}]$ for each different layer is presented in Table 3.7. In line with the findings from research by Rachwal et al. [136] and Froidevaux [189] no measurable barrier effect of the gesso layer was observed. When comparing the samples covered with paint layers to the wooden supports only covered with a gesso layer, a clear resistance against water vapour transfer was observed. No significant difference was found between the two paints. For the varnish layer, no measurable vapour resistance was detected compared to the samples covered with a gesso and a paint layer. Therefore, in Table 3.7, the S_d -value for the paint and varnish are presented as one and not for varnish as a separate layer.

Table 3.7: S_d -values $[\text{m}]$ for each layer found by numerical inverse method (PB =particle board – O =Oak).

Layer	(37 – 79)		(60-93)		(85 – 50)	
	PB	O	PB	O	PB	O
paint red	0.36	0.28	0.05	-	0.21	0.37
paint green	0.37	0.10	0.09	-	0.25	0.31
Paint red and varnish	0.34	0.29	0.06	-	0.31	0.32
Paint green and varnish	0.43	0.13	0.10	-	0.33	0.25
+wax (in case of a red paint layer)	0.27	0.44	0.10	-	0.46	0.33
+wax (in case of a green paint layer)	0.21	0.10	-	-	0.22	0.29

Furthermore, an influence of the relative humidity on the vapour resistance of the layers was observed. For the relative humidity increasing from 60% to 93% RH the barrier effect was 3 to 5 times lower than for the two other measurements. This observation is in accordance with general literature on polymer films and proteins [209]. The magnitude of the S_d -value is comparable with these found by Ruus [212] and Hendrickx [209]. For the samples for which the back had been impregnated with wax, an S_d -value similar to that of paint and varnish was observed.

3.3 Case Study of a Panel Painting: “The Mystic Lamb”

In this section the case study of an important panel painting is discussed, that is “The Mystic Lamb” by the brothers Van Eyck. The case represents the situation of a panel painting exhibited in a historic building with suboptimal conditions, which results in climate induced damage due to differential shrinkage and expansion of panel boards and top layers. As in many historical buildings, the owners and stakeholders attempted to improve the indoor climate conditions. The situation before and after the retrofitting will be assessed using different evaluation approaches.

3.3.1 Description of the Case Study

The panel painting “The Mystic Lamb”, shown in Figure 3.17, was painted by the brothers Van Eyck in 1432. It is generally accepted to be among the most important surviving works of art in the world and is part of the European cultural heritage. The original location was the Vijd-chapel for which the altar piece was commissioned. Since 1986, the altarpiece is exhibited in one of the chapels, namely the baptistery chapel, of the Saint-Bavo Cathedral in Ghent, Belgium (Figure 3.18). In that year, the polyptich was moved from its original location mainly because of security reasons.



Figure 3.17: “The adoration of the mystic lamb”, painted by H. & J. Van Eyck in the 15th century: (left) panel closed and (right) panel opened [227].

In 2008, a thorough examination raised concerns about the state of conservation of the altarpiece and the inadequate display conditions. As a consequence, a multi-year preservation project was set up. After an urgent conservation treatment, an assessment of the condition of the altarpiece indicated the need for a full restoration [228]. The restoration and conservation campaign of the Ghent altarpiece started in 2012 and is divided into three phases. One-third of the panels was consecutively moved to the restoration studio in the Museum of Fine Arts in Ghent, while the other two-thirds of the panels remained in Saint-Bavo Cathedral. This can be seen on Figure 3.19. Although there are plans to rehouse the altar piece in optimal display conditions, the panels will still be exhibited in the current shrine in the baptistery until a new visitor centre is

constructed within the cathedral [228,229]. Therefore, in 2011 modifications were made to the exhibition chapel to reduce the most problematic variations in indoor climate.

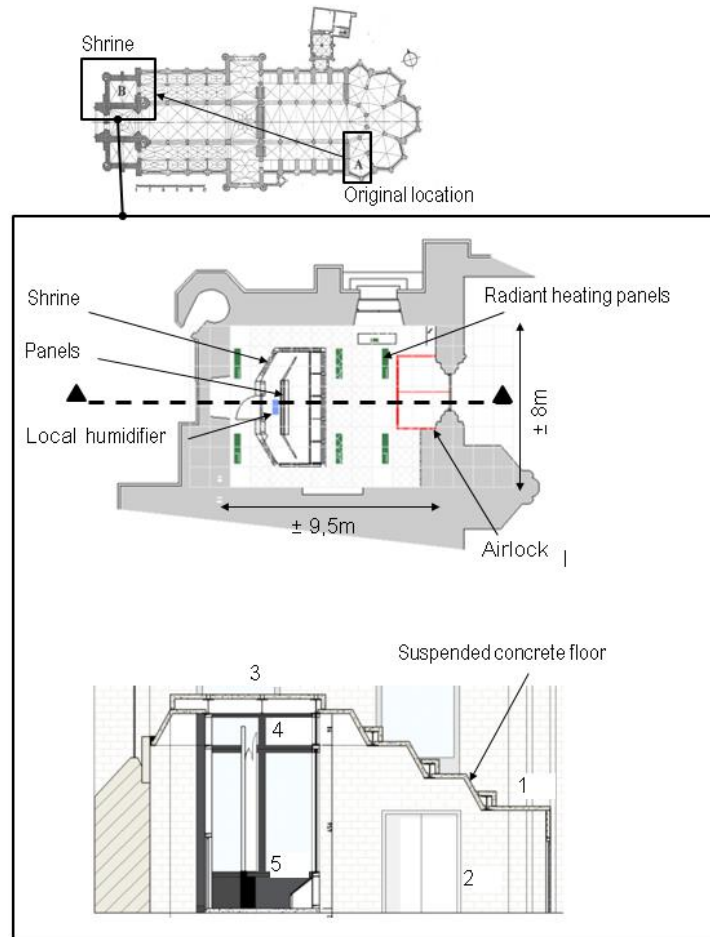


Figure 3.18: Floor plan of the Saint-Bavo Cathedral with location of the altar piece since 1986 (B). Floor plan and cross section of the baptistery and the shrine, located on the ground floor of the West tower. Location of the loggers (1-5) are indicated on the cross section.

To understand the relation between the state of preservation of the altarpiece and the display conditions, and to assess damage risks related to the current location, the measured indoor climate was evaluated using the different approaches discussed in chapter 2: a general approach and a more object based approach.

3.3.2 Measurement Campaign

Set-up measurement campaign

The monitoring campaign in the cathedral started in February 2010 and lasted for two years. Sensors of the Hobo H8 Pro Series were used for measuring temperature and relative humidity with an interval of 10 minutes. The measurement error of these sensors is $\pm 0.25^{\circ}\text{C}$ and $\pm 3\% \text{RH}$. The sensors were installed at various locations in the cathedral (Figure 3.18 – cross section): above the entrance hall of the baptistery (1), in the baptistery (2), in the space above the baptistery (3), in the upper part of the shrine ($\pm 4.5\text{m}$) (4) and in the lower part of the shrine ($\pm 1\text{m}$) (5). Furthermore, also the temperature and relative humidity of the outdoor climate were registered. Care was taken at each location to ensure that the loggers were placed away from draft, direct sunlight, and ceiling light fixtures. The measurements revealed that the temperature and relative humidity in the cathedral and above the baptistery were nearly the same and that the temperature and relative humidity measured at both positions in the shrine were nearly identical. Therefore, in the analysis of the monitoring data discussed in this work these measured values were averaged.

Boundary conditions in the Baptistery Chapel and the Shrine

In the baptistery, the altar piece is enclosed in a bulletproof glass chamber under a suspended concrete ceiling, called 'the shrine' (Figure 3.19). This shrine protects the painting against theft and vandalism and acts as a separate compartment in case of fire. The shrine is 5.56m high, 5.9m long and 3.5m wide and is constructed of 34mm thick glass panels, mounted in a steel frame.

Only electrical lighting, and thus no daylight, is present in the baptistery as the suspended ceiling is placed lower than the windows (Figure 3.18). The frame of the shrine contains the lighting system for lighting the polyptic. The original lighting system had been shut down and replaced by a temporary energy-efficient lighting system already in 2009 since it was soon understood that the heat gains due to the lighting had a negative impact on the display conditions and that the illuminance was too high. Therefore, it was reduced to a maximum illuminance of 150 lux. Access by the public is only allowed during opening hours, with up to 800 registered visitors on one day.

During the monitoring campaign, in February 2011, additional modifications to the baptistery were made to reduce the observed variations in indoor climate. Between the baptistery and the cathedral an airlock was installed to reduce draught. The airtightness of the shrine was improved by sealing seams between the glass panes and installing a climate barrier in the ceiling of the shrine. Further radiant heating panels (6x1700W) were placed at the ceiling of the baptistery to control temperature and reduce relative humidity during cold winter conditions (Figure 3.18). The heating system control consists of a room thermostat, with a set-point temperature of about 14°C , aiming at tempering extreme conditions in winter. To avoid a too low relative humidity at times of heating, a portable humidifier was installed in the shrine, with a set-point relative humidity of 40%. Until the moment that these modifications were made, the baptistery and shrine had never been heated nor conditioned.



Figure 3.19: The shrine in the baptistery where the panel painting the "Mystic Lamb" is located.

3.3.3 Evaluation of the Preservation Conditions for the Panel Painting

To compare the different assessment methods, the measurement period from March 2011 till Feb 2012 was used, equalling one year in which the heating system was in operation (Figure 3.20-RH Measured). During that period, the average temperature in the shrine measured 18.3°C, with a maximum of 24.0°C and a minimum of 9.6°C. Daily temperature variations between 2 and 5°C were observed. For the relative humidity, the annual average during the first monitoring year was 60.5%, with a maximum value of 74.7% and a minimum of 19.7%.

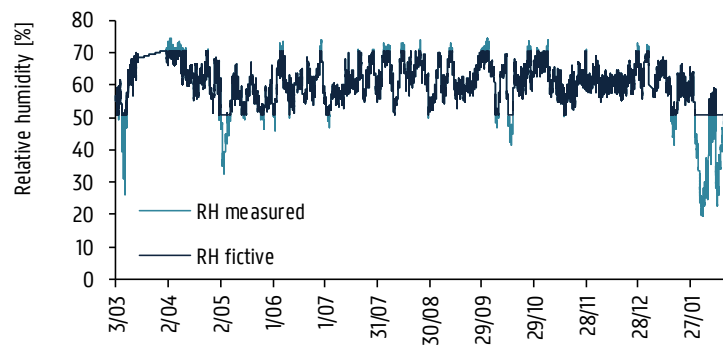


Figure 3.20: Relative humidity in the shrine from March 2011 till February 2012. Comparison between the measured relative humidity and a fictive case in which the too low or too high relative humidity is avoided by the use of a humidifier and dehumidifier.

ASHRAE classes of control

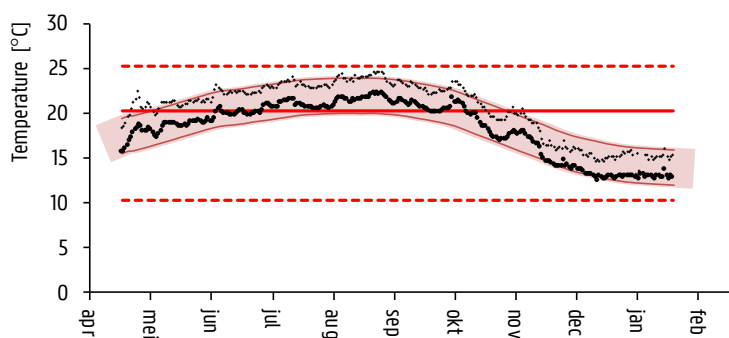
To evaluate the indoor climate according to the ASHRAE classes, the approach described in Chapter 2 was used. Because the panel painting is exhibited in a shrine, it is debatable whether class A or B should be achieved. Although climate class A is typically considered the optimum for most museums, as it is associated with a small risk of mechanical damage to highly vulnerable artefacts, it is also recognized as a target that is not feasible in most historic buildings, where classes B or C are the best that can be achieved [91].

Measured climate: failure?

Figure 3.21 illustrates the results for the evaluation of the indoor climate against the ASHRAE class A. A similar figure can be found for class B. For both classes A and B, the percentage of time that the measured indoor climate meets the ASHRAE criteria, is calculated. The results of this assessment are presented in Table 3.8 (actual situation).

The results show that target values for temperature variations were always met for control classes B. Only when more stringent limits for short-term temperature fluctuations are considered, as is the case for control classes A, the indoor temperature did not always achieve the target. The main reason of not achieving the higher control classes was a too high temperature in summertime or a too low temperature in wintertime.

The comparison of the measured relative humidity with the ASHRAE targets in Table 3.8 shows that the target values for all control classes were exceeded. A cause for not meeting the control class target values for relative humidity were the large short-term humidity variations, which often exceeded $\pm 10\%$ RH. The occurrence of short term relative humidity fluctuations was related to the daily visitor flows, leading to moisture production in the baptistery and draughts when entrance doors were opened.



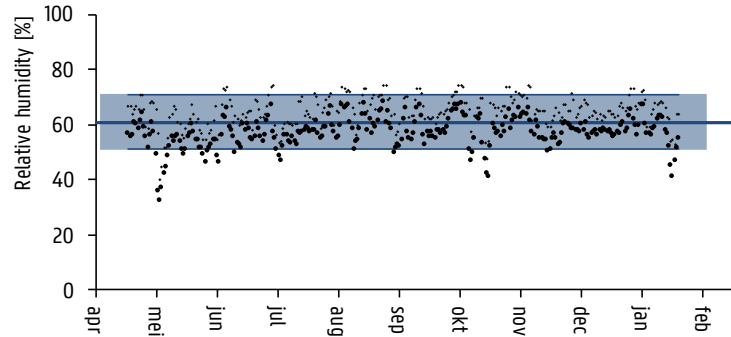


Figure 3.21: Comparison of measurements and target values of ASHRAE class A: temperature and relative humidity.

Fictive climate: Adaptations to improve indoor climate

Based on the evaluation of the measured indoor climate, a fictitious case was considered in which fluctuations in the indoor climate were limited. The limits are an offset of the annual average, allowing a fluctuation of $\pm 10\%$ RH. The progress of the relative humidity is shown in Figure 3.20. As a result, the occurrence of too low and too high values for the relative humidity was avoided and the seasonal fluctuation became smaller. Consequently, targets for relative humidity of control class A and B was met at all times (Table 3.8-improved situation (fictional case)).

Table 3.8: Percentage of time that measured time series of temperature, relative humidity or the combination of temperature and relative humidity meet the criteria of the ASHRAE classes: comparison between first and second monitoring year.

Class	Actual situation			Improved situation (fictional case)		
	T	RH	T & RH	T	RH	T & RH
A	73%	77%	60%	73%	100%	60%
B	100%	76%	76%	100%	100%	100%

This fictional year, which satisfies for control class B, is used further in the object-oriented method too study if the object-oriented leads to the same conclusion.

The three-types of degradation principle

In chapter 2, the three types of damage were described which will be used to evaluate the damage risk for the panel painting. For the assessment of the mechanical damage, boundaries suggested by Mecklenburg [118] were used (paragraph 2.1.2). The fatigue analysis is based on the research of Bratasz et al [183]. As criterion for the fatigue analysis the cracking of gesso was chosen and critical elongation values of the S-N curve were translated into critical magnitudes of relative humidity responsible for these elongations. In the analysis the rain flow counting method is used, thus for each time interval (1 day, 2days, ...,100days) the number of relative humidity cycles is counted.

Chemical deterioration

The concept of 'Lifetime Multiplier', defined by Michalski [112] and 'The equivalent Lifetime Multiplier' proposed by Silva and Henriques [147] is used to evaluate the risk of chemical damage. Two values for activation energy were used: 70kJ/mole for yellowing of varnish and 100kJ/mole for degradation of cellulose. The equivalent lifetime multiplier for the measured indoor climate is 1.27 for both activation energies. For the fictional indoor climate, a value of 1.30 was found for both activation energies. According to the classification method suggested by Silva and Henriques [147] for the eLM (Annex 2B), both years have 'some risk' on chemical degradation. These results are documented in Annex 3A.

Biological deterioration

The upper boundary for relative humidity set in the ASHRAE classes is 75%. This is because a relative humidity above 75% is associated with damages caused by deformation and mould growth. However, mould growth is less likely to occur in environments with a lower temperature, as observed in this case. To analyse whether there is a risk of mould growth or not, the bio-hygrothermal model of Sedlbauer [149] was used. Assuming a worst-case scenario, substrate class 0 was assumed. For both years no danger of mould growth is observed.

Mechanical deterioration

Three panel thicknesses were analysed (2mm, 10mm and 30mm) in the simulation study. The reason is that the polyptich consists of different panels with different thicknesses varying from 1mm to 34mm (Annex 3.B) and, as shown in Figure 3.22, the thickness determines the response time of the panel painting and therefore the acceptable relative humidity fluctuation..

At the start of the simulation study (time =0), it is assumed that the panel painting is in equilibrium with the environment and no damage is present. Material characteristics derived in the experiments were used. As the back of the polyptich is impregnated with wax, the sorption isotherm of oak impregnated with wax was used. For wax an Sd-value between 0.10 and 0.29m was observed. For the top layers, i.e. paint, gesso and varnish, an Sd -value between 0.10 and 0.37m was observed. This resulting simulated cases are listed in Table 3.9:

Table 3.9: Simulated cases for the tree thicknesses (2mm, 10mm and 30mm).

	Built-up of the panel	S_d wax	S_d top layers
Case 1	Asymmetric	0.10	0.37
Case 2	Asymmetric	0.29	0.10
Case 3	Asymmetric	0.29	0.37
Case 4	Symmetric	0.10	0.10

Figure 3.22 shows for case 1 the relative humidity at the back of the wooden panel, in the middle of the wooden panel and at the top of the wooden panel directly under the top layers. In this case, the diffusion resistance is the largest at the upper side of the panel. On the figure it can be noticed that for all panel thicknesses (2mm-10mm and 30mm), the upper side (wood/top layer) reacts slower to the indoor climate and thereby the relative humidity gradient is the largest between the back of the panel and the middle of the panel. Furthermore it can be noticed that only the thinnest panel follows the short-term humidity fluctuations.

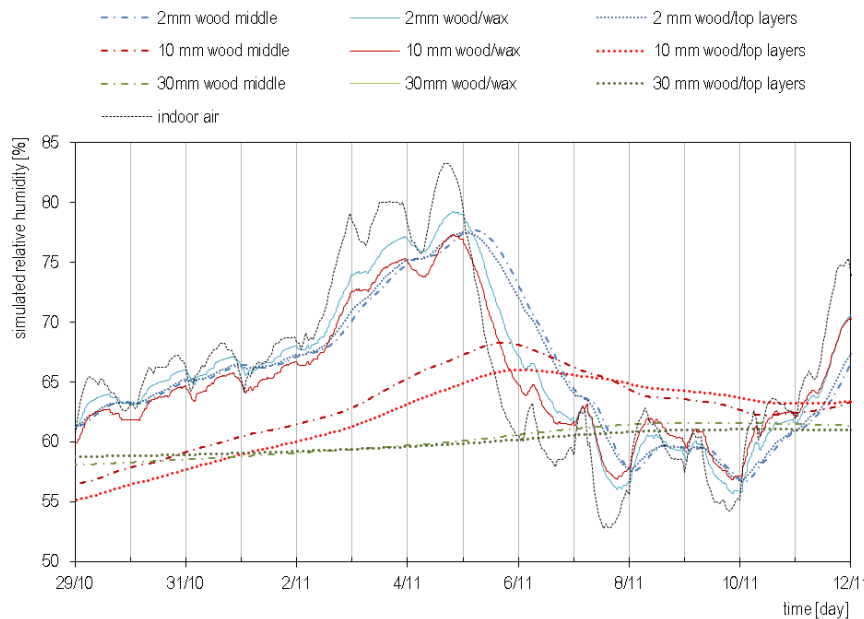


Figure 3.22: Calculated relative humidity in the middle of the wooden panel and at the surface of the wooden panel adjacent to the top layers.

As mentioned in paragraph 3.1, the calculated moisture response has to be compared with a pre-defined critical level. To evaluate the humidity fluctuations in the panel painting, former research of Mecklenburg [144] was used. He determined for different layers of a wooden panel painting

the domains of allowable relative humidity fluctuations (Figure 3.7). Tension and compression yield lines represent the upper and lower limits of relative humidity change at any given relative humidity. Beyond these limits, permanent wood deformation will occur (plastic region). The limits are valid for the worst case, i.e., restraint in the tangential direction²⁰. The x-axis represents the equilibrium relative humidity and the y-axis represents the end relative humidity. This is because the limits were determined in a lab by imposing a sudden change in relative humidity for the sample. To be able to use this method on real situations, the graph must be translated. For the starting relative humidity, the calculated relative humidity in the middle of the panel painting was chosen, for the ending relative humidity the relative humidity at the surface was used. A similar method for the evaluation of mechanical damage risk of a work of art was performed by Silva et al. [230] and Huijbregts et al. [231].

Figure 3.23 till Figure 3.25 show the results for case 1. Relative humidity boundaries of white oak were used to assess mechanical damage risk. Two positions were chosen at the surface of the wood: at the interface between wood and top layers (indicated as dark points on the graph) and at the back of the wooden panel (indicated as light points on the graph). The same analysis was performed for the other three cases, all of them providing similar results.

Two things are noticeable from the figures.

- The graphs indicate that for a relative humidity higher than 60%RH, risk of damage is observed for all three thicknesses of the wooden panel. The exceeding of the boundaries occurs more often for the back of the panel and is larger for the thicker panels than for the smaller ones. The boundaries of the safe region are exceeded for the measured case as well as for the fictional case. Contrary to the conclusion of ASHRAE, this graph indicates that there exists a possible risk of mechanical damage.
- Furthermore, it is also noticeable that in the measured case the variation in relative humidity is larger than in the fictional case. However, this does not result in a noteworthy increase of the mechanical damage risk since the fluctuations remain within the boundaries. So the measured drop in relative humidity does not necessarily have to lead to direct mechanical damage.

²⁰ in real-world conditions one assumes there is restraint [144]. Tangential worse than radial (same yield point, other swelling properties)

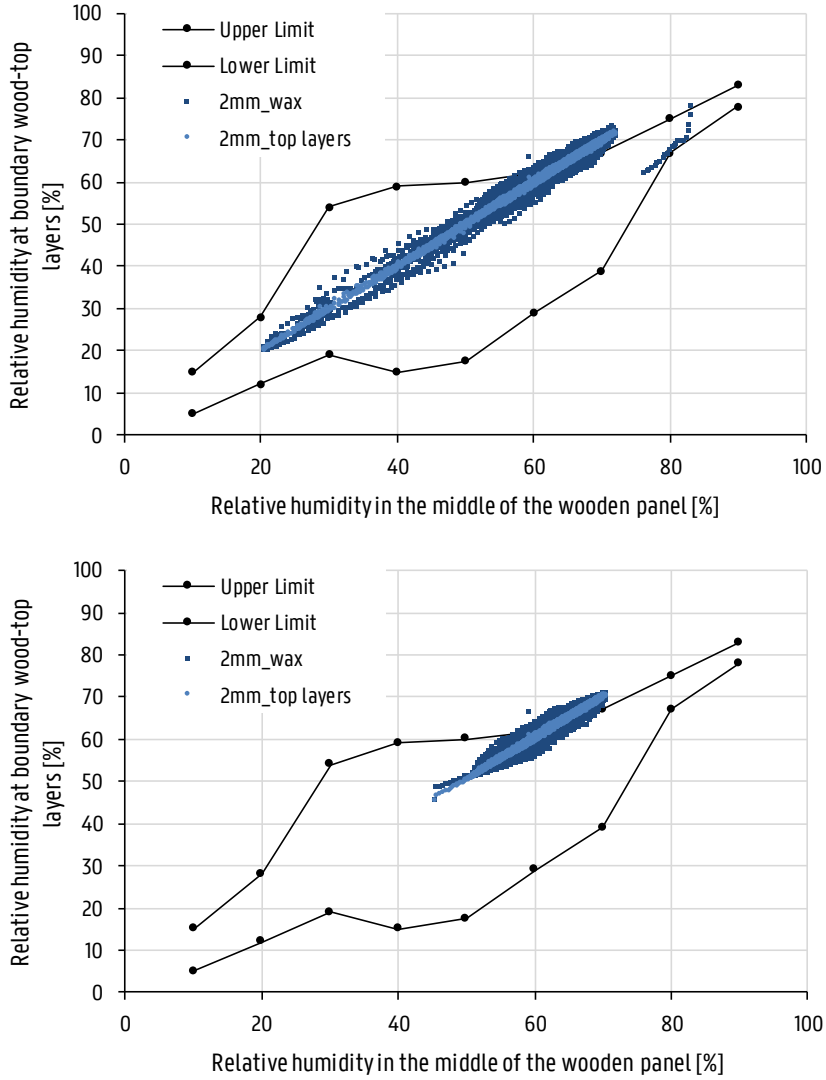


Figure 3.23: Domains of allowable RH fluctuation for case 1 for a panel with a thickness of 2mm. Above: free floating climate. Below: climate-controlled climate.

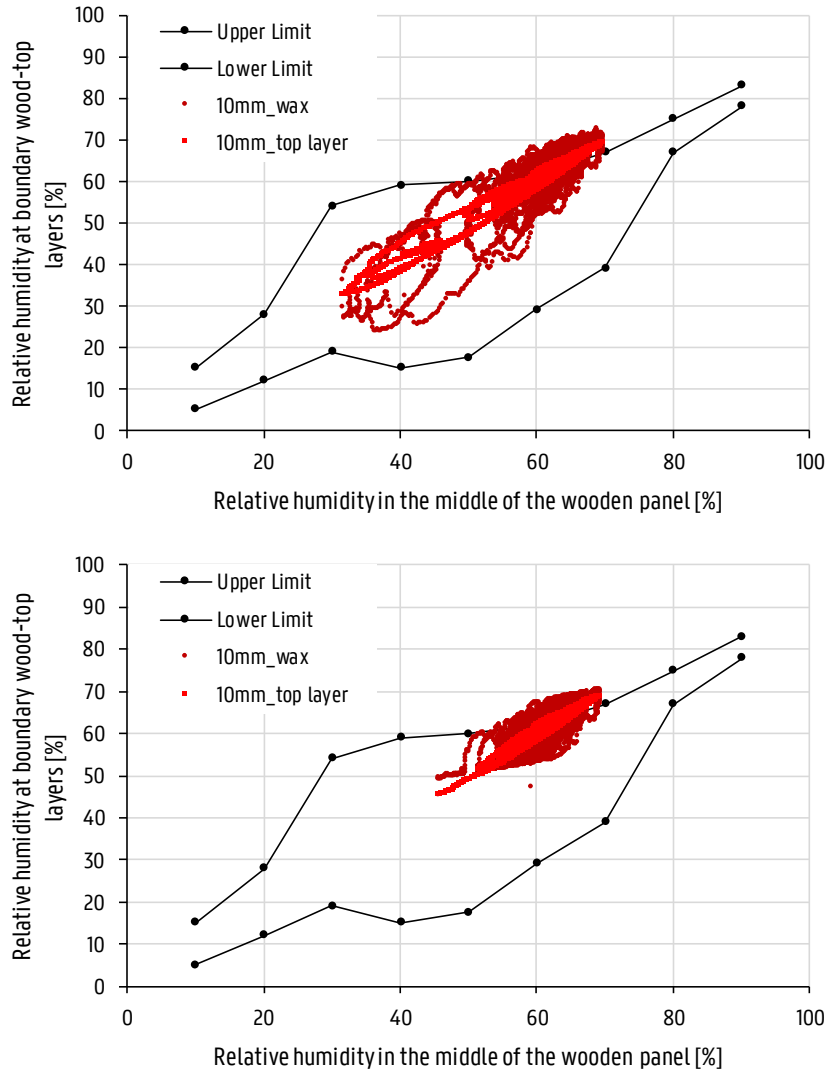


Figure 3.24: Domains of allowable RH fluctuation for case 1 for a panel with a thickness of 10mm. Above: free floating climate. Below: climate-controlled climate.

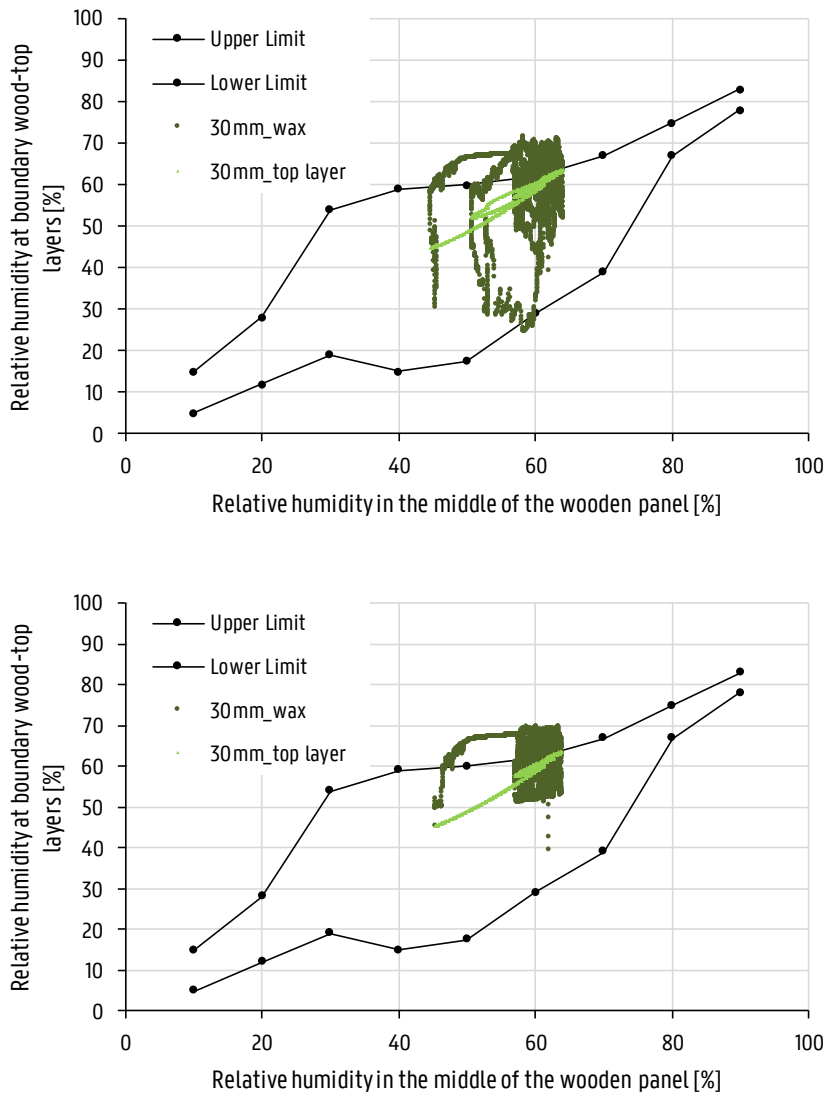


Figure 3.25: Domains of allowable RH fluctuation for case 1 for a panel with a thickness of 30mm. Above: free floating climate. Below: climate-controlled climate.

Fatigue Damage?

Large daily variations in relative humidity are associated with a higher risk of age crack formation of the paint layers. This is consistent with the damage detected during the preservation study of the altarpiece [229]. To study the risk of fatigue damage, the allowable amplitudes for relative humidity derived by Bratasz [136] were used to analyse the monitoring results of the case-study

in Ghent. The rain flow counting method in combination with the Palmgren-Miners rule was used to estimate the damage risk (Chapter 2). The evaluation of the measured humidity variations over the corresponding periods gives a **qualitative** indication of the improvement of the climate due to the modifications to the shrine and baptistery. The resulting total damage is:

$$D_{\text{tot,year2, measured}} = 2.56$$

$$D_{\text{tot,year2, fictional}} = 0.36$$

Following the Palmgren-Miner's rule, fatigue failure occurs when $D_{\text{tot}} > 1$. Consequently, for the fictional year in which too low or too high relative humidity was avoided, the risk on fatigue damage is largely decreased and the work of art is safe from fatigue damage.

3.4 Conclusion

The aim of this chapter was to evaluate in which case the simulated indoor temperature and relative humidity can be used to directly assess damage risk and in which case is it beneficial to model the relation between indoor climate and the work of art. Following conclusions are drawn based on the case-study.

- A general approach, like the approach proposed by ASHRAE, allows the modeller to assess climate conditions of a whole space by using the simulated temperature and relative humidity. These values are compared against boundaries which indicates a safe climate. However, in case boundaries were exceeded and thus failure is concluded, the percentage of exceeding can only give an indication of how far the climate lies from the desired preservation class. Therefore measuring the preservation conditions and expressing them in a percentage of time, does not give clear indications of about the damage risk.
- In case the relative humidity is in the mid-range, i.e. between 40%RH and 60%RH, the ASHRAE classes are useful to estimate damage risk. In case the relative humidity is outside this mid-range, ASHRAE preservation classes can give a different conclusion compared to the object-oriented method. Reasons are:
 - When exceeding the limit of 75%RH, even if it happens only once a year, the lower preservation classes of ASHRAE are not achieved. Therefore, in case of a high relative humidity, using a biological model allows a more nuanced prediction of the mould risk. Besides, not reaching any conservation class feels bad in the perspective of the owner.
 - When looking at the material specific stress-strain curves, it is noticed that in case of high relative humidity, smaller fluctuations are allowed than in the mid-range. The reason is that the moisture sorption curve of organic materials is S-shaped: it is flattened in the mid-range and steep at low and high relative humidities. As a consequence, relative humidities outside the mid-range will lead to larger expansion or shrinkage and therefore, also to a mismatch in dimensional behaviour of the different material layers (Figure 3.26). This implies that the use of an annual average for relative humidity instead of the value of 50%RH, can lead to an underestimation of the damage risk.
 - Using the values derived by Lukomski [171,182] to assess mechanical risk is very rough since the amplitudes were determined at 50%RH (Table 3.2). As noticed from the determination of allowable amplitudes based on the yield point, large amplitudes are allowed at the mid-range, but they need to be reduced significantly at very high or low relative humidities. Therefore this approach is not used in this dissertation.

A common criticism on the three-type-degradation principle is that one of the three types of degradation, namely the mechanical degradation, is difficult to assess. The reason is that the mechanical behaviour of a work of art is complicated and related to specific material composition and characteristics.

- A first contradiction however, is that the ASHRAE standard and classes were based on these researches. Therefore, using the more generalized approach because the object based approach is too specific, could somehow be relativized as the 'general' approach was also related to specific object behaviour.'
- A second contradiction is that for the three-type-degradation principle, material research is used and extrapolated for other similar works of art. This includes that the object-oriented approach, as used nowadays, is also 'general'. However, it gives a better understanding of the causes leading to damage.

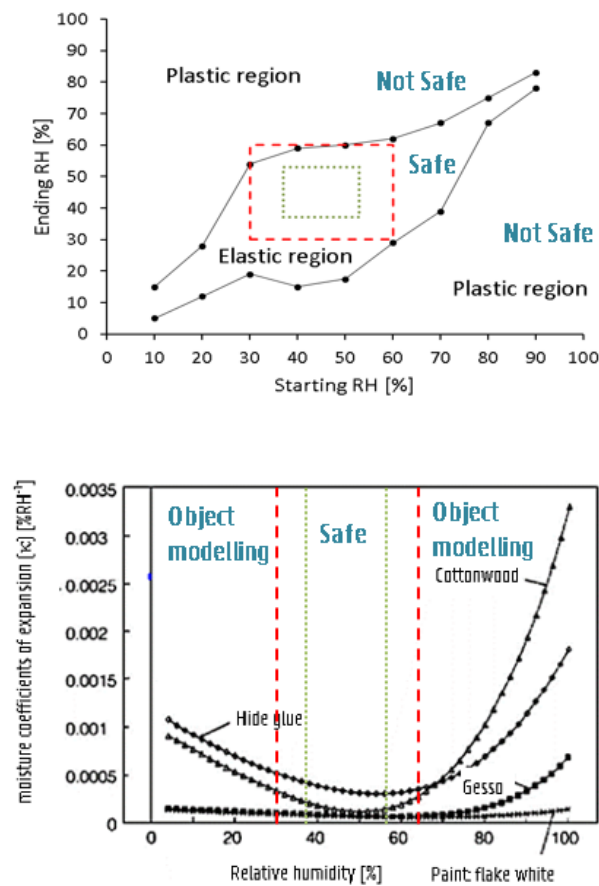


Figure 3.26: Mismatch in dimensional behaviour of the different material layers in case relative humidity is outside the mid-range. Therefore, in this dissertation, Object modelling is used if this is the case instead of a general method like ASHRAE.

A main disadvantage for the object based approach is that to be able to model the moisture transport, material characteristics are necessary. For the object in the case study, material characteristics were derived from experiments on wooden samples representative for restored Flemish panel paintings of the 15th-16th century. However, performing these experiments is time demanding as wood adapts slowly to moisture changes. In conclusion, the simulation with a coupled BES-HAM model is not time demanding, but the determination of the material characteristics is.

A main disadvantage for most methods is that they set an allowable range around an average value for the relative humidity. However, in case the mid-range is not achievable for the historical building, it would be interesting to have more information about allowable amplitudes. Therefore, research like Mecklenburg and Lukomski [171,182] is very useful and will hopefully be continued and extended.

4

Sub-Modelling Approaches to Predict Dynamic Moisture Response in Historic Buildings

To model the indoor climate of a building, a simulation model has to be made of the building and boundary conditions have to be defined. Historic buildings have typical characteristics that have an influence on the indoor climate. The way these are defined in the BES-tool and the way these are calculated by the BES-tool, will have an influence on the simulation results. In this chapter is looked to which extent the expansion of a BES tool with (simplified) moisture buffer models is sufficient for estimating the damage risk damage risk of a work of art related to conditions of the indoor environment.

4.1 Model Calibration and Model Uncertainties

The goal of a simulation study is to develop a model of the historic building which can be used to predict if the chosen measures will lead to the desired improvement concerning preservation conditions. In order for BES-models to be used with any degree of confidence, it is necessary that the existing model closely represents the actual behaviour of the building under study [36,45]. However, in the detailed physical simulation model variable inputs, like material characteristics, infiltration rate, occupancy and the control of systems, have a degree of uncertainty or are not known. Consequently, the chosen value for these inputs will influence the dynamic hygrothermal behaviour of the system and thus the simulation results. Therefore, to achieve a representative simulation model, the first step is to calibrate the model of the actual situation.

Uncertainty analysis, not sensitivity analysis²¹, represents an integral part of the modelling process, especially for calibrated simulations [233]. Namely, when reconciling measured and simulated values, two overall sources of error exist: measurement errors contained in the actual data and model errors emanating from the simulation process [234]. De Wit [235,236] classified the sources of uncertainty in the simulation model into the following:

- Uncertainties related to the specifications of the building and its systems because the building characteristics and systems are described partially or inaccurately.
- Uncertainties related to defined physical parameters (infiltration losses, occupancy,...) within the model which are different from reality.
- Uncertainties related to the model due to the fact that the simulation model is fundamentally a simplified description of reality.

This chapter focuses on the third uncertainty and it is studied how a simplified description of reality in the simulation model related to heat conduction and moisture buffering will influence the accuracy of the model. This is done using a case study. There is started with the most detailed description possible. In that case, for the first two types of uncertainties, a calibration technique is used to achieve through an iterative process a satisfactory model. This model will then be used as base case to compare with more rough approximations of the buffering and heat conduction process.

²¹ A subtle distinction exists between uncertainty and sensitivity analyses. The aim of a sensitivity analysis is to discover the input parameters to which the measured output of a model is sensitive. A crucial aspect of a sensitivity analysis is that it is unnecessary to quantify the likely variation in the model's parameters. Conversely, in an uncertainty analysis the variation in the input parameters is critical to the analysis, as the aim is to discover the likely variation in the output due to the actual variations in the input. A side effect of this is that the model may be sensitive to a specific parameter but, if the parameter is well known, it is not a critical parameter in an uncertainty analysis [232].

4.2 Calibration of a BES-Model

Development of a BES model using the forward approach (Chapter 1) involves prediction of the output variables using a detailed structure and parameters of the model subjected to a specific set of input variables. Models developed practicing such an approach are called white-box models [32]. In a historic building, however, not all input variables are known. As a consequence, values of some parameters are estimated. When one or more input parameters in a white-box model are estimated based on a fitting of the model to measurement data, the model becomes grey, no matter its complexity [237]. Figure 4.1 shows the approach which is also used in this work to achieve a validated BES-simulation model using calibration²².

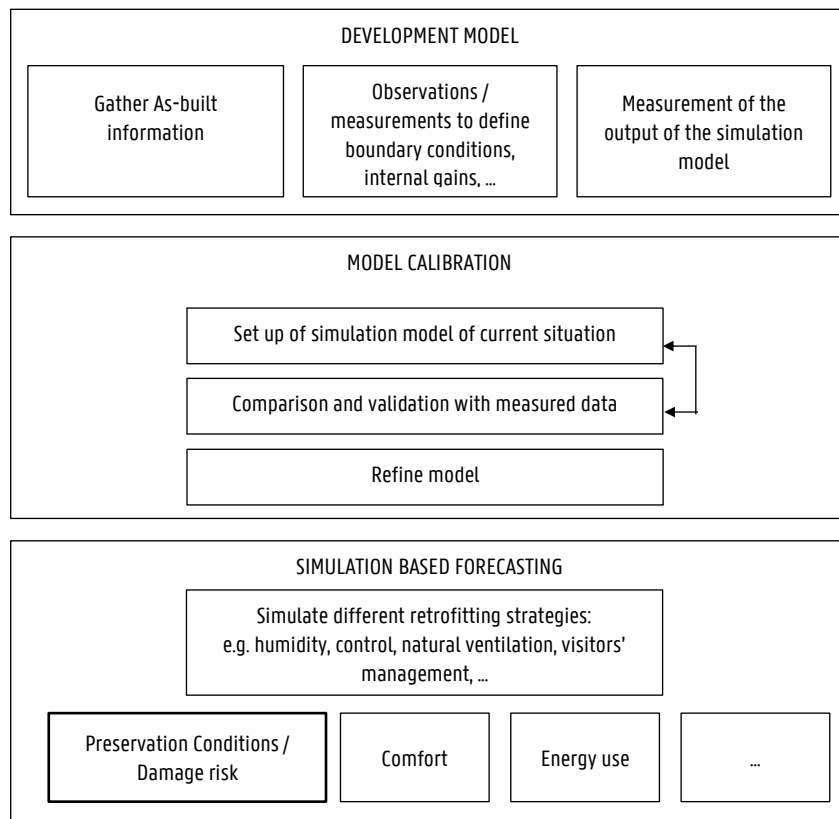


Figure 4.1: Approach used in throughout dissertation to achieve a simulation model. Based on [239,240].

²² Model calibration is an iterative process which, through the assessment of a series of simulations with different inputs, aims to reduce the discrepancies between simulated and actual building energy behaviour [238].

4.2.1 Development model

The first step is to build a simulation model that approximates the real behaviour of the (part of the) building as well as possible. Therefore, the following is needed [241]:

- As-built information to build up a simulation model (geometry of the building, envelope properties, infiltration rate, operation set-points of the heating system, ...)
- Survey observations or measurements to define the boundary conditions of the simulation model: occupant's behaviour, outdoor climate measurement, behaviour of adjacent rooms, ...

4.2.2 Model Calibration

Once the whole simulation model is developed, input parameters are set and measurements data have been collected, the model can be calibrated to represent more closely the actual behaviour of the building under study [36,45]. To perform the calibration, different methods exist. Roberti describes different methods applied on historical buildings [242]. In this dissertation, the calibration is done manually iterative. Other possible methods are automated, graphical and statistical methods [243,244].

Input Parameters

For the calibration process, different types of input parameters were considered. The first type contains data for which values remains unchanged and could be obtained from the building drawings, site survey and technical sheets [245]. The second type of data included parameters which were updated until an accurate model was achieved (Figure 4.2).

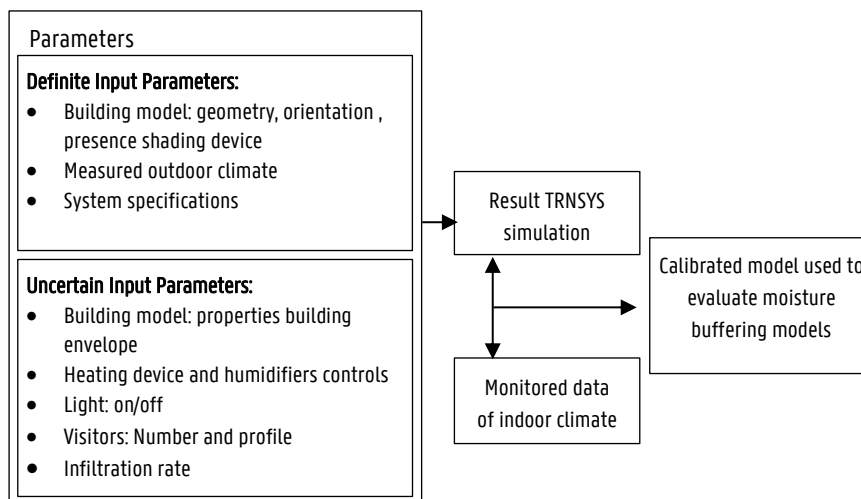


Figure 4.2: Schematic representation of the procedure followed in this case study to compare the moisture buffering models.

To achieve accurate results, the procedure suggested by Mustafaraj et al. [246] was used in this work. Based on earlier research, the authors proposed two stages of calibration during the manual iterative method process. In the first stage, the model is built using the collected data including as-built information with realistic occupancy, operating profiles and building use. In the second stage, sensitive parameters are defined and if possible extra field measurements are performed. A sensitivity analysis of the model to the input data is for historic buildings closely related to the calibration activity in order to assess the parameter influence on the building energy performance [238]. The chosen input parameters, that will be adapt, are updated through an iterative process until the accuracy of the calibrated model is satisfactory.

Chosen simulation output to compare with measured data

It was chosen in this work to use temperature and absolute humidity to calibrate the simulation model. The reason was that for estimating the preservation condition in a (historical) building, it is important to correctly model temperature and relative humidity course as these are the two most important parameters. Absolute humidity was chosen instead of relative humidity, because the absolute humidity is not dependent on temperature, contrary to relative humidity. Afterwards, once the model was calibrated on absolute humidity, relative humidity was used to estimate the preservation conditions. Simulation results of the models were compared with hourly and monthly mean temperature and absolute humidity. In addition to the average temperature and humidity course, it also is important to estimate as good as possible the short-term fluctuations. Therefore, also the daily variation in temperature and absolute humidity was used in the calibration process.

Furthermore, monitoring periods should be long enough and should allow to calibrate the model for each operation mode of the building: free floating, heating and or cooling [247]. Besides to evaluate the indoor climate, it is also advised to measure a longer time period to assess seasonal fluctuations. Therefore in this dissertation, one year was used.

Indicators to assess the fitting with measured data

To compare the deviation of the simulated results with the measured results, several data performance metrics exist. An extensive overview is provided by Afram et al [47]. In this work, the calibration process of the simulation model follows the method suggested by ASHRAE Guideline 14 [240]. ASHRAE Guideline 14 [240] suggests following two statistical indicators to calibrate the simulation model: "Mean Bias Error (MBE)" and "Coefficient of Variation of Root Mean Square Error (CV [RMSE])".

The mean Bias Error (MBE) measures how closely simulated data correspond to monitored data. It is a non-dimensional bias measure (relative error) between measured and simulated data and is calculated by the following equation:

$$\text{MBE} = \frac{\sum_{i=1}^n x_{\text{meas},i} - x_{\text{sim},i}}{\sum_{i=1}^n x_{\text{meas},i}} \quad (4.1)$$

Where: $x_{\text{meas},i}$ the measured data points for each model instance i ,
 $x_{\text{sim},i}$ the simulated data points for each model instance i
 n number of data points

The MBE it is subject to cancellation errors. Therefore, the Root Mean Squared Error (RMSE) approach or the Coefficient of Variation (CV) of the root mean squared error values are used more frequently [45,240]. The RMSE and CV(RMSE) are not subject to cancellation errors, because the error of every data point is squared. They allow one to determine how well a model fits the data by capturing offsetting errors between measured and simulated data. The advantage of using CV(RMSE) instead of RMSE is that it allows to compare which models provide better predictions of outcome, because the CV(RMSE) is non-dimensional. Equation (4.2) shows how the CV(RMSE) is calculated.

$$\text{CV(RMSE)} = \frac{\sqrt{\sum_{i=1}^n (x_{\text{meas},i} - x_{\text{sim},i})^2 / n}}{\sum_{i=1}^n x_{\text{meas},i} / n} \quad (4.2)$$

Data performance metrics

Common used criteria to calibrate a simulation model are the ones presented in ASHRAE Guideline 14/2002. These are shown in Table 4.1. Although this guideline was originally developed to quantify energy saving potentials of proposed retrofit schemes, it is also used for other variables like temperature, relative humidity, energy use, ... [234,246,248]. However, it is important to consider whether the requirements apply to the parameters of interest and whether the requirements lead to a sufficiently accurate simulation model. For example, an error of 10% on 20°C allows a deviation of 2°C. In literature, only a few works were found that use the internal temperature as a calibration goal [242,249]. Three of them, applied on historical buildings, are listed Table 4.1. In this dissertation, indicators suggested by ASHRAE Guideline 14/2002 were used. Furthermore, there was strived to never have an error larger than 5% for temperature and 10% for relative humidity.

4.2.3 Simulation Based Forecasting

Once there is reasonable agreement between measured and simulated data, new scenarios can be tested, parameter analysis can be performed, ... The authors are aware that it is inevitable that the vast volume of information that is required to describe a building model generally always leads to simplification and parameter reduction [234] and that other, more detailed methods are available calibration the simulation model. A comprehensive review of historical and current

calibration techniques and their advantages is given by Coakley, et al. [45] and by Reddy [250]. This is not in the scope of this work.

Table 4.1: Criteria used to calibrate the building simulation model described in ASHRAE Guideline 14 [240].

Source	Statistical indicator	Criterion
ASHRAE Guideline 14/2002	MBE	Hourly: 10 % Monthly: 5 %
	CV(RMSE)	Hourly: 30% Monthly: 15%
Paper of Roberti et al.[242]	RMSE MAE ²³	As no standard was found they tried to find the lowest value as possible. A RMSE of 0.78K was reported.
Book of Pretelli et al. [249]	MAE	5-10%
Paper of Enriquez et al. [247]	RMSE	0.5°C

²³ MAE is the mean absolute error. The same formula as the MBE is used. However, the absolute value of the numerator is used instead (always positive).

4.3 Uncertainties Related to the Simulation Model: Sub-Models for Moisture Buffering of the Building Envelope

4.3.1 Sub-models in a BES-simulation software

A BES-software, which is used in this work to model the behaviour of historic buildings, solves the heat and moisture balance for whole buildings. As shown in Figure 4.3, ASHRAE divides the heat balance into four distinct processes: outdoor-face heat balance, wall conduction process, indoor-face heat balance and air heat balance [43]. Similar to the heat balance, also a moisture balance is solved. To solve the distinct processes, building thermal performance software consists of sub-models to characterise each process. Because for each sub-model a choice is made how the balance will be solved (detailed, simplified), every sub-model will have an influence in the BES-simulation results [251].

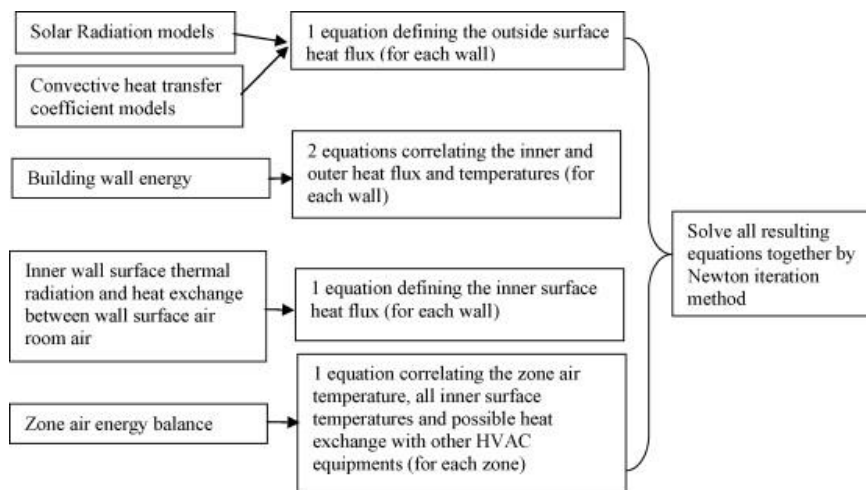


Figure 4.3: Sub-models in a BES-software. Outdoor face heat balance, wall behaviour, indoor heat balance, air heat balance [43,251].

In this chapter, two sub-models to describe the dynamic response of the building enclosure to variations in thermal and hygric boundary conditions are discussed in more detail. The reason is that historical buildings are characterized by thick walls with high thermal and hygric buffering capacity. The next paragraphs explain how the buffering behaviour of walls is integrated in a BES model, and how the choice of modelling the thermal and hygric behaviour affects the results.

4.3.2 Conductive Heat Transfer

For a wall with thickness d , made of one or more homogeneous layers, non-steady one-dimensional (1D) conductive heat transfer is expressed as a partial differential equation, known as Fourier's law, yielding:

$$\frac{\partial T}{\partial t}(x, t) = \alpha \frac{\partial^2 T}{\partial x^2} \text{ for } 0 < x < d \quad (4.3)$$

Where: α the thermal diffusivity ($\lambda/\rho \cdot c_p$) [m^2/s]

Different methods exist to solve this partial differential equation. One method is to solve the partial differential equation numerically by a finite difference or finite volume method. This is for example used by the BES-software ESP-r and optionally by EnergyPlus [252]. Due to the iterative computation for computing the temperature distribution inside the wall, the simulation program becomes more complicated and also the computational time and storage requirements can in some cases significantly increase [253–256]. To simplify the calculation of heat conduction through building multilayer constructions, many building energy performance simulation programs like TRNSYS, EnergyPlus and HVACSIM+ use the conduction transfer function (CTF) to solve the partial differential equation [257,258]. Other methods to solve the partial differential equation are the harmonic methods and response factor methods (e.g. DOE-2).

The CTF method is a numerical method to solve the partial differential equation without discretization. The idea is to determine the response of a system (=output) to some excitation relating to the boundary conditions (=input) [259]. Hereby walls are the system and treated as black boxes. Only the surface outputs, namely surface fluxes q_{si} and q_{so} , are of interest. Doing so, the CTF method results in a simple linear equation that expresses the current heat fluxes in time series dependent on the current surface temperatures, and histories of the surface temperatures and heat fluxes. By using this simplified method, the required computational effort compared to other numerical techniques gets reduced [258,260].

To solve the time series in the CTF-method, different methods exist. The Laplace transform method and the state-space method are the most widely used in cooling load and energy calculations [261]. TRNSYS uses the Laplace method as CTF calculation method described by Stephenson and Mitalas [262]. Other developed methods are state space (SS) methods, used by EnergyPlus, and frequency-domain regression (FRD) methods [256,258]. As TRNSYS is used in this dissertation study, the description is limited to the method used in TRNSYS.

The Conduction Transfer Function Method

Figure 4.4 illustrates the principle of the CTF method. Continuously changing boundary conditions of walls (=inputs), namely indoor and outdoor temperature, are simplified to a series of linear functions, consisting of consecutive triangular pulses with a base width of $2 \cdot \Delta t$ [263]. The input pulses are transformed into a response function (e.g. by Laplace transform method). The

response factors (RF), found by solving the response functions, represent the responses at time $i\Delta t$ of a wall to a single triangular temperature pulse. The response factors have the same unit as thermal transmittance, so the RF's are numerically equal to heat fluxes produced by unit triangular pulses of 1K [264].

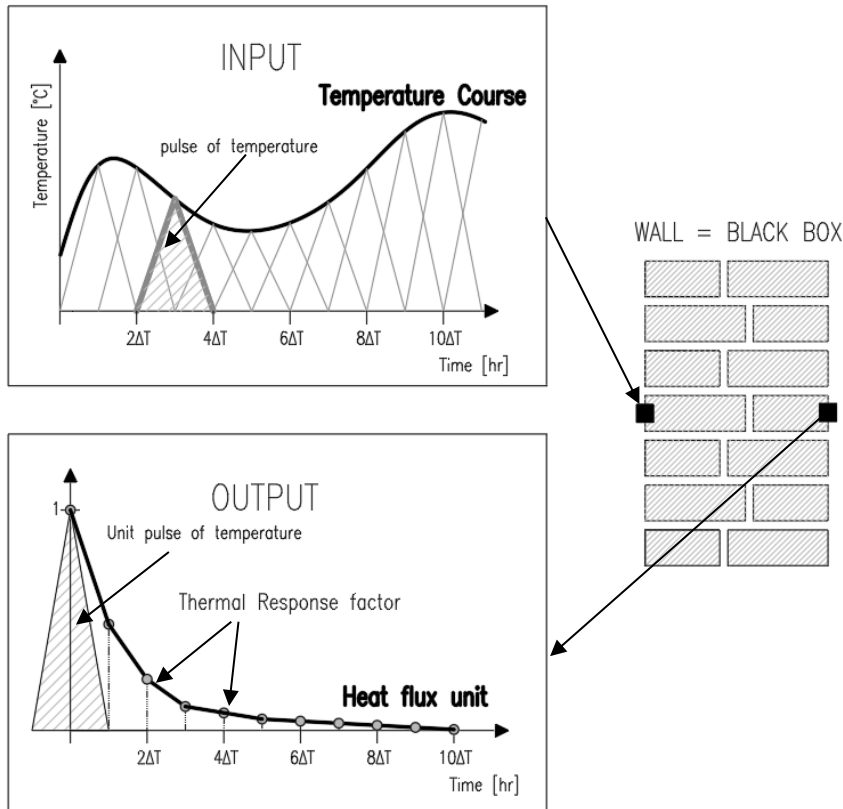


Figure 4.4: Schematic representation of the idea behind the black box treatment of walls and slabs for the conductive heat transfer [259,263].

The description following McQuiston and Lu is used to show the mathematical background of the method [265,266]. In the following equation $q_{s0,t}$ and $q_{si,t}$ are the heat fluxes at the exterior and interior surface at the current time $[W/m^2]$:

$$\begin{aligned} q_{s0,t} &= -Y_o T_{si,t} + X_o T_{so,t} + H_o \\ q_{si,t} &= -Z_o T_{si,t} + Y_o T_{so,t} + H_i \end{aligned} \quad (4.4)$$

The constant terms H_0 and H_i are the flux history terms [W/m²]. These are related to previous surface temperatures and to previous heat fluxes:

$$\begin{aligned}
 H_0 &= - \sum_{k=1}^{n_Y} Y_k T_{si,t-k\Delta t} + \sum_{k=1}^{n_X} Y_k T_{so,t-k\Delta t} + \sum_{k=1}^{n_\Phi} \Phi_k Q_{s0,t-k\Delta t} \\
 H_i &= - \sum_{k=1}^{n_Y} Z_k T_{si,t-k\Delta t} + \sum_{k=1}^{n_X} Y_k T_{so,t-k\Delta t} + \sum_{k=1}^{n_\Phi} \Phi_k Q_{si,t-k\Delta t}
 \end{aligned}
 \tag{4.5}$$

Equations (4.4) and (4.5) produces flux history terms are usually solved iteratively. The converged solution produces H_0 and H_i which correctly account for the thermal capacity of a given construction [266].

Where:	X, Y and Z	CTF's terms used to represent the exterior, interior, and cross terms, respectively.
	n_X, n_Y and n_Z	the number of CTF's terms
	n_Φ	the number of flux history terms
	Φ	the flux coefficient [-]

For lightweight materials, the thermal response is fast and few history terms are enough to accurately calculate the current heat flux, while for heavy weight materials, more history terms are needed [258].

Settings of time base

The key to success for the response factor method is the calculation of accurate, reliable conduction transfer function coefficients (CTF) for the walls [251]. The coefficients of the time series equations are generated once before the simulation for a certain timebase value (Δt) at a constant temperature, which is specified by the user [257]. The triangular pulses, shown in Figure 4.4, each have a base width of $2\cdot\Delta t$ and a height corresponding to the temperature.

The value of the time base plays a role in the accuracy and stability of modelling. The smaller the time base, the less time that passes between two temperature pulses, but the more CTF coefficients have to be calculated to capture the entire response of the wall [264]. In TRNSYS, the number of calculated coefficients varies only to a certain extent. Hence, the CTF coefficients in equation (4.4) and equation (4.5) become generally less precise. On the other hand, a larger time base means that temperatures and fluxes are recorded less frequently, which also causes inaccuracies [264,267].

Based on these commands for heavy and thick walls, ASHRAE recommends a time base of two or more hours [268].

4.3.3 Moisture Buffering

As discussed in chapter 2, the amplitude of relative humidity fluctuations is an vital parameter to define the preservation conditions of the work of art. In historical buildings, building materials and the furniture play a important role by their moisture buffering capacity in the amplitude of the relative humidity fluctuations [269]. Therefore, to make a more accurate assessment using a building simulation study, moisture buffering has to be taken into account.

The moisture balance for indoor air within a space under non-steady conditions is expressed by equation (4.6). In this equation, the humid air is assumed to be perfectly mixed within the zone and to behave as an ideal gas. Vapour pressure is used as driving potential. The terms in blue express the moisture sorption into or desorption out of the building materials. This can be calculated by equation (4.7). The term in green expresses the moisture gains or losses by condensation or evaporation at surfaces. In case no surface condensation is assumed in the BES-model, this term is omitted.

$$\frac{V_{\text{room}}}{R_v T_i} \frac{dp_{v,i}}{dt} = \sum_k (G_{v,\text{in}} - G_{v,\text{out}})_k + G_{\text{sys}} + G_p + \sum_j G_{\text{hyg},j} + \sum_l G_{c,l} \quad (4.6)$$

Where: V_{room}	volume of the room [m ³],
R_v	gas constant of water vapour [462 J/(kgK)],
T_i	interior air temperature [K]
dt	timestep [s].
$G_{v,\text{in}}$	netto-vapour flow added by infiltration (and natural ventilation) [kg/s]
$G_{v,\text{out}}$	netto-vapour flow removed by infiltration (and natural ventilation) [kg/s]
G_{sys}	vapour flow added or removed by an HVAC installation [kg/s]
G_p	vapour produced in the room by people, cooking, washing, ... [kg/s]
G_{hyg}	vapour flow by exchange with hygroscopic surfaces (building enclosures, as well as indoor objects, furnishing,...) [kg/s]
G_c	vapour flow by condensation or evaporation at surfaces [kg/s]

The term in blue expresses the moisture flow in or out of the building enclosure. It can be calculated by equation (4.7).

$$\sum_k G_{\text{hyg}} = \sum_k h_{p,k} A_k (p_{v,i} - p_{v,\text{surf},k}) \quad (4.7)$$

Where: $h_{p,k}$	the convective vapour mass transfer coefficient for wall k [kg/(Pa.m ² .s)],
A_k	area of wall k [m ²],
$p_{v,i}$	partial vapour pressure of zone i [Pa],
$p_{v,\text{surf},k}$	surface vapour pressure of interior wall surface k [Pa].

The term $p_{v,\text{surf},k}$ for each element can be found by solving the moisture storage and transport by vapour diffusion in an object k. The 1D-moisture transport equation is written as:

$$\frac{dw}{dt} = \frac{\partial w}{\partial \varphi} \frac{\partial \varphi}{\partial t} + \frac{\partial w}{\partial T} \frac{\partial T}{\partial t} = \frac{\partial}{\partial x} \left(\delta \frac{\partial p_v}{\partial x} \right) \quad (4.8)$$

Where:	φ	relative humidity [%]
	p_v	vapour pressure [Pa]
	$p_{v,sat}$	saturated vapour pressure at temperature T[°C]
	$\partial w/\partial \varphi$	slope of the sorption isotherm and expresses the moisture capacity
	δ	vapour permeability of the material [kg/(Pa.m.s)]

Analysing the interior humidity evolution in a building zone requires simultaneous solution of equation (4.6) for the room air and equation (4.7) and the differential equation (4.8) for each wall and object. Heat, Air and Moisture (HAM) models describe the combined heat and moisture transfer processes in complex porous building structures in detail and are appropriate to account for the hygrothermal interaction between the building air and the porous surfaces [270]. Therefore, to have a more accurate prediction of the interior relative humidity, some researchers have implemented finite-difference models in existing building simulation tools. Annex 41[34] gives an overview of implemented HAM-models in BES-software. Although they are more physically realistic, in most cases this approach yields a far too high computational load [271,272]. As a result, in building modelling moisture buffering has typically either been ignored or has been simplified. Two approaches generally exist to model moisture buffering in a simplified way [273].

In the first approach, moisture buffering has been lumped with the zone air using an effective moisture capacitance (EC) multiplier. In other words, the buffer effect of adsorptive and desorptive materials and furniture is not explicitly solved by the term G_{hyg} , but instead the moisture capacitance of the zone air is multiplied with a ratio EC. In the EC-model a value for the moisture capacitance multiplication factor is defined, which raises the capacitance of the air. This multiplication factor (EC) generally is in the range of 1 to 10 [268]. Equation (4.6) becomes:

$$EC \frac{V_{room}}{R_v T_i} \frac{dp_{v,i}}{dt} = \sum_k (G_{v,in} - G_{v,out})_k + G_{sys} + G_p \quad (4.9)$$

A second approach used in building modelling to incorporate the moisture exchange between the air and the materials, is the effective moisture penetration depth (EMPD) model [274,275]. In this approach, the assumption is that only a thin part of the interior surface of the moisture absorbent material, with a fictitious thickness d_{buf} , contributes to the moisture buffering process [271]. The thickness d_{buf} is related to the period of the moisture variation cycle and the moisture storage and sorption properties of the material. The contributing part of the interior surface can consist of one or two fictitious layers. In case two layers are present, two thicknesses are calculated, d_{buf} and d_{deep} . The first layer or surface layer accounts for short-term moisture buffering, while the other layer, the deep layer, accounts for long-term moisture buffering. The short-term period is usually defined as 24hours and the long-term period as one year. The effective penetration depth d_{buf} and in case two layers were used, d_{deep} , are calculated by equation (4.10), in which t_p is the period of cyclic variation (s).

$$d_{\text{buf/deep}} = \sqrt{\frac{\delta(\varphi)p_{v,\text{sat}}(T)t_p}{\rho\xi(\varphi)\pi}} \quad (4.10)$$

Where	$\delta(\varphi)$	vapour permeability [kg/(Pa.m ² .s)],
	$\rho\xi(\varphi)$	moisture capacity in terms of humidity derived from the material sorption isotherm [kg/m ³]
	$p_{v,\text{sat}}(T)$	saturation water vapour pressure at temperature T [Pa].
	t_p	period of cyclic variation [s]

A fundamental limitation of this model is that the material's thickness has to be wide enough, wider than the true moisture penetration depth calculated by Arfvidsson and Claesson [276], to allow the distinction between the surface layer where the moisture content varies with time and the remaining part of the material where the moisture content stays constant to the initial value [277].

Wood et al. [272] described two possibilities of formulations of the EMPD model, a non-isothermal formulation (e.g. EnergyPlus) and a more simplified isothermal formulation (TRNSYS). Following Wood et al. [272], the isothermal assumption includes that the non-isothermal term in equation (4.8) $\frac{\partial T}{\partial t}$ is neglected. Janssen [278] showed that this term, also called thermal diffusion, is of negligible magnitude and that thermal diffusion is of no importance for building science applications, leaving vapour pressure as the sole significant transport potential for the diffusion of water vapour in porous materials.

Apart from the building walls, also objects and furniture in the room will influence the humidity. In the work of Janssen and Christensen [269], it is suggested to use the EMPD-model for vapour release or uptake of the building walls and the 'effective moisture capacity' method for vapour release or uptake of the objects, given the many unknowns in relation to the stored objects. Roels and Janssen [271] state however that the 'moisture penetration depth'-concept implies the time-consuming determination of moisture capacities and permeabilities of all materials involved. Therefore, they proposed a method which relates the multiplication factor 'EC' for the room air moisture capacity to the measured moisture buffering value (MBV) [279] and is calculated by:

$$EC = 1 + 100 \frac{a\text{HIR}_{8h} + (1 - a)\text{HIR}_{1h}}{\rho_{v,\text{sat}}V} \quad (4.11)$$

Where:	$\rho_{v,\text{sat}}$	the saturated vapour concentration [kg/m ³]
	a	weighting factor related to the moisture production regime [-]
	$\text{HIR}_{8h/1h}$	the long and short term hygric inertia per cubic meter of room [kg/m ³ .%RH], calculated by:

$$\text{HIR}_{8h/1h} = \frac{\sum_k A_k \text{MBV}_{k,1/8h} + \sum_l \text{MBV}_{l,1/8h}}{V} \quad (4.12)$$

Where:	A_k	the moisture buffer area of finish type k [m ²]
--------	-------	---

V	volume of the room [m ³]
MBV _k	moisture buffer potential of the surface with finish k [kg/m ² .%RH]
MBV _l	moisture buffer potential of object l [kg/%RH]

Available Moisture models in TRNSYS building model

The main focus of thermal building simulation codes, like TRNSYS or EnergyPlus, is to predict the temperature fluctuations and energy demands of individual rooms [273]. As a result, the available models to describe water vapour exchange with surrounding materials are the simplified models; the EC-model and the EMPD-model.

Besides the EC-model, an EMPD-model is available. In the building model of TRNSYS, TRNBuild, the more simplified isothermal model had been implemented, which is named 'the buffer storage humidity model'.

The isothermal moisture model in TRNSYS consists of two buffering layers; one for short-term, and one for long-term moisture buffering. Both layers are related to each other as shown on Figure 4.5. The term G_{hyg} in equation 4.6 is calculated by solving following two differential equations:

$$\frac{\rho_{buf} d_{buf} [\xi(\varphi)]_{buf}}{P_{v,sat}} \frac{dP_{v,buf}}{dt} = \frac{(P_{v,i} - P_{v,buf})}{Z_{buf} + 1/\beta} - \frac{(P_{v,buf} - P_{v,deep})}{Z_{deep}} \quad (4.13)$$

$$\frac{\rho_{deep} d_{deep} [\xi(\varphi)]_{deep}}{P_{v,sat}} \frac{dP_{v,deep}}{dt} = \frac{(P_{v,buf} - P_{v,deep})}{Z_{deep}} \quad (4.14)$$

Where the buffer and deep layer are described by the following characteristics:

ρd	the mass of the layer per square meter surface area [kg/m ²]
$\xi(\varphi)$	gradient of the isothermal sorption curve of the layer [kg/kg]
Z	moisture transfer resistance for diffusion, $d_{layer}/\delta(\phi)$

For each zone, the characteristics of the two buffering layers have to be provided, knowing that the layer represents the average moisture storage properties of all room surrounding surfaces [273,280]. A further simplification in the EMPD-model of TRNSYS includes that constant material properties for the moisture transfer resistance for diffusion [Z] and the specific moisture capacity [$\rho\xi(\phi)$] are used. In other words, constant material properties for a certain temperature and relative humidity are provided before the simulation starts. During the simulation process, these material characteristics are not updated anymore. In reality, the mentioned material characteristics are dependent of the material moisture content. Although in the interval [30%RH; 70%RH] those properties are almost constant for most materials [277], outside this interval they are highly dependent of relative humidity. A last simplification is that the moisture model is not coupled with a model for heat transfer and thus assumes isothermal conditions.

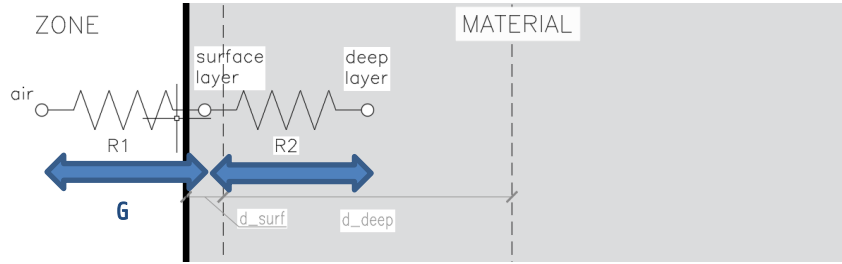


Figure 4.5: EMPD-model in TRNSYS consisting of a surface layer and a deep layer.

Extension to the original Moisture models of TRNBuild

The moisture model available in the building model of TRNSYS, named TRNBuild, has some limitations. The used EMPD-model is an isothermal moisture model with constant material properties and is not coupled with heat transfer in the wall. In insulated buildings, these model assumptions are accepted because the thin buffering layer has a constant temperature [273,281]. As shown by Janssens and De Paepe [273], in cases where a temperature gradient is present, the EMPD-model is not able to predict the initial fast response of indoor humidity to changes in moisture production. This could lead for example to an underestimation of the humidification load [281]. Because this study deals with historical buildings, where these non-isothermal effects could be important, two models are used to model the hygric behaviour: a non-isothermal EMPD model, coupled with heat transfer in the material and in which material properties are updated every time step and a more detailed continuous HAM-model.

User-defined TRNSYS type: coupled heat and simplified moisture model (EMPD-model) with updated material properties

This model is an extension of the isothermal EMPD model. Equations (4.13) and (4.14) are solved together with the heat balance equations under the non-steady-state (eq. 4.14 and 4.15). The conductive heat transfer is solved by.

$$d_{\text{buf}} c_{p,\text{buf}} \frac{dT_{\text{buf}}}{dt} = \frac{(T_i - T_{\text{buf}})}{R_{\text{buf}} + 1/\alpha} - \frac{(T_{\text{buf}} - T_{\text{deep}})}{R_{\text{deep}}} \quad (4.15)$$

$$d_{\text{deep}} c_{p,\text{deep}} \frac{dT_{\text{deep}}}{dt} = \frac{(T_{\text{buf}} - T_{\text{deep}})}{R_{\text{deep}}} \quad (4.16)$$

Every time step, material parameters $\delta(\varphi)$, $\rho\xi(\varphi)$ are updated, dependent on the calculated vapour pressure and temperature. More information about the TRNSYS component can be found in Annex 4A.

HAM-model

Because the incomplete modelling of the hygrothermal transfer in the envelope has direct effects on the simulation accuracy of the global thermal and hygric behaviour, several authors coupled BES and HAM simulation codes together [282]. HAM-models solve the conservation equations for heat and mass transfer in the porous materials and may be coupled to multi-zone building energy simulation models. To model the interaction between the porous material and the room in TRNSYS, a component was written by M. Steeman [226]. This model iteratively solves the coupled heat and mass transfer equations using a control volume method and an implicit discretization scheme. In this model, thermal diffusion is neglected and only the vapour diffusion is considered. Detailed information about the model and validation can be found in Steeman [283]. Starting from this HAM-component for TRNSYS, following adaptations were made:

- Translation from FORTRAN to C++. In this context, the original model was improved by lower computational time (convergence scheme, dealing with memory issues, ...).
- The code of the component is not programmed in one file anymore, but instead into multiple files (.cpp). By separating the code of the HAM-equations and the code which reads the TRNSYS-inputs, the HAM-code could also easily be used for interfacing with other software, such as MATLAB (flexibility).
- Different mathematical formulations of the moisture sorption curve, instead of only the empirical equation given by Hansen (flexibility).
- The water vapour resistance Z_{PE} between two nodes is now calculated as following:

$$Z_{PE} = \frac{\Delta X_{PE}}{\delta_e} = \frac{\Delta X_{Pe} \delta_E + \Delta X_{eE} \delta_P}{\delta_E \delta_P} \quad (4.17)$$

Where: ΔX_{PE} Distance between node P and node E
 $\Delta X_{Pe}, \Delta X_{eE}$ Distance between node P or E and boundary e
 δ_e Vapour permeability of element e
 δ_E, δ_P Vapour permeability at node E and node P respectively

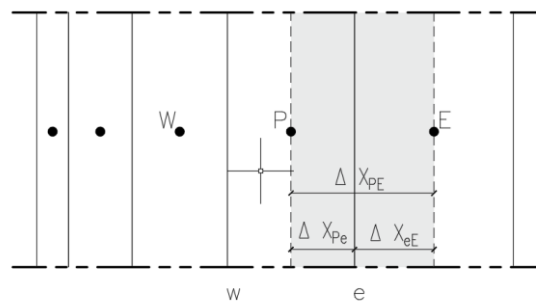


Figure 4.6: Spatial discretization scheme for heat and mass transfer.

4.4 Uncertainty Analysis

4.4.1 Description Case Study

To illustrate the effect of the defined characteristics for hygric and thermal buffering, this paragraph presents the simulation study of one of the spaces of the museum Plantin-Moretus, the library. The museum is located in Antwerp, Belgium and was the residence and workshop of Christophe Plantin. He was the founder of a printing dynasty (the Moretus family) that continued to operate at this location for three hundred years. The origin of the first buildings of the house dates from the 16th century. The museum opened to the public in 1877. Nowadays, the Museum Plantin-Moretus is a UNESCO world heritage site.

Besides the historical value of the building, also a mixed collection of works of art is housed here. Next to many books and prints, artefacts like (panel) paintings, textiles, gilded leather and furniture are exhibited. In 2012, Peckstadt and Moris investigated the condition of the exhibited books and they found that the books showed accumulated damage [284]. The observed damage could mainly be subscribed to two causes. Firstly, short-term fluctuations of the indoor climate, both temperature and relative humidity, were too large. Secondly, the seasonal fluctuation of the relative humidity, related to a too dry humidity during winter caused by heating, was too large. Since this problem was not new, the conclusion of this study was to search for a sustainable long-term solution. Therefore, commissioned by Museum Plantin-Moretus, a simulation study was performed.

Several rooms of the museum were selected to simulate, of which the Grand Library. A model was built in which the moisture buffering was included by using the most detailed available moisture model. This is the 1D-HAM model. First the effect of adapting the time base was calculated. Next, the effect of the used moisture model was studied. Therefore, the HAM model was replaced by the more simplified moisture buffering models. The results of the temperature and relative humidity course and fluctuations, on the achieved ASHRAE-classes will be compared against the most detailed model.

4.4.2 The Building Simulation Model

Geometric Model

To start, a 3D-building model of part of the building was made using Sketch-up and TRNBuild. The 3D-model included the whole building site along with the neighbourhood. This was done to quantify the shading effects on solar gain calculations. Only part of the building was modelled, representative of other parts containing a thermal zone for every orientation (north, south, east, west) per floor level. Other geometries were modelled as shading devices. The building geometry was derived from Autocad drawings. The geometric model, which includes the library, consists of four thermal zones.

Figure 4.8 illustrates the library and the geometric simulation model. The library was modelled as a single zone with following dimensions: 13.3m×7.24m×3.9m (interior floor area: 96m², interior volume: 372m³).

Because occupancy profile and internal load profile were similar for the adjacent zone, it was assumed that adjacent zones on the same floor level had a similar temperature and therefore they were not modelled. The adjacent adiabatic interior walls were maintained in the building model, since they provide a substantial part of the thermal and hygric inertia [269]. The basement, the room at the ground floor and the attic above the library were modelled as additional zones to include stack effect and the influence of the overheating of the attic in summertime on the library. The geometry and material characteristics in the model were assumed constant and were not changed to achieve a validated model.

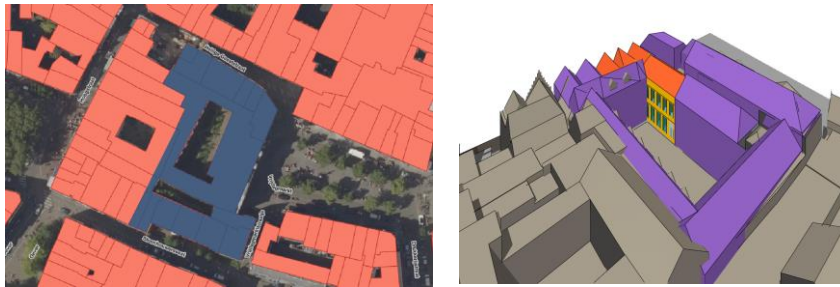


Figure 4.7: Illustration of the simulation models. Left: The Site Plantin-Moretus included in the 3D-building model (blue) – Right: Illustration of the model construction. The spaces in purple have the function of shadow objects, the spaces in yellow is the building model including the library.

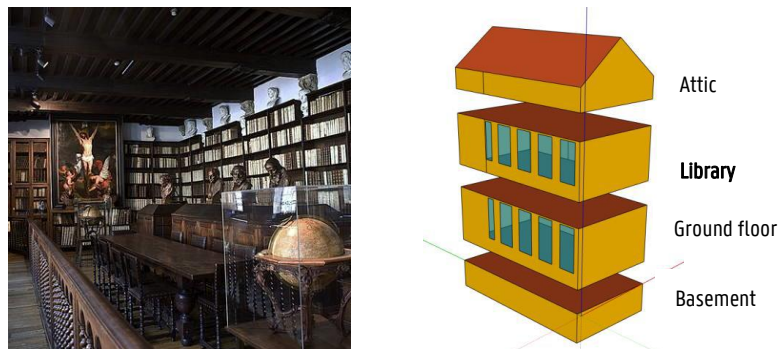


Figure 4.8: Interior view of the library showing the many books stored in the room and the building model including the library (located at first floor).

Material Characteristics

Both interior and exterior walls consist of masonry covered with plaster at the interior. The ceiling and floor consist of wood. It was only possible to measure the total wall thicknesses. Therefore, for the thickness of the separate material layers (masonry, plaster, wood) assumptions were made. Because the interior walls in the library were covered with bookcases, bookcases were included in the build-up of the interior wall. Windows are single glazed and the frame consists of wood and stone pillars. At the interior site, wooden shutters are presents. They were modelled as an additional thermal resistance of the window. Heat transport properties for these materials are summarized in Table 4.2. Windows and shutters were always closed.

Table 4.2: Material properties used in the building model of the library

Building part	Material	Thickness [m]	λ [W/m.K]	ρ [kg/m³]	c_p [kJ/kg.K]
Exterior wall	Masonry	0.35	1.00	1800	0.84
	Plaster	0.02	0.75	1300	1.00
Interior wall	Masonry	0.35	1.00	1800	0.84
	Plaster	0.02	0.75	1300	1.00
	Books	0.20	0.13	840	1.30
Ceiling/Floor	Wood	0.03	0.18	900	1.88

Building part	material	U-value [W/m²K]
Windows	Glazing: Single Frame: Wood + Stone	4.9
Correction closed shutter		2.9

Moisture Buffering

No information was available for the moisture properties of the materials. Hence, there was looked in literature to find information about the sorption isotherm and the water vapour diffusion coefficient of the different materials present in the building model. To model the moisture buffering of books by a HAM-model, the characteristics found in the work of Kupczak et al. [140] were used. These authors investigated the buffering effects of paper collections in libraries and proposed a 1D model of a book which can be used to investigate any number of books placed on a bookshelf. To use the HAM-component in TRNSYS, the equation for the moisture sorption isotherm have to be in the same format for all material layers in one composition (e.g. external wall). Therefore the sorption isotherm as presented by Kupczak et al. [140] is written in the format presented by Hansen [203]²⁴. Figure 4.8 shows the sorption isotherm as presented by

²⁴ $c = c_{\max} [1 - \ln(\varphi)/A]^{-1/b}$

Kupczak et al. [140] and as used in this work. The curve used in this work fitted well with the curve presented in literature, except for low relative humidities. For brick, gypsum and wood, characteristics presented in Annex 14 [203] were used. An overview of the used characteristics is presented in Table 4.3.

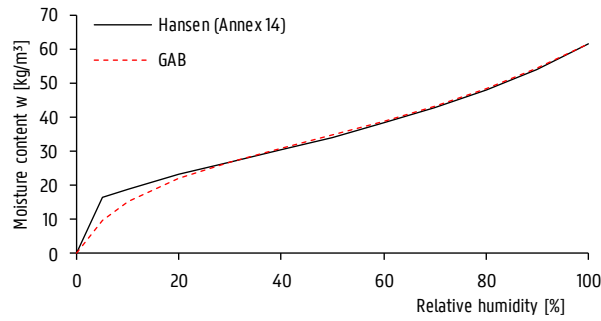


Figure 4.9: Sorption isotherm as presented by Kupczak et al. [140] and as used in this work written in the form of the equation presented by Hansen [203].

Table 4.3: Hygric Parameters used for the HAM model.

Characteristic	Value
<i>Books</i>	
Moisture content [kg/m ³]	$c = 61.5 \left(1 - \frac{\ln(\varphi)}{1.88}\right)^{\frac{1}{0.7}}$
Vapour diffusion [-]	$\mu = 2.45$
<i>Brick</i>	
Moisture content [kg/m ³]	$c = 16.3 \left(1 - \frac{\ln(\varphi)}{1.92}\right)^{\frac{1}{0.5}}$
Vapour diffusion [-]	$\mu = 7.69$
<i>Gypsum</i>	
Moisture content [kg/m ³]	$c = 310 \left(1 - \frac{\ln(\varphi)}{31.25}\right)^{\frac{1}{1.58}}$
Vapour diffusion [-]	$\mu = 1/(0.155 + 7.60 \cdot 10^{-4} e^{4.64\varphi})$
<i>Wood</i>	
Moisture content [kg/m ³]	$c = 223 \left(1 - \frac{\ln(\varphi)}{0.0865}\right)^{\frac{1}{1.88}}$
Vapour diffusion [-]	$\mu = 1/(0.0096 - 1.45 \cdot 10^{-3} e^{0.265\varphi})$

Weather data

The weather data was measured by a weather station providing following outputs; air temperature, relative humidity, wind speed and direction, barometric pressure, global solar radiation. All measurements were instantaneous values sampled at 10-minute intervals. Data was reformed to make hourly averaged weather files. To calculate the diffused radiation, TRNSYS type 16 was used which takes hourly integrated values of total horizontal solar radiation and estimates diffuse fraction internally.

Infiltration

The stack effect and the infiltration were modelled using the TRNSYS add-on TRNFLOW [285]. The air mass flow coefficient c_s (kg/s @1Pa), used in the power law equation, is based on the results of passive tracer gas measurements performed in cooperation with Pentiaq²⁵ [286]. The power law equation serves to calculate the instantaneous air flow rate Q based on pressure differences, which were dependent on temperature and wind velocity (eq. 4.18). In the performed measurement, an average infiltration rate of the library of 0.2 h^{-1} @2Pa was found. The standard value of 0.65 for the airflow exponent is not changed because most cracks have a mixed flow regime with a flow exponent of 0.6 to 0.7

$$Q = AC_s \Delta P^n \quad (4.18)$$

For more information about modelling with TRNFLOW, the reader is referred to the manual of TRNSYS and TRNFLOW.

HVAC

The library is heated by four radiators, located next to the exterior wall. To avoid low relative humidity due to heating, two mobile humidifiers are placed in the library which start working in case the relative humidity drops below 40%. The heating system and humidifiers are continuously in operation. This includes that there is no setback during night of for the summer season. The radiators were modelled in a simplified way using TRNSYS type 1231²⁶. The heat released to the room by one radiator is 800W and was modelled as a heat gain of 70% by convection and 30% by radiation. Radiators were controlled by a room thermostat. The setpoint of the room temperature is 18.5°C. The radiators switched of at a room temperature of 20.5°C.

Table 4.4: Input values of the radiator.

$T_{\text{rad,inlet}}$ [°C]	$T_{\text{rad,outlet}}$ [°C]	Mass flow rate [kg/s]	Type of Controller	n_{rad}
70	60	0-0.03	PID	1.3

²⁵ Pentiaq AB: www.pentiaq.se

²⁶ This type is not available in the standard library of TRNSYS, but is available in the TESS Libraries.

The humidifiers were defined as a moisture gain with a gain of 1kg/hr per humidifier using type 641. The operation of the humidifier was controlled by a hygrostat controller by an on/off controller. The deadband was $-3/+3\%$ RH.

Other Internal Gains and Losses

Other defined internal gains were the presence of visitors and the light equipment. The adopted values for these are summarized in Table 4.5. For their presence the following weekly scheme was implemented: from Tuesday till Sunday 10h-17h. (On Mondays, the museum is closed.). The amount of visitors was based on the monthly sold tickets. Furthermore, a daily occupancy profile was used as suggested by Schito and Testi [287].

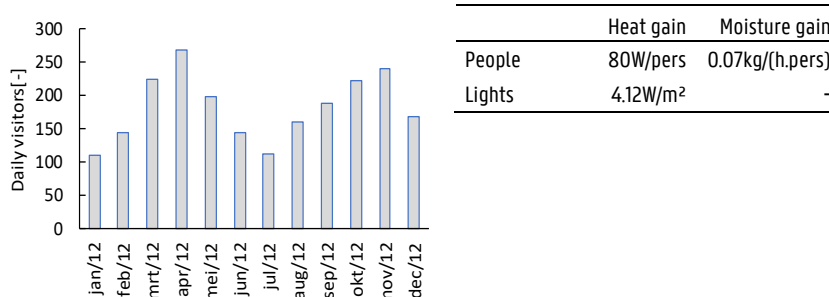


Table 4.5: Internal gains used in the building model of the library.

4.4.3 Model Calibration

Monitored indoor temperature and relative humidity over a full annual cycle were used to calibrate the model in order to accurately predict zone temperature. Data-loggers inside the building were located approximately 2m above the floor and all data loggers were placed out of draft or direct sunlight. Criteria used during the validation procedure are presented in Table 4.1. These criteria were applied to the hourly and monthly average temperature and absolute humidity. Because daily and seasonal temperature and relative humidity fluctuations are needed to estimate the preservation conditions, it was strived to achieve an as low as possible error for the hourly values. Input parameters which were varied in the model are illustrated in Table 4.6.

Table 4.6: Modified parameters in the simulation model.

Parameter	Range	Initial Value
Occupancy (heat gain and moist gain)	[-10%; +10%]	Monthly average
Infiltration rate	[-10%; +10%]	0.2 h ⁻¹
Setpoint heating	[-10%; +10%]	18.5
Walls: λ -value brick	[-10%; +10%]	1.00 W/(m.K)

After the completion of iterations, analysis of results showed satisfying consistency between calculations and measurements. Hourly and monthly MBE, RMSE and CV(RMSE) were calculated for each hour, month and for the total period. Table 4.7 shows the MBE, RMSE and CV(RMSE) values for temperature, absolute humidity and relative humidity on annual basis. MBE and CV(RMSE) values were below the predefined tolerance range for all parameters.

Figure 4.10 depicts the monitored and simulated temperature and relative humidity for the entire calibration period of 1 year. MBE and CV(RMSE) values for individual months showed that for the coldest months, temperature was underestimated, while in summer, temperatures were overestimated. Hence, the deviation was never more than 5%.

Table 4.7: MBE, RMSE and CV(RMSE) for the hourly and monthly average temperature, absolute humidity and relative humidity.

	MBE _{hour}	RMSE _{hour}	CV _{hour}	MBE _{month}	RMSE _{month}	CV _{month}
T	0.6%	0.7°C	3.5%	0.1%	0.4°C	1.7%
RH	-0.9%	2.6%RH	5.4%	-0.8%	1.0%RH	1.9%
AH	-0.7%	0.00048kg/kg	6.5%	-0.7%	0.00021kg/kg	2.6%

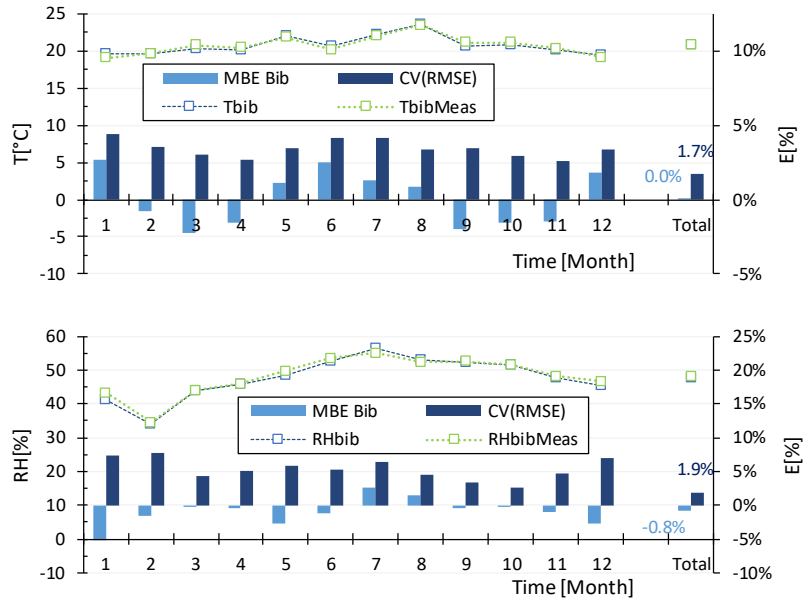


Figure 4.10: Simulated monthly average temperature and relative humidity for the entire calibration period of one year and hourly MBE and CV(RMSE) values for individual months.

Because the yearly relative humidity lies in the mid-range and the building is conditioned (heating system and humidifier), the guidelines of ASHRAE were used to assess the preservation class²⁷. Most important parameters are yearly average value and short and seasonal fluctuations. Figure 4.11 shows the measured and simulated percentages of time a preservation class was reached. For the highest preservation classes, AA, As or A, the simulated results did not predict the outcome as well as for the other preservation classes. This was due to the error on the daily temperature fluctuations, but mainly due to the error on daily relative humidity fluctuations (Figure 4.12). As for the highest preservation classes smaller short- and long-term fluctuations are allowed compared to the other preservation classes, errors for prediction the daily fluctuation have a higher impact for the higher preservation classes and as a consequence, the simulation result is more uncertain.

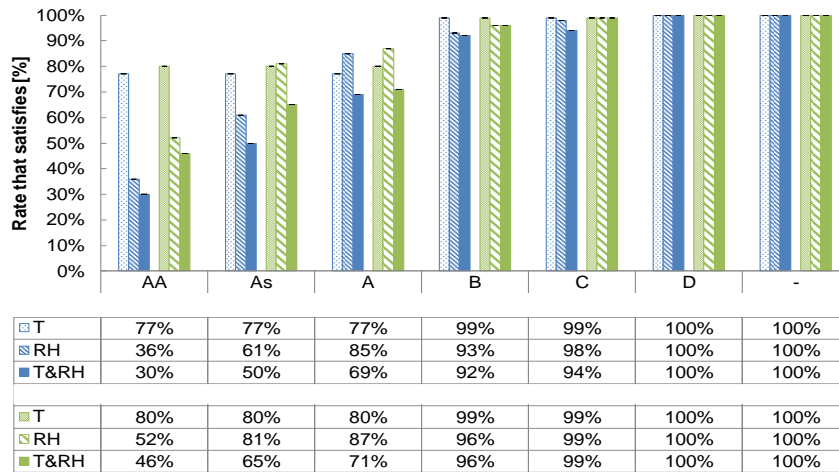


Figure 4.11: Comparison between the measured (blue) and simulated (green) percentages of time a preservation class is reached.

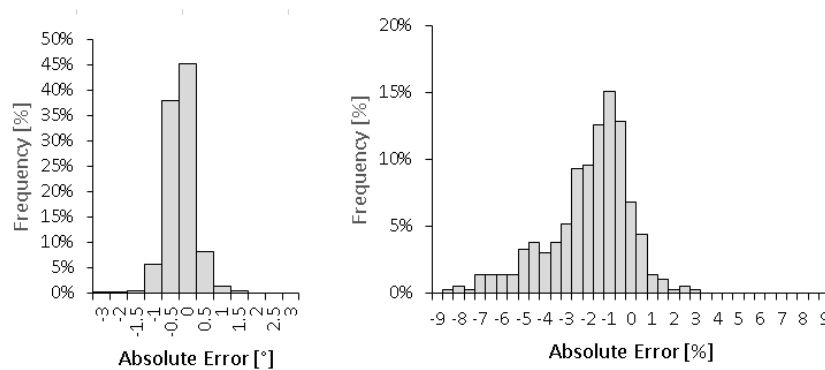


Figure 4.12: Histogram of absolute errors on hourly average temperature and relative humidity values.

²⁷ See Chapter 3.

4.4.4 Uncertainty Related to Time-Base

The building model of the library was simulated using three values for the time base: one hour, two hours and two and a half hours. The range of these values were the only possibilities with the same construction for the external wall. For values below 1 hour or larger than 2.5 hours, the calculation of the CFT-coefficients could not converge. As illustrated in Table 4.8, the setting of the timebase had no effect on the uncertainty of the simulation model. It had also no influence on the estimation of the percentage of time that a certain preservation class was reached.

Table 4.8: Performance comparison metrics for the temperature, absolute humidity and relative humidity.

		TB 1hr	TB 2hr	TB 2.5hr
Temperature				
MBE _{hour}	%	0.6	0.6	0.6
RMSE _{hour}	°C	0.7	0.7	0.7
CV _{hour}	%	3.5	3.6	3.56
MBE _{month}	%	0.1	0.1	0.1
RMSE _{month}	°C	0.4	0.4	0.4
CV _{month}	%	1.7	1.7	1.7
Absolute humidity				
MBE _{hour}	%	-0.7	-0.7	-0.7
RMSE _{hour}	kg/kg	0.00048	0.00048	0.00048
CV _{hour}	%	6.5	6.5	6.6
MBE _{month}	%	-0.7	-0.7	-0.7
RMSE _{month}	kg/kg	0.00021	0.00021	0.00021
CV _{month}	%	2.6	2.6	2.6
Relative humidity				
MBE _{hour}	%	-0.9	-0.9	-0.9
RMSE _{hour}	%RH	2.6	2.6	2.6
CV _{hour}	%	5.4	5.4	5.4
MBE _{month}	%	-0.8	-0.8	-0.8
RMSE _{month}	%RH	1.0	1.0	1.0
CV _{month}	%	1.9	1.9	1.9

4.4.5 Uncertainty Related to the Choice of Moisture Model: EC, EMPD-model and HAM-model

In the library, all interior walls are covered with book shelves. Because Derluyn et al. found that in these spaces, the daily maximum relative humidity at peak water production can be reduced by 80% [288] [289], next to the brick walls and the wooden floor and ceiling, the moisture buffering capacity of books was included in the moisture buffering sub-model defined in the simulation model of the library. Based on the floor plan, a total exposed area was assumed of 119m² of books, 204m² of wood and 45m³ of bricks covered with gypsum. The moisture buffering

capacity was calculated once with the buffer models available in TRNSYS (EC and EMPD), once with the non-isothermal EMPD-model (EMPD2) as a separate TRNSYS type and once with a HAM-model as a separate TRNSYS type.

For the EC-model, the so called EC-multiplier was derived by equation (4.11), in which a weighting factor α of one is used. Values used to calculate the value for the EC-multiplier are tabulated in Table 4.9. Parameters for the EMPD model in TRNSYS²⁸ were derived based on the materials characteristics as used in the HAM-model. Yearly average temperature (20.7°C) and relative humidity (48.2%RH) of the library were used to calculate the moisture capacity and the effective penetration depth. Furthermore, to estimate the penetration depth, the EMPD-model relies on a cyclical humidity load [272]. Hence, next to material properties also the duration of the cyclical loads should be defined. For the EMPD-model, the short-term period was defined as 24 hours and the long-term period was defined one year.

Table 4.9: MBV-values used in the simulation model to estimate EC [271,290].

Buffering materials	Surface area [m ²]	MBV _{in} [kg/m ² /RH]	MBV _{8h} [kg/m ² /RH]
Wooden Floor and Ceiling	204	0.36	1.15
Exterior wall (gypsum)	45	0.28	0.43
Interior wall (books)	119	0.72	2.45

Influence on Calibration Parameters

Table 4.10 summarizes the MBE, RMSE and CV(RMSE) for the temperature, absolute humidity and relative humidity. According to this table, all moisture buffer models provide satisfactory results. The averages hourly and monthly values were predicted well by every moisture buffering model.

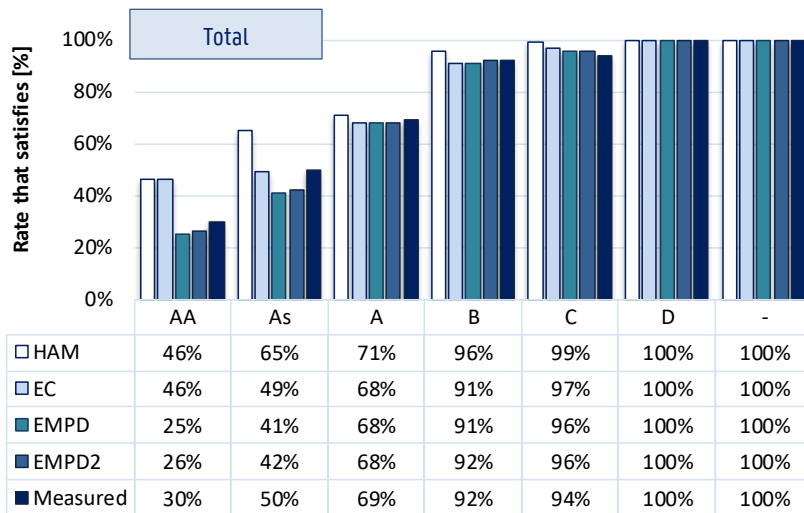
Figure 4.13 compares the percentages of time that a certain ASHRAE preservation class was reached for the different simulated cases. For the highest preservation classes, AA, As and A, the simulated results diverged the most and did not predict the outcome as well as for the other preservation classes. This was due to the absolute error for the daily fluctuations, and mainly due to the daily relative humidity fluctuations (Figure 4.12), and the fact that for the highest ASHRAE preservation classes, smaller short-term and long-term fluctuations are allowed compared to the other classes.

In this case, the leading influence on relative humidity is the infiltration and occupancy, so the influence of modelling with or without a detailed humidity models has less impact than modelling the infiltration and occupancy moisture gains. Taking into account that the calculation time increases by using the coupled HAM-BES model, for an historical building in which infiltration is important, it is not beneficial to use the most detailed HAM-model for including moisture buffering effects.

²⁸ Gradient of sorptive isotherm line, mass and exchange coefficient.

Table 4.10: Performance comparison metrics for the temperature, absolute humidity and relative humidity.

		HAM	EC	EMPD	EMPD2
Calculation time		20min	8min	10min	12min
Temperature					
MBE _{hour}	%	0.6	0.4	-0.1	0.4
RMSE _{hour}	°C	0.7	0.7	0.7	0.7
CV _{hour}	%	3.5	3.5	3.6	3.5
MBE _{month}	%	0.1	0.1	-0.1	0.1
RMSE _{month}	°C	0.4	0.4	0.4	0.4
CV _{month}	%	1.7	1.7	1.8	1.7
Absolute Humidity					
MBE _{hour}	%	-0.7	-0.2	-2.1	-0.9
RMSE _{hour}	kg/kg	0.00048	0.00065	0.00061	0.00055
CV _{hour}	%	6.5	8.8	8.2%	7.1
MBE _{month}	%	-0.7	-0.5	-2.3	-1.1
RMSE _{month}	kg/kg	0.00021	0.00031	0.00027	0.00025
CV _{month}	%	2.6	3.9	3.7	3.5
Relative Humidity					
MBE _{hour}	%	-0.9	-0.4	-1.8	-1.8
RMSE _{hour}	%RH	2.6	4.1	3.1	3.1
CV _{hour}	%	5.4	8.6	7.6	7.6
MBE _{month}	%	-0.8	-0.5	-1.8	-1.8
RMSE _{month}	%RH	1.0	1.9	1.9	1.9
CV _{month}	%	1.9	3.7	3.69	3.69



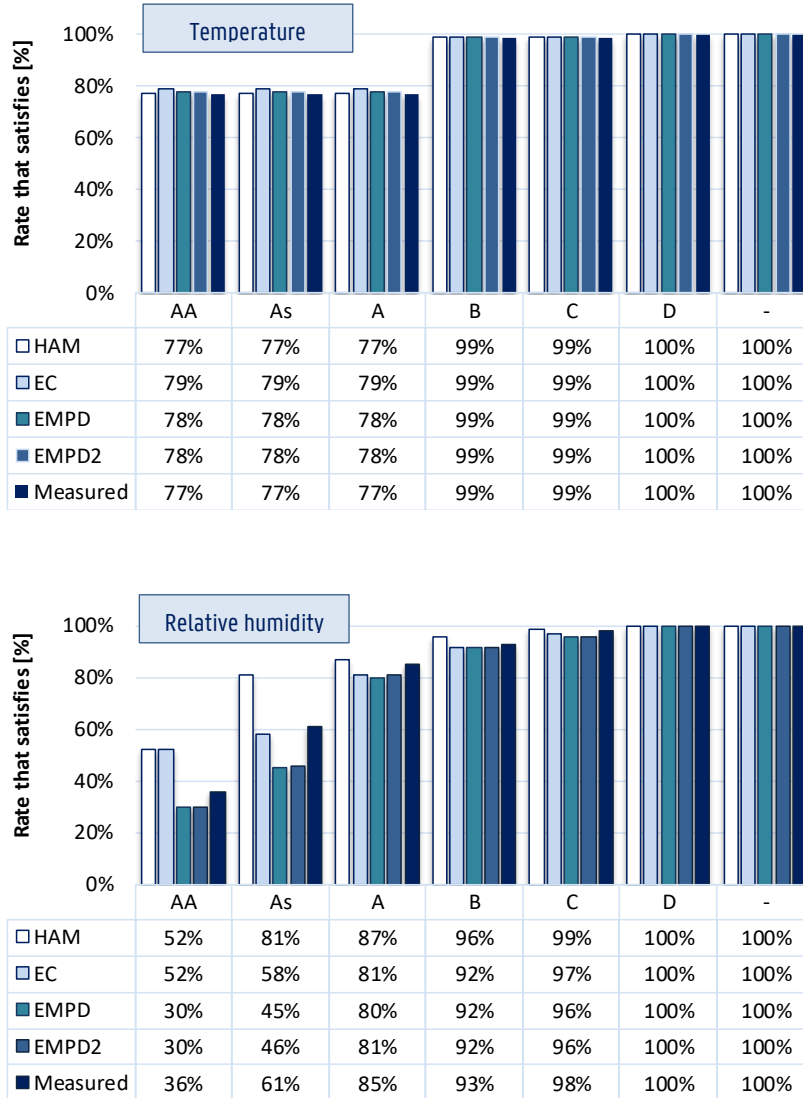


Figure 4.13: Comparison between the different moisture buffering models in TRNSYS for the percentage of time that a certain preservation class is reached.

4.5 Conclusion

Simulation tools are useful and powerful tools to investigate the outcome of an retrofitting option. Thereby, the forward modelling approach is appropriate to design a new system or to improve the existing system. For old historic buildings, however, information to build an accurate simulation model of the actual building is often lacking. To deal with the lack of some detailed information on required input parameters, it is common use to apply a grey box modelling approach in which uncertain inputs values are calibrated until the results are below a reasonable pre-defined error.

Different sources of uncertainty in the simulation model exist. This chapter focusses on one type of uncertainties. Namely, uncertainty related to the simulation model itself because the simulation model is a simplified description of reality. More precisely, there is looked at the sub-model for moisture buffering and the model related to the conductive heat transfer through the building envelope. The reason is that these two sub-models are supposed to have an influence on the average value and the amplitude of the temperature and relative humidity fluctuations, which are significant parameters to define the preservation conditions of the work of art.

The influence of these sub-models on the outcome of the simulated results were studied using a case study of a historical building with a high buffer load (library). Firstly, different values for the timebase were used to estimate the influence by this parameter. As the walls were massive stone walls, the timebase varied between 1 and 2.5. In the presented case, the value had no influence on the outcome of the simulation model. Secondly, a HAM-model was compared with an isothermal and non-isothermal EMPD-model and an EC-model. According to the MBE, RMSE and CV(RMSE) values for the absolute and relative humidity, all models provided satisfactory results. The HAM and non-isothermal EMPD model were the closest to the measurements. The EMPD model was also accurate to predict the preservation conditions. The advantage of using an EMPD model is that the calculation time is reduced. The EC model still provides reasonably result. Thereby the EC-model is more easy to implement, and the assessment and the calibration of EC value is more straightforward in use. Because the simulation case is rather complex, meaning that different input parameters cause uncertainty in the model, it was observed that infiltration gains and occupancy caused larger uncertainty than the choice for a simplified or more detailed buffering model.

5

Modelling Indoor Climate in Tall Enclosures

This chapter examines to which extent the expansion of a BES tool with a simplified stratification model allows to improve the simulation of the indoor climate in historic buildings. Firstly, different airflow models which can be coupled with a BES-software are presented. The original mathematical background of the chosen airflow model, the temperature-based zonal model, and the added equations for moisture transport are also presented. Finally, the coupling of the airflow model with the BES-software TRNSYS is explained and a validation of the model is performed to check the correctness of the coupled zonal-BES model. Part of this chapter was presented at the conference Building Simulation 2017 and published in the proceedings [291].

5.1 Tall Historic Buildings

5.1.1 Damage to works of art Related to Stratification

Works of art can become damaged in various ways due to inadequate indoor climate conditions. One possible cause is related to the installation of a HVAC system as an answer to the increased thermal comfort demand. Increased living standards since the Second World war have led to higher comfort demands [46], not only in residential dwellings, but also in churches. As a consequence, heating systems were installed which were designed to quickly heat the space during the service. Although these uncontrolled hot air system installations in churches improve thermal comfort, there has been an increase in damage and decay of their valuable works of art. [60,62,292,293].

When the church building is only heated during a service, there is a sudden increase in temperature, and thus a decrease in relative humidity, coupled with a moisture release by the churchgoers. In the building stratification occurs during heating caused by hot air, which is lighter than the surrounding cooler air, rising up into the ceiling (Figure 5.1). In addition to the fluctuations in time, the variation of temperature and humidity in space is important. This stratification phenomenon may not be neglected when assessing preservation conditions. Therefore, stratification also has to be estimated during the modelling of the indoor climate of the historic building.

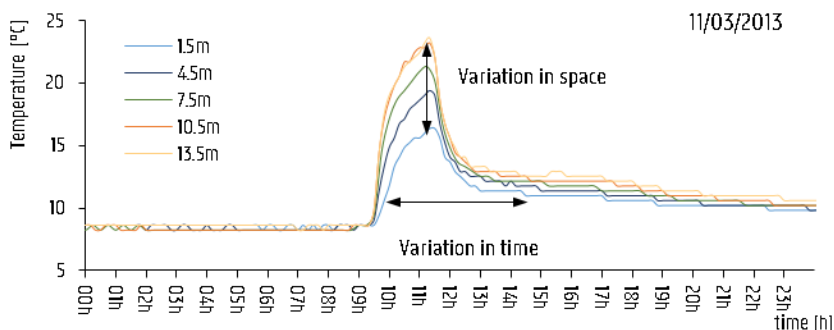


Figure 5.1: Measured temperature at different heights during a service in the church of Watervliet (Chapter 6). The heating causes a temperature variation in time and in space.

5.1.2 BES as an Analysis Tool

BES-tools commonly assume that the air in a space is well-mixed. Although these tools are adequate for the prediction of a space-average temperature and relative humidity in small rooms, they cannot predict detailed temperature and airflow distributions within the room. As described in Chapter 2, data quantifying about both variation of temperature and humidity in

time and in space is necessary to evaluate the preservation conditions. As a consequence, a simulation in which air is assumed well-mixed, suffers from a lack of accuracy for estimating damage risk in case stratification gets important [294]. Referring to Chapter 1 which discussed the groups of tools, this holds that an integration or linkage mechanism is needed between the tools for building energy modelling (group 1) and the tools for airflow modelling (group 3).

In this chapter a simplified method integrated into TRNSYS, is suggested in order to provide a more realistic representation of thermal and hygric conditions in a church building that takes into account the stratification during heating. Figure 5.2 illustrates the method used in this work to estimate the preservation conditions in a large volume, like a church building. This method is relatively fast and suitable for building engineering studies.

To estimate the airflow within a zone, a coupling between an airflow model and a BES-model is implemented. The next paragraph presents the theoretical background of airflow modelling. As illustrated, different airflow models exist which can be used to couple with a BES-software. The complexity ranges from coarse fully mixed models to very detailed Computational Fluid Dynamics (CFD).

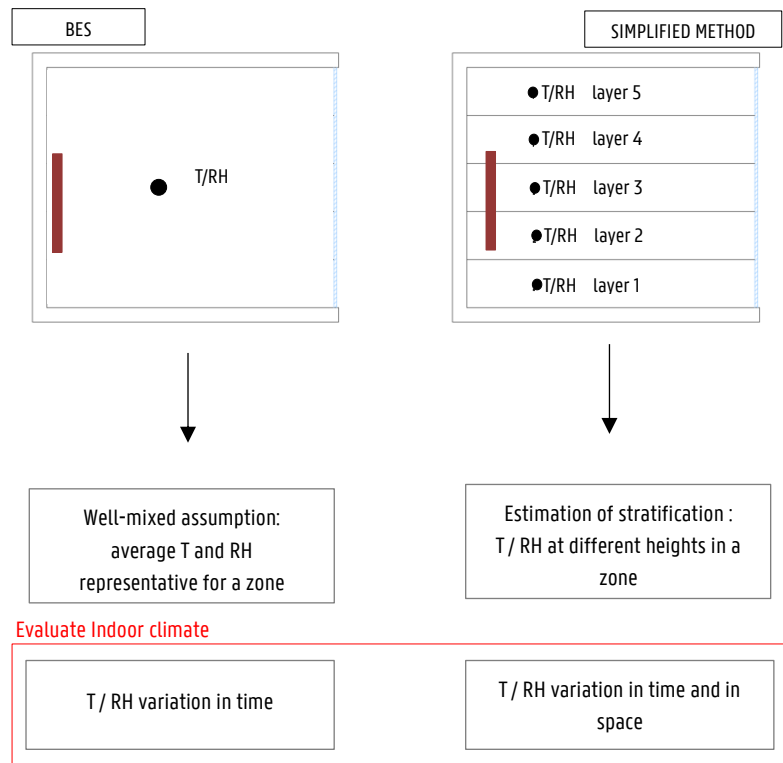


Figure 5.2: Integration of a method to estimate stratification into a classical BES-model.

5.1.3 Airflow Modelling in a Building

As noted by Griffith, a large variety of airflow modelling techniques have been developed and applied to building problems over the past 30 years [295]. This chapter only focusses on the modelling of air flow in buildings. Figure 5.3 shows a classification of available simulation models.

Course models are listed first; these are the so called one-zone and multi-zone models. This category includes the Building Energy Simulation (BES) programs. The term 'multi' suggests different interacting air nodes in one building. Each node represents the ambient, a plant, a room or even a collection of rooms. In each zone, air is assumed to be perfectly mixed and air pressure, temperature and relative humidity are represented as a single value. In other words, the airflow within one zone is not considered and effects like stratification are neglected. The BES-models may include a multi-zone airflow network model [296]. These airflow models allow to calculate flows such as airflow between adjacent rooms, infiltration, ventilation and HVAC systems of the building. Well-known examples of such a coupling are the integration of the airflow model COMIS [297] in the BES-software TRNSYS [50] (known as TRNFLOW [298]) or in the BES-software EnergyPlus [299]. However, these airflow models only calculate the air flow between different zones or nodes, while the air in one zone is assumed to be perfectly mixed. Because the focus of this study is on models which can predict the airflow in one room, these models are beyond the scope of this study.

At the other end of the spectrum are the CFD-models, which predict the temperature, velocity and other flow parameters by solving the complete set of the Navier-Stokes and energy equations. This method uses discretization techniques to develop approximations of these mathematical equations. To this end, the fluid volume of interest is divided into a set of very small cells (called a "mesh"). The conservation equations are applied to each cell and the set of algebraic equations are solved numerically for the flow field variables. The accuracy of the CFD solution is governed by the number of cells [300]. The use of Computational Fluid Dynamics (CFD) seems attractive to predict the airflow pattern in unsteady conditions. Hence, for CFD the domain boundary is usually the inside surface of a room and it needs to be dynamically fed with boundary conditions coming from the BES-tool [301]. Because of the detailed calculation, a CFD model is time consuming when making unsteady simulations for a room over a long period, such as a year. As a consequence, the study of the actual dynamics of large enclosures becomes difficult and time consuming, which is not practical in design work. Furthermore, coupled simulation of BES and CFD cannot be practically used to perform simulations involving controls of systems [296]. For these reasons, the third group of models (described next) still has benefits over complex models: user friendliness, are straight forward, and allow for fast calculation [302].

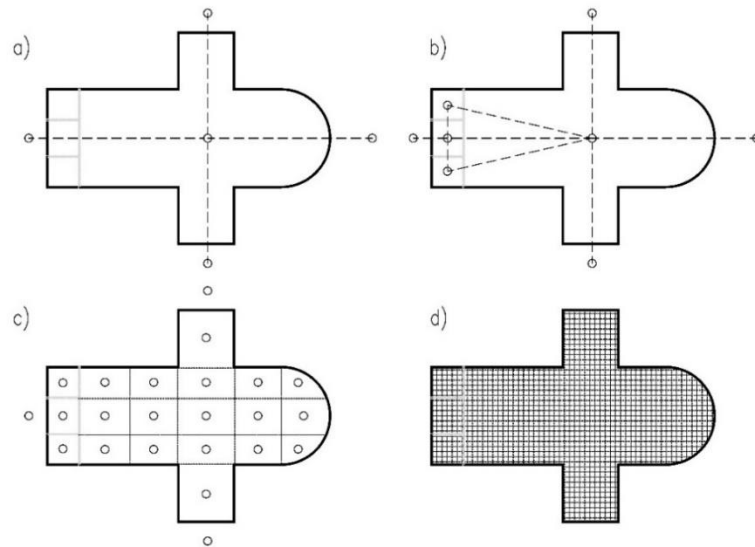


Figure 5.3: Schematic representation of airflow modelling techniques: (a) one-zone (b) multi-zone (c) zonal and (d) CFD approach

The third group of models is an intermediate solution between the coarse multi-zone models and the detailed CFD-models and includes the nodal and zonal models²⁹. These models predict the airflow in a room and thus provide a more detailed result compared to one-zone models, but they are less accurate than the CFD-models. In this intermediate approach, a rough flow pattern is calculated in each space by applying simplified mass and balance equations for each node or zone in the space. These models, which predict the airflow in one zone, can be linked to BES-software where the air in a zone is assumed to be perfectly mixed. By inclusion of such 'zonal' models in a BES-software the influence of airflow on the temperature distribution and vice versa can be estimated [303–305].

5.1.4 Intermediate Approach: Simplified Modelling Methods for Temperature and Humidity Distribution

A wide variety of models for the intermediate approach exist. Figure 5.4 schematically represents the airflow modelling techniques for the intermediate approach [306]. In ASHRAE RP-1222, Chen

²⁹ As mentioned by Griffith and Chen [295], care should be taken to avoid confusing zone with zonal, where the former refers to traditional building zoning (e.g. TRNFLOW) and the latter refers to one category of room airflow models.

and Griffith [307] make a distinction between so-called nodal and zonal models, based on how strictly and how resolved the geometry of the control volumes is defined [295,306].

Intermediate: Nodal and Zonal approach

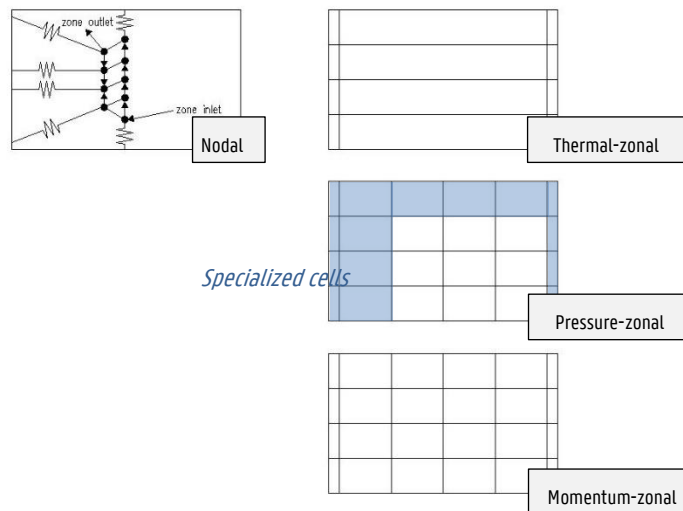


Figure 5.4: Schematic representation of nodal and zonal airflow modelling techniques (based on a figure of Griffith [306]). The zonal models are further subdivided into thermal-zonal, pressure-zonal and momentum-zonal models. [Blue = distinction made in grid cells, based on expected flow path].

Nodal models consist of a number of pre-defined nodes in a room, which are connected by flow paths. The first model was developed in 1970 by Lebrun [308] who suggested a nodal model which estimated the thermal stratification in a room heated by a radiator under a cold window. Subsequently, a series of nodal models were developed and nowadays there are numerous such models. Although some of these types of models can predict the temperature stratification with satisfactory precision, the main limitation is that pre-knowledge of the flow pattern is required [309].

Contrary to nodal models which consist of a predefined network, zonal models refer to air models that use a three-dimensional grid to divide the entire room into a system of control volumes and where no assumptions are needed for airflow direction [305]. The air flow between the gridsurfaces of the cells are calculated based on the corresponding conservation equations. The difference with a CFD model is that the cells are much coarser and the conservation equations are simplified. Depending on the simplifications made, the zonal models can be further subdivided into the pressure-zonal, temperature-zonal and momentum-zonal models [306].

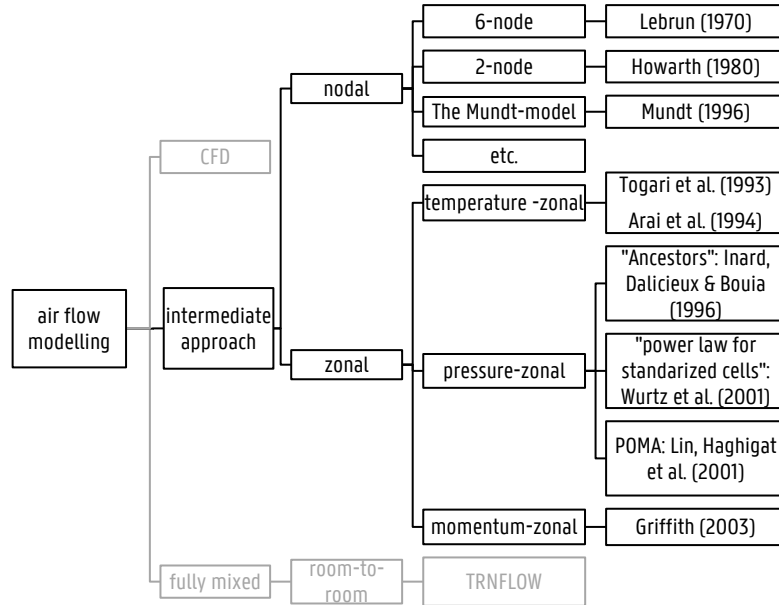


Figure 5.5: An overview of the different air flow models found in literature (non-exhaustive): narrow scope to buildings.

Pressure-zonal, temperature-zonal and momentum-zonal models

The starting point for these types of zonal models are the Navier-Stokes equations which are then simplified. The Navier-Stokes equations (eq. 5.1) include time-dependent equations for momentum and together with the continuity and energy equation they govern the motion of a Newtonian compressible fluid.

$$\rho \frac{Dv}{Dt} = -\nabla p + f_{visc} + F_{body} \tag{5.1}$$

Where the left hand-side describes two kinds of acceleration, consisting of time-dependent and advective effects. The right-hand side contains body forces (F), like gravity, and surface forces; one due to pressure (p) and a second due to viscous stresses (f_{visc}).

The pressure-zonal models predict the airflow between cells based on pressure differences and specific flow-pressure equations. Pressure-zonal models solve the mass and energy conservation equations, but the momentum equation is not considered [310]. The general idea is that the Navier-Stokes equation is simplified to the Bernoulli equation (eq. (5.2)) and the amount of air exchanged between two zones is calculated based on an equation, such as the power-law equation (eq. (5.3)), derived from the Bernoulli equation [311]. Over the last decades, a whole

range of pressure-zonal models were developed. An extended review of pressure-zonal models is provided by Megri and Haghghat [305]. In Figure 5.5 the most important ones are given.

$$p + \frac{1}{2}\rho v^2 = \text{const} \quad (5.2)$$

$$\dot{m} = \pm C_d A \rho \sqrt{2 \left| \frac{\Delta p}{\rho} + g \Delta h \right|} \quad (5.3)$$

Where: p air pressure in the cell [Pa]
 C_d discharge coefficient [-]
 A common surface between two adjacent cells
 g gravitational constant [9.81m/s²]
 h Height of the cell [m]

Bouia and Dalicieux [31] were the first to use this approach. The original two-dimensional model was later extended to a three-dimensional model by Inard, Dalicieux and Bouia [312]. Two types of cells were defined. First there were the so-called 'standard cells'. In these cells the flow velocity and thus also the momentum are of low magnitude, allowing for the simplification of the flow being driven by pressure alone. Wurtz [313] improved the method and showed that only the power law (eq. (5.3)) is appropriate to describe air flows in the standard cells [303]. However, when jets, plumes or thermal boundary layers are present, the viscous forces cannot be neglected. One solution was to no longer describe the mass flow in these regions by the standard cells, but by cells with specific equations for jet flow [312] or for thermal plumes [314]. Another solution is to adapt the discharge coefficients [311], as in the work of Teshome and Haghghat [315]. In subsequent years, many researchers developed zonal models. Two well-known models are POMA and CWSZ. POMA (Pressurized zonal Model with Air-diffuser) was a simplified numerical model developed in 2001 by Haghghat et al. [309] in the framework of Annex 35. CWSZ is a modified version of COMIS to simulate airflow, temperature, and concentration distributions inside a building [316,317]. The pressure-based zonal model also has limitations. One criticism is that these models made use of prior knowledge of the rough airflow pattern as expected by the modeller. This holds that the modeller had to define in advance of the simulation study, the type of cell (standard flow, jet flow, plume,...). A change in indoor conditions, e.g. a jet turned off, may change the predefined function of the cell-type [295,318]. A second criticism is that the pressure-based model is unsuccessful in predicting the temperature gradient in large buildings [secondary source: [319]] and in case of forced convection [303,309,320]. In literature, different alternatives are provided for the pressure-based zonal models.

An alternative to the pressure zonal models are the momentum-based zonal models. In contrast to the pressure zonal models, the momentum equation is not neglected. Griffith and Chen [295] formulated such a model. The velocity and viscosity of the fluid were assumed small enough to treat the fluid as inviscid. The Navier-Stokes equations were reduced to the steady three-dimensional Euler equation (eq.(5.4)), implying that the frictional forces were neglected. Similar to the model of Griffith and Chen, the VEPZO model [311,318] attempted to avoid the drawbacks of the pressure-zonal models by calculating the acceleration of the airflow between two adjacent

zones, but compared to the model of Griffith and Chen they also implemented a viscous loss model (eq.(5.5)).

$$(v\nabla)v = \frac{1}{\rho} \nabla P + g \tag{5.4}$$

$$\dot{v} = \frac{\frac{1}{\rho} \nabla P + \nabla(v^2) + g\Delta z}{\text{distance between two zones}} - f_{\text{loss}} \text{sign}(v)v^2 \tag{5.5}$$

Another alternative to the pressure zonal models and momentum-zonal models are temperature-zonal models. They use empirical correlations based on temperature differences in combination with mass and energy conservation laws for flows such as jets and plumes [306]. The temperature-zonal model has fewer unknowns and is easier to implement than the pressure-zonal models. It is a good alternative to pressure-zonal models when only the temperature prediction is required [319]. A widely used temperature-zonal model is based on the model proposed by Togari et al.[66] in 1993 [321–325].

The selected model in this dissertation is also based on the thermal zonal model proposed by Togari et al. [66]. In this model, the airflows along the vertical wall surfaces and supply airstreams are assumed to be the main components of the air movement in a large space. As illustrated in Figure 5.6, this assumption is reasonable for church buildings, where downdraught from cold surfaces, such as tall windows and most tall masonry surface are present [326].

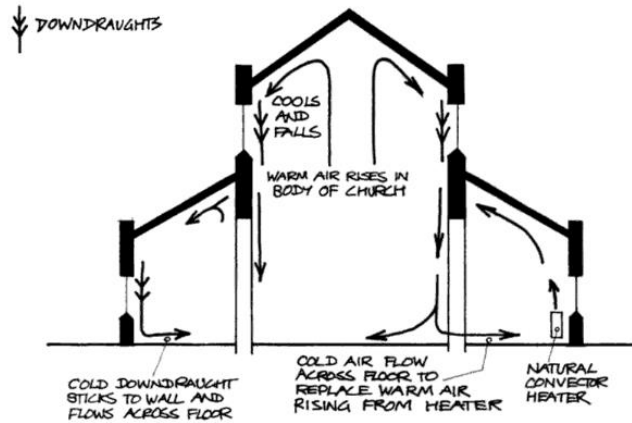


Figure 5.6: Common downdraughts in a church building [326].

5.1.5 The Thermal-Zonal Model

The developments of Togari's thermal zonal model

The thermal-based zonal model was first proposed in 1993 by Togari, Arai and Miura [66,327]. They intended to develop a simplified model which could be incorporated into an unsteady thermal analysis and which was able to predict the vertical temperatures in an atrium with a glass wall. The model consisted of three sub-models (Figure 5.7):

- a sub-model that computes the interior surface temperature by solving the heat transfer by conduction, convection, and radiation of a building envelope [327]. Wall surfaces temperatures were calculated with a resistance-capacitance model (Figure 5.8) using the vertical temperature distribution of the preceding time step.
- a sub-model for the wall currents which evaluates mass and heat transfer for air along interior surfaces of walls [66]
- a sub-model which solves the mass and heat balance for air in the vertical layers[66]. The calculated wall temperatures were used as boundary conditions for the thermal-zonal model to calculate the vertical temperature distribution in the room air for the actual time step. When a primary airstream is present, such as a jet is present, the mass and temperature of the primary stream is first calculated which is then be used in the mass and heat balance for air in the vertical layers.

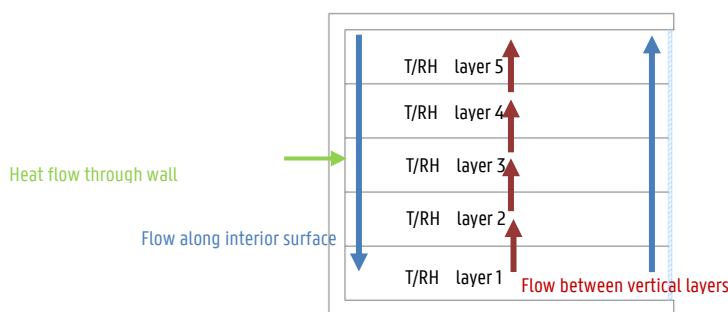


Figure 5.7: Three sub-models present in the thermal-zonal model: (1) a sub-model solving the heat transfer through the wall, (2) a sub-model which solving the mass and heat balance for air between the vertical layers, (3) a sub-model evaluating mass and heat transfer for air along interior surfaces of walls.

This model was originally validated using a 3mx3mx2.5m scale-model and was demonstrated to be adequate for practical use by Takemasa et al. [328]. Meanwhile, the model has been extended and applied to real buildings, such as a data centre [329] and an atrium [325], .

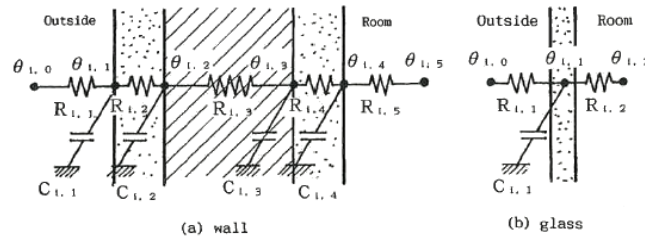


Figure 5.8: Resistance-capacitance model used in the original model: (a) opaque wall – (b) glazing. It was used to calculate the wall surface temperatures necessary to calculate the vertical temperature distribution of the actual time step [327].

In 2003, Gao et al. [321,330] extended the original model to calculate stratification cooling in combination with natural ventilation (hybrid ventilation). In this case only the lower zone, corresponding to the occupied zone, is cooled by multiple air jets, and the upper zones are naturally ventilated (Figure 5.9a). In one iteration step, first wall surface temperatures and convective coefficients are calculated and then these are used to calculate the vertical temperature distribution. In the surface heat balance model no heat capacity is taken into account (Figure 5.9b). The natural ventilation is assumed to be driven by only the buoyancy force, which results from the temperature difference between indoor and outdoor air and two-level openings. In the subsequent years, Gao et al. further investigated some assumed parameters used in the thermal-zonal model: the convective heat transfer coefficient [331] and the heat transfer factor between two adjacent zones in the zonal model due to temperature difference and turbulent penetration [319,332].

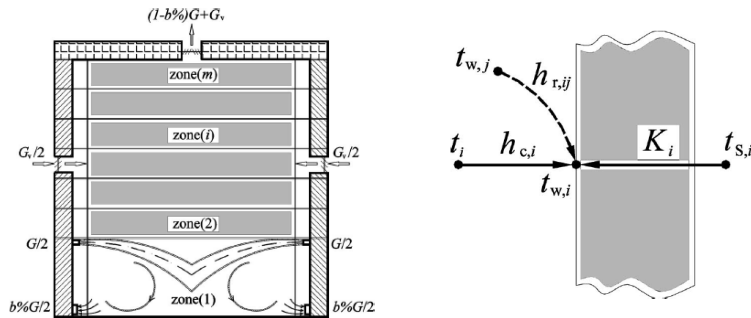


Figure 5.9: [a] Problem considered by Gao et al. [b] Model used to calculate the wall temperature by Gao et al. As can be noticed, the wall is treated as 'steady-state' [321].

In the same period, (2006) Huang C. [323] et al. and (2009) Wang X. et al. [322] also extended the original model to calculate stratification for hybrid ventilation. They incorporated a sub-model including wind-driven and temperature-driven natural ventilation and a sub-model for a cooling jet affected by an indoor heat source. In the surface heat balance model no heat capacity was taken into account and heat losses through the building envelope were taken into account

by providing a value for this heat flux. These authors further criticized a number of assumptions that have been made in the original model. The first criticism was that wall temperatures were provided and constant. From the original papers however, it was seen that a model was suggested to take into account unsteady conditions. Therefore, it is unclear whether the authors read the papers from Aria et al. [327] and Takemasa et al. [328] as there were no references to these sources in their paper. It is also unclear whether the authors meant that the wall temperature in the previous model was solved separately from the zone temperatures, since they used the zone temperature of the previous time step. The second criticism was that in the original model the humidity transfer had no effect on the temperature distribution. Although they mention that they improved the original model by including the aforementioned influence, it is unclear how they improved the model. Also no equations were provided to account for humidity transfer.

Aims of this thesis

In this work, the thermal-zonal model of Togari is used to estimate stratification during intermittent heating. However, to estimate the preservation conditions in a space, in addition to the temperature variation, the humidity variation in the space needs to be predicted. In the original thermal-zonal model, there were no equations for moisture transport. To be able to estimate the humidity stratification, the following transport equations were added to the thermal-zonal model as described by Togari et al. [66] (paragraph 5.2.4):

- addition of moisture transport in the air. Hereby the air was assumed a mixture of dry air and water vapour, each component (vapour and dry air) obeying the ideal gas equation.
- addition of moisture flux coming from a wall.

Furthermore, the model was coupled with a BES-software. The use of the zonal model together with the BES-software TRNSYS is explained in detail in paragraph 5.3. The coupling builds upon the existing simulation environment of TRNSYS (*Simulation Studio*). The model is written in C++ and is compiled as a component for the BES-software TRNSYS v17. The different sub-models, which are also shown in the flowchart (Figure 5.11) are solved as follows:

- Sub-model for wall heat transfer: The conductive heat transfer is solved by the Conduction Transfer Function (CTF) method (paragraph 4.3.2). To calculate the convective heat transfer, convective coefficients can be constant, temperature-dependent (a possibility in TRNSYS) or defined by the user in the form of an equation. The radiative heat transfer can be calculated by a star network method or by the more detailed Gebhart method (Annex 5.B).
- Sub-model for wall currents: The equations described by Togari et al. [66] are solved by the newly developed component.
- Sub-model for natural ventilation: Natural ventilation is calculated by a component available in the TRNSYS library (e.g. LBL model).
- Sub-model for primary air stream: Because the description of jet model implemented by Togari et al. was very concise and because no component was available in TRNSYS, a sub-model to include the mass and heat flow added by a non-isothermal free jet

was implemented in the same component as the thermal zonal model. This is described in 5.2.3.

Tables 5.1 and 5.2 summarize a comparison of the sub-models for surface heat balance, the jet and natural ventilation, applied in this work to the other models earlier presented in literature.

Table 5.1: Comparison of the sub-models used for surface heat balance, the jet and natural ventilation.

	Surface heat balance	Jet flow	Natural ventilation
Original model	Non-steady	Free non-isothermal air jets presented by Koestel. Not described in the paper.	-
Gao et al.	Steady	Model for multiple air jets	Natural ventilation by buoyancy
Wang et al.	Steady	-	Natural ventilation by buoyancy and wind
This work	Non-steady	Non-isothermal jet typical for a heating with air in a church building	Natural ventilation by buoyancy and wind

Table 5.2: Comparison of the sub-models used in the surface heat balance to calculate wall conduction, indoor convection and indoor radiation.

Wall conduction	
Togari et al.	RC-model
Gao	Steady by providing a heat transfer coefficient that accounts from outdoor air to the interior surface. (i.e. outside convection and radiation included)
Wang	Steady by providing the heat conduction per area (W/m ²)
This work	Non-steady: Conduction Transfer Function (CTF) method (§4.3.2)

Convection from interior wall surface K to layer I	
Togari et al.	Convection coefficient is constant
Gao	Convection coefficients outside the air-conditioned zone are temperature-dependent. Convection coefficients for air-conditioned zone are obtained using the Churchill and Usagi approach [333].
Wang	Convection coefficient is constant
This work	Convective coefficients can be constant or temperature-dependent (both possibility in TRNSYS) or provided by an user defined equation. In this work

	the second option is used and a TRNSYS-model was written by the author themselves. In case of natural convection, the equations presented by Alamdari and Hammond [96] were used. In case of a jet flow, convective heat transfer coefficients were predicted using the expressions presented by Beausoleil-Morrison [333]. (eq. Annex 5D)
--	--

Indoor radiation	
Togari et al.	Gebhart's Method: Direct + indirect radiation With $a_r = \dots (\sum_k (\epsilon_k F_{i,k} + \sum_l \rho_l F_{i,l} g_{l,k})) (T_{w_k} - T_{w_i})$
Gao	View factor ($F_{i,k}$) calculated by the ray tracing with a Monte Carlo method With $a_{r_{i-k}} = \frac{5.67E^{-8}(T_{w_k}^4 - T_{w_i}^4)}{(\frac{1-\epsilon_i}{\epsilon_i A_{w,i}} + \frac{1}{F_{i,k} A_{w,i}} + \frac{1-\epsilon_k}{\epsilon_k A_{w,k}}) A_{w,i}} (T_{w_k} - T_{w_i})$
Wang	Gebhart's Method: Direct + indirect radiation (includes one-time reflective radiation). The radiative heat transfer is linearized and holds: $4T_m^3 \epsilon_i 5.67E^{-8} \sum G_{ik} (T_{w_k} - T_{w_i})$
This work	Two methods are available in the building model in TRNSYS: a star network method or by the <u>more detailed Gebhart method</u>

5.2 Mathematical Description of the Thermal-Zonal Model

Because the description of the original model was concise, an outline of the calculation method for the original thermal zonal model is described here in detail.

5.2.1 The Original Model of Togari et al.

In this model, a zone is divided into a finite number of horizontal layers. The horizontal temperature of each layer is assumed to be uniform, except for the regions affected by supply air jet ventilation. Each layer consists of a core cell and wall cells, as shown in Figure 5.10. The core cell represents the mainstream air flow. Where the layer is bounded by a wall, a virtual wall cell is defined which accounts for the mass flows in the boundary layer at the wall. The wall cell is called 'virtual' as no separate volume or cell is defined in the geometric model of the thermal zone.

There is an exchange of mass and heat Between a "wall cell" and a "core cell". The method considers the three most significant paths for the heat and mass transfer (Figure 5.10): (1) heat and mass transfer between the layer and a wall surface, (2) heat transfer and air movement between the different layers and (3) heat transfer through the wall. Flows are defined as positive in the upward direction and from the wall cells to the layers.

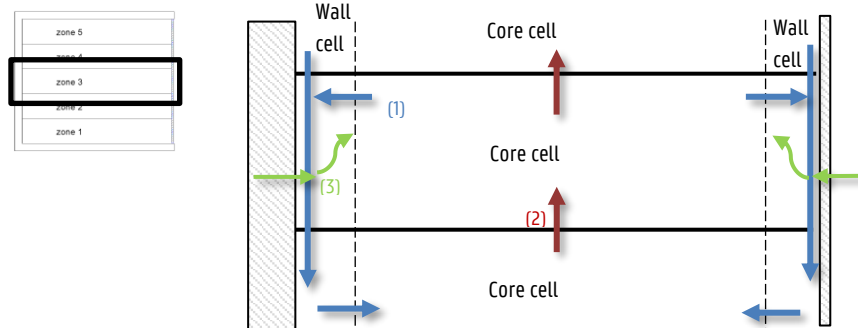


Figure 5.10: Schematic representation of the division of the zone into core cells and wall cells and the three major paths for heat and mass transfer.

A flow chart of the calculation procedure is shown in Figure 5.11. Firstly, data about the geometric model and initial conditions are specified. These initial conditions are the layer temperature and mass flow between the layers. Secondly, at every time step changed boundary conditions and wall surface temperatures need to be provided. Once all these values are known, the thermal-zonal model can start the calculation by solving the different sub-models one by one.

When a primary airstream is present (e.g. a jet) the mass flow and temperature of the primary airstream at the position entering a layer, first need to be calculated using layer temperatures of the preceding time step. One iteration loop then starts in which the temperature for every layer is calculated. The iteration loop consists of three sub-models. To start, the mass and heat transfer along interior surfaces of walls is calculated, which accounts for the near-wall flow. Next, the mass and heat balance for every core cell is determined by the sub-model for mass flow and by the sub-model for heat flow. Based on these three sub-models, the temperature for every layer is determined. This iteration loop is repeated until the algorithm converges to a solution.

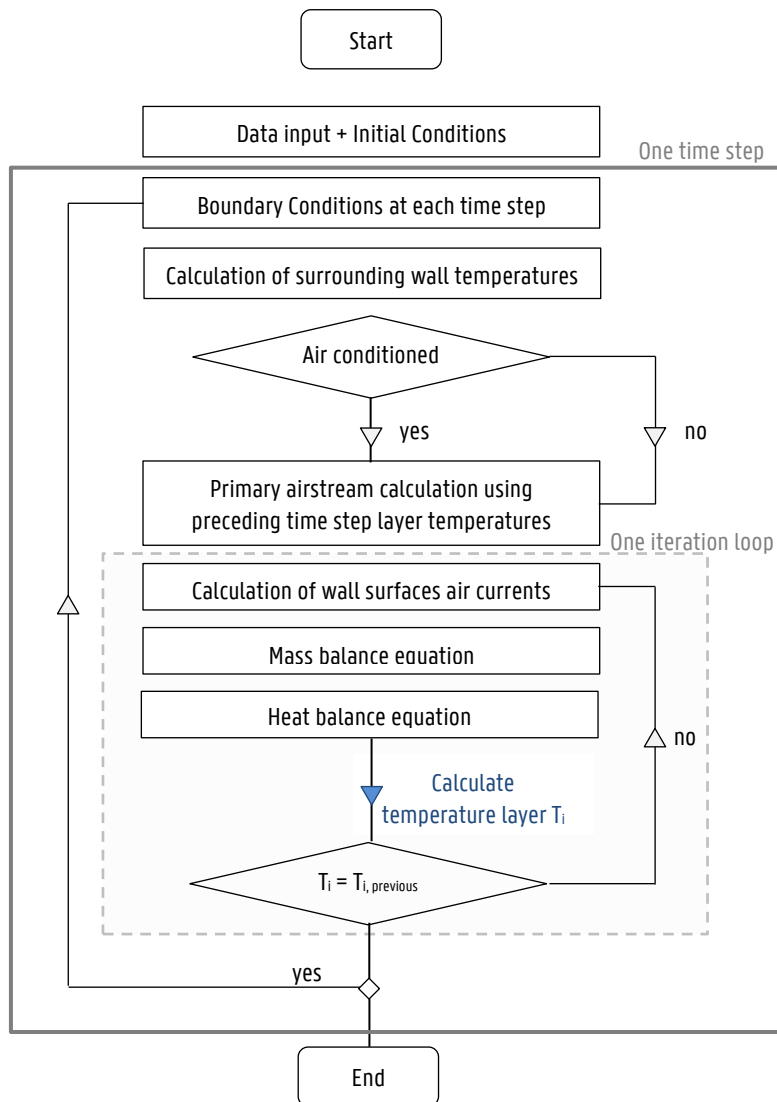


Figure 5.11: Flow chart used by Togari et al.

Sub-model for mass and heat transfer along interior surfaces of walls

If the inner surface temperature is not the same as the indoor temperature, a downward or upward airflow will be induced near the vertical wall. The heat transfer and mass flow along the surface are modelled using a so-called wall current model. This model assumes that the convective heat transfer drives a mass flow ($m_{\text{out}(i,K)}$) with an average temperature ($T_{D(i,K)}$) from layer i (core cell) to its related boundary layer at wall K (virtual wall cell).

To calculate the mass flow $m_{\text{out}(i,K)}$ and the temperature $T_{D(i,K)}$, the following assumptions are made:

- The mass transfer along the wall is modelled using a wall current model, based on the boundary layer theory for natural convection for a vertical wall. More specifically, it is based on the 1/7-law described by Eckert and Jackson [334] which counts for turbulent free convection along a flat plate. Based on their theory, the flow temperature of the air entrained from layer i to the corresponding current of wall K is calculated as follows (see appendix 5A):

$$T_{D(i,K)} = 0.75T_{(i)} + 0.25T_{w(i,K)} \quad (5.6)$$

- The rise or fall in temperature $T_{D(i,K)}$ in the boundary layer is dependent by the heat flow to the wall. To calculate the mass flow $m_{\text{out}(i,K)}$, the equation for a convective heat flow ($q_{w(i,K)}$) between a surface and its environment is used (5.7). By setting this heat flow equal to the heat flow leaving or going into layer i (5.8), and replacing $T_{D(i,K)}$ by the equation from above (eq. 5.6), $m_{\text{out}(i,K)}$ can be calculated as following:

$$q_{w(i,K)} = h_{C(i,K)} \cdot A_{(i,K)} \cdot (T_{w(i,K)} - T_{(i)}) \quad (5.7)$$

$$q_{w(i,K)} = C_i \cdot m_{\text{out}(i,K)} \cdot (T_{D(i,K)} - T_{(i)}) \quad (5.8)$$

$$m_{\text{out}(i,K)} = 4 \frac{h_{C(i,K)} \cdot A_{(i,K)}}{C_i} \quad (5.9)$$

Where	$q_{w(i,K)}$	heat flow [W]
	$T_{w(i,K)}$	average surface temperature of the wall K adjacent to layer i [$^{\circ}\text{C}$]
	$T_{(i)}$	average temperature of the layer i [$^{\circ}\text{C}$]
	$T_{D(i,K)}$	bulk temperature of the mass flow $m_{\text{out}(i,K)}$ [$^{\circ}\text{C}$]
	$h_{C(i,K)}$	heat convection coefficient [$\text{W}/\text{m}^2\text{K}$]
	$A_{w(i,K)}$	area of wall K adjacent to layer i [m^2]
	C_i	specific heat of the air in layer i [$\text{J}/\text{kg}\cdot\text{K}$]
	$m_{\text{out}(i,K)}$	mass flow leaving layer i to wall K [kg/s]

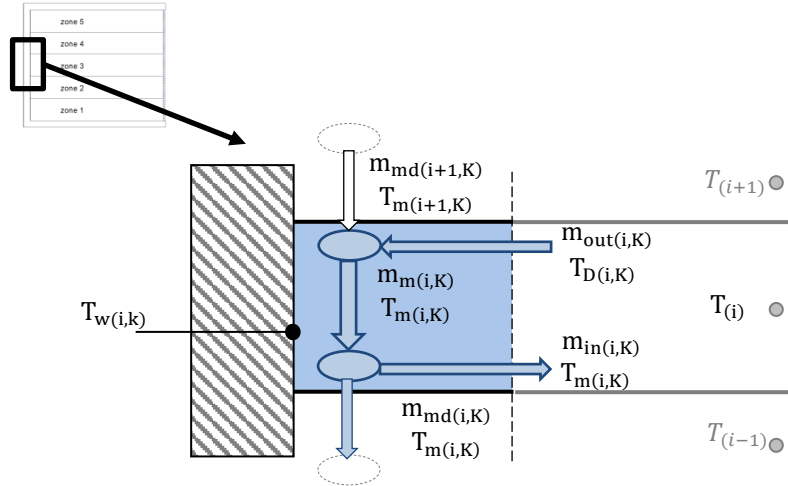


Figure 5.12: Schematic representation of the wall currents and air mass flows in one layer in case there is a downward stream along the wall. Flow streams belonging to layer i and wall K are indicated in blue.

If the current is downward, as shown in Figure 5.12, the current flows from wall cell $_{k,i+1}$ to wall cell $_{k,i}$. This flow will be mixed with the flow $m_{out(i,K)}$ coming from layer i . The same analogy holds if the current is upwards. The mass $m_{m(i,K)}$ and an average temperature $T_{m(i,K)}$ of the mixed flow is calculated as following:

$$m_{m(i,K)} = m_{out(i,K)} - \min(m_{md(i+1,K)}, 0) + \max(m_{md(i-1,K)}, 0) \quad (5.10)$$

$$T_{m(i,K)} = \frac{m_{out(i,K)} T_{D(i,K)} - \min(m_{md(i+1,K)}, 0) T_{m(i+1,K)} + \max(m_{md(i-1,K)}, 0) T_{m(i-1,K)}}{m_{m(i,K)}} \quad (5.11)$$

Where $m_{m(i,K)}$ mass of the wall current of wall K adjacent to layer i [kg/s]
 $m_{md(i\pm 1,K)}$ mass of the wall current of wall K coming from the layer above ($i+1$) or the layer below ($i-1$). The value is negative in case this current is downward and positive in case this current is upward [kg/s]
 $T_{m(i,K)}$ the temperature of the wall current of wall K adjacent to layer i [°C]

Some of the air of this current $m_{m(i,K)}$ may return to the air layer i ($m_{in(i,K)}$) and some may continue to the cell above or below ($m_{md(i,K)}$), depending on the direction of the current flow. The splitting of the mass $m_{m(i,K)}$ into $m_{in(i,K)}$ and $m_{md(i,K)}$ is defined by the ratio $P(i,K)$.

$$m_{in(i,K)} = (1 - P_{i,K})m_{m(i,K)} \tag{5.12}$$

$$m_{md(i,K)} = P_{i,K}m_{m(i,K)} \tag{5.13}$$

In case the airstream is downward, the ratio $P(i,K)$ is dependent on the relationship between the air temperature in layer i and in layer $i-1$. When the airstream is upwards, the ratio is dependent of the temperature in layer i and layer $i+1$. Table 5.3 presents the criteria for the airflow pattern, and how the value for ratio $P(i,K)$ is determined. The justification is described or a downward airstream along the wall. The same justification holds in case the airstream is upwards. When the temperature of the mixed air current $T_{m(i,K)}$ is higher than the temperature in the same layer, the mixed airstream will flow back into the core cell. When the temperature of the mixed air current $T_{m(i,K)}$ is lower than temperature in the same layer, but higher than the temperature of the next layer, a part of the mixed stream will flow back into the core cell, and a part will flow downwards along the wall. In case the temperature of the mixed air current $T_{m(i,K)}$ is lower than the temperature of the same layer and the temperature of the next layer, the mixed stream will completely flow into the next layer, where it will entrain mass $m_{out(i,K)}$ of the layer i [335].

Table 5.3: Criteria for the airflow pattern.

Flow direction	Temperature conditions	$P_{i,K}$
Descending	$T_{m(i,K)} \geq T_{(i)}$	0
	$T_{(i)} > T_{m(i,K)} > T_{(i-1)}$	$\frac{T_{(i)} - T_{m(i,K)}}{T_{(i)} - T_{(i-1)}}$
	$T_{m(i,K)} \leq T_{(i-1)}$	1
Ascending	$T_{m(i,K)} \leq T_{(i)}$	0
	$T_{(i)} < T_{m(i,K)} < T_{(i+1)}$	$\frac{T_{m(i,K)} - T_{(i)}}{T_{(i+1)} - T_{(i)}}$
	$T_{m(i,K)} \geq T_{(i+1)}$	1

Sub-model for mass balance between horizontal layers

Figure 5.13 represents the different mass flows from and to core cell of the layer. The calculation of the mass balance in every layer begins with the lowermost layer. The mass balance for layer i is calculated by:

$$0 = m_{source} + \sum_{K=1}^m m_{currents,K} + m_{layers} \tag{5.14}$$

Where m_{source} net air mass flow from a source or to a sink [kg/s]
 $m_{current}$ net air flow between the wall current and the zone,
 $=m_{in(i,K)} - m_{out(i,K)}$ [kg/s]

m_{layer} net air flow to the layer underneath (m_{i-1}) and above (m_j) kg/s
 $= m_{i-1} - m_j$ [kg/s]
 $m_{\text{out}(i,K)}$ mass flow from layer i to wall current of wall K, kg/s
 $m_{\text{in}(i,K)}$ mass flow from wall current of wall K to layer i, kg/s

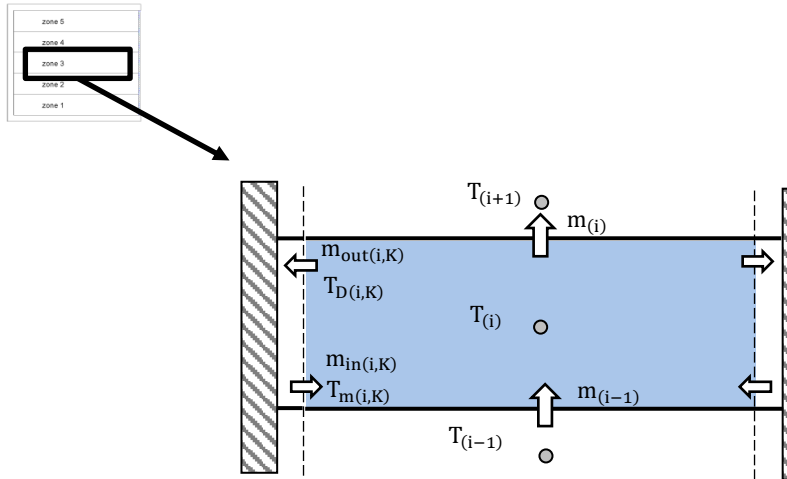


Figure 5.13: Schematic of the wall currents and air mass flows in one layer in case there is a downward stream along the wall.

Sub-model for heat balance between horizontal layers

Similar to the mass flows, the heat balance can be written as:

$$V_i \frac{(\rho C)T_i - (\rho C)T_i^{\text{prev}}}{\Delta t} = Q_{\text{source}} + Q_{\text{layer}} + Q_{\text{currents}} + Q_b \quad (5.15)$$

Where

V_i	volume of layer i [m ³]
Δt	time step [s]
prev	value of the previous time step
Q_{source}	heat sources or sinks [W]
Q_{layer}	heat flow due to mass transport between layer i and layer i-1 and between layer i and layer i+1 [W]
Q_{current}	heat flow between the core cell and the wall currents representing the heat flow by convection along vertical walls [W]
Q_b	heat flow by temperature difference between adjacent layers and by penetrative convection between adjacent layers. In case of inversion between layers, the heat flow becomes larger due to instability

As can be seen in the heat balance equation a term Q_b is added. This term represents the heat flow by penetrative convection between two adjacent layers. In case of inversion between layers, the heat flow becomes larger due to instability. The term is calculated as follows:

$$Q_b = C_b A_b (T_{(i-1)} - T_{(i)}) \quad (5.16)$$

Where: C_b the convective heat transfer coefficient at the interface between two layers [319]
 A_b cross section area of the top or bottom layer [m²]

Writing out the individual terms in the equation, the heat conservation equation becomes:

$$\begin{aligned} V_i \frac{(\rho C)T_i - (\rho C)T_i^{\text{prev}}}{\Delta t} &= Q_{\text{source}} \\ &+ \sum_{k=1}^m C_{m,i,k} \cdot m_{in,i,k} \cdot (T_{m,i,k}) - \sum_{k=1}^m C_{m,out,i,k} \cdot T_i \\ &+ C_{b,i} \max(0, m_{i-1}) \cdot (T_{i-1}) + C_{b,i} \min(0, m_{i-1}) \cdot (T_i) \\ &- [C_{b,i} \max(0, m_i) \cdot (T_i) + C_{b,i} \min(0, m_i) \cdot (T_{i+1})] \\ &+ C_{b,i} A_{b,i} (T_{i-1} - T_i) + C_{b,i+1} A_{b,i+1} (T_{i+1} - T_i) \end{aligned} \quad (5.17)$$

The values for the mass flows $m_{in,i,k}$, $m_{out,i,k}$ and m_i and their corresponding temperature are derived from the former described equations. It must be mentioned that for the bottom and top layer, convective heat transfer along the floor and ceiling surfaces are also included. The value for the surface A_b is obtained from the geometric model. The only unknown is the value for the heat transfer factor C_b .

Togari et al. [66] suggested the following values for the term C_b : when a stable temperature stratification is formed, 2.3W/m²K, and in case an unstable temperature stratification is formed, 112W/m²K. However, Togari et al. [66] stated that further research was needed to determine a more accurate value for C_b . From that point of view, these authors started a sensitivity analysis. They observed that the value of C_b had a small effect on the vertical temperature difference as long as air transfer is active between the layers. However, in case stable temperature stratification is formed and air flow rates between layers become small, the value of C_b has a larger effect on the vertical temperature difference. In this context, Gao et al. [319] searched for a physical definition of the heat transfer factor. They stated that the one-dimensional heat transfer Q_b represents the heat transfer between adjacent air layers due to the combined diffusion of laminar and turbulent conduction and that the term C_b can be expressed by the following theoretical equation:

$$C_b = \mu_m \left(\frac{\lambda_a}{l \mu_m} + \frac{c_p \cdot \mu_t}{Pr.l \cdot \mu_m} \right) \quad (5.18)$$

Where: λ_a thermal conductivity of air [W/(m.K)]
 l a characteristic length, defined as the height of a layer [m]
 Pr Prandtl number [-]
 μ_m and μ_t molecular and turbulent viscosity

Based on this formula, they found a linear relationship between the factor C_b and the turbulent viscosity ratio μ_t/μ_m , shown in Figure 5.14. The value for C_b is calculated by the CFD method.

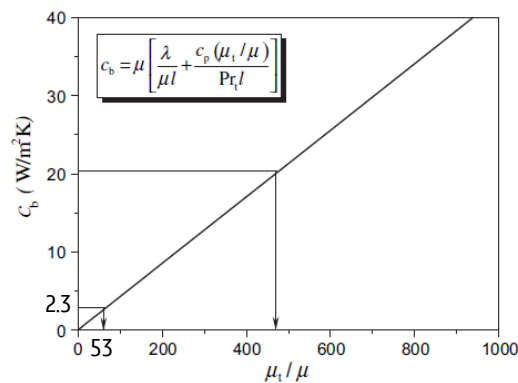


Figure 5.14: Linear relationship between the heat transfer factor C_b and turbulent viscosity ratio μ_t/μ_m , provided by Gao et al. [319].

5.2.2 Addition of Equations for Infiltration

Due to pressure differences, air will penetrate through small cracks, unintentional openings and through the normal use of doors [43]. Air infiltration is due to wind-driven or buoyancy-driven infiltration. Buoyancy-driven infiltration is due to pressure differences caused by air density differences, which in turn are due to temperature differences. The library of TRNSYS contains models to estimate the infiltration rate. The infiltration rate was then used as input in the thermal-zonal model. Descriptions of the equations making up this model can be found in Annex 5B.

5.2.3 Addition of a Jet Flow model for Non-Isothermal Free turbulent Jets

A free jet is principally a jet that flows in an infinitely large space and is not affected by surroundings [336,337]. This type of jet can be used for heating a large space like a church building. For this reason, heat transfer and mass equations of this type of jet were implemented in the zonal model. Figure 5.15 illustrates the principle of how the jet flow is integrated and calculated in the thermal-zonal model.

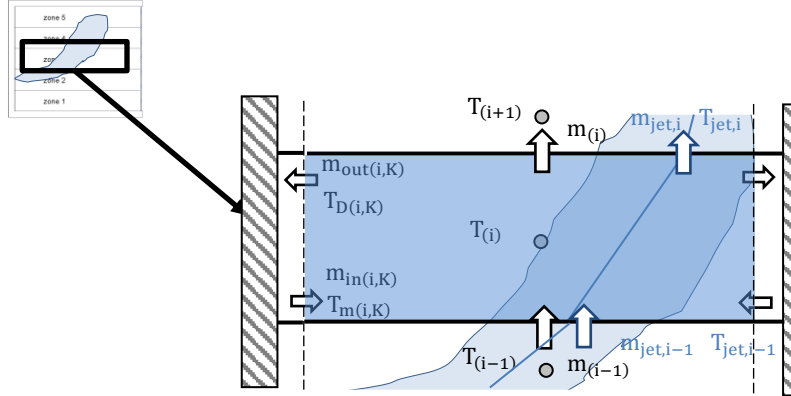


Figure 5.15: Schematic of jet flow in the thermal-zonal model.

The mass balance becomes:

$$0 = m_{source} + \sum_{k=1}^m (m_{in,i,k} - m_{out,i,k}) + m_{i-1} - m_i + m_{jet,i-1} - m_{jet,i} + m_{jet_in} + m_{jet_out} \quad (5.19)$$

Where $m_{jet,i}$ is the total air flow of the jet at the interface layer i and $i+1$
 $m_{jet_in} + m_{jet_out}$ mass added when there is an inlet opening, so the air of the jet is added the layer i . The last term is the mass leaving when there is an outlet opening, so the air is subtracted from layer i .

The following terms were added to the heat balance. The last two terms are non-zero in case there is a supply or an outlet.

$$\begin{aligned} V_i \frac{(\rho C)T_i - (\rho C)T_i^{prev}}{\Delta t} = & \\ & + Cmax(0, m_{jet,i-1})(T_{jet,i-1}) + \dots + \min(0, m_{jet,i-1})(T_{jet,i}) \\ & - Cmax(0, m_{jet,i})(T_{jet,i}) + Cmin(0, m_{jet,i})(T_{jet,i+1}) \\ & + Cm_{jet_in} T_{jet,supply} - Cm_{jet_out} T_i \end{aligned} \quad (5.20)$$

In every layer, the jet enters and leaves with a certain mass and temperature. Thus, to calculate the mass and heat balance in the zonal model, the air flow rate (m_{jet}) and the heat flow rate ($m_{jet}.C.T_{jet}$) are required. To calculate these, the jet trajectory, which is the centreline of the jet, is first determined. Once the jet trajectory is known, it is possible to calculate at which point on the

trajectory the jet enters and leaves a layer. At these intersection points, the mass flow and temperature were calculated.

Jet trajectory

When the jet temperature is different compared to the surrounding air temperature, the diffusion of the jet will be influenced both by the buoyancy forces as well as by inertia forces due to jet momentum [338]. For different types of supply openings, the equation of Frea and Billington [339] is used to calculate the jet trajectory.

$$\frac{y}{\sqrt{A_0}} = 0.226 \left(\frac{x}{\sqrt{A_0}} \right)^{2.61} Ar \quad (5.21)$$

Where	y	vertical distance [m]
	x	horizontal distance [m]
	A ₀	effective area of jet outlet [m ²]
	Ar	Archimedes number [-]

The Archimedes number is calculated as follows:

$$Ar = \frac{g\sqrt{A_0}(T_0 - T_{ref})}{v_0^2 T_{ref}} \quad (5.22)$$

Where	g	gravitational acceleration [9.81 m/s ²]
	v ₀	initial velocity [m/s]
	T ₀	supply temperature [°C]
	T _{ref}	Reference temperature. The average zone temperature, average of all layers, is used [°C]

Air flow rate

The air flow rate entering a layer ($m_{jet,i}$), is calculated as the area under the velocity profile at that position. This velocity profile is a function of the centreline velocity and the spread angle. Since the 1850's, many researchers have been studying how turbulent free jets are developed. According to Straub [340], the development of the jet is subdivided into four major zones. These zones are shown in Figure 5.16 and in the dimensionless graph in Figure 5.17. Each zone is characterized by an equation expressing the centreline velocity decay along the trajectory [338,341-343]. In the first three zones, room air is entrained into the jet and mixed with supply air. In the fourth zone, the jet collapses inward from the boundaries and the supply air is distributed to the room air as the jet disintegrates [344]. A description of each zone and the equation used to define the characteristics of each zone is shown in Table 5.4.

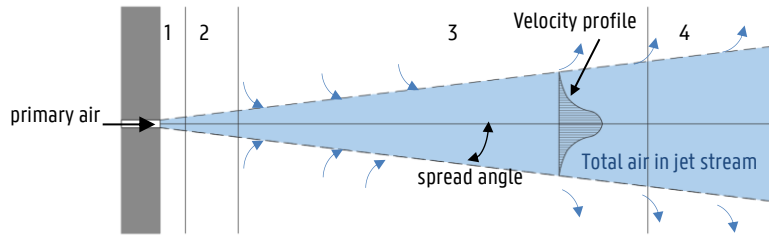


Figure 5.16: Schematic presentation of the four zones in an isothermal jet.

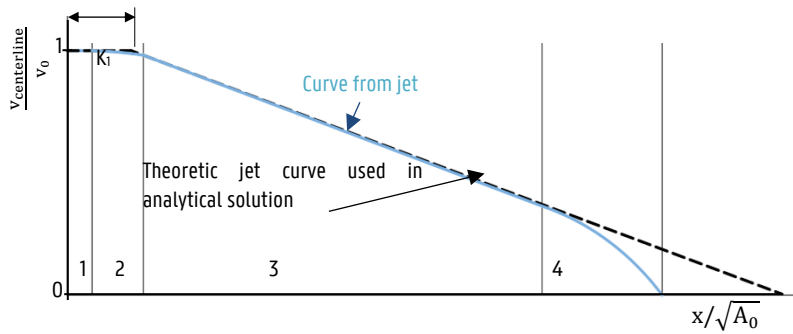


Figure 5.17: Four Zones of expansion of a jet. This graph can be generated for any type of grill. Based on this graph the jet trajectory and velocity profile can be generated.

Table 5.4: Boundaries adopted for the four zones of a free jet and their characteristic velocity decay [338,341,342].

Zone	Range	Velocity	Remarks
1. Core zone	$x \leq 4D$	$\frac{v_{centerline}}{v_0} = 1$	Centreline velocity and temperature are constant and equal to the supply velocity. The mixing of supply air and room air is minimal.
2. Transient zone <i>Characteristic decay region</i>	$4D < x < 8D$ $4D < x < b \cdot 4(b/h)$ (linear)	$\frac{v_{centerline}}{v_0} \sim \frac{1}{x^n}$ $n = 0.33 - 1$	Region in which the jet begins to mix with room air. Induction of room air causes the jet to expand and this in turn causes the centreline velocity to begin to decay. The extent of this region and the value of n depends on the shape of the supply opening and it is usually associated with

			large aspect ratio openings. It is negligible for circular or square openings.
3. Turbulent zone <i>Axisymmetric decay region</i>	$x \leq 25D-100D$	$\frac{v_{\text{centerline}}}{v_0} \sim \frac{1}{x}$	Most of induction of room air occurs in this zone. The flow is dominated by a highly turbulent flow. The spread angle of the jet is constant and depends on the geometry of the opening.
4. Degradation zone	$x > 100D$	$\frac{v_{\text{centerline}}}{v_0} \sim \frac{1}{x^n}$	Velocity and temperature degrade rapidly and the jet diffuses in the conditioned zone.

The 3rd zone is the most important, from an engineering point of view, as the jet enters the area occupied by people and compared to other zones, the jet has the most effect on room air velocities and room induction [342]. Figure 5.18 illustrates the velocity profile in this zone, which is usually expressed as a Gaussian distribution [344]:

$$v_{(x,r)} = v_{\text{centerline}}(x) \cdot \exp\left(-\left(\frac{r(x)}{\delta(x)}\right)^2\right) \tag{5.23}$$

Where $v_{\text{centerline}}(x)$ centreline velocity at position x [m/s]
 $r(x)$ radial coordinate [m]
 $\delta(x)$ distance to the jet boundary which is related to the spread of the profile across the centreline [m].

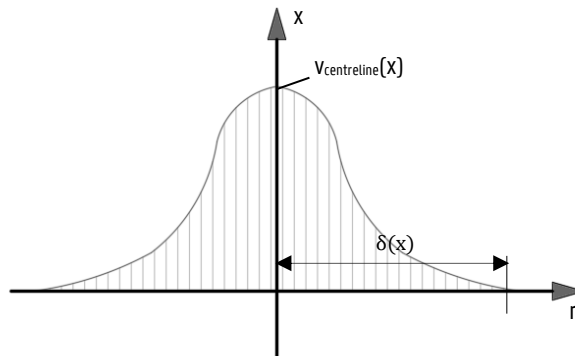


Figure 5.18: Velocity profile of a jet at position x .

The spread and the maximum velocity at the centreline of the jet is dependent on air discharging from the opening into the large enclosure. The following diffuser types are integrated in the zonal model ([345]):

- Circular air jet
- Compact air jet: The jet is formed by square or rectangular openings with a small aspect ratio ($1 < b/h < 40$). Compact air jets are three-dimensional and axisymmetric.
- Linear air jet: The jet is formed by rectangular slots with a large aspect ratio ($b/h > 40$). The jet flow is approximately two-dimensional. Air jets are symmetric in the plane. At some distance from the diffuser, linear air jets tend to transform into compact jets.

The isothermal jets are dependent on the type of opening, the spread and the maximum velocity at the centreline, and can be described by the equations in in Table 5.5.

Table 5.5: Equations used in the TRNSYS-component to calculate mean centreline velocity and flow rate in the third zone. The default value of the spread constant can be redefined in the TRNSYS-component.

Type of jet	Spread $\delta(x)$	Velocity
Compact: Circular jet	0.151x	$\frac{v_{\text{centreline}}(x)}{v_0} = \frac{K_1}{x/d_0}$
Compact 3D-Jet		$\frac{v_{\text{centreline}}(x)}{v_0} = \frac{K_1}{x/\sqrt{A_0}}$
Plane Jet (2D)	0.272x	$\frac{v_{\text{centreline}}(x)}{v_0} = \frac{K_1}{\sqrt{x/h}}$

Where v_0 average velocity at the supply [m/s]
 $v_{\text{centreline}}(x)$ velocity at the centreline [m/s]
 K_1 a constant usually referred to as the throw constant. Theoretical values of the characteristic K_1 depend upon the type of velocity profile equation and supply conditions assumed [345]. It refers to the value indicated in the non-dimensional graph in Figure 5.17. Average values for K_1 are provided in the ASHRAE handbook [342].
 d_0 effective diameter of the supply opening [m]
 h height of the opening

Based on the calculated centreline velocity, the flow rate for unit length at any section of the jet is then calculated by solving the following integral. In the developed TRNSYS-component this was solved by using a Riemann-sum .

$$m_{\text{jet},i} = \rho v_{\text{centreline}}(x_i) \cdot \int_0^\infty \exp\left(-\left(\frac{r(x_i)}{\delta(x_i)}\right)^2\right) r dr \tag{5.24}$$

For the other zones, the following equations were used to calculate the flow rate. It must be mentioned, that these zones are small compared to the third zone.

Table 5.6: Equations used to calculate mean centreline velocity and flow rate in all zones besides the third zone.

Zone	Velocity	Flow rate
1	$\frac{v_{\text{centerline}}}{v_0} = 1$	Spread angle = 0 $Q = Q_0$
2	$\frac{v_{\text{centreline}}(x)}{v_0} = \sqrt{\left(\frac{K}{x/\sqrt{A_0}}\right)}$	Use of spread angle
4	$\frac{v_{\text{centreline}}(x)}{v_0} = \left(\frac{K}{x/\sqrt{A_0}}\right)^2$	Use of spread angle

Temperature of the jet

To define the average temperature of the mass flow of a jet entering and leaving a layer, the temperature profile and the temperature decay need to be first calculated. The temperature profile of a jet is similar, but flatter than the velocity profile. In general, the two profiles are related by the following equation [338]:

$$\frac{v(x, r)}{v_{\text{centreline}}(x)} = \frac{(T(x, r) - T_{\text{ref}})^{1/Pr}}{(T_{\text{centreline}}(x) - T_{\text{ref}})^{1/Pr}} \quad (5.25)$$

Where $T_{\text{centreline}}(x)$ centreline temperature at position x [°C]
 T_{ref} a reference temperature, in this work the average zone temperature is used and not the temperature of each individual layer [°C]

This allows the temperature profile along the path line to be defined. Expressing the temperature profile similar to the velocity profile, as a Gaussian distribution [344] results in:

$$T(x, r) = T_{\text{ref}} + (T_{\text{centreline}}(x) - T_{\text{ref}}) \left[\exp\left(-\left(\frac{r(x)}{\delta(x)}\right)^2\right) \right]^{Pr} \quad (5.26)$$

Based on this equations, the average temperature of the jet entering and leaving a layer i is calculated by the following integral, which is solved in the TRNSYS-component by a Riemann-sum.

$$T_{\text{jet},i} = 1/\delta(x, i) \int_0^\infty T(x, r) r dr \quad (5.27)$$

The temperature decay in the centreline of the jet, needed to calculate the temperature profile at position x is calculated using the following equation.

$$\frac{T_{\text{centreline}}(x) - T_{\text{ref}}}{T_0 - T_{\text{ref}}} = \frac{K_2 \sqrt{A_0}}{x} \quad (5.28)$$

- Where
- T_0 supply temperature [°C]
 - T_{ref} average room temperature [°C], the average of all layers in the zonal model
 - $T_{\text{centreline}}(x)$ temperature at the centreline [°C]
 - K_2 constant calculated by the formula of Shepelev (see [345]):

$$K_2 = \frac{1}{K_1} \frac{(1 + \text{Pr})}{2\pi \cdot 0,082^2} \quad (5.29)$$
 - Pr Prandtl number

5.2.4 Addition of Moisture Transport Equations

To estimate the preservation conditions, next to temperature variation in space also the relative humidity in space has to be known. In the original thermal-zonal model, only mass and heat transport were calculated. To be able to estimate the humidity stratification, following transport equations were added to the original model:

- addition of moisture transport in the air,
- addition of a moisture flux coming from a wall.

Figure 5.19 shows the variables that were added to the thermal-zonal model when adding the two mentioned equations.

- To be able to calculate the moisture transport, for every layer and wall current a humidity ratio is defined, calculated as the partial pressure of vapour in the air to the partial pressure of the dry air.
- The moisture flux coming or going to the wall is expressed as a mass of moisture from or to the layer.

Addition of moisture transport in air

The model of Togari was extended by an equation for moisture conservation. Hereby the air is assumed as a mixture of dry air and water vapour, each component obeying the ideal gas equation. Figure visualises a schematic representation of the vapour flow in a layer.

Considering the time dependency of the moisture content of the air, the moisture balance equation for a layer i can be expressed as:

$$\rho_a V_i \frac{dY_i}{dt} = \rho_a V_i \frac{(Y_i^{t+\Delta t} - Y_i^t)}{\Delta t} = G_{\text{layer}} + G_{\text{currents}} + G_{\text{source}} + G_{\text{inf}} + G_{\text{jet}} + G_{\text{b}} \quad (5.30)$$

Where	G_{source}	vapour flow produced by people, systems activities such as washing... [kg _{moist} /s]
	G_{current}	vapour mass flow from or to the wall current [kg _{moist} /s]
	G_{layer}	vapour mass flow between the layers [kg _{moist} /s]
	G_{jet}	vapour mass flow added by the jet [kg _{moist} /s]
	G_{inf}	vapour mass flow added by infiltration [kg _{moist} /s]
	$+G_{\text{b}}$	it is assumed that the flow is driven by temperature difference. In case of temperature inversion between layers, the flow of the two layers is mixed. In case there is only inversion of moisture content in a layer, no mixing is assumed as the temperature flow is assumed to be dominant. Further research of this assumption can be interesting, but is not done in this dissertation.

The vapour mass flow from or to the wall currents and between the layers is calculated by multiplying the previous calculated mass flow by its absolute humidity.

$$G_{\text{current}} = \sum_{k=1}^m m_{\text{in}(i,K)} Y_{m(i,K)} - \sum_{k=1}^m m_{\text{out}(i,K)} Y_i \quad (5.31)$$

$$G_{\text{layer}} = \max(m_{c,i-1}, 0) Y_{c,i-1} + \min(m_{c,i-1}, 0) Y_{c,i} \\ - \max(m_{c,i}, 0) Y_{c,i} - \min(m_{c,i}, 0) Y_{c,i+1} \quad (5.32)$$

Where Y_i humidity ratio of the layer i [kg/kg]
 $Y_{m(i,K)}$ humidity ratio of wall current [kg/kg]

The vapour mass flow from the jet is calculated by calculating the absolute humidity of the mass flow entering and leaving the layer by calculating the mixture of the absolute humidity of the jet and the absolute humidity of the entrained air at that position.

$$G_{\text{jet},i} = m_{\text{jet},i-1} \cdot Y_{\text{jet},i-1} - m_{\text{jet},i} \cdot Y_{\text{jet},i} \quad (5.33)$$

$$Y_{\text{jet},i} = \frac{m_{\text{jet},\text{in}} \cdot Y_{\text{jet},\text{in}} + m_{\text{entr},i} \cdot Y_i}{m_{\text{jet},i}} \quad (5.34)$$

Where $Y_{\text{jet},i}$ humidity ratio of the mass $m_{\text{jet},i}$ [kg/kg]
 $Y_{\text{jet},\text{in}}$ humidity ratio of incoming mass flow rate of the jet [kg/kg]
 $m_{\text{entr},i}$ entrained air by the jet

Addition of a moisture flux coming from a wall

To integrate the possibility to include the hygrothermal behaviour of the walls, the moisture flux $m_{\text{wall}(i,K)}$ coming or going to the wall is added to the moisture balance equation for a wall current (Figure 5.19). How the hygrothermal behaviour of the envelope is calculated, leading to a value for $m_{\text{wall}(i,K)}$ is a decision of the modeller. Moisture buffering models discussed in Chapter 4 can be used for this task.

The mass $m_{\text{wall}(i,K)}$ is added in the equation to determine the humidity ratio of the wall current $Y_{m(i,K)}$, yielding:

$$Y_{m(i,K)} = \frac{Y_{i(i,K)} m_{\text{out}(i,K)} + \min(Y_{m(i+1,K)} m_{\text{md}(i+1,K)}, 0) \\ + \max(Y_{m(i-1,K)} m_{\text{md}(i-1,K)}, 0) + m_{\text{wall}(i,K)}}{m_{\text{md}(i,K)} + m_{\text{in}(i,K)}} \quad (5.35)$$

It must be mentioned that in case a moisture flux is coming from the floor and/or the ceiling, it is not added to a wall current. It is defined as an additional moisture source in the respective layer.

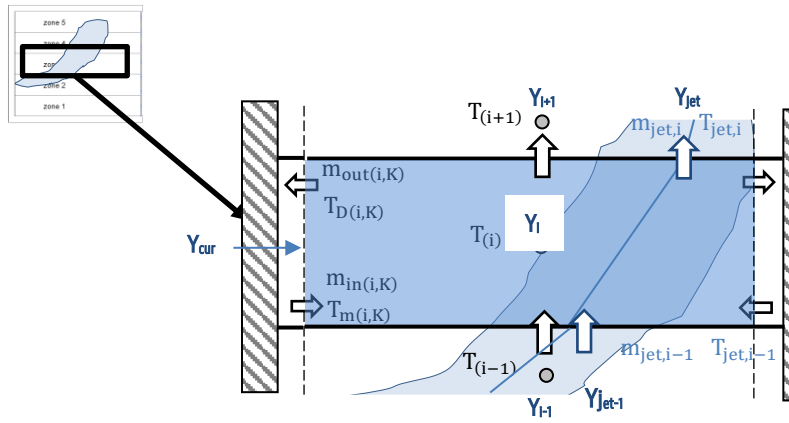


Figure 5.19: Schematic representation of flow in the thermal-zonal model.

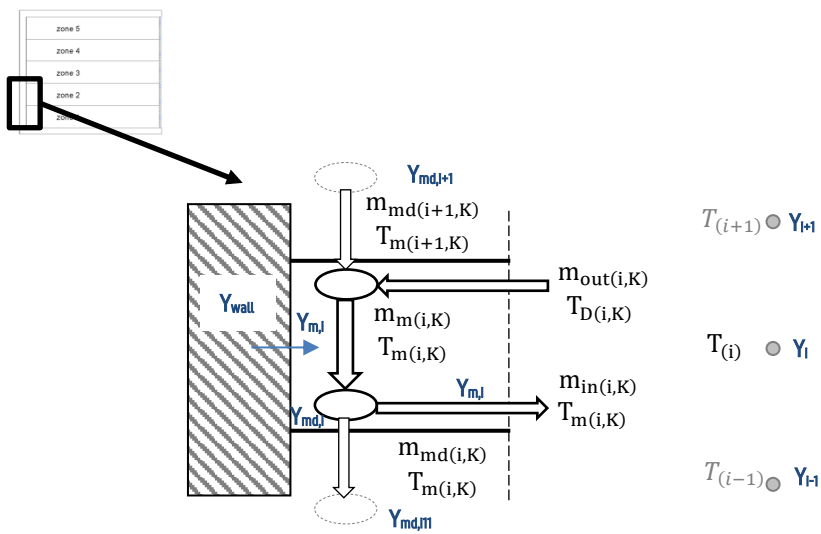


Figure 5.20: Schematic representation of current flow in the thermal-zonal model.

5.3 Coupling of the Thermal-zonal Model with TRNSYS

This section covers the integration of the thermal-zonal model into the TRNSYS simulation environment.

5.3.1 Possibilities of the BES-tool TRNSYS v17

TRNSYS simulates the behaviour of transient systems with a modular structure. In other words, one complex problem is subdivided into smaller sub-problems. In the release of TRNSYS v17, the multi-zone building model (Type 56) has been extended with some new features. A thermal zone can be subdivided into one or more air nodes defining the convective zones. Each air node may have up to two coupling airflows from adjacent air nodes. The heat exchange between building surfaces and the air node is based on convection only, whereas the shortwave radiation distribution and the longwave radiation exchange is performed over the whole radiative zone (Figure 5.21). This new feature simplifies the simulation of stratification effects [268,346].

Another new interesting feature in TRNSYS v17 is the possibility to select a more detailed calculation of the diffuse radiation distribution and longwave radiation exchange within a zone. In the previous version, diffuse radiation distribution was area weighted and longwave radiation exchange within a zone was calculated standard by the starnode model (Annex 5B). In the new version both can be calculated based on view factors, leading to a more accurate estimate of the surface temperature. Because the airflow is driven by surface temperatures, more detailed results of the surface temperature will influence the stratification in the thermal zone.

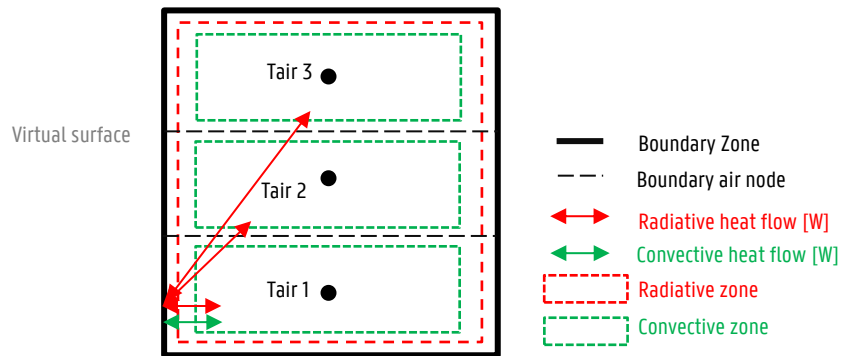


Figure 5.21: One radiative zone subdivided into three air nodes, each with their own convective gain (based on[346]).

5.3.2 Implementation of the Thermal-Zonal Model

As already mentioned, the advantage of TRNSYS is that next to the many standard components which are included in the TRNSYS library, the user has the possibility to write his own components. For this purpose, the thermal-based zonal model of Togari et al., as described and expanded in previous paragraphs is coded in C++.

To include the components in a simulation, they are put into the simulation environment, called the Simulation Studio. The thermal-zonal model is implemented in the Simulation Studio as a new component (Type 223). Parameters, inputs and output values of the model are defined in a so-called proforma file. Required parameters, input and output values for the component are listed in Table 5.7. Parameter values are assigned a constant value during the whole simulation. The first two parameters are the number of layers and the number of walls. Depending on the number of layers and number of walls, an array is defined in which the volume of each layer, the wall temperature and other input values can be set. Contrary, input values are updated every time step and can be coupled to other TRNSYS components in the simulation environment. For instance, the zone temperature, relative humidity, convective heat gain and wall temperature are calculated by the multi-zone building component and then transferred to the thermal-zonal model component. Furthermore, the value of C_b is also defined as input. In the dissertation the values suggested by Togari et al. are used. However, to leave the option open to fill in this value using the CFD method or a database which will perhaps be developed, the value is defined as an input value.

On the two following figures, it can be noticed that different components are used in the simulation model. What is done by the TRNSYS building, by the thermal zonal model and by the EMPD or HAM component is shown Figure 5.22. Figure 5.23 illustrates the principle of how the interaction with these three component is built up in the simulation environment. Firstly, a three-dimensional model is made with the TRNSYS-plugin in the software Sketch Up. This results in a file (.idf) containing geometrical information necessary to calculate the view factors for the radiation between surfaces. In the simulation environment of TRNSYS, the geometry file (.idf) is used both for the TRNSYS building component (type 56) and the thermal-zonal model (type 223). Secondly, boundary conditions are provided for both the building model as the zonal model. An own-written component which calculates the interior convective heat transfer is connected to both components. Furthermore, a component which calculates the moisture flux from or to the wall is connected to the thermal-zonal model (e.g. EMPD or HAM-component). The building-component and the thermal zonal component are coupled in both directions. The type 56 delivers the boundary conditions necessary to calculate the vertical temperature profile. The thermal-zonal model returns a convective heat gain and moisture gain for every layer. A detailed description of the inputs required for both models and how the coupling precisely works is given in the next paragraph.

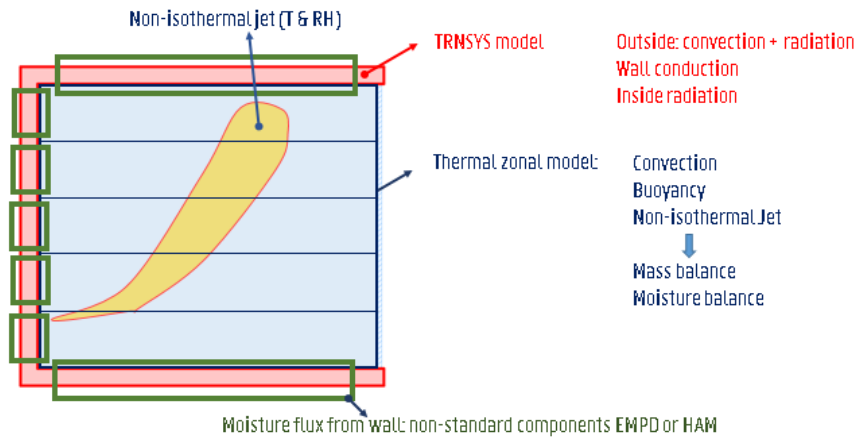


Figure 5.22: Principle of the coupling. What is done by the TRNSYS building, by the thermal zonal model and by the EMPD or HAM component.

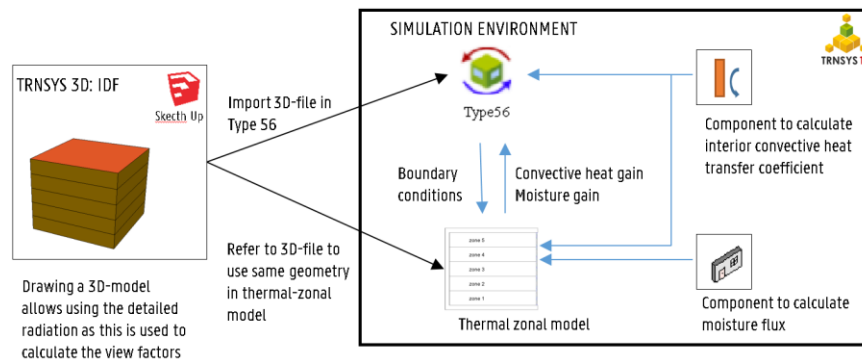


Figure 5.23: Schematic overview of the practical use of the thermal-zonal model in the TRNSYS environment.

Table 5.7: Parameters, input and output values for Type 223. (Green = related to modelling of jet, Blue = related to hygrothermal model).

Parameter Values	
layers	Number of layers in the thermal-zonal model - (= number of air nodes in the building model of TRNSYS)
walls	Number of walls in the thermal model and - building model

height layer [layers]	Height of each layer	m
Area between layers[layers-1]	Interface area between two horizontal layers	m ²
iterations	Maximum number of iterations	-
time step	Time step of the zonal model	s
volume [layers]	Volume of each layer	m ³
area opening	Area of the supply inlet	m ²
hydraulic area	Hydraulic area of the supply outlet (linear jet = h; compact jet = sqrt(area))	m
type jet	Diffuser types. [1] =Linear; [2] = compact	-
K1	Throw constant. Values for K1 can be derived from the table presented in ASHRAE (ASHRAE, 2005)	-
layer inlet	Layer in which the supply inlet is located	-
layer outlet	Layer in which the return air outlet is located	-
layer Infiltration		
layer Exfiltration		
Input Values		
T _{zone} [layers]	Temperature of the zone	°C
AH _{zone} [layers]	Absolute humidity of the zone	kg/kg
T _{wall} [walls]	Temperature of the wall	°C
h _{wall} [walls]	Convective heat transfer coefficient	kJ/m ² K
Q _{conv} [layers]	Convective heat gain for every layer, calculated by TRNSYS	kJ/h
C _b	Heat transfer factor	W/m ² K
m _{walls} [walls]	Moist flux from or to the wall	kg/hr
C _{p,air}	Heat capacity air	J/kg.K
C _{p,vap}	Heat capacity vapour	J/kg.K
h _{ev}	Latent heat vapour	J/kg
m _{jet}	Jet flow rate	kg/h
T _{jet}	Temperature of the jet at the supply	°C
AH _{jet}	Absolute humidity of the jet at the supply	kg/kg
m _{inf}	Infiltration rate	kg/h
T _{inf}	Temperature of the infiltration	°C
AH _{inf}	Absolute humidity of the infiltration	kg/kg
Moisture source[layers]	Moisture source in a layer	kg/hr
Output Values		
G _{gain}	Moisture gain related to the thermal-zonal model	kg/h
Q _{gain, conv}	Convective heat gain related to the thermal-zonal model	kJ/h

5.3.3 Detailed Representation of the Coupling Strategy

The previous paragraphs discussed the thermal-zonal model to calculate the mass transfer between the different air nodes leading to stratification. However, to be able to calculate the

mass, heat and moisture transfer some boundary conditions must be provided. These boundary conditions can easily be provided by the multi-zone model and other TRNSYS components. Figure 5.24 shows an overview of all the data streams and which information is needed for the coupled BES- thermal-zonal model.

1. The first step is providing the input data for the TRNSYS building and the thermal-zonal model. A distinction is made between necessary input data, shown in the first block, and information that is only needed in case a jet flow or in case a moisture flux from the walls is defined. This is shown in block two and three.
 - a. The TRNSYS building model needs geometrical data, properties of the building envelope, outside boundary conditions and the convective heat transfer coefficients.
 - b. For the thermal-zonal model, information of the geometric data is needed. The geometrical model is the same as used for the multi-zone building model (.idf). The thermal-zonal model needs this information to know the positions of all the walls to be able to calculate the wall streams. Furthermore, the same values for the interior convective heat transfer coefficients are needed.
 - c. In case a jet flow of moisture flux is present, this data need to be provided only for the thermal-zonal model.
2. The second step is setting the initial air temperature and relative humidity for every layer in the TRNSYS building model. The model assumes that walls are in equilibrium with the indoor air and therefore the initial interior surface temperatures are the same as the air temperature.
3. Next, necessary boundary conditions are passed by the TRNSYS building component to the thermal-zonal model. The interior surface temperatures and the temperature and absolute humidity of the air nodes act as boundary conditions for the thermal-zonal model. Once the boundary conditions are passed to the thermal-zonal model, the latter calculates the wall currents and solves the heat, mass and moisture transport for all layers until temperature and absolute humidity reach convergence below a step change of $1e-6^{\circ}\text{C}$ and $1e-9\text{kg/kg}$ ³⁰. To achieve, a simple adaptive relaxation technique is used in which is switched between two relaxation parameters; one for under-relaxation and one for over-relaxation.
4. Once convergence is reached, results are passed on to the multi-zone building model to the corresponding air node. To integrate the thermal-zonal model in TRNSYS, the logical approach would seem to make use of the possibility to implement a user defined mass flow between the different air nodes. Instead, a user defined convective heat gain ($Q_{\text{gain,conv}}$) and moisture gain ($G_{\text{gain,conv}}$) were defined by the thermal-zonal model for every air node. The reason was to avoid that the convective heat gain will be calculated twice: once by the thermal-zonal model and once by the multi-zone building model in TRNSYS. Therefore, the convective heat gain from the walls to the air node in the building model in TRNSYS ($Q_{\text{gain,TRNSYS}}$) is subtracted from the total heat gain calculated by the thermal-zonal model

³⁰ If desired, the convergence criteria can be adapted, but increasing the accuracy has influence on the simulation time.

($Q_{\text{gain,zonal model}}$). The residual heat flow will be implemented in TRNSYS as a convective heat gain.

$$Q_{\text{gain,conv},i} = Q_{\text{gain,zonal model},i} - Q_{\text{conv,TRNSYS},i} \quad (5.36)$$

To define the moisture gain in an air node, the moist gain entering the layer is calculated as following:

$$G_{\text{gain},i} = G_{\text{gain,layer},i} + G_{\text{gain,current},i} \quad (5.37)$$

$$G_{\text{gain,layer},i} = G_{\text{layer}} + G_{\text{source}} + G_{\text{inf}} + G_{\text{jet}} \quad (5.38)$$

$$G_{\text{gain,current},i} = Y_{m(i+1,K)} m_{\text{md}(i+1,K)} - Y_{m(i,K)} m_{\text{md}(i,K)} + m_{\text{wall}(i,K)} \quad (5.39)$$

5. In the TRNSYS building model, a new temperature and relative humidity is then calculated for every air node.
6. Step 1,3,4 and 5 are repeated every time step

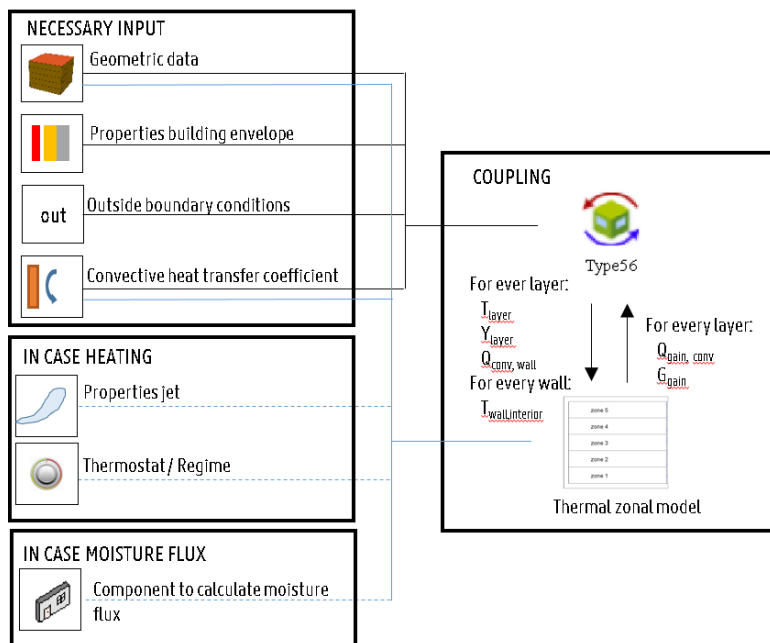


Figure 5.24: Schematic overview of the coupling between the multi-zone building model in TRNSYS and the developed thermal-zonal model.

5.4 Verification Studies

5.4.1 Case Description

To verify the coupled model, and thus the own written component, the cases of the experiment presented in the report of Togari et al. were simulated and compared with the measurements [66]. They performed a scale-model test using a test room (Figure 5.25). The geometrically simple test room has a ground plane of 3m x 3m and measures 2,5m in height. The room consist of insulated boards (three vertical walls, ceiling and floor) and one glass wall. In the wall opposite to the glass wall, two openings were made in the symmetry plane: a supply inlet at 0,625m above the floor and a return outlet at 0,250m above the floor. Air temperatures, and interior and exterior surface temperatures were measured using Cu-Co thermocouples at 160 locations on the symmetry and its perpendicular plane [66,319]. Besides, heat flow sensors coated with aluminium foil were installed to infer the convective heat transfer coefficient [66].

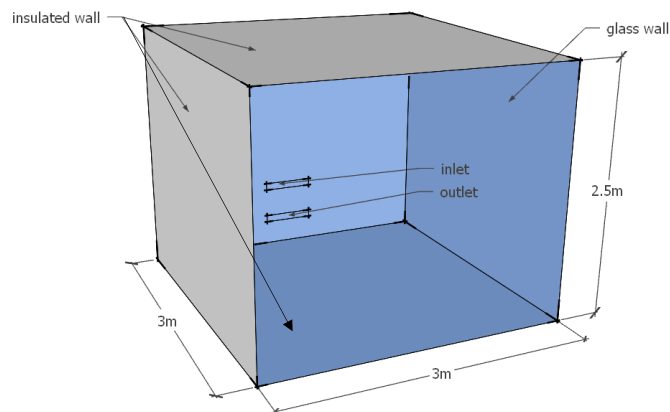


Figure 5.25: Configuration of the test room used in the experiments of Togari et al. [66].

Originally, several configurations were measured in this test room (Table 5.8). In two cases, natural convection was intended. To achieve this condition, outside temperature was abruptly changed (N-11 and N-10). In the other cases, there was forced convection: in three cases hot air was supplied (H-100, H-101 and H-110) and in two cases cool air was supplied (C-200 and C-210). In this dissertation the simulated results of two cases, N10-natural convection and H100-forced convection are presented. These cases were of main interest for heating in a tall building.

Table 5.8: Overview of the case studies performed by Togari et al. Cases used to verify the coupled model are highlighted in grey.

Name Case	Supply air condition					Inlet location	Outside temp
	outlet size	air volume	velocity	temp	momentum		
	[mm x mm]	[m ³ /h]	[m/s]	[°C]	[kg m/s ²]		[°C]
N-11							42 -> 14
N-10							12 -> 42
H-100	500 x 74	150	1,13	40,7	0,053	layer 1	11
H-101	500 x 74	150	1,13	40,7	0,053	layer 5	11
H-110	250 x 74	135	2,03	40,4	0,086	layer 1	12
C-200	250 x 74	135	2,03	12,1	0,095	layer 1	34
C-210	250 x 74	100	1,5	13,8	0,052	layer 1	34

5.4.2 The TRNSYS model

The room described above was fully modelled in TRNSYS. The space is vertically divided into five layers (Figure 5.26). For this verification study, it was chosen to use the same number of layers as used by Togari et al. [66]. In the model described by Togari et al., calculations of the stratification started based on measured wall surface temperatures, while in the model in TRNSYS only outdoor conditions were used. The behaviour of the walls and the inside surface temperature is calculated by TRNSYS. The convective heat transfer coefficients were fixed and the ones measured by Togari et al. This resulted in a k -value of $5.8 \text{ W/m}^2\text{K}$ for glass and of $0.8 \text{ W/m}^2\text{K}$ for the insulated walls. The specific heat capacity for all walls was 840 J/(kg.K) . The radiation is calculated based on view factors (see paragraph 5.5.2 for a discussion about the radiative heat transfer). To verify if the thermal-zonal model was well-defined in TRNSYS, the thermal resistance for the insulated walls and the glass wall were defined by fitting the model for natural convection on measured indoor surface temperatures. Figure 5.27 shows schematically the principle of the two simulated cases.

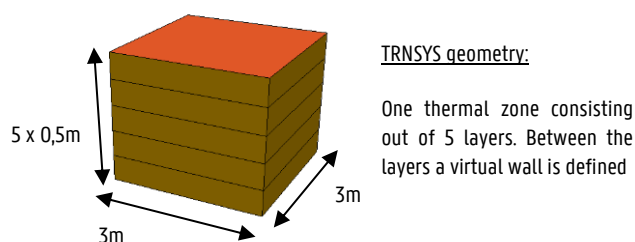


Figure 5.26: The simulation model of TRNSYS, where the room was vertically divided into 5 layers.

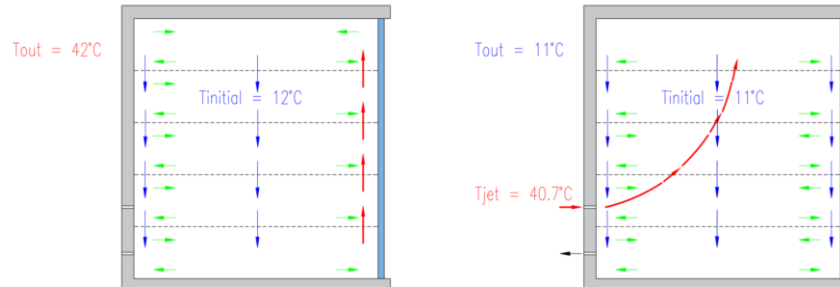


Figure 5.27: Schematic representation of case N10: natural convection (left) and case H100: forced convection (green: to or from walls currents – blue/red: direction of flow for every zone and wall current).

5.4.3 Cases without Moisture Source

Case of natural convection: case N10

In case N10, natural convection was created inside the test room. This was done by raising the temperature outside the room from 12°C to 42°C , while 24 hours later it was again lowered to 12°C . The response of the test room was monitored, while no air was supplied into the room. The mean convective heat transfer coefficient used in the simulation study were the ones measured by Togari et al. [66]: it is 3.5 W/m^2 at the vertical walls and glazing, and 2.3 and $4.6 \text{ W/m}^2 \text{ K}$ at the floor and ceiling, respectively.

Figure 5.28 depicts results of the air temperature for the first nine hours when outdoor temperature was raised from 12 to 42°C ; respectively at 1:00, 2:00, 3:00, 4:00, 5:00, 7:00 and 9:00. The simulated results were compared to the measurements in the test room and to the calculations performed by Togari et al. with the simplified model. Out of Figure 5.28, it can be concluded that the temperatures found by the coupled BES-zonal model were in good agreement with the measurements. Differences between the simulated results and the results presented by Togari et al., can be subscribed to differences in interior surface temperature leading to a difference in mass flows (Figure 5.29 right).

Figure 5.29 (left) shows simulated interior surface temperature and measured interior surface temperatures, which are used by Togari et al. as boundary condition, after two hours as measurements at that time were provided in the paper. The simulated surface temperature of the glass surface was underpredicted for the three lowest layers ($\text{RMS} = 1.25^{\circ}\text{C}$). This deviation has no effect on the flow rate calculation. Because for the glass surface, there was no airflow back to the layer ($m_{in} = 0$), only the value of m_{out} determines the upward current (m_m). In the original model, the value for m_{out} is independent of the surface temperature and therefore, the difference in simulated interior surface temperature has no influence on the wall current. The surface temperature for the insulated walls were in good agreement with the measured wall

surface temperatures (RMS = 0.53°C). However, small deviations were observed leading to a difference in the value for the mass flows (m_{in} , m_m and m_c) and thus layer temperatures.

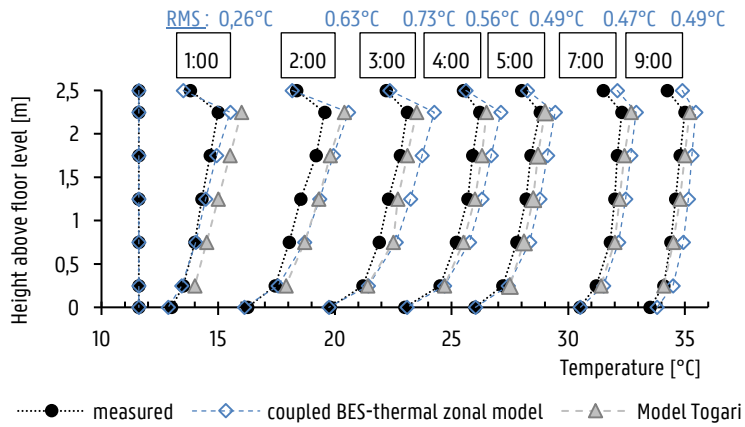


Figure 5.28: The temperature for the first nine hours while heating outside the chamber. Comparison between the measured values and the values calculated by the thermal-zonal model in TRNSYS. Root mean square errors are provided together with the time step.

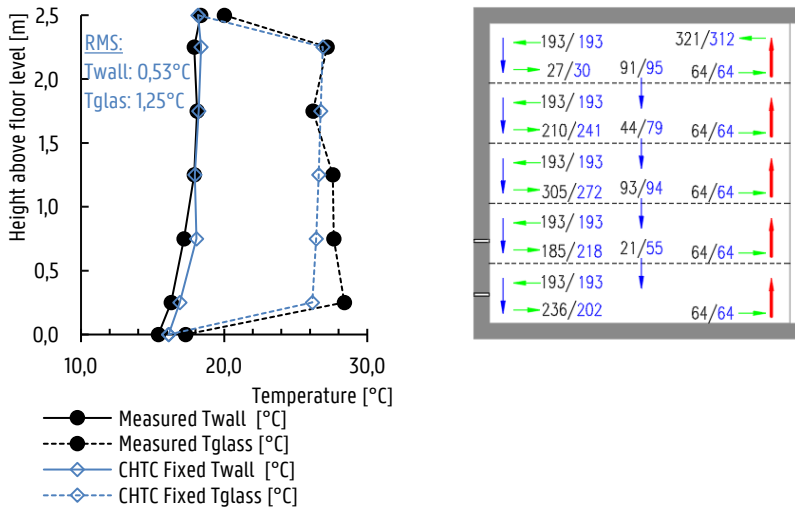


Figure 5.29: Left: Interior surface temperature for the insulated wall and the glass surface. Comparison between the measured values and the simulated values by TRNSYS. Right: Values the mass flow [kg/hr] from the layer to the wall current and between the layers. Comparison between the calculated values by Togari et al. and by the coupled BES-zonal model.

Case of forced convection (Implementation of a jet): case H100

In case H100, the outside temperature of the test room was kept between 11°C and 12°C. Hot air was supplied to the test room at 0h00. The temperature of the supplied air was 40,7°C and the supply air volume was 150m³/h. The convective heat transfer coefficients used in the simulation study were the ones measured by Togari et al. [66]. It is 3.5 W/m²K at the insulated walls, and 2.3 and 9.3 W/m² K at the floor and ceiling, respectively. At the glass surface, the convective heat transfer coefficient for the uppermost layer is 9.3W/m²K, for the other layers it is 5.8W/m²K. Characteristics of the jet and supply were not described for the experiment.

Figure 5.30 shows the measured air temperatures and the air temperatures calculated by the thermal-zonal model and by the simplified model of Togari et al. [66]. The coupled zonal model achieved in predicting the temperature profile during heating with a heated jet flow. Differences between the simulated results and the results presented by Togari et al. have mainly two causes.

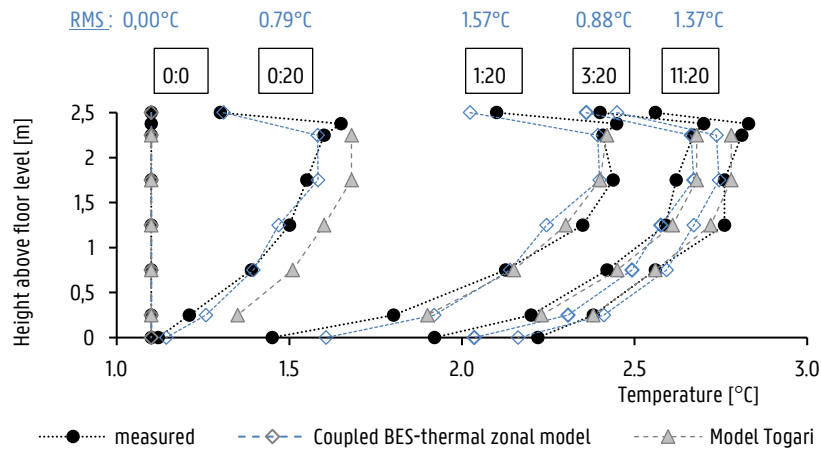


Figure 5.30: The progress of the temperature in case of hot air supply condition (jet).

Firstly, the difference in interior surface temperature leads to a difference in current flows. Figure 5.31 (left) shows simulated interior surface temperature and measured interior surface temperatures, which are used by Togari et al. as boundary condition, after two hours of heating. Measurements at other times were not presented. Glass and wall temperatures were in good agreement with the measured values. As visualized in Figure 5.31 (right), the simulated surface temperature of the interior surfaces were underpredicted, leading to other values for the backflow from the current to the layer (m_{in}).

Secondly, because the characteristics of the real jet and the implemented jet model used by Togari et al. were not described, typical values for the characteristics from literature were used. For the spreading a value of $0.151 \cdot s(x)$ was used (Table 5.5). As a result, other values were found for the flow rate of the jet. Compared to the values presented in the paper for the entrained air flow, significantly lower values were obtained (red numbers in Figure 5.31 (right)). However, since

there was no measurement of these flow rates, it was assumed that the stated values for the jet flow rate are the theoretical values and that these were not validated. To have an idea of the importance of the value of these flow rates, the case study was also calculated with values for the flow rate that approach the values presented in the paper. To do so, the spreading was increased to $0.195 \cdot s(x)$. As a result, higher values for the indoor air were obtained (Figure 5.32) and the indoor air temperature was overestimated.

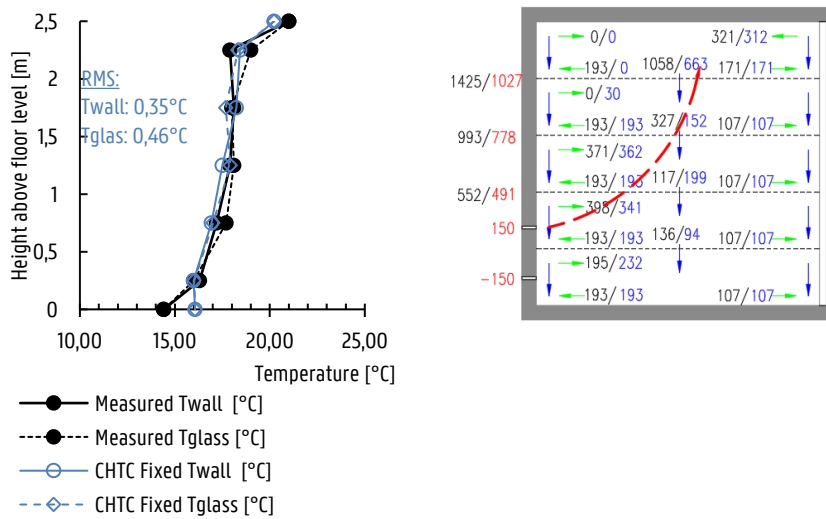


Figure 5.31: Left: Interior surface temperature for the insulated wall and the glass surface. Comparison between the measured values and the simulated values by TRNSYS. Right: Values of the mass flow from the layer to the wall current, by the jet (values left outside wall) and between the layers. Comparison between the calculated values by Togari et al. and by the coupled BES-zonal model.

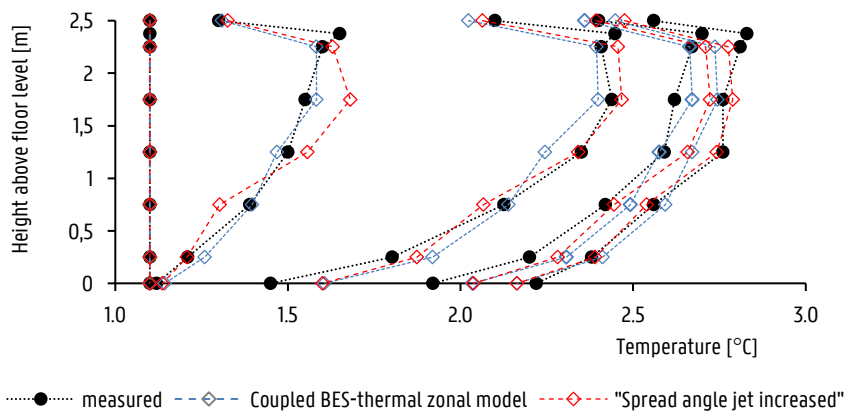


Figure 5.32: The progress of the temperature in case of hot air supply condition (jet) with two different values for the spreading.

5.4.4 Issues Using the Coupled Zonal Model Starting from Outside Boundary Conditions

The influence of Convective Heat Transfer Coefficients

A first point of attention is the influence of the defined value of the heat transfer coefficients. It must be remarked that the convective heat transfer coefficients have an influence on the results of the thermal-zonal model as this is based on convective heat flow.

In the original calculation of the case studies presented by Togari et al. [66], a constant heat transfer coefficient was used to calculate the mass and heat flows. As a consequence, the value of the mass m_{out} is constant during the whole calculation (eq.(5.9)).

- In case of natural convection (case N10) a fixed value of 3.5 W/m²K was chosen for the glass wall and the insulated wall. For the floor and the ceiling, the convective heat transfer coefficient was 4.6W/m²K when heat flow was upward, and 2.3W/m²K when the heat flow was downward.
- In case of mixed convection (case H100) a fixed value of 5.8 (zone 1-4) and 9.3 W/m²K (zone 5) was chosen for the glass wall. For the ceiling, the convective heat transfer coefficient was 9.3W/m²K. For the insulated walls and the floor, the convective heat transfer coefficients were the same as in the case of natural convection.

To reveal the effect of the heat transfer coefficient on the temperature distribution in the room, the two cases used in the verification of the coupled model, N10 & H100, are recalculated using a variable convective heat transfer coefficient. Values for the convective heat transfer coefficients were recalculated every time step dependent on other time-variant parameters like wall temperature and flow regime. In case of natural convection, the equations presented by Alamdari and Hammond [96] were used. These authors suggested correlations for buoyancy-driven convective heat transfer. In case of jet flow, convective heat transfer coefficients were predicted using the equations presented by Beausoleil-Morrison [333] for mixed convection. Equations are given in Annex 5D. This author applied the Churchill and Usagi method, which is a technique commonly used to derive the convective heat transfer coefficient in case of mixed convection. These equations combine the equations of Alamdari and Hammond [96] for natural convection, and of Fisher and Pedersen [347] for forced convection. Although Beausoleil-Morrison classified his equations as fit for mechanically ventilated rooms which are heated or cooled with air – without validation, further research is regarded necessary on free non-isothermal jets [348]. This is however out of scope for this dissertation. In case in future, improved algorithms are developed to predict the convective heat transfer coefficients, it can be easily adapted in the coupled approach used in this work.

Figure 5.33 compares the results for the case of natural convection. Simulated air temperatures for the first nine hours are shown. For both variations, namely fixed and variable convective heat transfer coefficients, the root mean square errors were calculated (Table 5.9). In case the convective heat transfer coefficients were dependent on the interior surface temperatures, smaller root mean square errors were observed. However, the improvement was small. To gain insight into the precise influence on the convective heat gain calculated by the thermal zonal

model, these gains were compared for both variations in Figure 5.34. The largest observed discrepancy is found in layer one and layer two and measures 7W. This leads to a difference of 0.5-0.6°C for the calculated air temperature in these layers.

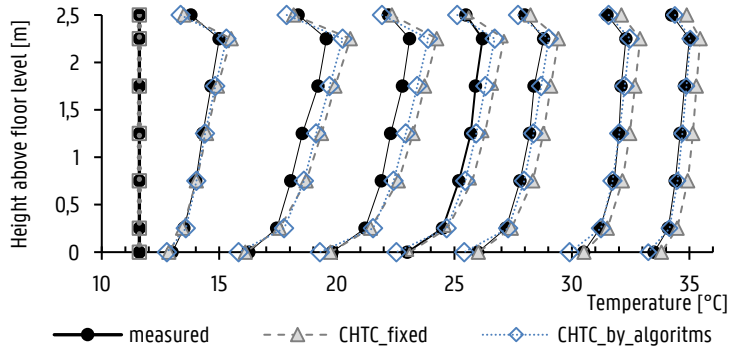


Figure 5.33: Case of natural convection [N10].

Table 5.9: Root Mean Square of the temperature for a constant heat transfer coefficients and for a heat transfer coefficient calculated by the expressions given by Alamdari and Hammond [96].

Time	1:00	2:00	3:00	4:00	5:00	7:00	9:00
Fixed CHTC	0.26	0.63	0.73	0.54	0.55	0.48	0.22
CHTC A&H	0.23	0.52	0.55	0.37	0.30	0.24	0.12

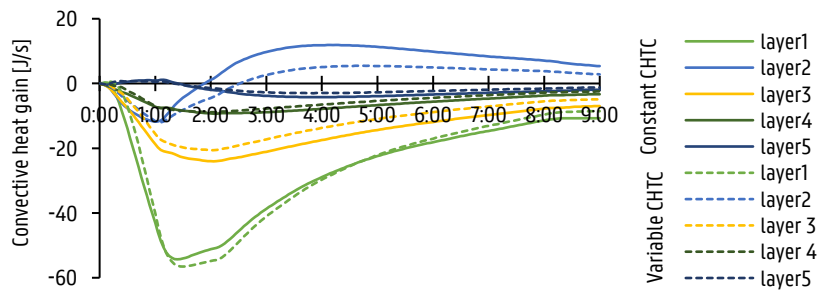


Figure 5.34: Convective heat gain calculated by the thermal zonal model for a constant heat transfer coefficients and for a heat transfer coefficient calculated by the expressions given by Alamdari and Hammond [96].

Figure 5.35 compares the results for the case of a heated jet flow. For this case, the influence of using the algorithms to calculate the convective heat transfer coefficient for each surface instead of using a fixed coefficient was the largest in the first layer. The root mean square error measures about 1°C in case convective heat transfer coefficients were not fixed. Overall, the fixed heat transfer coefficients led to a better estimate in this case (Table 5.10). However, this must be put into perspective because measured values were used in this simulation. If one does not know them and one would use a supposed fixed value, it will depend on how close this fixed value approaches reality. In that case variable coefficients give a decent estimate as shown in the figure below. Finally, convective heat gains are also shown in Figure 5.36. It can also be seen from this figure that the difference between a fixed or a variable convective heat transfer coefficients is small.

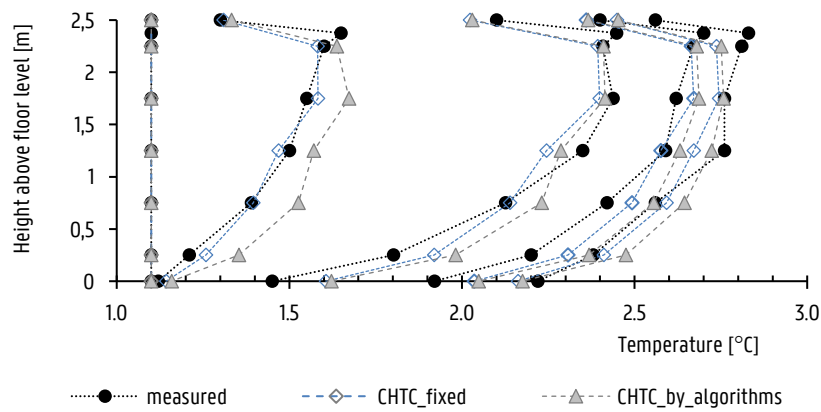


Figure 5.35: Case of forced convection [H100].

Table 5.10: Case of jet flow [H100]. Root Mean Square of the temperature for a constant heat transfer coefficients and for a heat transfer coefficient calculated by the expressions given by Beausoleil-Morisson [333].

Time	0:20	1:20	3:20	11:20
Fixed CHTC	0.37	1.01	0.83	1.04
CHTC B-M	0.95	1.08	1.00	0.70

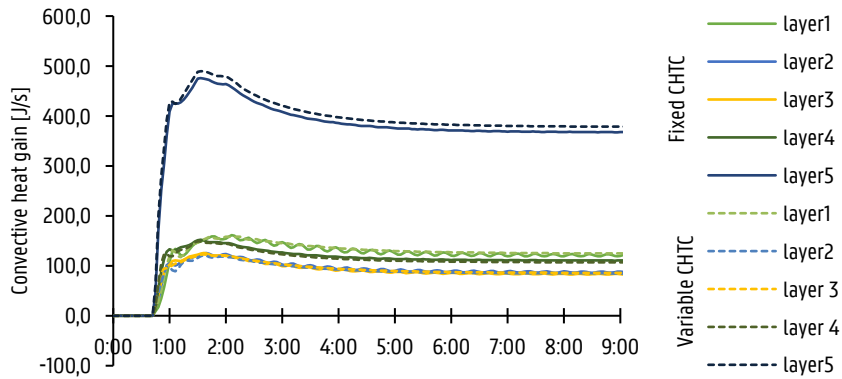


Figure 5.36: Convective heat gain calculated by the thermal zonal model for a constant heat transfer coefficients and for a heat transfer coefficient calculated by the expressions given by Beausoleil-Morisson [333].

The Influence of the Chosen Radiation Model

TRNSYS considers three different types of radiation. Surfaces within the zone are modelled as grey surfaces at two different wavelengths, namely long-wave and short-wave radiation. Short-wave radiation is further subdivided into diffuse and direct radiation. Since TRNSYS17 different radiation modes for these three types are available within each thermal zone (Figure 5.21). Besides the standard mode, which exist in previous versions, new detailed modes can be selected. The standard model to calculate longwave radiation is the star network given by Seem [349]. The new radiation model applies so-called Gebhart factors for a detailed treatment of longwave radiation and shortwave diffuse radiation [346]. The increased level of detail, however, increases computing time. It also increases the input effort because a 3D-geometrical model has to be made in SketchUp instead of only defining the surface properties for every zone in TRNBuild [268]. Therefore, it is examined whether the increased level of detail has a significant impact on the results.

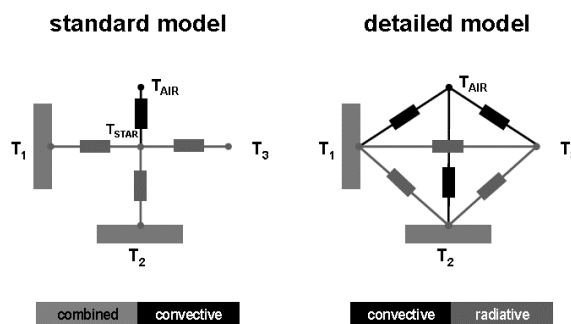


Figure 5.37: Standard method and detailed method in TRNSYS 17 to model longwave radiation [268].

Figure 5.38 shows the surface temperature for the insulated wall and the glass wall in the case of natural convection (N10) after two hours of outside heating. Temperatures calculated by TRNSYS using the simplified radiation method and the detailed radiation method are compared against the measured values. The deviation is caused by the differences in energy absorbed on the inside floor and ceiling surface by longwave radiation exchange. Using the standard method, the surface temperature of the floor was underestimated, while surface temperatures for the indoor ceiling and insulated wall were overestimated. As a result, indoor air temperature was overestimated.

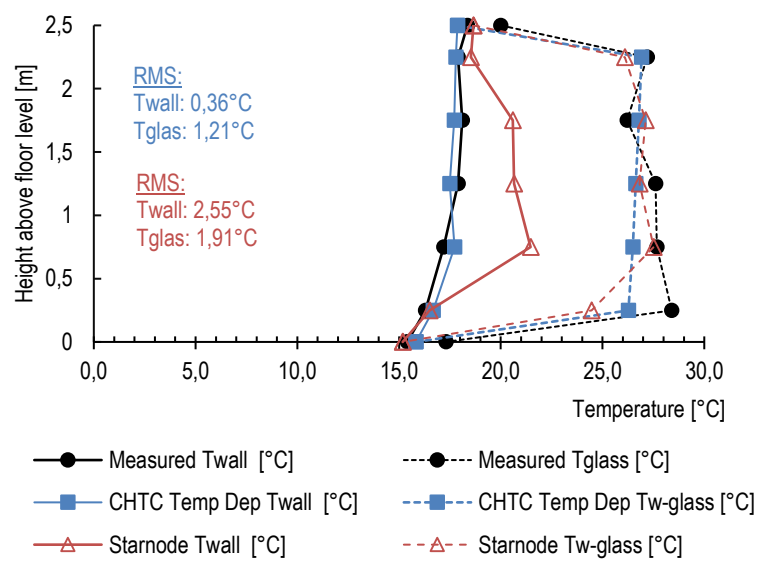


Figure 5.38: Surface temperature for the insulated wall and the glass wall. Comparison between the measured values and the calculated values by TRNSYS by the simplified and detailed radiation method.

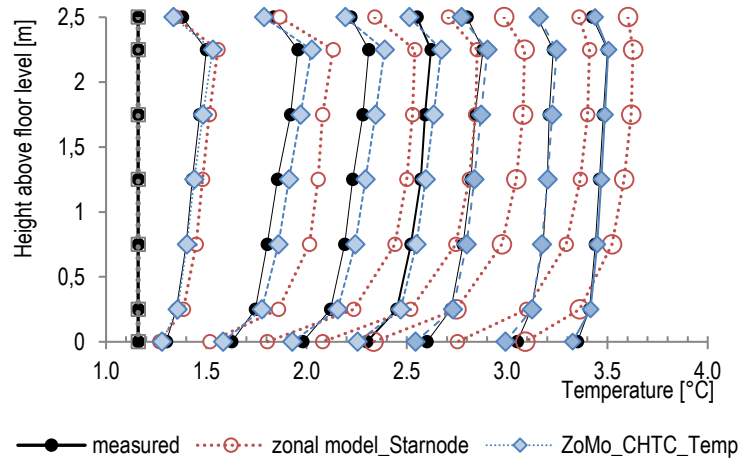


Figure 5.39: Temperature for the first nine hours while heating outside the chamber. Comparison between the measured values and the values calculated by the thermal-zonal model in TRNSYS when using the simplified method or the detailed method for longwave radiation.

Table 5.11: Root Mean Square error of the air temperature. Comparison between the simplified and detailed radiation method.

	1:00	2:00	3:00	4:00	5:00	7:00	9:00
Simplified method	0.45	1.55	2.10	2.08	2.05	1.86	1.50
Detailed method	0.23	0.52	0.55	0.37	0.30	0.24	0.12

5.4.5 Cases with Moisture Source

Addition of Moisture Source

In this section the effect of the addition of a moisture source is examined numerically. The two cases, N10 and H100, used for verification were used for this purpose. A moisture source was added in the lowest zone with a moisture generation rate of 10g/hr. This situation presents the situation where visitors are present in the church or in the church during heating. The overall initial temperature was 11 (Case N10) and 12°C (Case H100) and the initial relative humidity for the cases was assumed to be 50%RH.

In the case with a jet flow, two variants were calculated. Figure 5.40 gives a schematic representation of these variants. In the first variant, the supply air has a constant temperature of 40.7°C and a constant relative humidity of 5%. In the second variant, the air blown in by the jet in the second layer is the reheated air extracted from the lowest layer. It has a constant

temperature of 40.7°C. The relative humidity of the supplied air by the jet will be dependent on the absolute humidity of the reheated air (AH = AH layer 1) and the constant temperature.

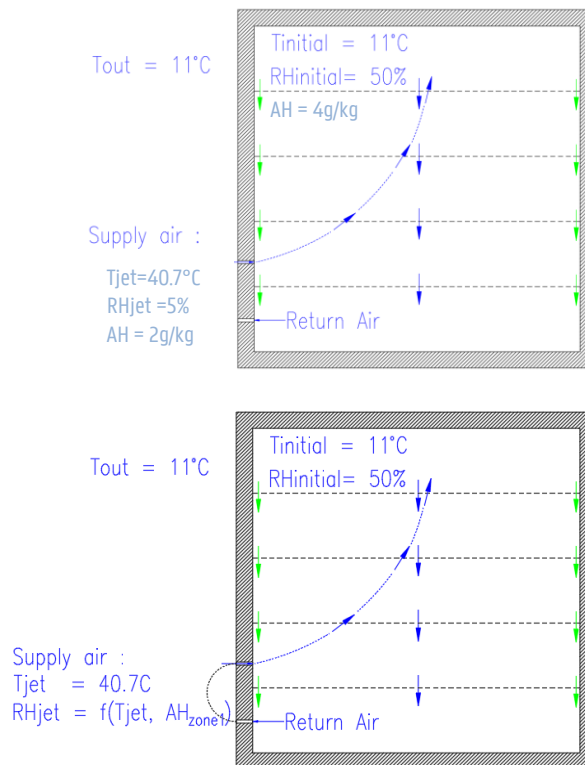


Figure 5.40: Flow regime in case with a jet flow (H100): Variant 1 and Variant 2.

Case of natural convection

Figure 5.39 shows the calculated absolute humidity and indoor relative humidity versus time for the case of natural convection. Air temperature versus time is not shown, as the temperature course remains the same. If a moisture source was defined in the lowest layer, the absolute humidity of all layers increased linearly. The sum of the linear increase from each layer corresponds to the value of the added moisture source. Comparing the absolute humidity in each layer to the absolute humidity in case air in all layers is perfectly mixed, the absolute humidity in the first layer is slightly higher, while the absolute humidity in the other layers is slightly lower. This could be explained by the vapour flow rate into a layer as illustrated in Figure 5.42.

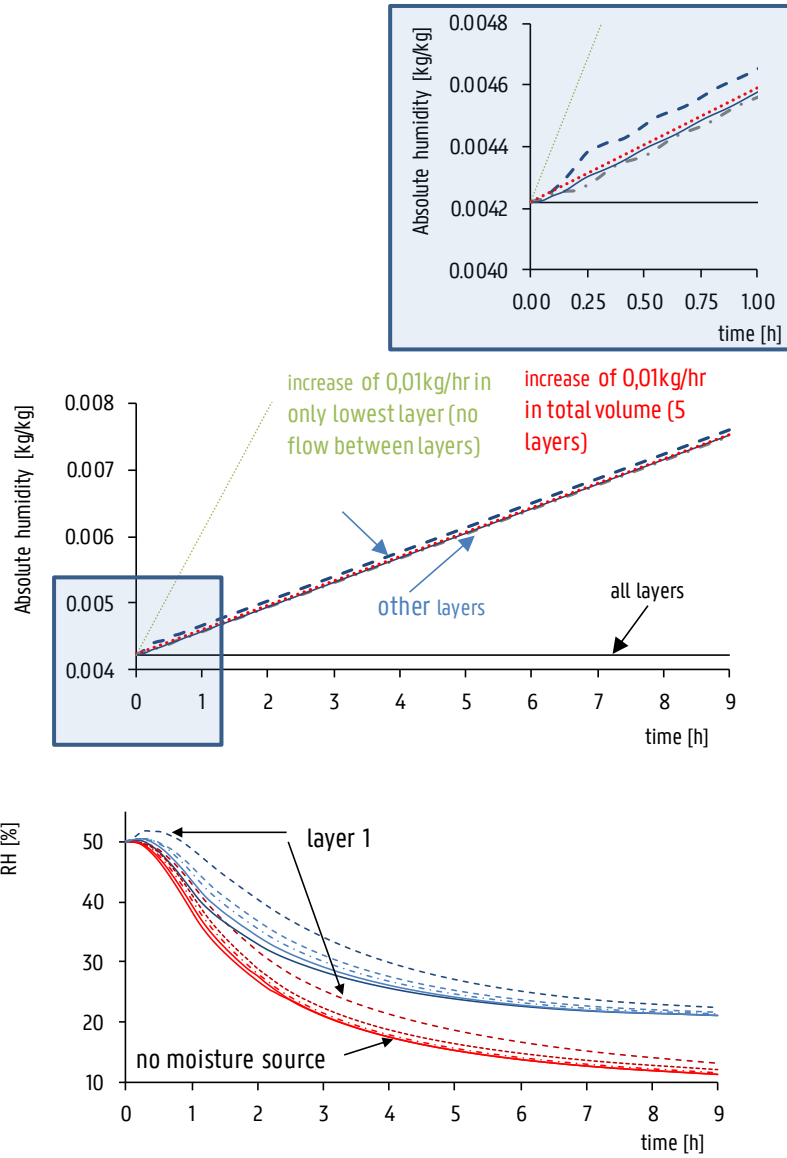


Figure 5.41: Absolute humidity and relative humidity for case N10. Comparison between the case without a moisture source (red) and the variant in which a moisture source is defined in the lowest layer (blue).

Figure 5.42 shows the vapour flow rate into a layer from other layers ($G_{\text{gain, layer}}$ eq. (5.38)) and from the wall currents ($G_{\text{gain, current}}$ eq. (5.39)). The sum of these two will be the total moist gain (G_{gain} eq. (5.37)(5.38)). At the right the values of the absolute humidity in the air current and in the layers after at 2h00 is visualised to illustrate the flows. At the location of the glass wall an upward air

flow occurs driven by the warmer glazed surface. The lowest layer has a higher absolute humidity due to the presence of a source of moisture. The upward wall current takes out dryer air from each layer above. As a result the absolute humidity in the wall current (Y_m) decreases. Finally, this air flow enters the upper layer. The flow mixes with the air present in the layer and will flow down along the colder walls and between the layers. The absolute humidity in the wall currents along the colder walls will decrease. As a result, the absolute humidity in layers two till five will increase. The absolute humidity in layer one will also increase, but not as much in case no air flow would be present, because of the incoming dryer air of the wall currents along the colder walls and from the layers above.

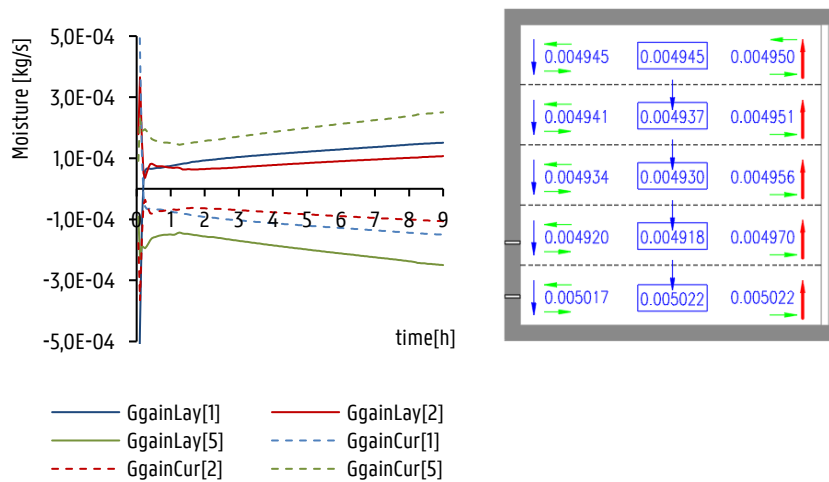


Figure 5.42: left: Vapour flow rate into a layer from other layers (moisture source included) or from the wall currents. Right: Visualisation of absolute humidity in the air current and in the layer at 2h00.

Case of forced convection

Figure 5.43 and Figure 5.45 show the calculated absolute humidity and indoor relative humidity versus time for the case of a jet flow. The temperature distribution for the case without a moisture source and for the two variants with a moisture source is identical. Therefore, this course is not shown. This temperature course was expected as the variants only define a variation in moisture transport. Hence, in case no moisture source is defined, the absolute humidity of every layer remained the same over time and the occurring distribution in relative humidity can be entirely ascribed to the distribution in temperature. Furthermore, in the first part when no air is supplied, no temperature differences occur. Consequently, no air flow between the layers initiates. Accordingly, the absolute humidity only increased linearly in layer one and thus also the relative humidity increase is linear. In the other layers, no increase in absolute humidity was observed. The reason is that when no air is supplied, no airflow is defined.

At the moment air through the jet is supplied into layer two and air is withdrawn from layer one, the jet is an upward flow from layer two till layer five. As a result, a downward flow occurs from layer five to layer one between the layers and at the walls (Figure 5.40).

In the first variant, the supplied air by the jet has a lower absolute humidity than the air in the layers. As a result, the moisture ratio in layer one till five decreases. This moist loss results in a similar absolute humidity for the layers two till five. In layer one, the absolute humidity no longer increases linearly. Instead, mixing occurs with the dryer air coming from layer two into layer one. Because of the presence of the moist source, the absolute humidity remains higher in this layer. Figure 5.44 shows the moist losses or gains for layer one and layer two calculated by the thermal zonal model. Large moisture losses and gains occurs at 0.75h by the jet, dominating the wall and layer currents.

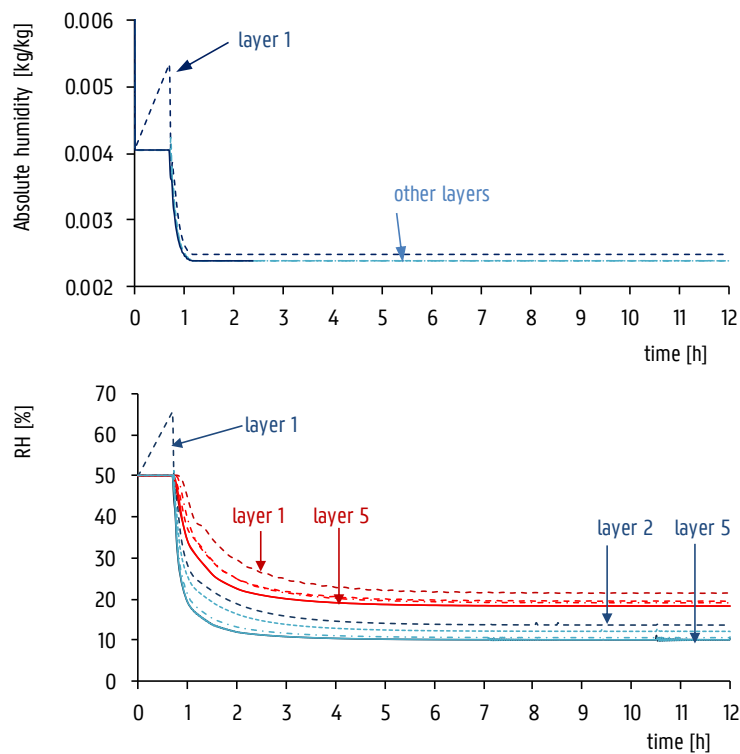


Figure 5.43: Absolute humidity and relative humidity for case H100-variant 1. Comparison between the base case (red) and the variant 2 in which a moisture source is added in the lowest zone (blue) and in which the supplied air is dry air.

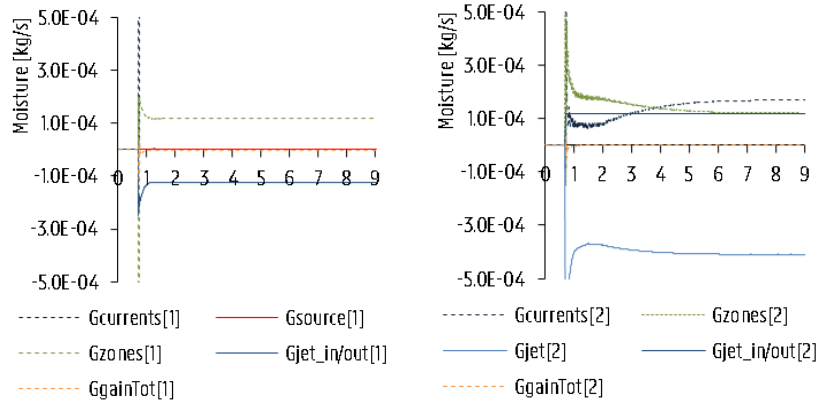
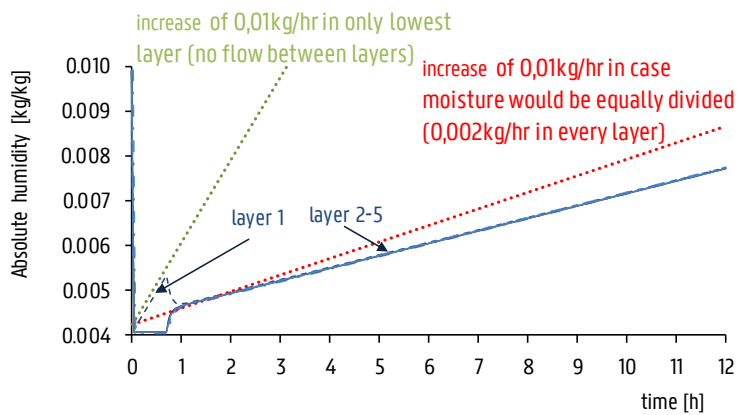


Figure 5.44: Additional moist gain for layer one and layer two in case H100 – variant 1.

In the second variant, the absolute humidity of the supplied air by the jet is equal to the absolute humidity of the lowest layer. This ratio is higher than in the other layers because of the presence of a moist source. As a result, the moisture ratio in layer two till five increases when the jet starts. From then on, the absolute humidity in layer one no longer increases linearly. Instead, mixing occurs with the dryer air coming from the layers above. Figure 5.46 shows the moist losses or gains for layer one and layer two calculated by the thermal zonal model. Large moisture losses and gains occurs at 0.75h by the jet, dominating the wall and layer currents. In this figure can also be noticed that the absolute humidity in the jet increases.



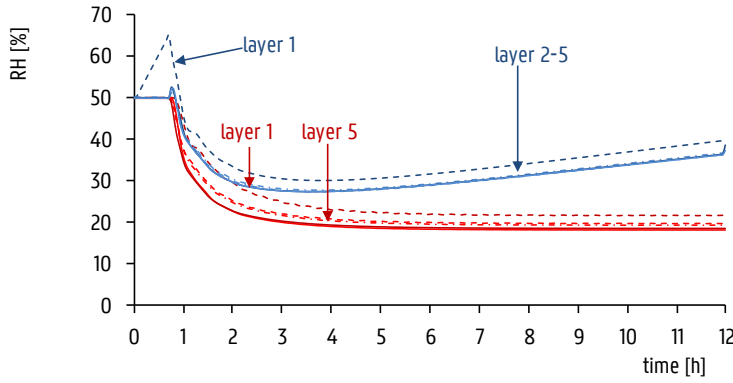


Figure 5.45: Absolute humidity and relative humidity for case H100-variant 2. Comparison between the base case (red) and variant 2 in which a moisture source is added in the lowest zone (blue). The supplied air by the jet is the reheated air subtracted from the lowest layer.

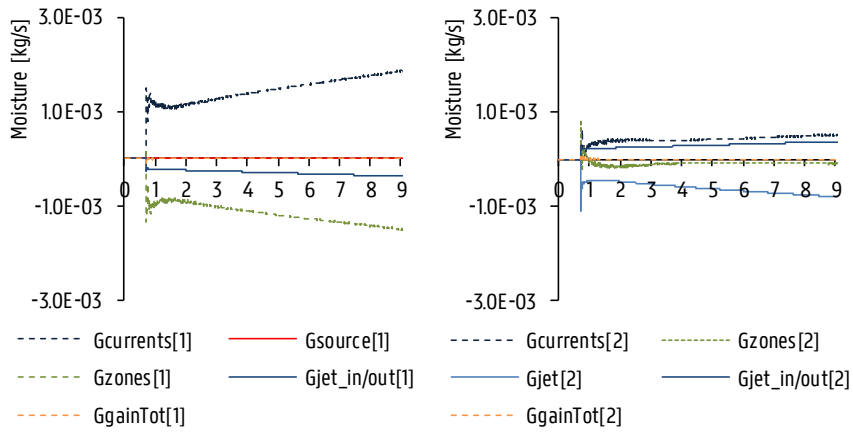


Figure 5.46: Additional moist gain for each layer in case H100 – variant 1. Moist gain of 0.01kg/hr in layer one by moisture source is not shown.

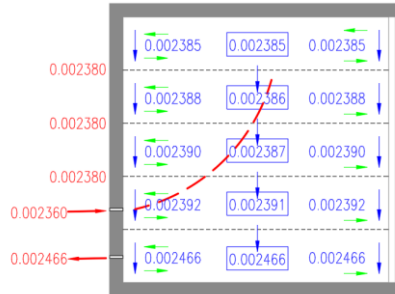


Figure 5.47: Additional moist gain for each layer in case H100 – variant 2.: absolute humidity in the layers and wall currents after two hours.

Addition of Moisture Buffering

In this section the effect of the moisture buffering of the walls was examined numerically. The cases, H100, was used for verification, as this represents the case when heating in a church building. For all vertical walls, except for the glazing, moisture buffering in TRNSYS was included by an individual EMPD-model (15 EMPD-components). The overall initial temperature was 11 (Case N10) and 12°C (Case H100) and the initial relative humidity for the cases was assumed to be 50%RH. The same conditions were used as initial temperature and relative humidity of the walls. In the variant was assumed that the vertical walls consisted of massive brick walls covered with two centimetres of plaster. Parameters used in the EMPD model are shown in Table 5.12.

Table 5.12: Hygric Parameters used for the EMPD-model.

Characteristic	Value
<i>Brick</i>	
Moisture content [kg/m ³]	$c = 16.3 \left(1 - \frac{\ln(\varphi)}{1.92}\right)^{-\frac{1}{0.5}}$
Vapour diffusion [-]	$\mu = 7.69$
<i>Gypsum</i>	
Moisture content [kg/m ³]	$c = 310 \left(1 - \frac{\ln(\varphi)}{31.25}\right)^{-\frac{1}{1.58}}$
Vapour diffusion [-]	$\mu = 1 / (0.155 + 7.60 \cdot 10^{-4} e^{4.64\varphi})$

Case of forced convection

Figure 5.45 shows the calculated absolute humidity and indoor relative humidity versus time for the case of a jet flow. Online the second variant, in which air of the lowest layer was blown into layer two by the jet, was simulated. The temperature distribution for the case without a moisture source and for this case was identical. Therefore, this course is not shown.

The courses for absolute humidity and relative humidity of every layer were compared to the courses of the same case in case no moisture buffering was present. It can be noticed, when moisture buffering was included, lower absolute humidities were found for every layer. This was due to moisture absorption of the walls. Consequently, also lower relative humidities were found.

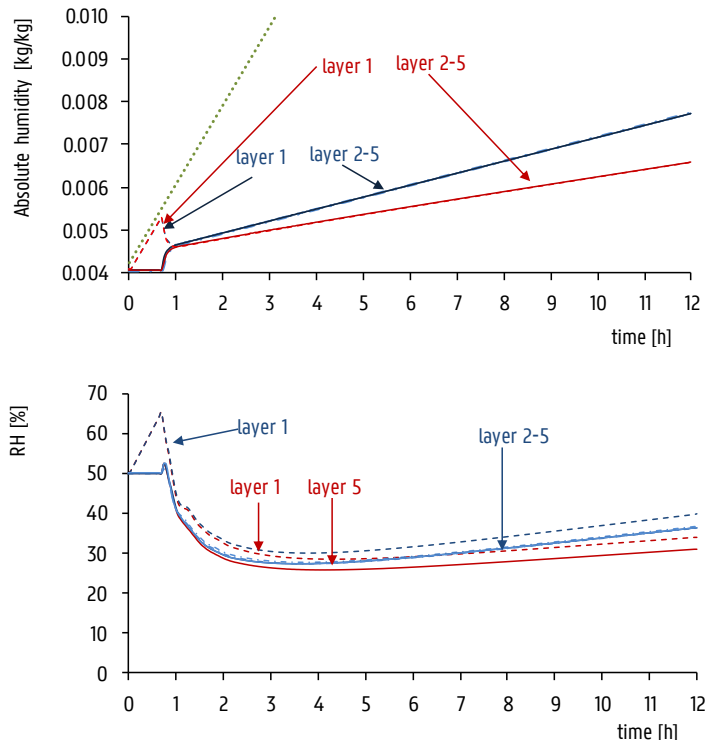


Figure 5.48: Absolute humidity and relative humidity for case H100-variant 2. Comparison between the same case without moisture buffering (blue) and the variant in which moisture buffering was include for all vertical walls, except for the glazing (red).

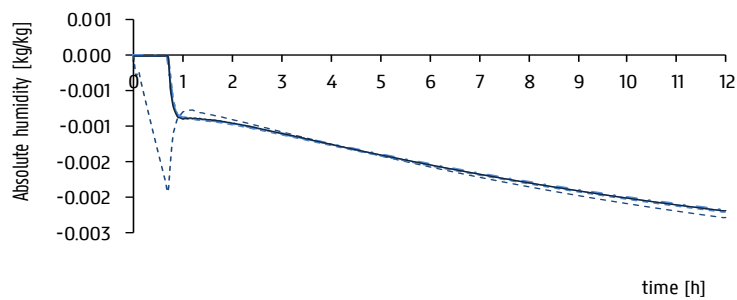


Figure 5.49: Total moisture gain for every layer. Comparison between the same case study (jet – variant 2) without and with moisture buffering included.

5.5 Discussion and Conclusion

This chapter presented the coupling of the thermal-zonal model with the BES-software TRNSYS. The coupled-zonal-BES model serves as an intermediate solution between the very detailed air flow modelling and the fully mixed assumption to evaluate the spatial temperature and relative humidity variation in tall buildings. The advantage of this coupling is that it has a short calculation time and can predict longer time periods (minimum one year).

The chosen simplified airflow model subdivides one zone into several horizontal layers, in which the temperature is uniform. It is assumed that the main components of the air movement in a large space are airflows along the vertical wall surfaces and primary supply airstreams, e.g. from a jet. To this end, equations were added for a non-isothermal free jet, which is representative of heating with a bulk air inlet in a large space, which is commonly present in old church buildings in Flanders.

A verification is performed to check the correctness of the coupled thermal-zonal-BES model. The original model, however, started from measured wall temperatures and measured heat transfer coefficients. This is not useful for simulating building behaviour, because these values are commonly not known. As a consequence, interior surface temperatures are also simulated. Following issues should be taken into account when simulating the interior surface temperature.

- Using unsteady values for of the convection transfer coefficients calculated by algorithms suggested in former studies, instead of using constant values improved the agreement between the measured and simulated results. This is due to the fact that the wall streams in the thermal zonal model are dependent on wall temperature and convective heat transfer coefficients.
- Calculating longwave radiation and shortwave diffuse radiation using so-called Gebhart factors increased computing time, but had a significant improvement on the agreement between measured and simulated temperature. The deviation between the simplified radiation model based on surface area and the more detailed radiation model, based on view factors, is caused by the differences in energy absorbed on the inside floor and ceiling surface by longwave radiation exchange. In the simplified model, the surface temperature of the floor was underestimated, while the surface temperatures for the indoor ceiling and insulated wall were overestimated. As a result, indoor air temperature was overestimated.

To estimate the preservation conditions, next to temperature variation in space also the variation in relative humidity in the space has to be known. In the original thermal-zonal model, however, there were no transport equations to model the moisture conditions. Therefore, to estimate the humidity stratification following equations were added to the original model:

1. Addition of moisture transport equation in the air. Hereby the air was assumed as a mixture of dry air and water vapour, each component (vapour and dry air) obeying the ideal gas equation.
2. Addition of moisture flux coming from a wall. This is done by defining a value for the moisture flux (kg/hr) for each wall element present in the zonal model. This values are

defined as an input. It can be a constant value or the input can be provided by another component which predicts the moisture flux by a simplified model (EMPD) or by a more detailed model (HAM) (Chapter 3).

6

Preventive Conservation of a Panel Painting in a Church Building: A Simulation Study

Wooden panel paintings are commonly displayed in traditional churches, where they are subject to uncontrolled microclimatic variations that include weekly heating periods [172]. The objective of this chapter is to introduce the coupled approach to assess the hygro-mechanical response of a panel painting in an intermittent heating regime. To do so, the ideas of Chapter 3, Chapter 4 and Chapter 5 are brought together in a case study of a historic church building in which an important panel painting is exhibited. For all simulated cases, the hygro-mechanical response of the painted panels was studied by coupling the thermal-zonal BES model (chapter 5) with a HAM-model (Chapter 3). The moisture buffering of the walls was modelled using an EMPD-model (Chapter 4).

The measurement campaign of the presented case study was presented by K. Maroy at the 6th International Building Physics Conference and published in the proceedings [350].

6.1 Background of the Church Building

The investigated church building is based on the Church of Our Lady in Watervliet (Figure 6.1), located in Belgium. The church, dating from the 16th century, is located in a rural area with a maritime temperate climate³¹. This climate is characterized as climate with a cool winter and a warm summer. The church is most of the time not acclimatised. Only during a service or a concert, the church is heated with an air heating system to a setpoint temperature of 16°C. An exception is in wintertime when the heating device is put on to maintain a minimum temperature. This heating system is put into operation when the temperature of the church drops below 5°C. The heating device is located in a technical room built next to the church building (Figure 6.3). Hot air is blown into the church through a large grill.

Due to the many works of art exhibited in the church, the Church of Our Lady in Watervliet is also called "The Cathedral of the North". The interior includes woodcarving and panel paintings from the 16th, 17th and 18th century. The most important and valuable painting of the church is the triptych "God's need" (Figure 6.2). It was painted in the 16th century by an unknown artist and is included on the list of masterpieces of Belgium heritage [352]. It should be noted that the work is currently in the southern choir and not above the main altar anymore, as was the case in the 16th century [353]. Unfortunately, this triptych has been damaged by hanging in an unfavourable climate. As can be observed in Figure 6.2, there is a joint between the horizontal and vertical boards of the central panel. This joint cannot be maintained. The reason is that in normal operation of the wood, the vertical boards along the joint experience larger dimensional changes than the horizontal boards. Consequently, numerous traces of restorations can be noticed on this joint [354].



Figure 6.1: Church of Our Lady in Watervliet, Belgium.

³¹ Köppen climate classification: Cfb [351].

As a result of an inspection report by Monument Watch Flanders, a measurement campaign was started in 2011 to gain information about the indoor climate of the church and to detect causes of damage. Meanwhile, in the winter season of 2013, an urgent conservation was carried out on the panel painting to fix the paint layers with support of a grant of the Flemish government. However, the Flemish minister of culture, Joke Schauvliege, said the following: "*The grant gives the church council time to look for a more permanent solution for the problematic climatic conditions in which the triptych is conserved. A further restoration is desirable, but only makes sense when improving the storage conditions in the Church of Our Lady*" [355]. Following from this, it was decided to increase the minimum temperature in the church building from 5°C to 11°C (starting the winter of 2013-2014) as described in the circular ML/11 [64].

To look for a more permanent solution in terms of preservation condition, a dynamic building simulation is applied. Firstly, the measurement results were analysed to find the causes of damage. Secondly, a simulation study was made. This study looked at the solution chosen as an temporary measure - increasing the minimum temperature - and other possibilities. An overview of the simulated cases is provided in Table 6.1. The selection of simulated solutions was based on the guidelines presented in the circular ML/11 [64]. If a proposed solution did not comply with these guidelines, an alternative was simulated which complied with these guidelines as far as possible.

Table 6.1: Heat loss calculation as formulated in DIN 4701.

	T_{\min}^{32}	T_{service}^{33}	ΔT^{34}	Heating system
Base Case	5°C	16°C		Jet
Intermittent Solution	11°C	16°C		Jet as in base case
Variant 1	11°C	15°C	2°C/h	Jet with decreased supply temperature and jet with decreased flow rate
Variant 2	11°C	15°C	2°C/h	Underfloor Heating

³² The minimum temperature in the church must be between 10 to 12°C, regarding permanent heating in colder periods.

³³ When heating during the service, the temperature must be limited to 15°C, and this limitation holds not only at the place where visitors are located, but also at the organ.

³⁴ The temperature of the space may not be increased more than 2°C per hour.



Figure 6.2: The panel painting "God's need" painted by an unknown artist. Above: The central panel - Below: Side-panels. [354]

6.2 Two Causes of a Non-optimal Indoor Climate

Different periods were measured starting from July 2011. Wireless sensors of the Hobo ZW3 Pro Series were used for measuring temperature and relative humidity with an interval of 10 minutes. The measurement error of these sensors was $\pm 0.54^{\circ}\text{C}$ and $\pm 2.5\% \text{RH}$. The sensors were installed at different locations in the church building (Figure 6.3): at the main entrance under the organ, at the out-and inlet of the heating system in the side aisle, at different points in the church building and at the triptych. Care was taken at each location to ensure that the loggers were placed away from draft, direct sunlight and ceiling light fixtures.

From the analysis of the measurement results, following problems have emerged: a too high relative humidity and too large short time fluctuations in relative humidity and temperature which is caused by the heating system.

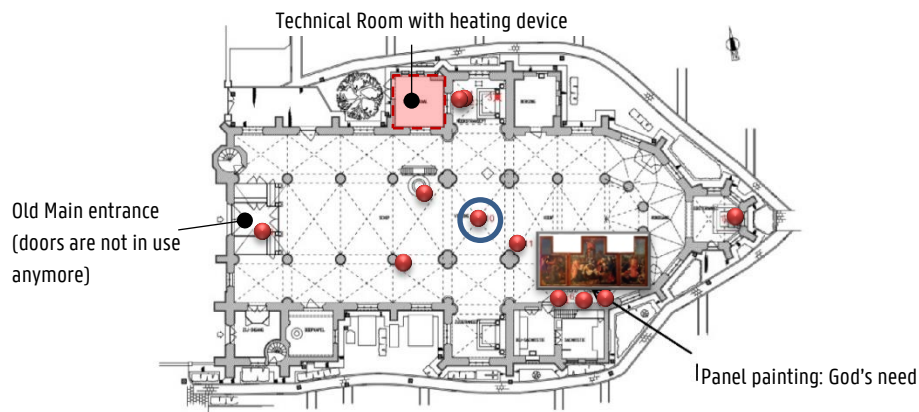


Figure 6.3: Floor plan of the Church of Our Lady with the original location of the panel painting "God's need". The location of the heating device and the positions of the Hobo-loggers (red points).

Problem 1: Intermittent heating

From the beginning it was quite clear that the heating system was the cause of excessive short-term fluctuations and spatial gradients (Figure 6.8). Therefore, additional measurements were carried out for one month from 6/3/2012 till 29/3/2012 to collect data of the occurring stratification during the heating event. The vertical temperature and relative humidity distribution was measured by hanging a rope vertically from the ceiling. Ten Hobo H8 Pro Series loggers were placed on the rope with a distance of 1.5m between each logger (see Figure 6.4). Measured temperature and relative humidity courses are shown in Figure 6.5 and Figure 6.6. During this period, the church building was heated twice; on the 11th and 25th of March. This measured data is used for the model calibration of the coupled BES-thermal zonal model to estimate stratification during the heating events.

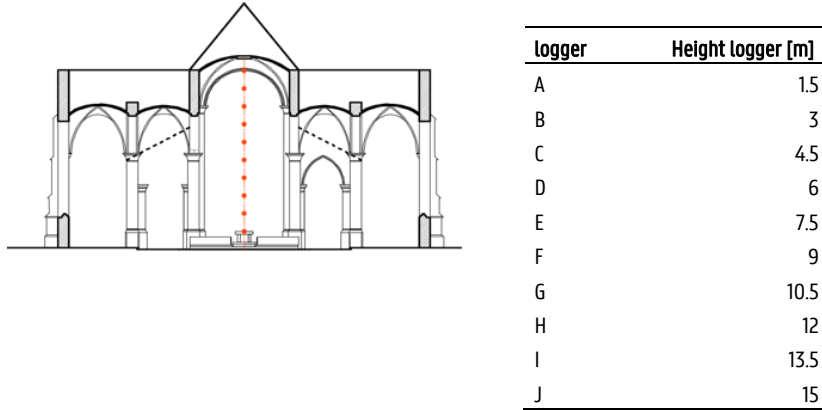


Figure 6.4: Schematic representation of the node and the position of the loggers.

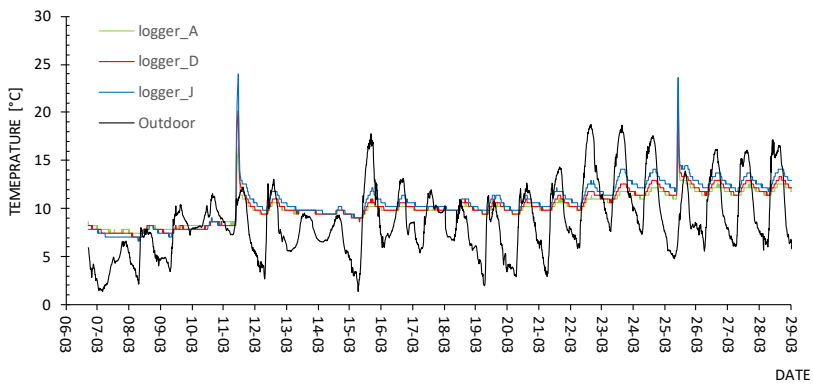


Figure 6.5: Air temperature profile at three measurement points (A: 1.5m – D: 6m – J: 15m) for the whole period of additional measurement.

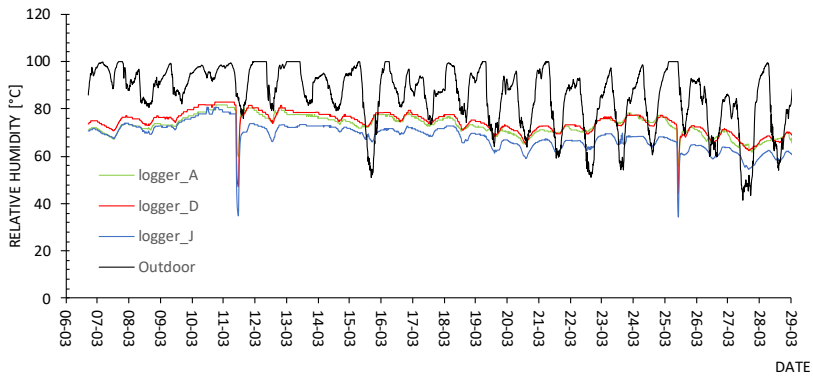


Figure 6.6: Relative humidity profile at three measurement points (A: 1.5m – D: 6m – J: 15m) for the whole period of additional measurement.

Problem 2: Too high relative humidity

Another problem was the too high relative humidity during the whole year. The figure below shows the annual course of the relative humidity in the church building. This shows that the fluctuations in relative humidity fall most of the time within the limit of 10%, with the exception of the heating events. The problem, however, is that the relative humidity for most of the time is above 75%RH. As mentioned in chapter 3, this will not only increase the risk of fungal growth, but will also decrease the allowable amplitude for the RH-fluctuations responsible for mechanical damage.

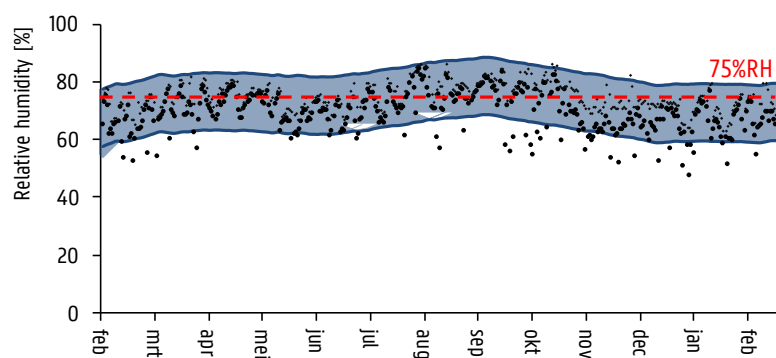


Figure 6.7: Measured relative humidity against ASHRAE class B.

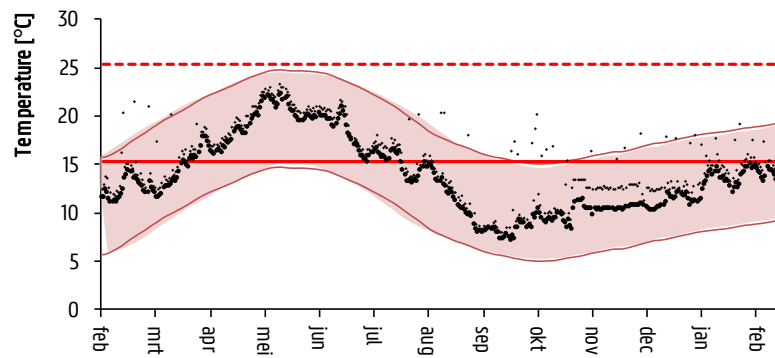


Figure 6.8: Measured temperature against ASHRAE class B.

6.3 Method of the Simulation Study

The modelling process consists of two models:

- A **whole building simulation model** was set-up of the church building in which the coupling of a BES-model with the simplified stratification model was used. The first step was to design a model of the actual situation, which was calibrated using the measurement data. Using the calibrated model, three types of adjustments to the heating system were tested. Firstly, the temporary situation in which the minimum temperature was raised from 5 to 11°C was simulated to get an idea of the impact of this adjustment on the preservation conditions. Secondly, other adjustments were tested to verify if other, perhaps better solutions are possible. To build up the building simulation model, the approach shown in Figure 4.1 was used.
- Because the relative humidity is very high in the church building, not the ASHRAE method was used. Instead the moisture distribution in a **panel painting** was modelled using a **1D-HAM model**. This was done because Chapter 3 concluded that in higher RH-regions, fluctuations are very restricted.

The simulation time step was set at 150s. Other values for the time step were tested but this value was the maximum value that could be used which still captured the jet behaviour and the switching on and off of the heating system during a day.

The initial temperature and relative humidity in all layers was set to the yearly average: 74%RH and 14°C. To avoid the effect of initial condition on the results, the simulation lasted four months in which only the period starting from the measurements for stratification (6th of March 2012-29th of March 2012) was used to calibrate and verify the model (Figure 6.9).

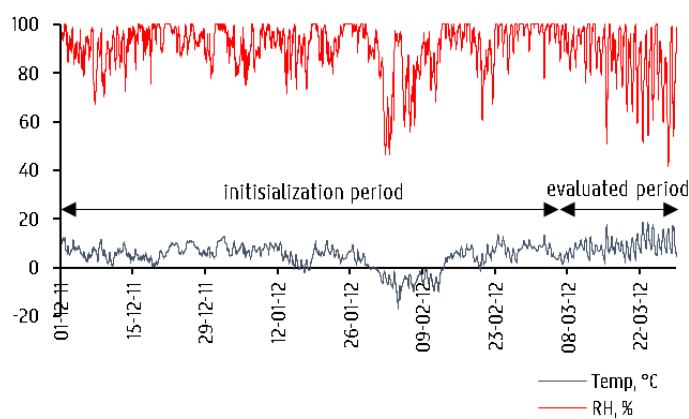


Figure 6.9: Exterior climate during the simulated period which is subdivided into initialization period and evaluated period.

6.3.1 The Building Model

Geometric model

Figure 6.10 shows the geometric model developed in Sketch Up. This 3D-model is converted in TNRBuild to a geometric model with necessary boundary conditions so it can be used in the simulation environment TRNSYS 17. The model of the church building is a multi-zone model consisting of three zones; the church volume and two attics. Furthermore, also the tower adjacent to the church building was drawn. This tower is not a part of the geometric model and thus the conditions in the adjacent tower are not simulated. The tower geometry only serves to take into account the shadow related to solar radiative gains. The main geometric characteristics of the church were obtained from architectural drawings and are approximately the following:

- Internal dimensions:
 - length: 40m,
 - depth: 17m,
 - height: 10m (left and right aisle)
16m (nave)
 - north and south transept: 5m x 5m x 10m
- Ground surface: 730m²
- Volume: 8836m³

Due to the detailed radiation which uses view factors, the geometry of the church building has been simplified to a convex zone with straight surfaces and columns and arcs were neglected. Instead the internal capacity of the volume was raised by adding the material's capacity by raising the effective air capacity.

The church building (zone 1) was further refined into horizontal layers to estimate the stratification in this part. The more layers the model contained, the larger computation time. The computation time not only increased by the use of a zonal model, but also by the building model itself to calculate the radiative heat transfer using view factors. Besides, the more layers, the longer it takes to build up the simulation model. Since the aim is to gain insight into stratification in a fast, simplified manner, an equilibrium was chosen between what is required and what is sufficient. Therefore, in this case the studied volume was divided into six horizontal layers (Figure 6.11)³⁵. Layer one, at the bottom, corresponds to the occupied area. For the other layers the position of the windows was taken into account. This resulted in four layers of 2.5m and two layers of 3m.

³⁵ Other studied variation where five and ten layers.

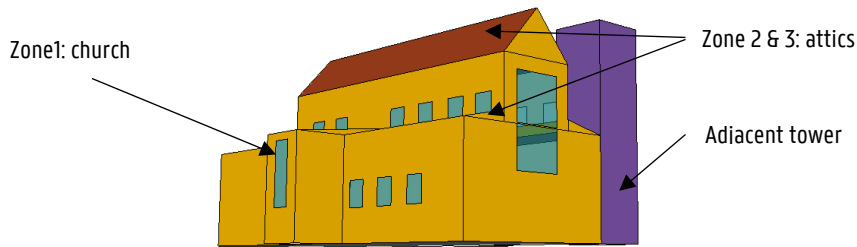


Figure 6.10: Geometry of the multi-zonal model of the church building.

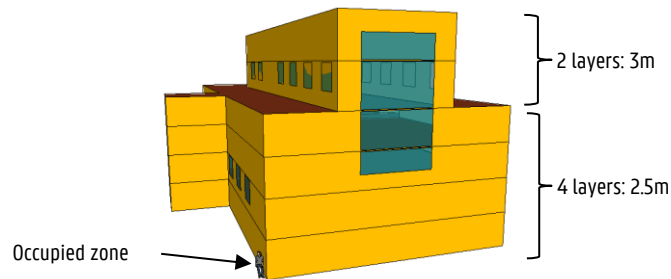


Figure 6.11: Refinement of zone 1: Thermal-zonal model of the church building.

Material Characteristics of the Church building

Table 6.2 summarizes the material input data used in the simulation model. The outdoor walls of the church are made of masonry and have a mean thickness of 0.75m. At the interior surface, walls are covered with a plaster. The glazing in the outdoor walls is stained single glass. The vaults of the ceiling of the church have a similar construction as the walls and consist of masonry with a thickness of 0.2m covered with plaster. The construction of the floor was unknown. Based on a typical floor used in old church buildings, the following construction was assumed in the simulation model: a stone floor, laid on mortar and sand [356]. Furthermore, the floor was modelled based on the method described in ISO EN 13370, which provides methods of calculation of heat flow rates for building elements in thermal contact with the ground, including slab-on-ground floors [357].

Table 6.2: Material properties.

Building part	Material	Thickness [m]	Thermal conductivity [W/m.K]	Density [kg/m ³]	Specific heat capacity [kJ/kg.K]
Outdoor wall	brick	0.75	1.39	2100	1.00
	plaster	0.02	0.80	1900	0.84
Ceiling	brick	0.1	1.39	2100	1.00
	plaster	0.02	0.80	1900	0.84
Floor	stone floor	0.02	3.50	2550	0.84
	mortar	0.05	1.20	1600	1.00
	sand	0.5	2.00	1800	1.00
	virtual layer		0.05	1000	1.00

Building part	Material	U-value W/ m ² K
windows	Stained glass	5.7

Moisture Buffering

The original EMPD-model available in the building model of TRNSYS cannot be used for the newly developed thermal-zonal model, because it only calculates one value representing the average moisture storage properties of all room surrounding surfaces [273,280]. In the zonal model, in which one zone is subdivided into a number of horizontal layers, for each separate wall surface a vapour mass flow is desired. This mass flow of every surface is necessary to calculate the moisture in the surface air streams. To this end, a new TRNSYS type was programmed which consisted of a non-isothermal EMPD-model and is coupled with each wall element (chapter 3). For each wall element, material definitions were provided for the plaster and brick. The duration for the short term period was one day and for the long term period one year. The material properties of plaster and brick along are shown in Table 6.3.

Table 6.3: Material properties and boundary conditions.

Property	Value
Internal surface coefficient for vapour transfer β [kg/(Pa.m ² .s)]	$2.0 \cdot 10^{-8}$
Internal surface coefficient for heat transfer	Temperature dependent Provided by TRNSYS
Brick: Vapour permeability δ [kg/(Pa.m.s)]	$\delta_a/0.13$
Brick: sorption isotherm [kg/m ³]	$16.3(1-0.52\ln(\varphi))^{-1/0.5}$
Plaster: Vapour permeability δ [kg/(Pa.m.s)]	$\delta_a/(0.155+0.00076e^{4.64\varphi})$
Plaster: sorption isotherm [kg/m ³]	$310(1-0.032\ln(\varphi))^{-1/1.58}$
Boundary Condition	
Initial RH layer 1	100%
Initial RH layer 2 – layer 6	74% (yearly average relative humidity)
Initial T	14°C (yearly average temperature)

Heating System

The set-point temperature of the heating system was 16°C during services and 5°C during other periods. In the simulation, services took place every fourteen days from 9h30 till 11h30. Other events, like a funeral or a concert, were not taken into account. The heating system is controlled by a simple on-off controller and is located in the lowest layer. The defined dead-band is 1°C and was based on measurement data (Figure 6.12)

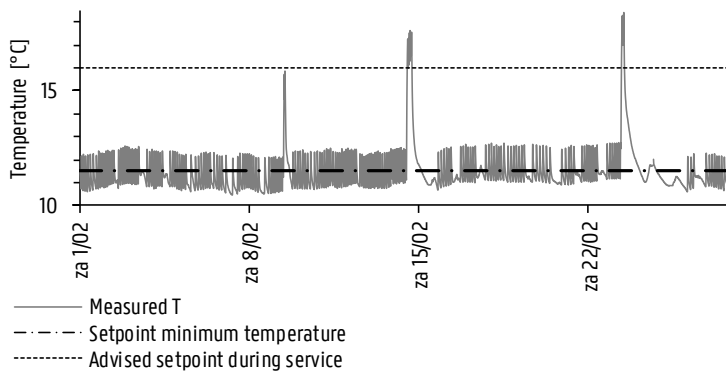


Figure 6.12: Measured temperature in the church near the on-off controller. The setpoint at that moment was 11°C.

The hot air was brought into the church by a re-circulation system. The inlet is defined as a grille of 0.5m by 2m at 2.5m above floor level and is therefore defined in the second layer. The return outlet is defined in the first layer. It was assumed that the same amount of air was extracted as supplied.

Based on the data from the current installation, which can be found in the figure below, an estimation is made of the actual airflow determined by the power of the installation. The heating system is a direct hot air system of Wanson Industries. The capacity of the plant is 325 000 kcal/h. After converting to kW, the obtained power is 377kW. Using the following formula, the air flow rate to use in the simulations of the current heating system is calculated:

$$Q = \dot{m}c_p\Delta T \quad (6.1)$$

Where: Q nominal power of the installation [W]
 c_p specific heat capacity for air [1005 J/(kg.K)]
 ΔT temperature difference [K]

Using the measured temperature of the supply air of 45°, this results in an air flow rate of 9.40kg/s.



Figure 6.13: Speciation of the heating installation in the church of Watervliet.

This value, however, resulted in an unrealistically outcome for the simulated indoor temperature. Therefore, the required flow rate was estimated by means of a simplified stationary calculation method for the heat load of a church made from solid masonry. This method is based on the work of Krischer and Kast from 1957 [358], which is formulated in the German standard DIN 4701. Although the method is old, this method for the heat demand for rarely heated buildings is still

typically used [22,359]. The equations as described within DIN 4701-1 state that the heat loss in the building is subdivided into three parts:

$$Q = Q_F + Q_W + Q_L \quad (6.2)$$

Where: Q_F heat loss through non-accumulating surfaces like windows [W]
 Q_W heat loss due to accumulating surfaces like walls and vaults [W]
 Q_L ventilation heat losses [W]

The heat loss due to accumulating surfaces Q_W is calculated as following:

$$Q_W = \frac{A_w \Delta T}{R_z} \quad (6.3)$$

The value R_z is a heating resistance [$K \cdot m^2/W$] which is dependent on the pre-heating time and the thermal effusivity of the material. The thermal effusivity b [$J/(m^2 K \cdot s^{1/2})$] can be calculated with the following material properties by:

$$b = \sqrt{\lambda \rho c_p} \quad (6.4)$$

Where: λ thermal conductivity [$W/(m \cdot K)$]
 ρ density [kg/m^3]
 c_p Specific heat capacity [$J/(kg \cdot K)$]

The value R_z can be determined from Figure 6.13 or can be calculated by the formula given by Krischer or by Gröber und Sieler [22,360]:

$$R_z = \frac{1}{H} + \frac{2\sqrt{z_0}}{b\sqrt{\pi}} \quad (6.5)$$

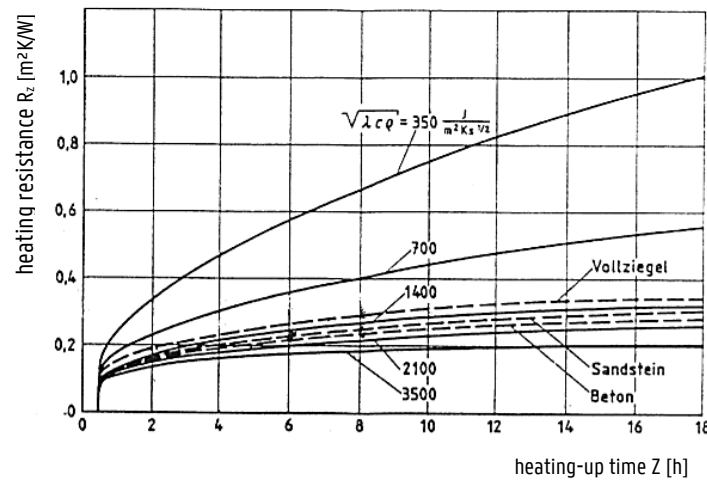
Where: H total indoor heat transfer coefficient [$W/(m^2 \cdot K)$]
 z_0 heating-up time [s]

For the temperature difference used in the calculation of Q_F and Q_L , the room air temperature ($16^\circ C$) and outside temperature mentioned in the standard NBN EN 12831:2003 ($= -8^\circ C$) were used. For the calculation of Q_W , the difference between the indoor temperature before ($= 5^\circ C$) and after the heating process ($= 16^\circ C$) was used.

The heat loss calculated with the above formulas results in 246kW. Using the measured temperature of the supply air of 45° ($\Delta T = 40^\circ C$), This results in an air flow rate of 6.12kg/s.

Table 6.4: Heat loss calculation as formulated in DIN 4701.

heat loss through non-accumulating surfaces Q_F	$A \cdot U \cdot \Delta T$	77.67 kW
heat loss due to accumulating surfaces Q_W	$\frac{A_w \Delta T}{R_z}$	96.32 kW
ventilation heat losses Q_L	$0.34 \cdot V_{\text{building}} \Delta T$	72.10 kW

Figure 6.14: Value R_z [$K \cdot m^2/W$] dependent on the pre-heating time and the thermal effusivity of the material presented in DIN 4701 and based on [360].

Internal Gains and Losses: Infiltration and Occupancy

In the current situation, there is only naturally ventilation (infiltration). The infiltration takes place through cracks in the walls and vaults and at the windows and doors. The infiltration rate of the church has not been measured. However, it was preferred to take infiltration losses into account in an old church building like in the case study, because these buildings are often leaky and therefore air infiltration has a great impact on indoor climate conditions and energy usage especially during the heating season [361]. Based on literature, a value of 0.25 air changes per hour was assumed [326]. Further, it was assumed that the leakage distribution at the building envelope was proportional to its area. To model the dynamic infiltration losses, the LBLN Infiltration Model was used. This model is available in the TESS library, an additional TRNSYS library.

In Figure 6.15 the assumed air flow path for natural ventilation is schematized. Here you can see in the cross-section that the fresh outside air enters the building through the windows and chinks in doors. The polluted air leaves the building through the holes in the vaults and the windows and chinks in the attic. A similar flow path was assumed in the simulation study. At this moment,

it is only possible to define one position for supply of infiltrated air, and one position where the air leaves the church building again.

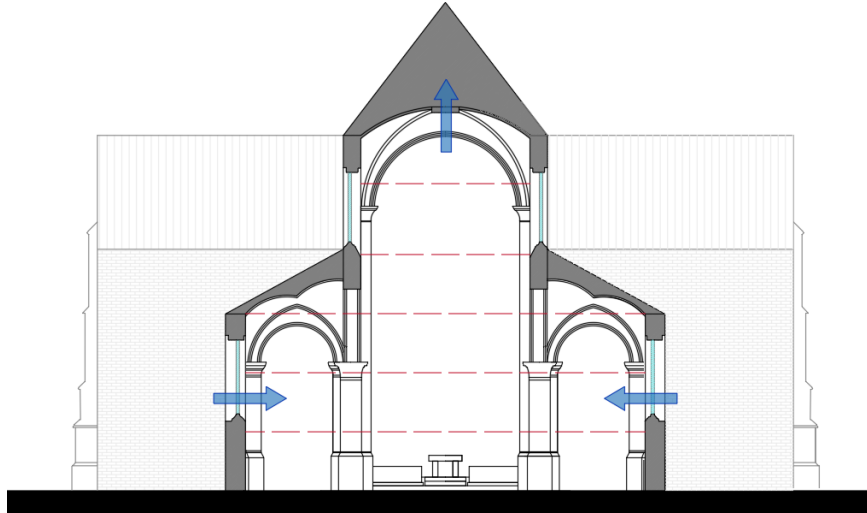


Figure 6.15: Assumed air flow path for natural ventilation in the case study.

Thermal loads from churchgoers and electrical fixtures were estimated because they could not be measured. The heat gain and moisture gain from the church goers were defined as class 4 (seating) from the ASHRAE Handbook of Fundamentals [43]. It is assumed that churchgoers are present every fourteen days from 10h30 till 11h00. Visit of the church by tourists is not taken into account, since the church is closed in the colder periods. The height of the occupancy zone is considered to be 1.8m, thus only present in the lowest zone. Internal gains from lights were not taken into account. Values used in the simulation study are tabulated in Table 6.5

Table 6.5: Internal gains used in the building model of the library.

	Number	Heat gain	Moisture gain
People	20	65W/person	0.03kg/(h.person)
Lights	neglected	neglected	neglected

6.3.2 The HAM-model for the Panel Painting

The altarpiece is between 1.555 and 2.385m high. The middle panel is 2.36m long and the two sides panels are 1.22 and 1.22m. The panel consists of quarter sawn oak, with a thickness varying

between 7 and 16mm [354]. The gesso layer consists of a mixture of animal glue and ground chalk. The thickness of this layer varied between 150 and 240 μm . A primer layer of oil is applied on top of this gesso layer to avoid adsorption of the paint into the gesso. On the layer of primer, several layers of paint were applied. The thickness and pigment depending on the colour (thickness 16 μm -35 μm). The identified pigments include pigments as described in Chapter 3 (vermilion pigment, lead-tin yellow,...). On top, a varnish layer consisting of resin was noticed with a thickness between 8 till 24 μm . After an extensive restoration treatment in Brussels, the blistering paint layers were fixed and the back of the panel was impregnated with beeswax. The old yellowed varnish layers were removed and new varnish used for restoration purposes was applied [354].

As the composition and layers are similar to those described in Chapter 3, the properties of the studied materials are used for the HAM model.

The HAM-model in TRNSYS is a one-dimensional model. Because the panel painting is located in two layers, namely layer 1 and layer 2, two HAM components are used. Each component has the same material characteristics and initial conditions. However, temperature and relative humidity which serve as boundary conditions for the two HAM-components are different; namely calculated conditions of layer 1 and of layer 2. Furthermore, the wall temperature was used for the back of the panel painting, while the air temperature was used for the front of the panel painting.

6.3.3 Evaluation of preservation Conditions

To study the influence of the heating system on the preservation conditions and on the indoor climate, three environmental effects were looked into. Firstly, the short-term temperature and relative humidity change caused by the heating system was studied. Secondly, because for estimating damage to works of art, also the spatial gradient is of importance, the gradient for both temperature and relative humidity was calculated. Two gradients were studied:

- The difference in temperature and relative humidity between the two lowest layers. This was done because the painting was divided over these two layers.
- The difference in temperature and relative humidity between the lowest and the highest layer. This was done to have an idea of the order of magnitude of stratification that occurs in the church.

6.4 Results found by the Simulation Study

6.4.1 Jet: Actual Situation

Indoor Temperature and Relative humidity

First, the actual situation was modelled. After the manually iterative calibration, a maximum root mean square error of 1.01°C was found. For the absolute humidity the maximum root mean square error was 0.000312 kg/kg. Root mean square errors for the entire period are listed in Table 6.6. The mean bias error and the measured and simulated profile for layer 1 and layer 6 are shown in Coefficients of variation of the root mean squared error values are not presented as these are mainly interesting when comparing which models provide better predictions.

The following pages visualize the simulated results of a day during the measurement campaign on which heating occurred during a short period of time, namely 11/3/2012. Figure 6.17 shows the measured and simulated vertical profile for indoor temperature and relative humidity. The simulated results by the simplified hygro-thermal zonal model shows a reasonable level of agreement between the measured and simulated values. The part during the warming up, at 9:45 and 9:30, has the largest inaccuracy. This was due to the steep slope in the beginning, which is sensitive to parameters related to the jet flow model; the throw constant of the jet ($K1$), the spread angle of the velocity profile (δ) and the chosen sub-model (mathematical representation) for the jet-model.

Table 6.6: Root mean square error for temperature and absolute humidity for each layer for the entire period in which stratification was measured.

Layer	RMSE	
	T [°C]	AH [kg/kg]
6	1.1	0.000310
5	1.1	0.000312
4	1.1	0.000263
3	1.0	0.000246
2	1.0	0.000260
1	0.8	0.000248

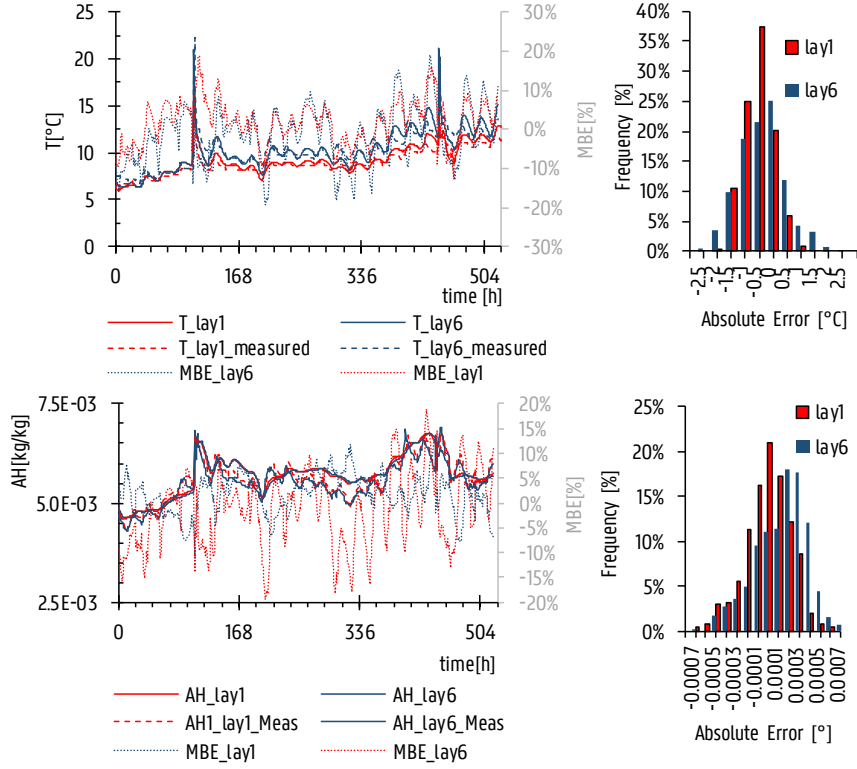


Figure 6.16: Comparison between measured and simulated temperature and absolute humidity for the entire period in which stratification was measured (6-29/3/2012). Mean bias Error is presented in the secondary axis.

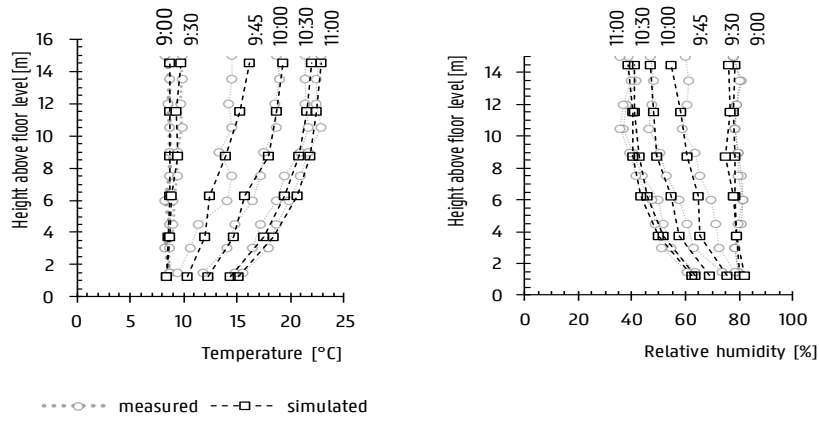


Figure 6.17: Measured and simulated vertical temperatures and relative humidity profile on a day with intermittent heating.

Figure 6.19 shows the measured and simulated spatial gradient for the two lowest layers (layer 2 - layer 1) and for the lowest and the highest layer (layer 6 - layer 1). The presented figures shows that the simplified model achieves in predicting the temperature gradient. The largest differences between measured and simulated value are 0.9°C and 4%RH. These are noticed during the warming-up of the church, at 9:30 and 9:45. At the end of the heating period, in which the temperature and relative humidity course remain stable, the temperature and relative humidity gradient is slightly overestimated; 0.7°C and +2%RH.

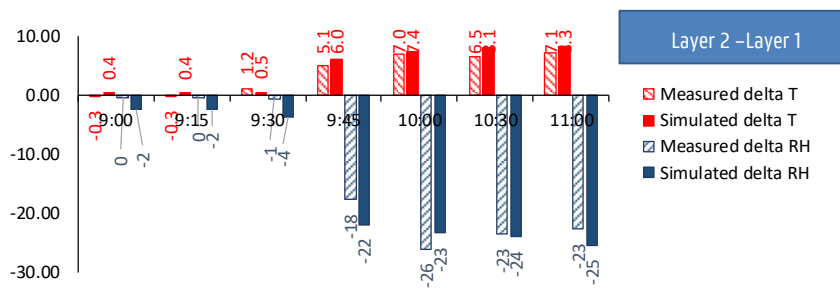


Figure 6.18: Spatial gradient in temperature (red) and relative humidity (blue) between layer 1 and layer 2. Difference between the simulated and measured values.

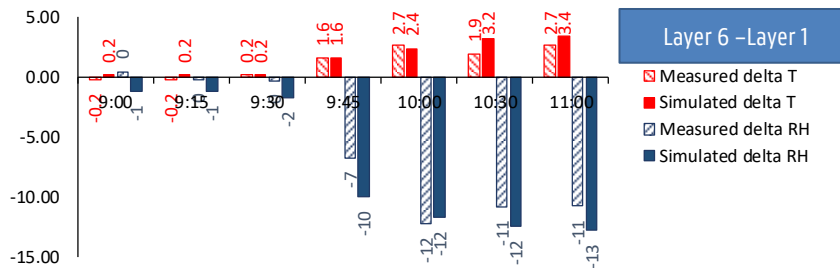


Figure 6.19: Spatial gradient in temperature (red) and relative humidity (blue) between layer 1 and layer 6. Difference between the simulated and measured values.

Influence on the panel painting

Figure 6.20 shows the relative humidity inside the panel painting calculated by the HAM-component. Simulated indoor temperature and relative humidity in air and wall acted as boundary condition. During the heating event a relative humidity decrease can be noticed. However, the drop in relative humidity is largely reduced in the material (10%RH).

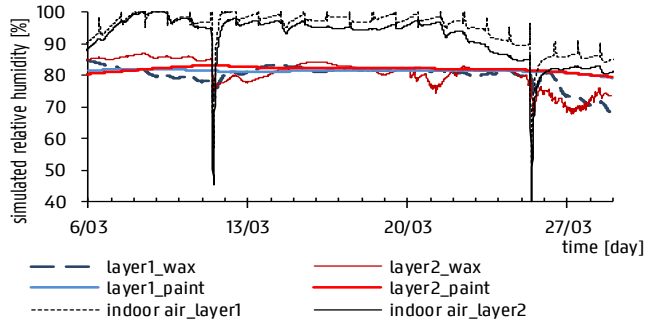


Figure 6.20: Relative humidity of three positions in the wooden panel.

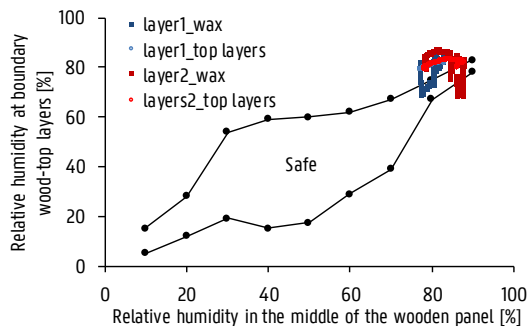


Figure 6.21: Domains of allowable RH fluctuation ($S_d \text{ wax} = 0.1 - S_d \text{ top layers} = 0.37$) at the height of layer 1 (blue) and at the height of layer 2 (red) for a wooden panel with a thickness of 7mm.

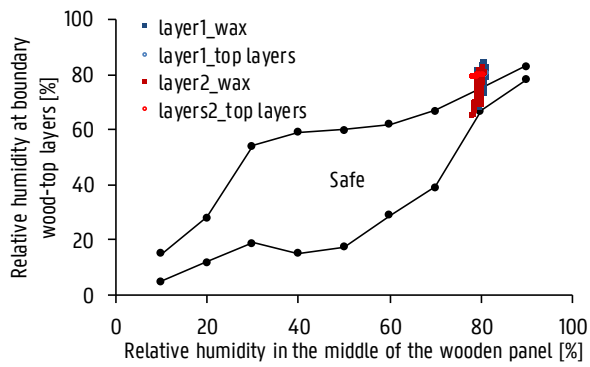


Figure 6.22: Domains of allowable RH fluctuation ($S_d \text{ wax} = 0.1 - S_d \text{ top layers} = 0.37$) at the height of layer 1 (blue) and at the height of layer 2 (red) for a wooden panel with a thickness of 16mm.

To evaluate the risk of mechanical damage, the calculated relative humidity in the middle of the panel painting is compared to the relative humidity at the interface “wood-top layers” or at the back of the wooden panel. Figure 6.21 and Figure 6.22 visualise the domains of allowable relative humidity fluctuation for a wooden panel with a thickness of 7mm or 16mm. The graphs indicate that the relative humidity fluctuations are exceeding the boundaries. This is due to the high relative humidity in the church. Furthermore, a difference can be noticed for layer 2 and layer 1. For layer 2, relative humidity difference between the middle and the top of the wood is larger. This is due to the stratification during heating, leading to higher temperatures and lower relative humidity. Although this modelling is very rough, it shows that the stratification will cause a difference in behaviour in the painting itself.

6.4.2 Temporary solution - Jet: Raising Minimum temperature to 11°C

Secondly, the solution chosen as a temporary measure was analysed; increasing the minimum temperature to 11°C as advised by the circular ML/11 [64]. Using the calibrated model the same period as above was simulated to study the effect of this proposal, but instead of using the actual setpoint of 5°C, the setpoint was raised to 11°C. It was studied which outcome this has on the gradient in time and in space.

Indoor Temperature and Relative humidity

Figure 6.23 shows on a day with intermittent heating the comparison between the simulated vertical profile in case the minimum temperature is 5°C or 11°C. It can be noticed that during heating almost the same profiles for temperature and relative humidity were found. Only in the beginning, the warming-up was less steep. This can also be noticed in Figure 6.24 which shows the temperature and relative humidity course for the two cases. In the base case in which the minimum temperature was 5°C, the intermittent heating causes in the lowest layer a temperature increase of 7°C and a relative humidity drop of 21%RH. In the highest layer, a temperature increase of 12°C and a relative humidity drop of 36%RH is noticed. By raising the setpoint, the gradient in time decreased to 5°C and -17%RH and to 9°C and -28%RH (Figure 6.25).

The warm air heating system also led to a thermal stratification up to 8°C and 25%RH over the height of the church (Figure 6.27). This spatial gradient remained the same in case the setpoint was raised. Furthermore, the heating device switches more frequent on and off in case temperature drops below the setpoint. On the 11th of march, indoor temperature was 8°C without heating. In the base case, the heating device only switched on during service, while in case the minimum temperature was raised to 11°C, the heating was permanently in operation. This resulted in an increase of the amplitude for daily temperature and relative humidity fluctuations. This can for example be seen in Figure 6.26 and Figure 6.27 which show the spatial gradient between the two lowest layers and between the lowest and highest layer. At 9o'clock the temperature difference between layer 1 and 2 measures 1°C instead of 0.2°C. The relative humidity in layer 2 is 5%RH lower than in layer 1, compared to 1%RH in the base case. Although the simulated value for the spatial gradient can contain some uncertainty, it makes sense that when heating switches on more often, a spatial gradient initiates.

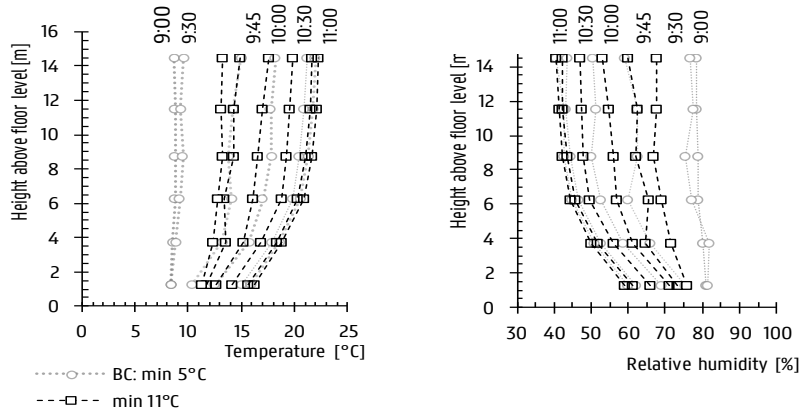


Figure 6.23: Comparison between the base case and the case in which the setpoint is raised to 11°C for the vertical calculated temperature profile on a day with intermittent heating.

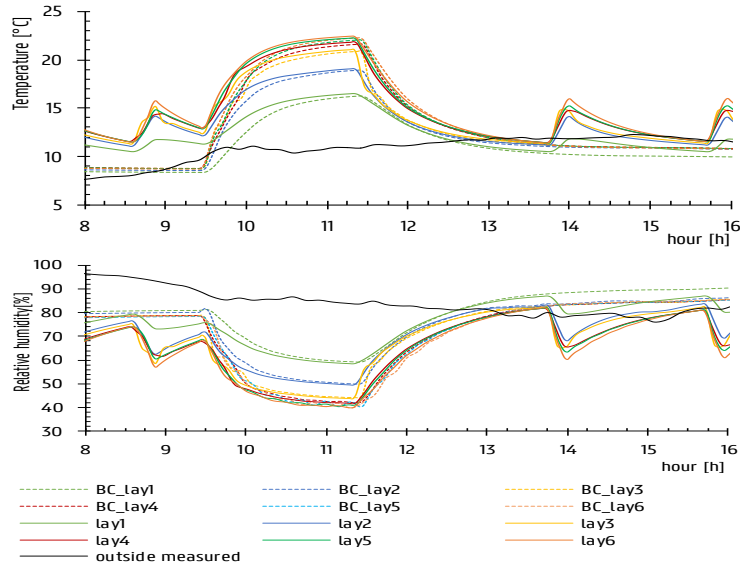


Figure 6.24: Temperature and relative humidity course for the base case and the case in which the setpoint is raised to 11°C.

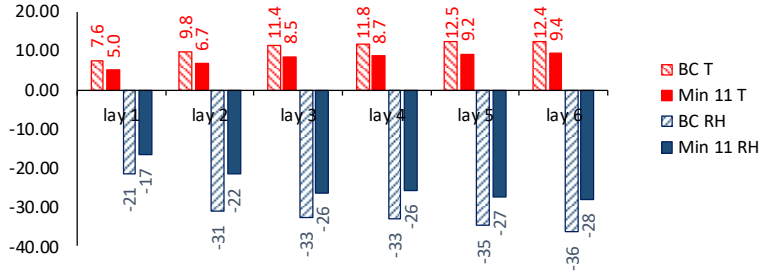


Figure 6.25: Gradient in time for temperature (red) and relative humidity (blue) for all layers. Difference between the start time and end of the intermittent heating. Comparison between simulated base case (BC) and in case the setpoint is raised until 11°C (Min 11).

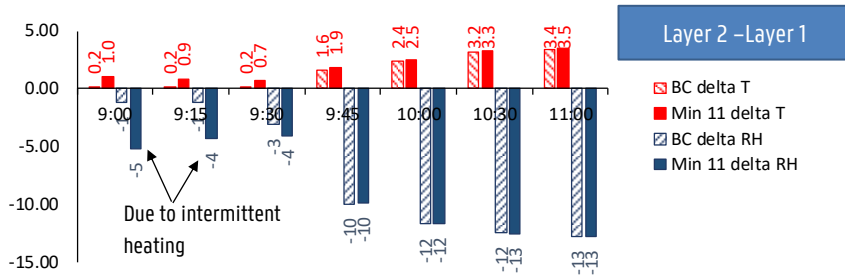


Figure 6.26: Spatial gradient in temperature (red) and relative humidity (blue) between layer 1 and layer 2. Difference between the simulated base case and in case the setpoint is raised until 11°C.

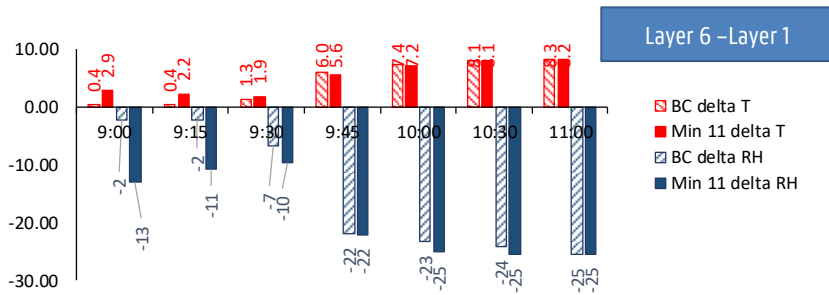


Figure 6.27: Spatial gradient in temperature (red) and relative humidity (blue) between layer 1 and layer 6. Difference between the simulated base case and in case the setpoint is raised until 11°C.

Influence on the panel painting

Figure 6.28 shows the influence of the more frequent relative humidity fluctuations on the relative humidity in the panel. The back of the wooden panel, which is in this case study more sensitive to changes of the indoor environment, shows all the time small fluctuations related to the on/off control and the sudden drop during by heating during a service is still present. However, as shown in Figure 6.29, fluctuations caused by the permanent heating can be nuanced. Because of the lower relative humidity in this period due to the higher minimum temperature, larger fluctuations are allowed. Furthermore, Figure 6.29 indicates that in some cases, relative humidity remains too high. This is certainly the case in case the temperature in church rises above the minimum setpoint. From that moment on, relative humidity is not controlled anymore.

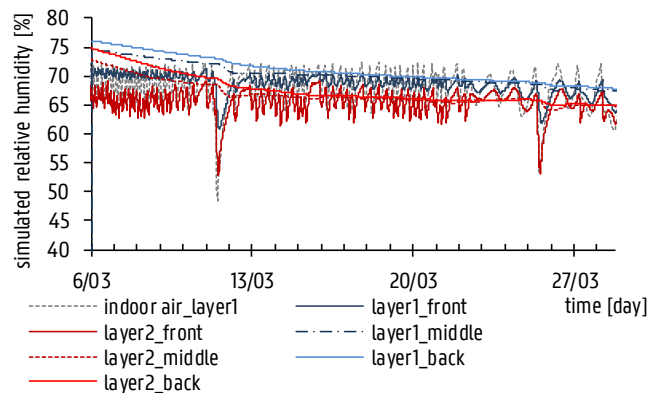


Figure 6.28: Relative humidity of three positions in the wooden panel.

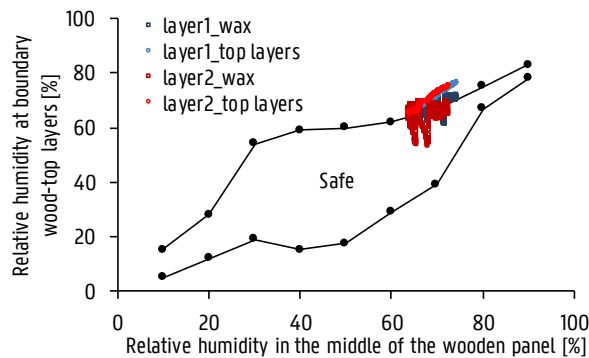


Figure 6.29: Domains of allowable RH fluctuation ($S_d \text{ wax} = 0.1$ - $S_d \text{ top layers} = 0.37$) at the height of layer 1 (blue) and at the height of layer 2 (red) for a wooden panel with a thickness of 7mm.

6.4.3 Variant 1 -Jet: Warming up time of 2°C per hour

In the circular ML/11 [64] was also advised that the temperature of the space may not increase more than 2°C per hour. The same value was advised by Schellen [22] and some authors advised even a lower temperature increase in time (Table 2.3). To do so, two options are possible:

- decreasing the supply temperature,
- decreasing the flow rate.

The minimum temperature of 11°C is maintained. The maximum temperature during service is lowered from 16°C to 15°C as was advised by the circular ML/11.

The first step was to recalculate the heat loss the method described within DIN 4701. Because the minimum temperature is raised to 11°C, the value for Q_w is recalculated. This results in a value of 172.6kW (Table 6.7). In case the flow rate is kept at 6.12kg/s, the supply temperature decreases from 45°C to 39°C ($\Delta T = 28^\circ\text{C}$). In order to obtain a lower temperature, the flow rate must be increased. Assuming a supply temperature of 35°C, results in a flow rate of 7.2kg/s. In case the supply temperature is kept at 45°C³⁶, the flow rate decreases from 6.1kg/s to 5.0kg/s. A further decrease in mass flow rate is not possible, as this will lead to a higher supply temperature. The supply temperature then contradicts to what is advised in the circular letter in which a maximum of 45°C is prescribed.

Table 6.7: Heat loss calculation as formulated in DIN 4701 ($T_{out} = -8^\circ\text{C}$ and $T_{in} = 11/15^\circ\text{C}$).

heat loss through non-accumulating surfaces Q_F	$A \cdot U \cdot \Delta T$	70.87 kW
heat loss due to accumulating surfaces Q_w	$\frac{A_w \Delta T}{R_z}$	32.64 kW
ventilation heat losses Q_L	$0.34 \cdot V_{\text{building}} \Delta T$	69.10 kW

Indoor Temperature and Relative humidity

Figure 6.30 shows on a day with intermittent heating the comparison between the temperature and relative humidity course in case the minimum temperature is 5°C or in case the minimum temperature is 11°C and the supply temperature or flow rate is decreased. The results displays that in case the supply temperature is decreased, less stratification is observed between the higher layers. If the mass flow rate is decreased, the same temperature in layer 1 is achieved, but more stratification remain between the other layers. This is due to the lower velocity along the jet path, resulting in less mixing of the layers.

Compared to the base case, the warming-up was less steep, however the demand that the temperature should only decrease 2K per hour is not achieved. This can also be noticed in Figure 6.27 which lists temperature and relative humidity difference after one hour of preheating for a service. In case the supply temperature was lowered, the temperature in all layers increased by

³⁶ In the circular ML/11 [64] was advised that the supply temperature of the heating should be between 40°C to 45°C. For this reason, no temperature higher than 45°C is taken.

3.8 to 5.9°C. In case the flow rate was decreased, the temperature in all layers increased by 2.5 to 5.6°C. As the ambition is to follow the guidelines of the circular, the minimum temperature was increased to 12°C to achieve an as low as possible temperature difference while heating during a service. Heat losses, supply temperature and flow rate were recalculated. The lowest temperature increase was found when decreasing the mass flow rate. In that case temperature in all layers increased by 1.8 to 4.5°C. In case of the decreased supply temperature, temperature in all layers increased by 2.3 to 4.1°C (Figure 6.29). Although the recommended temperature rise of 2°C per hour was not achieved for all layers, this was the best result that could be achieved with the jet heating in case there was strived for a comfort temperature of 15°C.

The results for the spatial gradient are shown in Figure 6.32 and in Figure 6.33. In case of decreasing the supply temperature, the warm air heating system led to difference up to 2.1°C and 7.9%RH between layer 1 and layer 2. Over the height of the church, a thermal stratification up to 3.5°C and 8.7%RH was observed. In case of decreasing the flow rate, the warm air heating system led to difference up to 3.0°C and 11.3%RH between layer 1 and layer 2. Over the height of the church, a thermal stratification up to 7.5°C and 20.1%RH was observed.

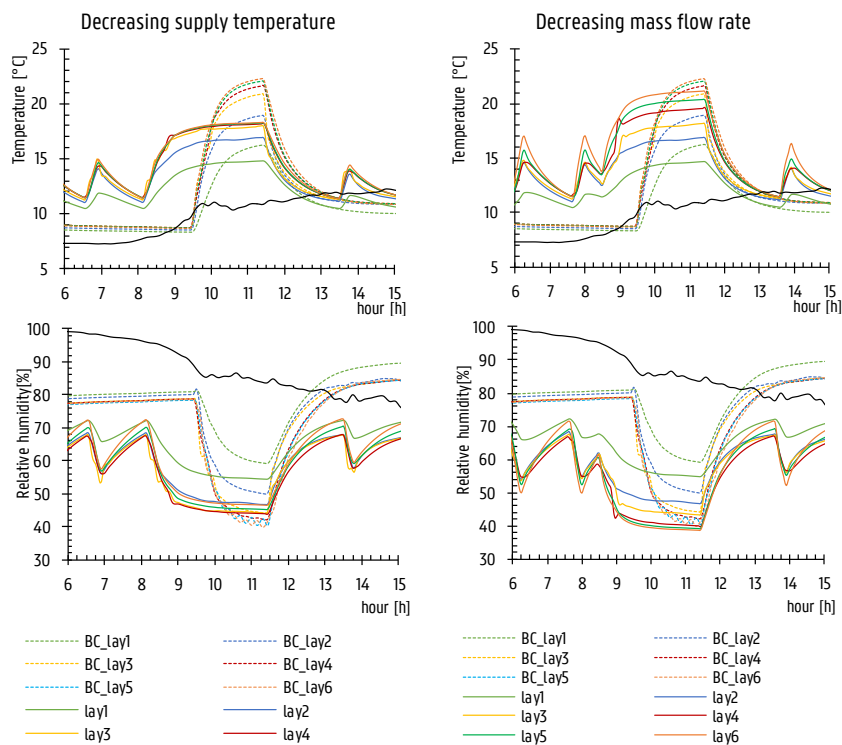


Figure 6.30: Temperature and relative humidity course for the base case and in case the setpoint is raised until 11°C and the temperature is decreased or the rate flow is decreased.

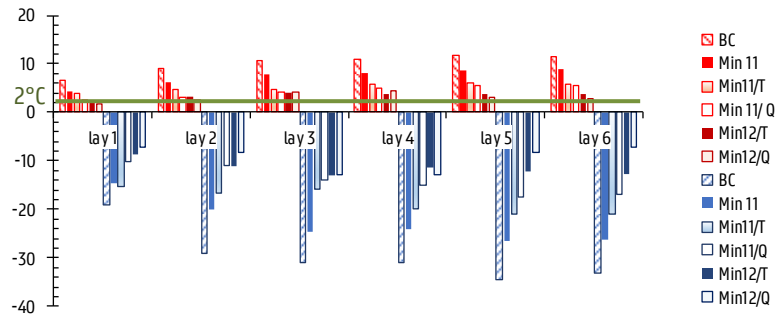


Figure 6.31: Gradient in time for temperature (red) and relative humidity (blue) for all layers. Difference for the first hour of heating during service. Comparison between simulated base case (BC), in case the setpoint is raised until 11°C (Min 11), in case the setpoint is raised until 11°C and the flow rate is decreased (Min 11/Q) or the temperature is decreased (Min 11/T) and in case the setpoint is raised until 12°C and the flow rate is decreased (Min 12/Q) or the temperature is decreased (Min 12/T).

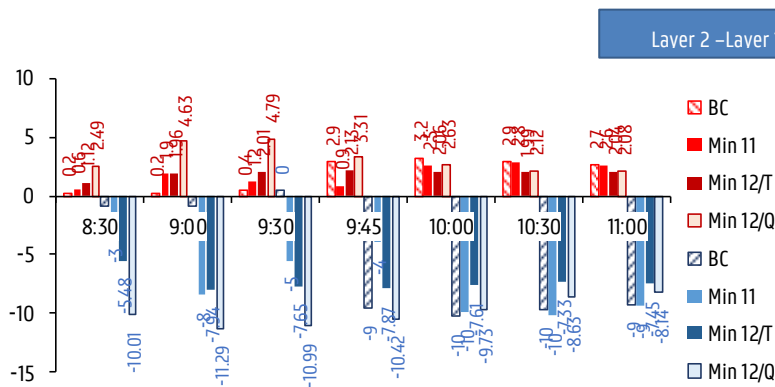


Figure 6.32: Spatial gradient in temperature (red) and relative humidity (blue) between layer 1 and layer 2. Difference between the simulated and measured values.

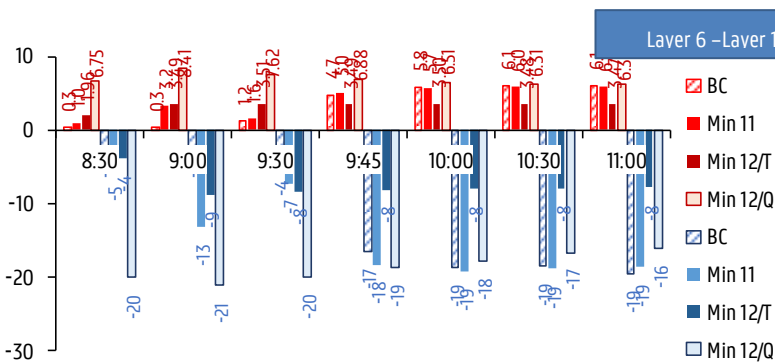


Figure 6.33: Spatial gradient in temperature (red) and relative humidity (blue) between layer 1 and layer 6. Difference between the simulated and measured values.

Influence on the panel painting

Figure 6.34 shows the relative humidity profile in the wooden panel with a thickness of 7mm for the case in which the supply temperature was decreased and the minimum temperature was set to 12°C. Figure 6.33 show the domains of allowable relative humidity fluctuation. Compared to the case in which only the minimum temperature was increased from 5°C to 11°C, fluctuations were smaller. Furthermore a lower average humidity can be observed. Consequently, data points in Figure 6.33 have shifted to the left. However, relative humidity is still too high so that the limits are still being exceeded.

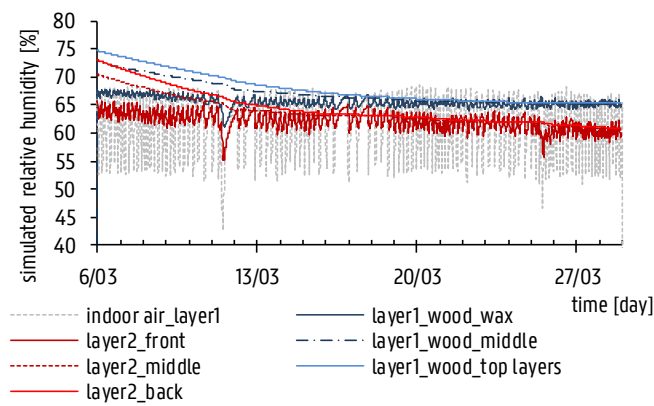


Figure 6.34: Relative humidity of three positions in the wooden panel.

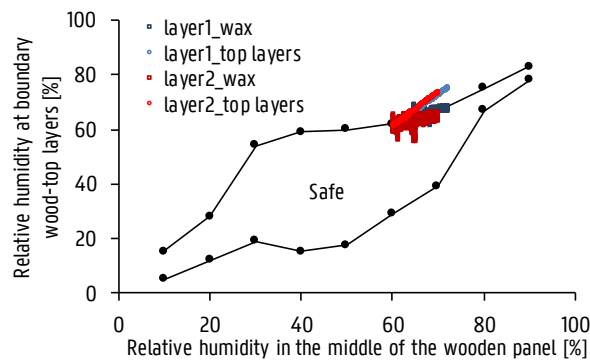


Figure 6.35: Domains of allowable RH fluctuation ($S_d \text{ wax} = 0.1$ - $S_d \text{ top layers} = 0.37$) at the height of layer 1 (blue) and at the height of layer 2 (red) for a wooden panel with a thickness of 7mm.

6.4.4 Variant 2 - Underfloor Heating

To model underfloor heating, the floor of the church building is defined in TRNSYS as an active layer. Characteristics of the radiant floor system are listed in Table 6.8. The supply temperature of the warm water had a constant value of 40°C. The mass flow rate for the total area of 730m² was 7600kg/h. A thermostat controls when heating is needed. The same setpoint temperatures as in the previous cases are used; during a service a temperature of 15°C, otherwise a minimum temperature of 12°C.

Indoor Temperature and Relative humidity

Figure 6.36 shows on a day with intermittent heating the comparison between the temperature and relative humidity course in case the minimum temperature is 5°C or in case the minimum temperature is 12°C and underfloor heating is used. Almost no stratification was found and the temperature in layer one was not higher than the other layers. Reason for this is that the simplified thermal zonal model assumes mixing in cases temperature inversion occurs. It can be noticed that during a service, underfloor heating did not achieve to obtain the desired 16°C. Since this is not realistic, a second case with underfloor heating was simulated in which there was additional heating during service with the jet heating.

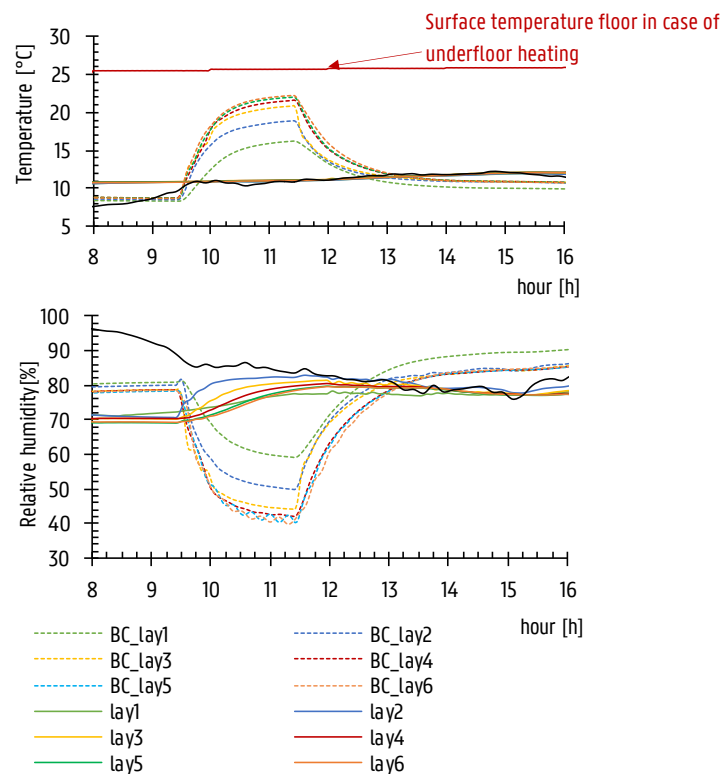


Figure 6.36: Temperature and relative humidity course for the base case and in case of floor heating in which the setpoint is raised until 12°C.

Table 6.8: Characteristics of the radiant floor.

Active Layer	Value
Specific thermal capacity of fluid	4.19J/(kg.K)
Pipe wall conductivity	0.35 W/(m.K)
Pipe spacing	0.2m
Pipe outside diameter	0.02m
Pipe wall thickness	0.002m

To obtain a minimum temperature of 12°C; a power of 165kW is needed. The TRNSYS simulation of the case with underfloor heating showed that the maximum power supplied by the underfloor heating was 86kW. This means that for heating the space from 12 to 15°C, still 79kW is required in addition. Because previous simulation showed that reducing the supply temperature led to better results than decreasing the jet flow rate, a jet with a lower supply temperature was chosen in this case. This yields in a jet flow with a supply temperature of 30°C ($\Delta T = 18^\circ\text{C}$) and with a flow rate of 4.4kg/s. The simulated course on a day with intermittent heating is shown in Figure 6.37.

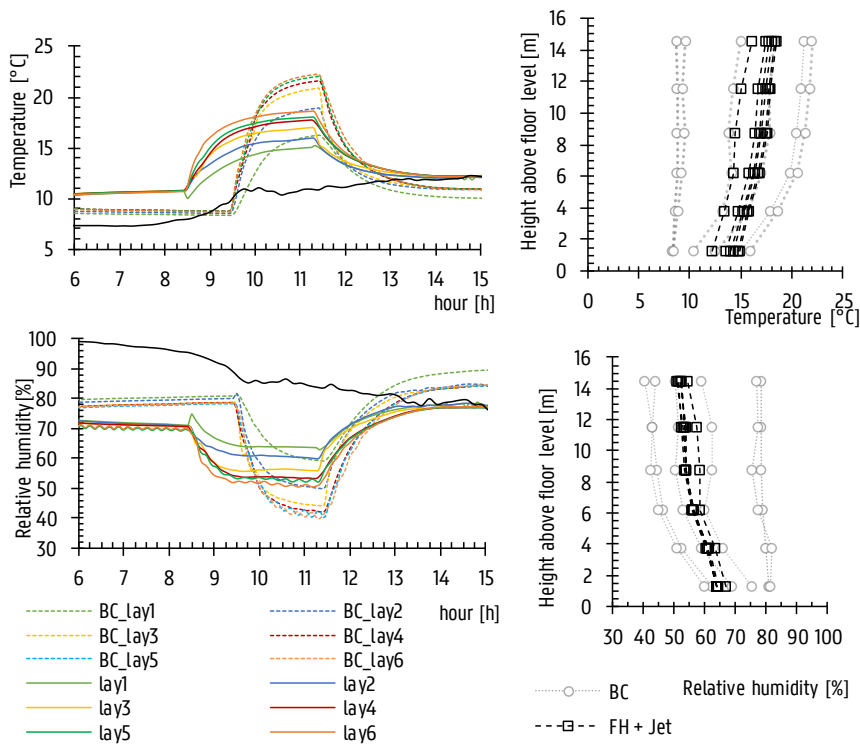


Figure 6.37: Temperature and relative humidity course for the base case and in case of floor heating combined with a jet. The minimum temperature is raised until 12°C.

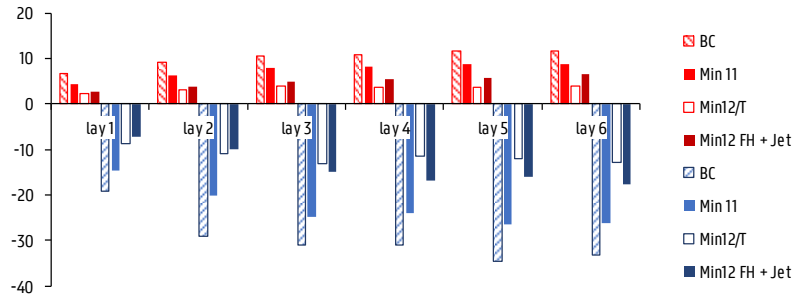


Figure 6.38: Gradient in time for temperature (red) and relative humidity (blue) for all layers. Difference between the start time and end of the intermittent heating. Comparison between the base case (BC), the intermittent solution (Min 11) and in case with floor heating whether or not combined with a jet (Min). The setpoint for the minimum temperature is 12°C (Min 11).

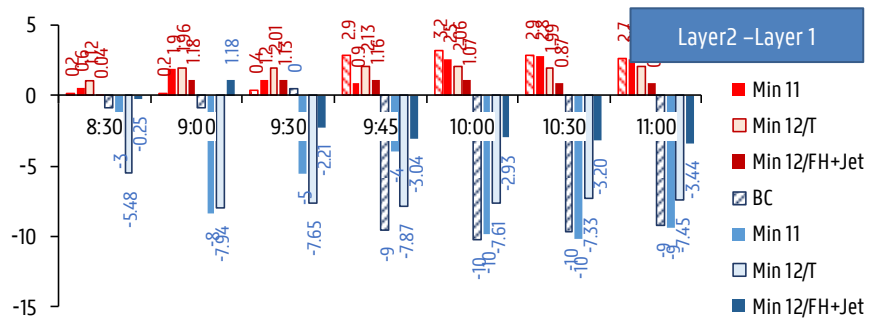


Figure 6.39: Spatial gradient in temperature (red) and relative humidity (blue) between layer 1 and layer 2. Difference between the simulated base case and in the case with floor heating combined with a jet.

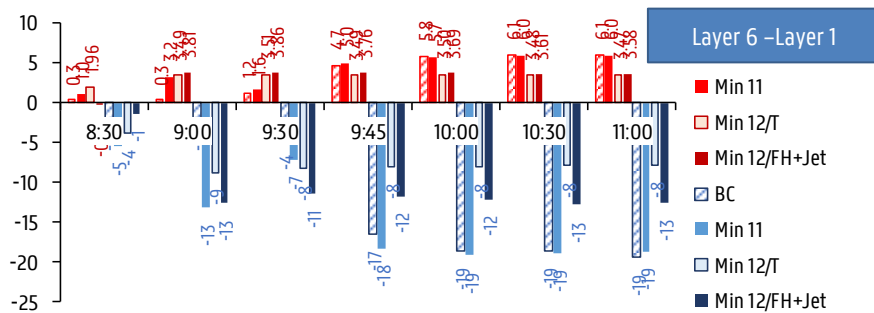


Figure 6.40: Spatial gradient in temperature (red) and relative humidity (blue) between layer 1 and layer 6. Difference between the simulated base case and in the case with floor heating combined with a jet.

During service, a similar temperature and humidity course is found as in the case with jet heating. However, Slightly higher temperature increases were obtained for layer 3 till 6: the temperature in all layers increased by 2.3 to 5.6°C (Figure 6.38). a possible explanation for the higher temperatures in the upper layers is the following. The underfloor heating does not cause stratification. Consequently, temperatures across all layers are the same, which is not the case when heating with a jet. When the jet heating is started to heat up the church during service, stratification occurs. This causes larger temperature differences in one layer during the preheating.

The results for the spatial gradient are shown in Figure 6.39 and Figure 6.40. During service the heating between layer 1 and layer 2 remained quite small: 2.2°C and 3%RH. Only at 9:30 a somewhat higher difference in relative humidity was observed. Over the height of the church, a thermal stratification up to 3.6°C and 13%RH was observed. Compared to the other simulated cases, floor heating has the lowest spatial differences in relative humidity.

Influence on the panel painting

Figure 6.41 shows the relative humidity profile in the wooden panel with a thickness of 7mm. A smoother temperature and relative humidity course is found compared to the cases with only jet heating. Figure 6.33 show the domains of allowable relative humidity fluctuation. It can be noticed that relative humidity was also in this case too high, leading to a possible risk of mechanical damage.

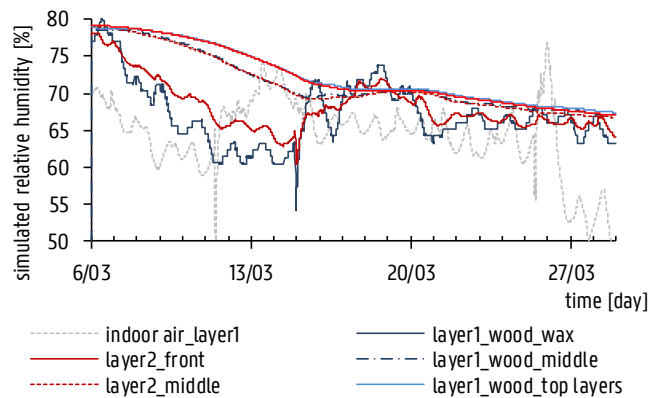


Figure 6.41: Relative humidity of three positions in the wooden panel.

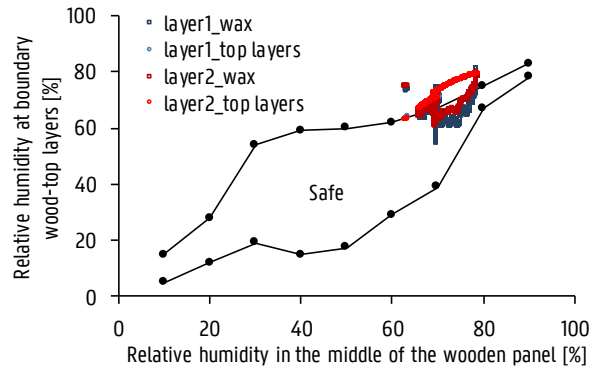


Figure 6.42: Domains of allowable RH fluctuation ($S_d \text{ wax} = 0.1$ - $S_d \text{ top layers} = 0.37$) at the height of layer 1 (blue) and at the height of layer 2 (red) for a wooden panel with a thickness of 7mm.

6.5 Conclusion

In this chapter the possibilities of the developed hygrothermal-zonal model were used to assess preservation conditions of an actual case of a church building. After an analysis of the measurement data, two problems were found. A first problem was the relative humidity in the church was too high for conservation of wooden artefacts when the church was not heated. At every measurement location, a relative humidity higher than 75% was registered. In Chapter 3 was noticed that in case of high relative humidity, smaller relative humidity fluctuations were allowed than in the mid-range. A second problem were too large short time fluctuations in relative humidity and temperature caused by the actual heating system. As a consequence, the existing situation was a risk for damage to the wooden objects in the church and thus also for the most important work; a wooden altarpiece.

The simulation study compared the base case (minimum temperature of 5° and 16°C during service) to the solution chosen as an temporary measure - increasing the minimum temperature to 11°C - and other possibilities. For the other possibilities, the circular ML/11 [64] written in 2011 by the department of Urban Planning of the Flemish government was used as guideline (Chapter 2-paragraph 2.1.3). The chosen systems, were systems also found in practice, and the goal was then also to demonstrate the practical use of the newly developed coupling.

The main conclusions of the simulation study were:

- For all cases with a jet, stratification occurred. This confirms what was described by Bordass [326] and Schellen [22]. Namely, stratification is almost inevitable unless air distribution is very carefully considered.
- The intermittent solution caused too high fluctuations in relative humidity.
- It was not possible to achieve a temperature increase lower than 2°C per hour in case the minimum temperature of 11°C was kept, even when supply temperature or mass flow rate was decreased. Hence, the minimum temperature was raised up to 12°C, which is still allowed following the circular ML/11 [64]. In that case, it was not possible for the higher layers to achieve a temperature decrease lower than 2K.
- Best results were found in case heating occurred with a low supply temperature and a higher flow rate.
- More fluctuations were observed in case of increasing the minimum temperature to 11°C or 12°C. This was due to the constant switching on and off of the heating device. In this case study, however, the fluctuations can be nuanced. Due to the lower level of relative humidity achieved by the permanent heating larger fluctuations in relative humidity are allowed (Chapter 3). When underfloor heating was used to achieve the minimum temperature, no fluctuations in relative humidity were observed.
- Underfloor heating did not result in heating up the church till 15°C. The explanation for this can be found in the work of Schellen[22]. Firstly, walls and vaults are not insulated so the area of the heated floor is relatively small compared to the heating loss area of walls and vaults. Secondly, the height of the space is large.

7

Conclusion and Perspectives

7.1 Conclusions

The dissertation studied the issues of how damage risk of valuable artworks in historical buildings, with particular attention to panel paintings, could be estimated more accurately by using simulation studies. The main cause of deterioration of organic works of art, and moreover panel paintings, is the mechanical deterioration related to indoor relative humidity. To avoid extensive treatment or irreversible damage, preventive conservation tries to elongate the lifetime of the work of art. This is done by improving the indoor climate until it is as stable as possible. Methods of stabilization consist of control of the environment, whether of whole buildings, whether of localized climate vitrines.

This PhD-dissertation aimed at developing a simulation strategy to estimate the predicted risk for works of art in historical buildings, while taking into account two typical conditions in these buildings. These were:

- the presence of moisture in heavy building walls
- the occurrence of stratification in the often very large interior volumes due to the limited control by (older) climate installation system.

The emphasis lied on developing a fast calculating modelling approach intended for practical use which predicts if the measures lead to the desired improvement concerning preservation conditions as well as possible. This holds that there was started from a 'classical' BES tool and it has been studied which adjustments to the tool are required to contain the mentioned conditions. Because the results of the simulation study are used to assess and to compare the outcome on the indoor climate of different retro-fitting measures, it was also studied which assessment tool is suitable.

Assessment

It was started with a literature review of guidelines and damage risk functions to answer following questions :

- “Which indoor climate conditions are necessary for preserving works of art?” (Chapter 2)
- “How can we assess the risk of damage to a work of art, which is related to the indoor climate?” (Chapter 3).

Many guidelines advice an average value and an allowed fluctuation. The temperature is usually around 20°C and the value of the average relative humidity is usually defined in the so-called mid-range (40-60%RH). Some authors or guidelines also make a distinction between an allowed short-term and allowed seasonal fluctuation.

In case the relative humidity is in the mid-range, these guidelines give a good indication of allowable fluctuations. However, Chapter 3 shows, using a case study of a panel painting, that the danger lies when these guidelines are used to estimate the damage risk and especially when an extrapolation outside the mid-range is performed. The reason is the guidelines were designed to define a safe zone. The background of defining the boundaries is based on the behaviour of materials, whether it is based on experience or on lab research. Once outside the boundaries, there is damage risk. Expressing the change on damage risk outside these boundaries is not possible. This results in the conclusion that either there is damage or not.

Experience shows that other climates than those defined in the guidelines are possible. If one wants to assess if this kind of climate is allowable, one should use the so-called object-related method to estimate the damage risk. This method will assess damage risk based on three types of deterioration; chemical, biological and mechanical. The third type, mechanical deterioration, is based on an object's dimensional behaviour. It is dependent on dimensional changes related to changes in the material's moisture content. The moisture sorption curve allows to define the moisture content in the material using indoor air relative humidity. For organic materials, like used for the works of art, this curve is S-shaped. This means that the curve is flattened in the mid-range (40-60%RH) and steep at low or high relative humidities. As a consequence, relative humidity changes outside the mid-range will lead to larger expansion or shrinkage.

The difficulty to assess damage risk using the object-based method is that material characteristics have to be known. In this dissertation moisture characteristics were experimentally derived for finishing layers representative of a wooden panel painting from the 15th-16th century and the moisture distribution in the object was modelled by a 1D-HAM model, based on a code developed by M. Steeman [226]. This 1D-HAM model can be directly integrated in the BES-software. Use was made of a previous study of Mecklenburg [118] to link the changes of moisture content in the object to dimensional changes and thus damage risk.

This is often done as experiments are time-consuming. The question, however, is to what extent these and the material characteristics can be generalized. Namely:

- In the mid-range, for which also the mentioned guidelines can be used, the flat course of the sorption curve allows a larger inaccuracy of material characteristics. Outside these boundaries, inaccuracy in material characteristics cause a larger uncertainty in predicting dimensional changes and thus estimating risk of damage.
- In reality, an object has a complex structure (cracks, different thickness in material layers...). Consequently, simplifications and assumptions have been made, both in a simulation study and in an experiments, leading to an uncertainty in predicting object behaviour. Consequently, also the risk on damage is more uncertain.

The object-oriented method thus allows you to estimate damage in individual situations or outside the defined boundaries by the more generalized guidelines. However, the background of material behaviour and the uncertainty of the prediction method must be kept in mind. This is especially the case when working in high or low humid conditions.

Modelling

Chapter 4 and 5 examined to which extent the expansion of a BES tool with simplified moisture buffer models and simplified stratification models allowed to improve the simulation of the indoor climate in historic buildings.

Chapter 4 focussed on the modelling of hygric and thermal buffering capacity in historical buildings. Because of the high thermal and hygric capacity of the building envelope, the indoor temperature and humidity of historic buildings is attenuated. As the amplitude of the fluctuations is an essential cause of damage to works of art, it is important to estimate these amplitudes appropriately. Therefore, buffering characteristics must be taken into account in simulating the indoor climate. To solve in a BES-software the transient behaviour for a longer time period relative fast, the buffering behaviour is solved in a simplified way. Chapter 4 goes deeper into detail in the mathematical background of the sub-model which solves the wall heat conduction process, responsible for the thermal capacity of the wall and the sub-model which calculates the moisture buffering of the envelope. As shown, the effect of changing the value for the timebase for the sub-model in TRNSYS, was negligible for the case study. For the second sub-model, namely moisture buffering, four models were compared. The most simple model was the moisture capacitance (EC) model available in TRNSYS. For the detailed modelling of moisture flux, a slightly adapted moisture transport model (HAM) intended to use in the BES software TRNSYS, was used (former model developed by M. Steeman). In between the very simplified and detailed approach, the EMPD model of TRNSYS was used. It was found that very detailed modelling of the moisture buffering by the building envelope had no significant improvement in the prediction of the relative humidity course compared to the more simplified EMPD-model. This was due to different reasons:

- Uncertainty in moisture gains or losses (visitors, infiltration) which were more relevant in case of a leaky building.
- Uncertainty in material characteristics necessary for the moisture buffering models.

The big advantage of using an EMPD model instead of a HAM model is that the calculation time is reduced. Also, the EC model still provided reasonable results. The gain of time by using an EC-model instead of an EMPD, is smaller, compared to the gain of time by using an EC model instead

of a HAM-model. However, because the calibration of an EC value is more straightforward in use, the time to build this simulation model is shorter.

Chapter 5 described the coupling of a zonal model with a BES-software (in this case TRNSYS) in order to predict the transient hygrothermal response of tall historical buildings while taking into account the vertical hygrothermal gradients in one zone. The advantage of this coupling is that it still has a short calculation time and can predict longer time periods. Based on a literature review, it was opted to use a temperature-based zonal model. A validation was performed to check the correctness of the coupled thermal-zonal-BES model. To do so, the same cases studies were used as these that were used for the original model. There are two important comments :

- Using unsteady values for of the convection transfer coefficients calculated by algorithms instead of using constant values improved the agreement between the measured and simulated results.
- Calculating longwave radiation and shortwave diffuse radiation using so-called Gebhart factors increased computing time, but had a significant improvement on the agreement between measured and simulated temperature.

Because to estimate the preservation conditions also the variation in relative humidity in the space have to be known, equations for calculating moisture distribution in the zone were added to the original model as the original model only calculated temperature distribution. To analyse the moisture equations, the effect of the addition of a moisture sources was examined numerically. The studied cases were variations on the cases used to validate temperature distribution. The results found for the moisture distribution were logical and could be explained by analysing the air flow in the zone.

7.2 Perspectives

The aim of the PhD-dissertation was to develop a simulation strategy to estimate the predicted risk for works of art, taking into account the presence of moisture in heavy building walls and the occurrence of hygrothermal gradients (stratification) in the often very large interior volumes due to the limited control by (older) climate installation system. Although the proposed modelling approach was shown to be valuable to estimate preservation conditions more accurately (Chapter 6), this is certainly not the end of the research on damage to historical works of art.

Assessment

Last years, different interesting studies were presented on estimating damage risk of museum objects and different numerical models were developed to model the behaviour of these objects. However, the gap stays between numerical models validated by laboratory tests, and the behaviour and damage observed at museum objects under real indoor conditions. One reason is that modelling the exact museum object is very difficult as the exact geometry and the thickness of different material layers is irregular. Furthermore, knowledge about material characteristics of the aged (and damaged) materials is limited. However, a recent study of Ekelund et al.[362] coupled an examination of empirical data obtained from naturally aged museum objects, i.e. the collection analysis, with numerical modelling and experimental testing. It would be interesting to integrate these with the methods for damage assessing applied in this work.

Modelling

In this dissertation, a thermal-zonal model was used to assess stratification. It succeeded to estimate fast the stratification in a tall building. Of course, this is only one model and in future research, also other strategies to assess the stratification can be implemented in BES. Concerning the modelling with the hygro-thermal zonal model, the following points are remarked:

- The disadvantage is that the code of the building model in TRNSYS, Type 56, is not precompiled and is not accessible. As a consequence, the coupling between the thermal-zonal model and the TRNBUILD model could only performed indirectly in the simulation environment. This makes it more laborious than needed. Furthermore, the most recent version of TRNSYS, version 18, allows to couple six air nodes instead of two, which opens new perspectives for zonal airflow modelling. So, it would be beneficial that the TRNBUILD code becomes open source, like e.g. Modelica, Energyplus,...
- There was started from the thermal zonal model presented by Togari at al. in which equations were added to assess moisture transfer. The next step should be to validate the moisture flow in the simplified model with a validation study in reality.
- The model, as it is now, is not capable of taken into account the local effect of underfloor heating. The reason for this is that if temperature inversion occurs, direct

air mixing occurs in the stratification model (value C_b in (5.16)). It would be an added value to also implement underfloor heating in the model. In this context, consideration is initially given to implement a plume equation (similar as the jet equation). However, further research is needed.

Furthermore, the air change rate in ancient churches and other historical and monumental buildings has a significant influence on the indoor temperature and humidity. This is because these buildings are often leaky, and the sealing possibilities are often limited by esthetical and preservation considerations [361]. In the model of the case study of the church building, the LBL available in TRNSYS was used. As infiltration is important, it would be interesting to go deeper into the infiltration part in the BES model. The recent work of Hayati [361,363] describes this more into detail and suggest some adapted infiltration models, which could be interesting.

As already mentioned in this work, the use of Computational Fluid Dynamics (CFD) is probably the most suitable method to predict the airflow pattern, but it is quite time consuming and requires a powerful computer. Because the objective in this work was the opposite, this approach was not taken into account and there was focused a simple model. It would be interesting, however, to compare and adapt the simplified model in the future based on results found in a (steady) CFD study. One example is, inter alia, the fine-tuning of the mixing coefficient used when temperature inversion occurs. Another possibility is to check whether the moisture flow is also dominated by temperature differences.

Publications

Journal publications as first author

De Backer L, Laverge J, Janssens A, De Paepe M. Evaluation of the diffusion coefficient and sorption isotherm of the different layers of early-Netherlandish wooden panel paintings; 2017. (accepted for publication – online version available).

De Backer L, Steeman M, Janssens A, De Paepe M. Evaluation of display conditions of the Ghent altarpiece at St. Bavo cathedral. *Journal of Cultural Heritage*; 2017. (accepted for publication - online version available)

Publications in proceedings of conferences as first author

De Backer L, Van Den Bossche N, Janssens A, De Paepe M. Evaluation of the hygric properties of a wooden panel painting to perform HAM simulations. XIV DBMC CONFERENCE. Ghent, Belgium; 2017.

De Backer L, Laverge J, Janssens A, De Paepe M. A coupled BES-zonal model to predict stratification in a large building. Healthy Buildings Conference. International Society of Indoor Air Quality and Climate (ISIAQ); 2015.

De Backer L, Laverge J, Janssens A, De Paepe M. The use of a zonal model to calculate the stratification in a large building. 35th AIVC Conference Proceedings. AIVC; 2014. p. 522–31.

De Backer L, De Paepe M, Janssens A. On the coupling of a zonal model with a BES model for predicting vertical temperature distribution. 10th International Conference on Heat Transfer, Fluid Mechanics and Thermodynamics, Proceedings. Orlando, Florida, USA; 2014. p. 2008–13.

De Backer L, Laverge J, Janssens A, De Paepe M. On the coupling of a zonal model with a multizone building energy simulation model. In: Arfvidsson J, Harderup L-E, Kumlin A, Rosencrantz B, editors. 10th Nordic Symposium on Building Physics, Proceedings. 2014. p. 71–8.

De Backer L, Janssens A, Van Belleghem M, De Paepe M. The aid of TRNSYS simulation for the conservation of an work of art: a case study. In: Mahdavi A, Martens B, editors. CONTRIBUTIONS TO BUILDING PHYSICS. Vienna, Austria: Vienna University of Technology. Department of Building Physics and Building Ecology; 2013. p. 351–5.

De Backer L, Janssens A, De Paepe M. Evaluation of the indoor climate for conservation of the polyptic “The Adoration of the Mystic Lamb” in the St. Bavo cathedral in Ghent. 5th International Building Physics Conference, Proceedings. Kyoto: 5th IBPC organizing committee; 2012. p. 1263–70.

De Backer L, De Paepe M, Janssens A. Evaluation of the climate for conservation of the adoration of the mystic lamb in the St. Bavo Cathedral in Ghent. 8th international conference on heat transfer, fluid mechanics and thermodynamics, Proceedings. Ghent, Belgium: Ghent University, Department of Flow, heat and combustion mechanics; 2011. p. 660–5.

De Backer L, Van Belleghem M, Steeman M, Janssens A, De Paepe M. Evaluation of the climate for conservation of the adoration of the mystic lamb in the St. Bavo Cathedral in Ghent. In: Vinha J, Piironen J, Salminen K, editors. Proceedings of the 9th Nordic symposium on building physics (NSB 2011). Tampere, Finland: Tampere University of Technology. Department of Civil Engineering; 2011. p. 791–8.

References

- [1] ICC- International Institute for Conservation of Historic and Artistic Works n.d. <https://www.iiconservation.org> (accessed July 22, 2017).
- [2] ICOM - ICOM-CC n.d. <http://www.icom-cc.org/> (accessed July 23, 2017).
- [3] Behoudsmedewerker erfgoed | FARO. Vlaams steunpunt voor cultureel erfgoed vzw n.d. <https://www.faronet.be/kalender/behoudsmedewerker-erfgoed> (accessed March 2, 2017).
- [4] UNESCO. Safeguarding our documentary heritage 2014. <http://webworld.unesco.org/safeguarding/>.
- [5] Krus M, Kilian R, Sedlbauer K. Mould growth prediction by computational simulation on historic buildings. In: Padfield T, Borchersen K, editors. Museum Microclimates, The National Museum of Denmark; 2007.
- [6] Erfgoedinspectie/Collectie Nederland. Luchtspiegelingen - De mens en het museale binnenklimaat. Erfgoedinspectie / Collecties; 2007.
- [7] The Mystic Lamb. Saint-Bavo's Cathedral- Ghent 2012. <http://users.skynet.be/sintbaafskathedraal-gent> (accessed February 17, 2010).
- [8] NGA. Preventative conservation. NGA (National Gallery of Australia): Collection Conservation 2017. <https://nga.gov.au/Conservation/prevention/index.cfm> (accessed May 17, 2017).
- [9] AIC. About Conservation - Definitions of Conservation Terminology 2015. <http://www.conservation-us.org/>.
- [10] ICOM C. Terminology for conservation 2008. <http://www.icom-cc.org/242/about/terminology-for-conservation/#.WMEZqjvvtEY> (accessed March 9, 2017).
- [11] The Getty Conservation Institute. Preventive Conservation Overview 2009. http://www.getty.edu/conservation/about/science/preventive_cr.html (accessed December 14, 2016).

- [12] UNESCO World Heritage Centre. Preventive Conservation: Course outline. UNESCO World Heritage Centre n.d. <http://whc.unesco.org/> (accessed December 14, 2016).
- [13] Charney N. Restored and ravishing: the magnificent Ghent Altarpiece gives up its centuries-old mysteries. *The Guardian* 2016.
- [14] Bret J, Jaunard D, Mandron P. The Conservation-Restoration of Wooden Painting Supports. In: Dardes K, Rothe A, editors., Getty Publications; 1998.
- [15] Vlaamse Gemeenschap. Decree protecting the moveable cultural heritage of extraordinary importance. Decreet houdende bescherming van het roerend cultureel erfgoed van uitzonderlijk belang (In Dutch). 2003.
- [16] Dahlin E, Grønøft T, López-Aparicio S, Odlyha M, Scharff M, Larsen T, et al. PROPAIN: Improved Protection of Paintings during Exhibition, Storage and Transit Final Activity Report. 2010.
- [17] Wadum J. Microclimate Boxes for Panel Paintings. In: Dardes K, Rothe A, editors. vol. Proceedings of a Symposium at the J. Paul Getty Museum., The Getty Conservation Institute; 1995, p. 497–524.
- [18] Richard M. The benefits and disadvantages of adding silica gel to microclimate packages for panel paintings. In: Padfield T, Borchersen K, editors., Copenhagen, The National Museum of Denmark: The National Museum of Denmark; 2007, p. 237–44.
- [19] Hackney S. The Evolution of a conservation framing policy at Tate. In: Padfield T, Borchersen K, editors., Copenhagen, The National Museum of Denmark: 2007.
- [20] Camuffo D, Sturaro G, Valentino A. Showcases: a really effective mean for protecting artworks? *Thermochimica Acta* 2000;365:65–77. doi:10.1016/S0040-6031(00)00614-6.
- [21] Glasbau Hahn. Clean Air and Climate Control Systems for Display Cases. *DISPLAY CASES* n.d.
- [22] Schellen H. Heating monumental churches : Indoor Climate and Preservation of Cultural Heritage. PhD dissertation. Technische Universiteit Eindhoven, 2002.
- [23] Bratasz Ł, Kozłowski R. Entwicklung der neuen EU-Normen –The CEN TC346 draft standard on heating historic churches: minimizing disturbance to the indoor climate. *Klimagegestaltung im Spannungsfeld zwischen Kulturgutschutz und Nutzerwünschen, Tagungsblatt des 1. Konservierungswissenschaftlichen Kolloquiums*, Berlin: 2007, p. 24–31.
- [24] Napp M, Wessberg M, Kalamees T, Broström T. Adaptive ventilation for climate control in a medieval church in cold climate. *International Journal of Ventilation* 2016;15:1–14. doi:10.1080/14733315.2016.1173289.
- [25] Napp M, Kalamees T. Energy use and indoor climate of conservation heating, dehumidification and adaptive ventilation for the climate control of a mediaeval church in a cold climate. *Energy and Buildings* 2015;108:61–71. doi:10.1016/j.enbuild.2015.08.013.
- [26] Straube DJ, Burnett DE. Review of Modeling Methods for Building Enclosure Design. 1999.
- [27] Augenbroe G, Malkawi A, editors. *Advanced Building Simulation*. Taylor & Francis Group; 2004.
- [28] Parys W. Cost optimization of cellular office buildings based on building energy simulation. PhD dissertation. KU Leuven, 2013.
- [29] Wetter M. A View on Future Building System Modeling and Simulation. In: Hensen JLM, Lamberts R, editors. *Building Performance Simulation for Design and Operation*, Routledge, UK: 2011.

- [30] Underwood C, Yik F. *Modelling Methods for Energy in Buildings*. John Wiley & Sons; 2008.
- [31] Bouia H, Dalicieux P. Simplified modeling of air movements inside dwelling room, 1991, p. 106–10.
- [32] Harish VSKV, Kumar A. A review on modeling and simulation of building energy systems. *Renewable and Sustainable Energy Reviews* 2016;56:1272–92. doi:10.1016/j.rser.2015.12.040.
- [33] Hens H. *Technical Synthesis Report on Heat, Air and Moisture Transfer in Highly Insulated Building Envelopes*. Physics International Energy Agency (IEA); n.d.
- [34] Woloszyn M, Rode C. IEA Annex 41: whole building heat, air, moisture response. Volume 1: *Modelling Principles and Common Exercises*. Energy Conservation in Buildings and Community Systems (ECBCS); 2008.
- [35] Widström T, Mattsson M. Multifunctional whole building simulation as a method in assessing retrofitting strategies in historical buildings. *Building Simulation 2011*, Sydney, Australia: 2011.
- [36] Chae YT, Lee YM, Longinott D. Assessment of Retrofitting Measures for a Large Historic Research Facility Using a Building Energy Simulation Model. *Energies* 2016;9:466. doi:10.3390/en9060466.
- [37] Corgnati S, Bednar T, Jang Y, Yoshino H, Filippi M, Danov S, et al. *Statistical analysis and prediction methods*. Institute for Building Environment and Energy Conservation; 2013.
- [38] Steeman HJ, Van Belleghem M, Janssens A, De Paepe M. Coupled simulation of heat and moisture transport in air and porous materials for the assessment of moisture related damage. *Building and Environment* 2009;44:2176–84. doi:10.1016/j.buildenv.2009.03.016.
- [39] Pitsch S, Holmberg S, Angster J. Ventilation system design for a church pipe organ using numerical simulation and on-site measurement. *Building and Environment* 2010;45:2629–43. doi:10.1016/j.buildenv.2010.05.022.
- [40] Troi A, Franzen C, Hauslade G. *Computational fluid dynamics can ensure high quality conservation interventions. A case study*, 2006.
- [41] Steeman H-J, Janssens A, De Paepe M. On the applicability of the heat and mass transfer analogy in indoor air flows. *International Journal of Heat and Mass Transfer* 2009;52:1431–42. doi:10.1016/j.ijheatmasstransfer.2008.09.006.
- [42] Van Belleghem M, Ameel B, Janssens A, De Paepe M. *Modelling heat and moisture transport in porous materials with CFD for building applications*, 2011.
- [43] ASHRAE. *ASHRAE Handbook: Fundamentals*. Atlanta, GA: ASHRAE; 2013.
- [44] Kramer R, van Schijndel J, Schellen H. Simplified thermal and hygric building models: A literature review. *Frontiers of Architectural Research* 2012;1:318–25. doi:10.1016/j.foar.2012.09.001.
- [45] Coakley D, Raftery P, Keane M. A review of methods to match building energy simulation models to measured data. *Renewable and Sustainable Energy Reviews* 2014;37:123–41. doi:10.1016/j.rser.2014.05.007.
- [46] Kramer R, van Schijndel J, Schellen HL. Inverse modeling of simplified hygrothermal building models to predict and characterize indoor climates. *Building and Environment* 2013;68:87–99.
- [47] Afram A, Janabi-Sharifi F. Review of modeling methods for HVAC systems. *Applied Thermal Engineering* 2014;67:507–19. doi:10.1016/j.applthermaleng.2014.03.055.

- [48] De Coninck R, Magnusson F, Åkesson J, Helsen L. Toolbox for development and validation of grey-box building models for forecasting and control. *Journal of Building Performance Simulation* 2016;9:288–303. doi:10.1080/19401493.2015.1046933.
- [49] Xiwang L, Wen J. Review of building energy modeling for control and operation. *Renewable and Sustainable Energy Reviews* 2014;37:517–37.
- [50] Klein SA. TRNSYS 17: A Transient System Simulation Program. Madison, USA: Solar Energy Laboratory, University of Wisconsin-Madison; 2009.
- [51] Crawley DB, Hand JW, Kummert M, Griffith BT. Contrasting the capabilities of building energy performance simulation programs. *Building and Environment* 2008;43:661–73. doi:10.1016/j.buildenv.2006.10.027.
- [52] Robert S, Mazza D, Hilaire B, Sette P, Vinot B. An approach to enhancing the connection between BIM models and building energy simulation – HVAC systems in the loop. *ECPPM 2014*, 2014, p. 149–54.
- [53] Hong T, Chou SK, Bong TY. Building simulation: an overview of developments and information sources. *Building and Environment* 2000;35:347–61. doi:10.1016/S0360-1323(99)00023-2.
- [54] Price H, Blair N. Current TES Capabilities in TRNSYS, Golden, Colorado: 2003.
- [55] Widström T. Enhanced energy efficiency and preservation of historic buildings – methods and tools for modeling. KTH Royal Institute of Technology, Stockholm, Sweden, 2012.
- [56] AIC. AIC Wiki. Environmental Guidelines 2016. http://www.conservation-wiki.com/wiki/Environmental_Guidelines#Historical_background (accessed November 15, 2016).
- [57] Erhardt D, Mecklenburg MF, Tumosa CS, McCormick-Goodhart M. The Determination of Allowable RH Fluctuations. *Waac* 1995;17:19.
- [58] Bratasz Ł. Allowable microclimatic variations in museums and historic buildings: reviewing the guidelines, 2012, p. 11–9.
- [59] Padfield T. Exploring the limits for passive indoor climate control. Experts roundtable on sustainable climate management strategies, The Getty Conservation Institute; 2008.
- [60] Camuffo D, Pagan E, Rissanen S, Bratasz L, Kozłowski R, Camuffo M, et al. An advanced church heating system favourable to artworks: A contribution to European standardisation. *Journal of Cultural Heritage* 2010;11:205–19. doi:10.1016/j.culher.2009.02.008.
- [61] Camuffo D, della Valle A. Church Heating: A Balance between Conservation and Thermal Comfort (PDF Download Available). Contribution to the Experts' Roundtable on Sustainable Climate Management Strategies, Tenerife, Spain: The Getty Conservation Institute; 2007.
- [62] Bratasz L, Kozłowski R, Camuffo D, Pagan E. Impact of indoor heating on painted wood - Monitoring the altarpiece in the Church of Santa Maria Maddalena in Rocca Pietore, Italy. *Stud Conserv* 2007;52:199–210.
- [63] Troi A, Hausladen G. Indoor Climate & Damage Risk Due To Heating Systems In South Tyrolean Churches, 2006.
- [64] Ruimtelijke Ordening W en O erfgoed. Omzendbrief ML/11 van 19 november 2002 betreffende de kerkverwarming van beschermde monumenten. Brussel: Ruimtelijke Ordening, Woonbeleid en Onroerend erfgoed; 2011.

- [65] Gowreesunker BL, Tassou SA, Kolokotroni M. Coupled TRNSYS-CFD simulations evaluating the performance of PCM plate heat exchangers in an airport terminal building displacement conditioning system. *Building and Environment* 2013;65:132–45. doi:10.1016/j.buildenv.2013.04.003.
- [66] Togari S, Arai Y, Milura K. A Simplified Model for Predicting Vertical Temperature Distribution in a Large Space. *ASHRAE Transaction* 1993;99:84–90.
- [67] Brown J, Rose WB. Development of humidity recommendations in museums and moisture control in buildings 1997. <http://cool.conservation-us.org/byauth/brownjp/humidity1997.html>.
- [68] Michalski S. Climate Guidelines for Heritage Collections: Where We Are in 2014 and How We Got Here. In: Stauderman S, Tompkins WG, editors. In Proceedings: Summit on the museum preservation environment, Smithsonian Institution Scholarly Press; 2016.
- [69] Church AH. *The chemistry of paints and painting*. 4th edition. London: Seeley, Service & Co. limited; 1915.
- [70] Ankersmit B. *Klimaatwerk: richtlijnen voor het museale binnenklimaat*. Amsterdam University Press; 2009.
- [71] Erhardt D, Tumosa CS, Mecklenburg A f. Applying science to the question of museum climate. In: Padfield T, Borchersen K, editors., *The National Museum of Denmark*; 2007.
- [72] Brown JP, Rose WB. Humidity and Moisture in Historic Buildings: The Origins of Building and Object Conservation. *APT Bulletin* 1996;27:12–23.
- [73] Luciani A. *Historical climates and conservation environments - historical perspectives on climate control strategies within museums and heritage buildings*. Politecnico Di Milano, 2013.
- [74] Coremans P. Le conditionnement de l'air dans les musées. *Bulletin Des Musées Royaux d'art et d'histoire*, Novembre-Décembre 1935:146–8.
- [75] Lambert S. 2014. The Early History of Preventive Conservation in Great Britain and the United States (1850–1950). *CeROArt* 2014.
- [76] Boersma F, Dardes K, Druzik J. PRECAUTION, PROOF, AND PRAGMATISM. *Evolving Perspectives on the Museum Environment*. Conservation Perspectives, vol. Collection Environments, The Getty Conservation Institute; 2014.
- [77] Davies M, Rawlins I. The War-Time Storage in Wales of Pictures from the National Gallery, London (1946). In: Staniforth S, editor. *Historical Perspectives on Preventive Conservation*, Getty Conservation Institute; 2013.
- [78] Plenderleith HJ, Werner AEA. *The Conservation of Antiquities and Works of Art*. Second Edition. London: Oxford University Press; 1962.
- [79] Buck RD. A Specification for Museum Airconditioning. *Museum News Technical Supplement*, 1964.
- [80] Thomson G. *The museum environment*. London: Butterworths; 1978.
- [81] Thomson G, editor. *Butterworth—Heinemann Series in Conservation and Museology. The Museum Environment (Second Edition)*, Butterworth-Heinemann; 1986, p. ii. doi:10.1016/B978-0-7506-1266-1.50001-9.
- [82] IPI. Climate Notes. Issue 19. Summary of the Museum Preservation Environment Summit 2013. <https://www.imagepermanenceinstitute.org/resources/newsletter-archive/v19/preservation-environment-summit> (accessed June 22, 2017).

- [83] Erhardt D, Mecklenburg MF. Relative humidity re-examined. Preventive conservation: practice, theory and research. Preprints of the Contributions to the Ottawa Congress, 1994, p. 32–8.
- [84] Michalski S. Relative humidity: a discussion of correct/incorrect values. ICOM Committee for Conservation tenth triennial meeting, Washington, DC: International Council of Museums Committee for Conservation; 1993, p. 624–9.
- [85] Mecklenburg MF. Resolving the Conflict between Building Preservation and the Proper Temperature and Relative Humidity Requirements of Collections. Smithsonian Institute; 2003.
- [86] Feilden BM. Conservation of historic buildings. Oxford: Butterworth-Heinemann Ltd; 1994.
- [87] Oreszczyń T, Cassar M, Fernandez K. Comparative study of air-conditioned and non air-conditioned museums. In: Roy A, Smith P, editors. Preventive conservation: practice, theory and research. Preprints of the contributions to the Ottawa Congress, International Institute for Conservation of Historic and Artistic Works; 1994, p. 144–8.
- [88] Camuffo D, Pagan E, Bernardi A, Becherini F. The impact of heating, lighting and people in re-using historical buildings: a case study. *Journal of Cultural Heritage* 2004;5:409–16. doi:10.1016/j.culher.2004.01.005.
- [89] ASHRAE. ASHRAE Handbook: Fundamentals, Atlanta, GA: American Society of Heating, Refrigerating and Air-Conditioning Engineers; 1999.
- [90] Michalski S. Setting Standards for Conservation: New Temperature and Relative Humidity Guidelines Are Now Published. *CCI Newsletter* No 24 1999:3–4.
- [91] Michalski S. The Ideal Climate, Risk Management, the ASHRAE Chapter, Proofed Fluctuations, and Toward a Full Risk Analysis Model. In: Contribution to the Experts' Roundtable on Sustainable Climate Management Strategies, 2007.
- [92] Mecklenburg MF, Tumosa CS, Pride A. Preserving legacy buildings. *ASHRAE Journal* 2004;46:S18–23.
- [93] Conrad E. A table for classification of climatic control potential in buildings 1995.
- [94] Coblenz E. Clin d'œil. Le « Groupe Bizot » : une cartellisation des grandes institutions muséales ? *Entreprises et histoire* 2014;2014/3:143–5.
- [95] ICOM-CC, ICC. Declaration on Environmental Guidelines - ICOM-CC 2014. <http://www.icom-cc.org/332/-icom-cc-documents/declaration-on-environmental-guidelines/#.WXMtpliGNPY> (accessed July 22, 2017).
- [96] Standardization EC for. EN 15757: Conservation of Cultural Property — Specifications for temperature and relative humidity to limit climate-induced mechanical damage in organic hygroscopic materials. Brussels: 2010.
- [97] ASHRAE. ASHRAE handbook: Heating, ventilating, and air-conditioning applications, SI edition, Atlanta, GA: American Society of Heating, Refrigerating and Air-Conditioning Engineers; 2015, p. 23.1-23.22.
- [98] Troi A. Kirchenheizung. Technische Universität München, 2010.
- [99] Camuffo D. The friendly heating project and the conservation of the cultural heritage preserved in churches. In: Kilian R, Vyhlídal T, Broström T, editors., 2010.
- [100] Standardization EC for. EN 15759: Conservation of Cultural Property - Indoor Climate – Part 1: Heating Churches, Chapels and other Places of Worship. Brussels: 2011.
- [101] Mecklenburg MF, Tumosa CS. Practical Guide: Temperature and Relative Humidity Effects on the Mechanical and Chemical Stability of Collections. *ASHRAE Journal* 1999;41:77–82.

- [102] Hueck HJ. The biodeterioration of materials as part of hylobiology. *Material Und Organismen* 1965;1:5–34.
- [103] Sterflinger K, Piñar G. Microbial deterioration of cultural heritage and works of art — tilting at windmills? *Appl Microbiol Biotechnol* 2013;97:9637–46. doi:10.1007/s00253-013-5283-1.
- [104] Merritt J, Reilly JA. *Preventive Conservation for Historic House Museums*. Rowman & Littlefield; 2010.
- [105] Konsa K, Tirrul I, Hermann A. Wooden objects in museums: Managing biodeterioration situation. *International Biodeterioration & Biodegradation* 2014;86, Part B:165–70. doi:10.1016/j.ibiod.2013.06.023.
- [106] Simon-Nobbe B, Denk U, Pöll V, Rid R, Breitenbach M. The spectrum of fungal allergy. *Int Arch Allergy Immunol* 2008;145:58–86. doi:10.1159/000107578.
- [107] Blanchette RA. A Guide to Wood Deterioration Caused by Microorganisms and Insects. In: Dardes K, Rothe A, editors. vol. Proceedings of a Symposium at the J. Paul Getty Museum., The Getty Conservation Institute; 1995, p. 55–68.
- [108] Unger A, Schniewind A, Unger W. *Conservation of Wood Artifacts: A Handbook*. Springer Science & Business Media; 2013.
- [109] Sedlbauer K. Prediction of mould fungus formation on the surface of and inside building components. Fraunhofer Institute, 2001.
- [110] Parra R, Magan N. Modelling the effect of temperature and water activity on growth of *Aspergillus niger* strains and applications for food spoilage moulds. *J Appl Microbiol* 2004;97:429–38. doi:10.1111/j.1365-2672.2004.02320.x.
- [111] Henry W, et al. Mold/Fungi. Chapter 12. *Paper Conservation Catalog*, Washington, DC: American Institute for Conservation Book and Paper Group; 1997.
- [112] Michalski S. Technical Bulletin No.23: guidelines for humidity and temperature in Candeian Archives 2000.
- [113] Michalski S. Agent of Deterioration: Incorrect relative humidity 2009. <http://www.cci-icc.gc.ca/crc/articles/mcpm/chap10-eng.aspx>.
- [114] Onions AH., Allsopp D, Eiggins HOW. *Smith's Introduction to Industrial Mycology*. 7th ed. London: Cambridge University Press; 1992.
- [115] Lankester P. *The Impact of Climate Change on Historic Interiors*. 2013.
- [116] Vereecken E, Saelens D, Roels S. A comparison of different mould prediction models, 2011.
- [117] Viitanen H, Krus M, Ojanen T, Eitner V, Zirkelbach D. Mold Risk Classification Based on Comparative Evaluation of Two Established Growth Models. *Energy Procedia* 2015;78:1425–30. doi:10.1016/j.egypro.2015.11.165.
- [118] Mecklenburg MF. Determining the Acceptable Ranges of Relative Humidity And Temperature in Museums and Galleries: Part 1, Structural Response to Relative Humidity 2007.
- [119] Mecklenburg MF. Determining the Acceptable Ranges of Relative Humidity And Temperature in Museums and Galleries: Part 2, Structural Response to Temperature 2007.
- [120] Michalski S. Stufing everything we know about mechanical properties into one collection simulation. *Climate for Collections - Standards and Uncertainties*. Postprints of the Munich Climate Conference 7 to 9 November 2012, 2013, p. 349–62.
- [121] Michalski SW. Correction to the proofed fluctuation concept by stress relaxation and fatigue. In *Proceedings: Allowable microclimatic variations for polychrome wood*, 18-19

- February 2010, International Focussed Meeting of COST Action IE0601, Norwegian Institute for Cultural Heritage Research – NIKU, Oslo: 2010.
- [122] Ashley-Smith J. Climate for Culture: Report on damage functions in relation to climate change. 2013.
- [123] Glinka G, Socie DF. *Advances in Fatigue and Fracture Mechanics* 2014.
- [124] François D, Pineau A, Zaoui A. Chapter 6: Fatigue. *Mechanical Behaviour of Materials*, 2013, p. 307–62. doi:10.1007/978-94-007-4930-6_6.
- [125] Downing SD, Socie DF. Simple rainflow counting algorithms. *International Journal of Fatigue* 1982;4:31–40. doi:10.1016/0142-1123(82)90018-4.
- [126] Rychlik I. A new definition of the rainflow cycle counting method (PDF Download Available). ResearchGate n.d.
- [127] Matsuishi M, Endo T. Fatigue of metals subjected to varying stress. *Japan Soc Mech Engineering* n.d.
- [128] ASTM Standard E1049-85(2011)e1 Standard Practices for Cycle Counting in Fatigue Analysis. West Conshohocken, PA: American Society for Testing and Materials; 2011.
- [129] Miner MA. Cumulative Damage in Fatigue. *Journal of Applied Mechanics* 1945;12.
- [130] Michalski S. The power of history in the analysis of collection risks from climate fluctuations and light. In: Bridgland J, editor. *ICOM-CC 17th Triennial Conference-Preprints*, Melbourne: Paris: International Council of Museums; 2014, p. art. 1506, 8 pp.
- [131] Champney EW, Champney F. Chapter XIV: Notable examples of Japanese architecture. *Romance of Old Japan*, The Knickerbocker Press; 1917.
- [132] Steven M. Technology for Wind Turbine Inverter with Increased Reliability on Portal. Infineon Technologies AG, Bodo's Power Systems 2009:24–7.
- [133] Pedersen MM. Theory reference | FatigueToolbox.org. FatigueToolboxOrg Free Open Source Fatigue Analysis Software n.d. <http://fatiguetoobox.org/documentation/theory-reference> (accessed October 22, 2017).
- [134] Laboratory (U.S.) FP, Kommers WJ. The fatigue behavior of wood and plywood subjected to repeated and reversed bending stresses. Madison, Wis. : U.S. Dept. of Agriculture, Forest Service, Forest Products Laboratory; 1960.
- [135] Krause W, Mathis RS, Grimes LW. Fatigue properties of acrylic bone cement: S-N, P-N, and P-S-N data. *J Biomed Mater Res* 1988;22:221–44.
- [136] Rachwal B, Bratasz Ł, Krzemien L, Łukomski M, Kozłowski R. Fatigue damage of the gesso layer in panel paintings subjected to changing climate conditions. *Strain* 2012;48:474–81.
- [137] Bratasz Ł, Kozłowski R, Lasyk Ł, Łukomski M, Rachwal B. Allowable microclimatic variations for painted wood: numerical modelling and direct tracing of the fatigue damage. In: *Conservation IC for*, editor., Bridgeland, J.; 2011.
- [138] Vanderauwera M. Keuze van verwarmingsinstallaties in functie van het monument of van zijn gebruikers? In: De Clercq H, Vernimme N, editors. *Energieprestaties en monumentale constructies*, 2008.
- [139] Steeman M, De Paepe M, Janssens A. Impact of whole-building hygrothermal modelling on the assessment of indoor climate in a library building. *Building and Environment* 2010;45:1641–52. doi:10.1016/j.buildenv.2010.01.012.
- [140] Kupczak A, Sadłowska-Sałęga A, Krzemien L, Radoń J, Kozłowski R. Modelling impact of collections on indoor climate and energy consumption in libraries and archives. *Energy*

- Efficiency and Comfort of Historic Buildings (EECHB-2016), Brussels, Belgium: Flanders Heritage Agency; 2016.
- [141] Martens MHJ. Climate risk assessment in museums. Degradation risk determined from temperature and relative humidity data. Technische universiteit Eindhoven, 2012.
- [142] Martens MHJ, Schellen H, Ankersmit B. Conserverende eigenschappen van museumklimaten. Voorspellen van objectdegradatie uit gemeten binnenklimaten. *Bouwfysica* n.d.;21e jaargang.
- [143] Anon. ASHRAE handbook: Heating, ventilating, and air-conditioning applications, SI edition, American Society of Heating, Refrigerating and Air-Conditioning Engineers; 2011, p. 23.1-23.22.
- [144] Mecklenburg MF, Tumosa CS, Erhardt D. Structural response of painted wood surfaces to changes in ambient relative humidity. In: Dorge V, Howlett FC, editors. *Painted wood: history and conservation (Part 6: Scientific Research)*, Los Angeles: The Getty Conservation Institute; 1998, p. 464–83.
- [145] Bratasz L, Rachwał B. Computer modelling of dimensional response and stress fields in wooden artworks. *Proceedings of Conference on Allowable microclimate variations for polychrome wood*, Oslo, Norway: 2010.
- [146] Bernikola E, Nevin A, Tornari V. Rapid initial dimensional changes in wooden panel paintings due to simulated climate-induced alterations monitored by digital coherent out-of-plane interferometry. *Appl Phys A* 2009;95:387–99. doi:10.1007/s00339-009-5096-3.
- [147] Silva HE, Henriques FMA. Preventive conservation of historic buildings in temperate climates. The importance of a risk-based analysis on the decision-making process. *Energy and Buildings* 2015;107:26–36. doi:10.1016/j.enbuild.2015.07.067.
- [148] Sedlbauer K, Krus M. A new model for mould prediction and its application in practice. In: Carmeliet J, Hens H, Vermeir G, editors. *Research in Building Physics: Proceedings of the Second International Conference on Building Physics*, Leuven, Belgium, 14-18 September 2003, CRC Press; 2003.
- [149] Sedlbauer K, Krus M, Zillig W. WUFI Bio. Fraunhofer Institute for Building Physics; n.d.
- [150] Reijnen S, Jorissen AJM. On shape stability of panel paintings exposed to humidity variations - A numerical study between science & art part 1: Modeling isothermal moisture movement. *Heron* 2013;58:113–26.
- [151] Saitzyk S. Sizing Painting Surfaces. Excerpts from *ART HARDWARE: The Definitive Guide to Artists' Materials* 1987. http://www.trueart.info/?page_id=186 (accessed June 23, 2017).
- [152] Hayashi M. The Effect of Preservative Interventions on the Chemical-Physical and Structural Characteristics of Panel Painting. *Università di Bologna*, 2009.
- [153] Buck RD. The use of moisture barriers on panel paintings. *Studies in Conservation* 1961;6:9–20.
- [154] Sozzani LSG. An Economical Design for a Microclimate Vitrine for Paintings Using the Picture Frame as the Primary Housing. *Journal of the American Institute for Conservation* 1997;36:95–107.
- [155] Billinge R, Campbell L, Dunkerton J, Foister S, Kirby J, Pilc J, et al. *Methods and materials of Northern European painting in the National Gallery, 1400–1550*. London: 1997.

- [156] Uzielli L. Historical Overview of Panel-Making Techniques in Central Italy. In: Dardes K, Rothe A, editors. vol. Proceedings of a Symposium at the J. Paul Getty Museum., The Getty Conservation Institute; 1995, p. 110–35.
- [157] Wadum J. Historical Overview of Panel-Making Techniques in the Northern Countries. In: Dardes K, Rothe A, editors. vol. Proceedings of a Symposium at the J. Paul Getty Museum., The Getty Conservation Institute; 1995.
- [158] Haneca K, Wazny T, Van Acker J, Beeckman H. Provenancing Baltic timber from art historical objects: success and limitations. *Journal of Archaeological Science* 2005;32:261–71. doi:10.1016/j.jas.2004.09.005.
- [159] Gezici-Koç Ö, Erich SJF, Huinink HP, Ven LGJ van der, Adan OCG. Bound and free water distribution in wood during water uptake and drying as measured by 1D magnetic resonance imaging. *Cellulose* 2017;24:535–53. doi:10.1007/s10570-016-1173-x.
- [160] Wang J, Mukhopadhyaya P, Morris PI. Sorption and capillary condensation in wood and the moisture content of red pine. *Journal of Building Physics* 2014;37:327–47. doi:10.1177/1744259112453829.
- [161] Niemz P. Water Absorption of Wood and Wood-Based Panels – Significant Influencing Factors. In: Thoemen H, Irle M, Sernek M, editors. COST | Publications | 10/35 Wood-Based Panels: An Introduction for Specialists, vol. Chapter 2, Brunel University Press; 2010.
- [162] Tiemann HD. Effect of Moisture Upon the Strength and Stiffness of Wood. *Bulletin* 70 1906.
- [163] Krabbenhøft K. Moisture Transport in Wood. A Study of Physical-Mathematical Models and their Numerical Implementation. PhD dissertation. Department of Civil Engineering. Technical University of Denmark, 2003.
- [164] Englund ET, Thygesen LG, Svensson S, Hill CAS. A critical discussion of the physics of wood–water interactions. *Wood Sci Technol* 2013;47:141–61. doi:10.1007/s00226-012-0514-7.
- [165] Simpson W, Tenwolde A. Wood Handbook - Wood as an engineering material. In: Department of Agriculture FS Forest Products Laboratory, editor., Madison, WI: U.S.: 1999, p. 463.
- [166] Leenaars J, Schellen H. Wood works - free and restrained deformation of wood in fluctuating climate conditions. *Hout werkt - vrije en verhinderde vervorming van hout bij wisselende klimaatomstandigheden*. (In Dutch). *Bouwfysica* 2009;4:30–7.
- [167] Bergman R, Cai Z, Carll CG, Clausen CA, Dietenberger MA, Falk RH, et al. Chapter 04: Moisture Relations and Physical Properties of Wood. *Wood Handbook - Wood as an engineering material*. General Technical Report FPL-GTR-190, Madison, WI: U.S. Department of Agriculture, Forest Service, Forest Products Laboratory: 2010, p. 508.
- [168] De Willigen P. A Mathematical Study on Craquelure and other Mechanical Damage in Paintings. Delft, The Netherlands: Delft Univeristy Press; 1999.
- [169] Benton JR. Painting on Wooden Panels: Egg Tempera, the Introduction of Oil. *Materials, Methods, and Masterpieces of Medieval Art*, Praeger; 2009, p. 303.
- [170] Colmars J. Hygromécanique du matériau bois appliquée à la conservation du patrimoine culturel : étude sur la courbure des panneaux peints. *l'Université Montpellier 2*, 2011.
- [171] Łukomski M. Painted wood. What makes the paint crack? *Journal of Cultural Heritage* 2012;13:S90–3. doi:10.1016/j.culher.2012.01.007.

- [172] Colmars J, Marcon B, Maurin E, Remond R, Fabrice M, Mazzanti P, et al. Hygromechanical response of a panel painting in a church: monitoring and computer modeling. In: Noldt U, editor. COST IE0601 Wood in Cultural Heritage, Hambourg: 2009.
- [173] Dionisi Vici P, Mazzanti P, Uzielli L. Mechanical response of wooden boards subjected to humidity step variations: climatic chamber measurements and fitted mathematical models. *Journal of Cultural Heritage* 2006;7:37–48. doi:10.1016/j.culher.2005.10.005.
- [174] Marcon B. Hygromécanique des panneaux en bois et conservation du patrimoine culturel: des pathologies... aux outils pour la conservation. Dissertation. Université Montpellier 2 - università degli studi di Firenze, 2009.
- [175] Mohen JP, Menu M, Mottin B. *Mona Lisa: Inside the Painting*. Harry N. Abrams; 2006.
- [176] Cornelis B, Ruzic T, Gezels E, Doods A, Pizurica A, Platisa L, et al. Crack detection and inpainting for virtual restoration of paintings: The case of the Ghent Altarpiece. *Signal Processing* 2013;93:605–19. doi:10.1016/j.sigpro.2012.07.022.
- [177] Bucklow S. The Description and Classification of Craquelure. *Studies in Conservation* 1999;44:233–44. doi:10.2307/1506653.
- [178] Bucklow S. The Description of Craquelure Patterns. *Studies in Conservation* 1997;42:129–40. doi:10.2307/1506709.
- [179] Mecklenburg MF, Tumosa CS. Mechanical Behaviour of Paintings Subjected to Changes in Temperature and Relative Humidity in Art in Transit: Studies in the Transport of Paintings. In: Mecklenburg MF, editor., National Gallery of Art; 1991.
- [180] Mecklenburg MF, Tumosa CS. An introduction into the mechanical behavior of paintings under rapid loading conditions. In: Mecklenburg MF, editor., National Gallery of Art; 1991.
- [181] Richard M, Mecklenburg MF, Tumosa CS. Technical Considerations for the Transport of Panel Paintings. International symposium, The structural conservation of panel paintings, Malibu: The Getty Conservation Institute; 1995, p. 32.
- [182] Łukomski M. Addendum to "Painted wood. What makes the paint crack?" [doi:10.1016/j.culher.2012.01.007]. *Journal of Cultural Heritage* 2014. doi:10.1016/j.culher.2012.02.009.
- [183] Bratasz Ł, Harris I, Lasyk Ł, Łukomski M, Kozłowski R. Future climate-induced pressures on painted wood. *Journal of Cultural Heritage* 2012;13:365–70. doi:10.1016/j.culher.2012.01.013.
- [184] Barradas Berglind JJ, Wisniewski R. Fatigue Estimation Methods Comparison for Wind Turbine Control. ArXiv 2014.
- [185] Carmeliet J, Roels S, Bomberg M. Chapter 29: Towards Development of Methods for Assessment of Moisture-originated Damage. *ASTM Manual 18 on Moisture Control in Buildings: The key factor in mold prevention edition*, ASTM International; 2009, p. 591–605.
- [186] Rachwał B, Bratasz Ł, Łukomski M, Kozłowski R. Response of Wood Supports in Panel Paintings Subjected to Changing Climate Conditions. *Strain* 2012. doi:10.1111/j.1475-1305.2011.00832.x.
- [187] Dureisseix D, Marcon B. A partitioning strategy for the coupled hygro-mechanical analysis with application to wood structures of Cultural Heritage. *International Journal for Numerical Methods in Engineering*, Wiley-Blackwell 2011;88:228–56.
- [188] Allegretti O, Raffaelli F. Barrier Effect to Water Vapour of Early European Painting Materials on Wood Panels. *Studies in Conservation* 2008;53:187–97.

- [189] Froidevaux J. Wood and paint layers aging and risk analysis of ancient panel painting. Dissertation. Université Montpellier II - Sciences et Techniques du Languedoc, 2012.
- [190] Welty J, Wicks CE, Rorrer GL, Wilson RE. Fundamentals of Momentum, Heat and Mass Transfer, 5th Edition. John Wiley & Sons, Inc; 2008.
- [191] Liu JY. A New Method for Separating Diffusion Coefficient and Surface Emission Coefficient. *Wood and Fiber Science* 1989;21:133–41.
- [192] Olek W, Weres J. Effects of the method of identification of the diffusion coefficient on accuracy of modeling bound water transfer in wood. *Transport in Porous Media* 2007;66:135–44.
- [193] Jakięta S, Bratasz Ł, Kozłowski R. Numerical modelling of moisture movement and related stress field in lime wood subjected to changing climate conditions. *Wood Science and Technology* 2008;42:21–37.
- [194] van der Zanden AJJ, Goossens ELJ. The measurement of the sorption isotherm of water in paint films. *Chemical Engineering and Processing: Process Intensification* 2004;43:739–43. doi:10.1016/S0255-2701(03)00073-4.
- [195] Brunauer S, Deming LS, Deming WE, Teller E. On a Theory of the van der Waals Adsorption of Gases. *Journal of the American Chemical Society* 1940;62:1723–32. doi:10.1021/ja01864a025.
- [196] Simpson W. Sorption Theories Applied To Wood. *Wood and Fiber Science* 1980;12:183–95.
- [197] van der Wel GK, Adan OCG. Moisture in organic coatings — a review. *Progress in Organic Coatings* 1999;37:1–14. doi:10.1016/S0300-9440(99)00058-2.
- [198] Donohue MD, Aranovich GL. Classification of Gibbs adsorption isotherms. *Advances in Colloid and Interface Science* 1998;76–77:137–52. doi:10.1016/S0001-8686(98)00044-X.
- [199] Zhang X, Zillig W, Künzel HM, Zhang X, Mitterer C. Evaluation of moisture sorption models and modified Mualem model for prediction of desorption isotherm for wood materials. *Building and Environment* 2015;92:387–95. doi:10.1016/j.buildenv.2015.05.021.
- [200] Bratasz Ł, Kozłowska A, Kozłowski R. Analysis of water adsorption by wood using the Guggenheim-Anderson-de Boer equation. *Eur J Wood Prod* 2012;70:445–51. doi:10.1007/s00107-011-0571-x.
- [201] Freiesleben Hansen P. Coupled Moisture/Heat Transport in Cross Sections of Structures (in Danish). Dissertation. Concrete and Structural Research Institute (BKI), 1985.
- [202] Carmeliet J, De Wit MHD, Janssen H. Hysteresis and moisture buffering of wood. Symposium of Building Physics in the Nordic Countries, 13-15 June, Reykjavik, Iceland: 2005, p. 55–62.
- [203] Hansen KK. Sorption Isotherms. A Catalogue. Buildings Materials Laboratory. Technical University of Denmark; 1986.
- [204] Bratasz Ł, Kozłowski R, Kozłowska A, Rachwał B. Sorption of moisture and dimensional change of wood species used in historic objects. In: Gril J, editor. *Wood Science for Conservation of Cultural Heritage - Braga 2008, 2010*, p. 11–6.
- [205] Grosser D, Geier E. The types of wood used in panel painting and carving and their determination by microscopic features. Part one. Softwoods. Die in der Tafelmalerei und Bildschnitzerei verwendeten Holzarten und ihre Bestimmung nach mikroskopischen Merkmalen. Teil I. Nadelhölzer (In German). *Maltechnik/Restauro* 1975;3:127–48.

- [206] Grosser D, Grässle E. The types of wood used in panel painting and carving and their determination by microscopic features. Part one. European Hardwood. Die in der Tafelmalerei und Bildschnitzerei verwendeten Holzarten und ihre Bestimmung nach mikroskopischen Merkmalen. Teil II. Europaeische laubhoelzer (In German). *Maltechnik/Restauro* 1976:40–5.
- [207] Perkowski Z, Świrska-Perkowska J, Gajda M. Comparison of moisture diffusion coefficients for pine, oak and linden wood. *Journal of Building Physics* 2016;1744259116673967. doi:10.1177/1744259116673967.
- [208] Boon JJ, Hendrickx R, Eijkel G, Cerjak I, Kaestner A, Ferreira ESB. Neutron radiography for the study of water uptake in painting canvases and preparation layers. *Appl Phys A* 2015;121:837–47. doi:10.1007/s00339-015-9381-z.
- [209] Hendrickx R, Desmarais G, Weder M, Ferreira ESB, Derome D. Moisture uptake and permeability of canvas paintings and their components. *Journal of Cultural Heritage* 2016;19:445–53. doi:10.1016/j.culher.2015.12.008.
- [210] Huldén M, Hansen CM. Water permeation in coatings. *Progress in Organic Coatings* 1985;13:171–94. doi:10.1016/0033-0655(85)80025-X.
- [211] Perera DY, Heertjes. Water transport in paint films. AATA, 1971.
- [212] Ruus A, Peetsalu P, Tohvri E, Lepasaar T, Kirtsi K, Muoni H, et al. Water vapour transmission properties of natural paints. *Agronomy Research Biosystems Engineering* 2011:195–201.
- [213] Allegretti O, Raffaelli F. External Resistance to Water Vapour Transfer of Varnishes on Wood. In: Uzielli L, editor. *Wood Science for Conservation of Cultural Heritage*, Firenze University Press; 2007.
- [214] Salin JG. Almost all wooden pieces have a damaged surface layer - impact on some properties and quality. In proceedings: European COST Action E53 Conference, October 29–30, Delft, The Netherlands: 2008, p. 135–43.
- [215] Hukka A, Oksanen O. Convective Mass Transfer Coefficient at Wooden Surface in Jet Drying of Veneer. *Holzforschung* 1999;53:204–8.
- [216] Yeo H, Smith WB. Development of a Convective Mass Transfer Coefficient Conversion Method. *Wood and Fiber Science* 2007;37:3–13.
- [217] Siau JF, Avramidis S. The Surface Emission Coefficient of Wood. *Wood and Fiber Science* 2007;28:178–85.
- [218] van Meel PA, Erich SJF, Huinink HP, Kopinga K, de Jong J, Adan OCG. Moisture transport in coated wood. *Progress in Organic Coatings* 2011;72:686–94. doi:10.1016/j.porgcoat.2011.07.011.
- [219] Lesar B, Straže A, Humar M. Sorption properties of wood impregnated with aqueous solution of boric acid and montan wax emulsion. *J Appl Polym Sci* 2011;120:1337–45. doi:10.1002/app.33196.
- [220] BIN. NBN EN ISO 12570: Hygrothermal performance of building materials and products - Determination of moisture content by drying at elevated temperature. 2000.
- [221] Feng C, Janssen H, Wu C, Feng Y, Meng Q. Validating various measures to accelerate the static gravimetric sorption isotherm determination. *Building and Environment* 2013;69:64–71. doi:10.1016/j.buildenv.2013.08.005.
- [222] BIN. NBN EN ISO 12571: Thermische en vochtwerende eigenschappen van bouwmaterialen en bouwwaren - Bepaling van de thermische sorptie-eigenschappen. 2000.

- [223] Blahnik R. Problems of measuring water sorption in organic coatings and films, and calculations of complicated instances of moistening. *Progress in Organic Coatings* 1983;11:353–92. doi:10.1016/0033-0655(83)85008-0.
- [224] Albalak R. *Polymer Devolatilization*. Massachusetts: CRC Press; 1996.
- [225] Crank J. *The mathematics of diffusion*. Second edition. Oxford: Clarendon Press; 1975.
- [226] Steeman M, Janssens A, Steeman HJ, Van Belleghem M, De Paepe M. On coupling 1D non-isothermal heat and mass transfer in porous materials with a multizone building energy simulation model. *Building and Environment* 2010;45:865–77. doi:10.1016/j.buildenv.2009.09.006.
- [227] (KIK-IRPA) KI voor het K, Lukasweb, (VUB) VUB, Foundation TG, (NWO) NO voor WO. Closer to Van Eyck: Rediscovering the Ghent Altarpiece 2012. <http://vaneeyck.kikirpa.be> (accessed January 1, 2012).
- [228] Van Grevenstein-Kruse A, Spronk R. Lasting support: an interdisciplinary research project to assess the structural condition of the Ghent altarpiece, Final project report. 2011.
- [229] Royal Institute for Cultural Heritage. Het adembenemende resultaat van de eerste fase van de restauratie van het Lam Gods (the breath taking result of the first phase of restoration of the Mystic Lamb, in Dutch). Press Conference Map: 2016.
- [230] Silva HE, Henriques FMA, Henriques TAS, Coelho G. A sequential process to assess and optimize the indoor climate in museums. *Building and Environment* 2016;104:21–34. doi:10.1016/j.buildenv.2016.04.023.
- [231] Huijbregts Z, Kramer RP, Martens MHJ, van Schijndel AWM, Schellen HL. A proposed method to assess the damage risk of future climate change to museum objects in historic buildings. *Building and Environment* 2012;55:43–56. doi:10.1016/j.buildenv.2012.01.008.
- [232] Macdonald IA. *Quantifying the Effects of Uncertainty in Building Simulation*. PhD dissertation. Department of Mechanical Engineering, University of Strathclyde, 2002.
- [233] Fabrizio E, Monetti V. Methodologies and Advancements in the Calibration of Building Energy Models. *Energies* 2015;8:2548–74. doi:10.3390/en8042548.
- [234] Royapoor M, Roskilly T. Building model calibration using energy and environmental data. *Energy and Buildings* 2015;94:109–20. doi:10.1016/j.enbuild.2015.02.050.
- [235] de Wit S, Augenbroe G. Analysis of uncertainty in building design evaluations and its implications. *Energy and Buildings* 2002;34:951–8. doi:10.1016/S0378-7788(02)00070-1.
- [236] de Wit S. Influence of modelling uncertainties on the simulation of building thermal comfort performance. In: *Proceeding of Buildings Simulation '97: 5th International IBPSA conference*, September 8-10, Prague, Czech Republic: 1997.
- [237] De Coninck R, Magnusson F, Åkesson J, Helsen L. Grey-box Building Models for Model Order Reduction and Control. *Proceedings of the 10th International Modelica Conference*, Lund; Sweden: Linköping University Electronic Press; Linköpings universitet; 2014, p. 657–66.
- [238] Perneti R, Prada A, Baggio P. On the influence of several parameters in energy model calibration: the case of a historical building. *IBPSA Italy*, Free University of Bolzano, Bolzano, Italy: 2013.
- [239] Sulaiman R, Schellen HL, Hensen JLM. Pilot study on indoor climate investigation and computer simulation in historical museum building: Amerongen Castle, the Netherlands. *Journal of Design and the Built Environment* 2010;7:75–94.

- [240] Habert JS, Claridge DE, Culp C. ASHRAE's Guideline 14-2002 for Measurement of Energy and Demand Savings: How to Determine What Was Really Saved by the Retrofit. Energy Systems Laboratory ([Http://EslTamuEdu](http://EslTamuEdu)); Texas A&M University ([Http://WwwTamuEdu](http://WwwTamuEdu)) 2005.
- [241] Andre P. Energy Performance Analysis. Institute for Building Environment and Energy Conservation; 2013.
- [242] Roberti F, Oberegger UF, Gasparella A. Calibrating historic building energy models to hourly indoor air and surface temperatures: Methodology and case study. *Energy and Buildings* 2015;108:236–43. doi:10.1016/j.enbuild.2015.09.010.
- [243] Reddy TA. Literature review on calibration of building energy simulation programs: uses, problems, procedure, uncertainty, and tools. *ASHRAE Transactions* 2006;112:226–40.
- [244] Clarke JA, Strachan P, Pernot C. An approach to the calibration of building energy simulation models. *ASHRAE Transactions* 1993;99:917–27.
- [245] Soebarto V. Calibration of hourly energy simulations using hourly monitored data and monthly utility records for two case study buildings. In: *Proceeding of Buildings Simulation '97: 5th International IBPSA conference, September 8-10, Prague, Czech Republic: 1997.*
- [246] Mustafaraj G, Marini D, Costa A, Keane M. Model calibration for building energy efficiency simulation. *Applied Energy* 2014;130:72–85. doi:10.1016/j.apenergy.2014.05.019.
- [247] Enríquez R, Jiménez MJ, Heras MR. Towards non-intrusive thermal load Monitoring of buildings: BES calibration. *Applied Energy* 2017;191:44–54. doi:10.1016/j.apenergy.2017.01.050.
- [248] Paliouras P, Matzaflaras N, Peuhkuri RH, Kolarik J. Using Measured Indoor Environment Parameters for Calibration of Building Simulation Model- A Passive House Case Study. *Energy Procedia* 2015;78:1227–32. doi:10.1016/j.egypro.2015.11.209.
- [249] Pretelli M, Fabbri K. *Historic Indoor Microclimate of the Heritage Buildings: A Guideline for Professionals who care for Heritage Buildings.* Springer; 2017.
- [250] Agami R. Literature review on calibration of building energy simulation programs: Uses, problems, procedure, uncertainty, and tools. *ASHRAE Transactions*, vol. 112 PART 1, 2006, p. 226–40.
- [251] Luo C, Moghtaderi B, Page A. Modelling of wall heat transfer using modified conduction transfer function, finite volume and complex Fourier analysis methods (PDF Download Available). *Energy and Buildings* 2010;42:605–17. doi:<http://dx.doi.org/10.1016/j.enbuild.2009.10.031>.
- [252] Delcroix B. *Modelling Of Thermal Mass Energy Storage In Buildings With Phase Change Materials.* PhD dissertation. University of Montreal, 2015.
- [253] Chen Y, Wang S. Frequency-domain regression method for estimating CTF models of building multilayer constructions. *Applied Mathematical Modelling* 2001;25:579–92. doi:10.1016/S0307-904X(00)00067-6.
- [254] Abadie M, Mendes N. Comparative Analysis of Response-factor and Finite-volume based Methods for predicting Heat and Moisture Transfer through Porous Building Materials. *Journal of Building Physics* 2006;30:7–37. doi:10.1177/1744259106064599.
- [255] Mazzarella L, Pasini M. CTF vs FD Based Numerical Methods: Accuracy, Stability and Computational Time's Comparison. *Energy Procedia* 2015;78:2620–5. doi:10.1016/j.egypro.2015.11.324.

- [256] Prada A, Cappelletti F, Baggio P, Gasparella A. On the effect of material uncertainties in envelope heat transfer simulations. *Energy and Buildings* 2014;71:53–60. doi:10.1016/j.enbuild.2013.11.083.
- [257] Delcroix B, Kummert M, Daoud A, Hiller M. Improved conduction transfer function coefficients generation in TRNSYS multizone building model. In: Wurtz E, editor. 13th International Conference of the International Building Performance Simulation Association, Chambéry, France: 2013, p. 2667–74.
- [258] Li XQ, Chen Y, Spittler JD, Fisher D. Applicability of calculation methods for conduction transfer function of building constructions. *International Journal of Thermal Sciences* 2009;48:1441–51. doi:10.1016/j.ijthermalsci.2008.11.006.
- [259] Clarke J. 2 - Integrative modelling methods. *Energy Simulation in Building Design (Second Edition)*, Oxford: Butterworth-Heinemann; 2001, p. 22–63. doi:10.1016/B978-075065082-3/50002-4.
- [260] Athienitis A, O'Brien W, editors. *Modeling, Design, and Optimization of Net-Zero Energy Buildings*. John Wiley & Sons; 2015.
- [261] Chen Y, Li X, Zhang Q, Spittler J, Fisher D. Investigation of the Accuracy of Calculation Methods for Conduction Transfer Functions of Building Construction 2006.
- [262] Stephenson DG, Mitalas GP. Calculation of Heat Conduction Transfer Functions for Multilayer Slabs. *AHRAE Transactions* 1971;77:117–26.
- [263] Duška M, Barták M, Drkal F, Hensen J. Analytical Approach To Transient Heat Conduction In Cooling Load Calculations. *Proceedings of the 17th Int. Air-conditioning and Ventilation Conference, Prague: STP - Society of Environmental Engineering: 2006*, p. 7.
- [264] Giuliani M, Avesani S, Oberegger UF. Quantitative Comparison Of Massive Walls Thermal Response Among Commercial Software. In: Wurtz E, editor. 13th International Conference of the International Building Performance Simulation Association, Chambéry, France: 2013.
- [265] McQuiston FC. *Cooling and Heating Load Calculation Manual*, 2nd edition 1992:2.1-2.14.
- [266] Iu I, Fisher D. Application of Conduction Transfer Functions and Periodic Response Factors in Cooling Load Calculation Procedures. *ASHRAE Transactions* 2004;110:829–41.
- [267] Delcroix B, Kummert M, Daoud A, Hiller M. Conduction Transfer Functions in TRNSYS Multizone Building Model: Current Implementation, Limitations and Possible Improvements. *SimBuild 2012: Fifth National Conference of IBPSA-USA, Madison, Wisconsin: 2012*.
- [268] SEL. Volume 5: Multizone Building modeling with Type 56 and TRNBuild, TRNSYS 17: A TRansient SYstem Simulation Program: Solar Energy Laboratory, University of Wisconsin-Madison; 2012.
- [269] Janssen H, Christensen JE. Hygrothermal optimisation of museum storage spaces. *Energy and Buildings* 2013;56:169–78. doi:10.1016/j.enbuild.2012.08.043.
- [270] Steeman M, Van Belleghem M, De Paepe M, Janssens A. Experimental validation and sensitivity analysis of a coupled BES–HAM model. *Building and Environment* 2010;45:2202–17. doi:10.1016/j.buildenv.2010.04.003.
- [271] Janssen H, Roels S. Qualitative and quantitative assessment of interior moisture buffering by enclosures. *Energy and Buildings* 2009;41:382–94. doi:10.1016/j.enbuild.2008.11.007.
- [272] Woods J, Winkler J, Christensen D. Evaluation of the Effective Moisture Penetration Depth Model for Estimating Moisture Buffering in Buildings. Washington, D.C. : United

- States. Office of the Assistant Secretary of Energy Efficiency and Renewable Energy ; 2013.
- [273] Janssens A, De Paepe M. Effect of moisture inertia models on the predicted indoor humidity in a room. 26th AIVC Conference, 2005.
- [274] Kerestecioglu A, Swami M, Kamel A. Theoretical and computational investigation of simultaneous heat and moisture transfer in buildings: Effective penetration depth theory. *ASHRAE Transactions* 1990;96:447–54.
- [275] Cunningham MJ. Effective penetration depth and effective resistance in moisture transfer. *Building and Environment* 1992;27:379–86. doi:10.1016/0360-1323(92)90037-P.
- [276] Arfvidsson J, Claesson J. Isothermal moisture flow in building materials: Modelling, measurements and calculations based on Kirchhoff's potential. *Building and Environment* 2000;35:519–36.
- [277] Abadie MO, Mendonça KC. Moisture performance of building materials: From material characterization to building simulation using the Moisture Buffer Value concept. *Building and Environment* 2009;44:388–401. doi:10.1016/j.buildenv.2008.03.015.
- [278] Janssen H. Thermal diffusion of water vapour in porous materials: Fact or fiction? *International Journal of Heat and Mass Transfer* 2011;54:1548–62. doi:10.1016/j.ijheatmasstransfer.2010.11.034.
- [279] Rode C, Peuhkuri R, Svennberg K, Dean SW. Moisture Buffer Value of Building Materials. *Journal of ASTM International* 2007;4.
- [280] Janssens A, Rode C, De Paepe M, Woloszyn M, Sasic-Kalagasidis A. From EMPD to CFD – overview of different approaches for Heat Air and Moisture modeling in IEA Annex 41. Copenhagen: IEA ECBCS Annex 41, Closing Seminar; 2008.
- [281] Steeman M, Goethals K, Laverge J, Janssens A, De Paepe M. On modelling moisture buffering when evaluating humidity controlled HVAC systems. *Proceeding of Building Simulation 2009*, Glasgow, Scotland: 2009.
- [282] Ferroukhi MY, Djedjig R, Limam K, Belarbi R. Hygrothermal behavior modeling of the hygroscopic envelopes of buildings: A dynamic co-simulation approach. *Build Simul* 2016;9:501–12. doi:10.1007/s12273-016-0292-5.
- [283] Steeman M. Hygrothermal modelling for building energy simulation applications. Ghent University, 2010.
- [284] Peckstadt A, Moris H. Eindverslag schadeonderzoek van de gepresenteerde boekbanden, documenten en vitrines. Stad Antwerpen Musea en Erfgoed; 2012.
- [285] Weber A, Koschenz M, Dorer V, Marion H, Holst stefan. TRNFlow, a new tool for the modelling of heat, air and pollutant transport in buildings within TRNSYS, 2003.
- [286] Stymne H, Hansson P, Boman CA. Experimental testing of a homogeneous tracer pulse technique for measurement of ventilation and air distribution in buildings. *Proceedings 21st Annual AIVC Conference "Innovations in ventilation technology,"* vol. paper 30, The Hague, Netherlands: 2000.
- [287] Schito E, Testi D. A visitors' presence model for a museum environment: Description and validation. *Build Simul* 2017:1–11. doi:10.1007/s12273-017-0372-1.
- [288] Derluyn H, Janssen H, Diepens H, Derome D, Carmeliet J. Can Books and Textiles Help in Controlling the Indoor Relative Humidity? 10th International Conference on Thermal Performance of the Exterior Envelopes of Whole Buildings, Clearwater Beach, Florida, USA: 2007.

- [289] Derluyn H, Janssen H, Diepens H, Derome D, Carmeliet J. Hygroscopic behavior of paper and books. *Journal of Building Physics* 2007;31:9–34.
- [290] Vereecken E, Roels S. Review of mould prediction models and their influence on mould risk evaluation. *Building and Environment* 2012;51:296–310. doi:10.1016/j.buildenv.2011.11.003.
- [291] De Backer L, Laverge J, Janssens A, De Paepe M. A strategy for Modelling Typical Indoor Climates in Historic Buildings: moisture buffering of massive walls and stratification by heating. *Proceedings of the 15th International Conference of IBPSA: Building Simulations 2017, San Fransisco, California, USA: 2017.*
- [292] Schellen HL, van Schijndel J, Limpens-Neilen D, van Aarle MAP. Damage to a monumental organ due to wood deformation caused by church heating (PDF Download Available). *ResearchGate* 2003.
- [293] Larsen PK. Climate control in Danish churches. In: Padfield T, Borchersen K, editors. *Museum Microclimates*, National Museum of Denmark: 2007.
- [294] Barbason M, Reiter S. Coupling building energy simulation and computational fluid dynamics: Application to a two-storey house in a temperate climate. *Building and Environment* 2014;75:30–9. doi:10.1016/j.buildenv.2014.01.012.
- [295] Griffith B, Chen QY. A Momentum-Zonal Model for Predicting Zone Airflow and Temperature Distributions to Enhance Building Load and Energy Simulations. *HVAC&R Research* 2003;9:309–25. doi:10.1080/10789669.2003.10391072.
- [296] Zuo W, Wetter M, Tian W, Li D, Jin M, Chen Q. Coupling indoor airflow, HVAC, control and building envelope heat transfer in the Modelica Buildings library. *Journal of Building Performance Simulation* 2016;9:366–81. doi:10.1080/19401493.2015.1062557.
- [297] Laboratory LBN. COMIS. Berkeley: 1988.
- [298] Weber A, Koschenz M, Holst S, Hiller M, Welfonder T. TRNFLOW: Integration of COMIS into TRNSYS TYPE 56, 2002, p. 801–6.
- [299] Huang J, Winkelmann F, Buhl F, Curtis Pedersen, Daniel Fisher, Richard Liesen, et al. Linking the COMIS Multi-Zone Airflow Model With the EnergyPlus Building Energy Simulation Program. vol. II, IBPSA; 1999, p. 1065–70.
- [300] Henk Kaarle Versteeg, Malalasekera W. *An Introduction to Computational Fluid Dynamics: The Finite Volume Method*. 2nd edition. Pearson Education; 2007.
- [301] Djunaedy E. External coupling between building energy simulation and computational fluid dynamics. Technische Universiteit Eindhoven, 2005.
- [302] Wang S, Chen Y. A novel and simple building load calculation model for building and system dynamic simulation. *Applied Thermal Engineering* 2001;21:683–702. doi:10.1016/S1359-4311(00)00073-9.
- [303] Teshome EJ, Haghghat F. Zonal Models for Indoor Air Flow – A Critical Review. *International Journal of Ventilation* 2004;3:119–29. doi:10.1080/14733315.2004.11683908.
- [304] Megri AC, Snyder M, Musy M. Building Zonal Thermal and Airflow Modelling – A Review. *International Journal of Ventilation* 2005;4:177–88. doi:10.5555/ijov.2005.4.2.177.
- [305] Megri AC, Haghghat F. Zonal Modeling for Simulating Indoor Environment of Buildings: Review, Recent Developments, and Applications. *HVAC&R Research* 2007;13:887–905. doi:10.1080/10789669.2007.10391461.
- [306] Griffith BT. Incorporating Nodal and Zonal Room Air Models into Building Energy Calculation Procedures. Massachusetts Institute of Technology, 2002.

- [307] Chen, Griffith BT. RP-1222 -- incorporation of nodal room heat transfer models into energy calculation procedures. ASHRAE; 2003.
- [308] Lebrun J. Exigences physiologiques et modalités physiques de la climatisation par source statique concentrée. University of Liege, 1970.
- [309] Haghghat F, Li Y, Megri AC. Development and validation of a zonal model — POMA. *Building and Environment* 2001;36:1039–47. doi:10.1016/S0360-1323(00)00073-1.
- [310] Megri AC, Yu Y. New calibrated zonal model (POMA+) for temperature and airflow predictions. *Building and Environment* 2015;94, Part 1:109–21. doi:10.1016/j.buildenv.2015.07.014.
- [311] Norrefeldt V, Nouidui TS, Gruen Gunnar. Development of an isothermal 2D zonal air volume model with impulse conservation | Energy Technologies Area. Proceedings of: Clima 2010, 10th Rehva World Congress "Sustainable Energy Use in Buildings," Antalya, Turkey: 2010.
- [312] Inard C, Bouia H, Dalicieux P. Prediction of air temperature distribution in buildings with a zonal model. *Energy and Buildings* 1996;24:125–32. doi:10.1016/0378-7788(95)00969-8.
- [313] Wurtz E. Modélisation tridimensionnelle des transferts thermiques et aérodynamiques dans le bâtiment en environnement orienté objet. Ecole nationale des ponts et chaussées, 1995.
- [314] Inard C, Meslem A, Depecker P. Energy consumption and thermal comfort in dwelling-cells: A zonal-model approach. *Building and Environment* 1998;33:279–91. doi:10.1016/S0360-1323(97)00074-7.
- [315] Teshome EJ, Haghghat F. A new generation of zonal models. *ASHRAE Transactions* 2005;112:163–74.
- [316] Ren ZE, Stewart J. Simulating air flow and temperature distribution inside buildings using a modified version of COMIS with sub-zonal divisions. *Energy and Buildings* 2003;35:257–71.
- [317] Stewart J, Ren ZG. CoWZ - A subzonal indoor airflow, temperature and contaminant dispersion model. *Building and Environment* 2006;41:1631–48. doi:10.1016/j.buildenv.2005.06.015.
- [318] Norrefeldt V, Grün G, Sedlbauer K. VEPZO – Velocity propagating zonal model for the estimation of the airflow pattern and temperature distribution in a confined space. *Building and Environment* 2012;48:183–94. doi:10.1016/j.buildenv.2011.09.007.
- [319] Gao J, Zhang X, Zhao JN, Gao FS. A heat transfer parameter at air interfaces in the BLOCK model for building thermal environment. *International Journal of Thermal Sciences* 2010;49:463–70. doi:10.1016/j.ijthermalsci.2009.08.002.
- [320] Mora L, Gadgil AJ, Wurtz E. Comparing zonal and CFD model predictions of isothermal indoor airflows to experimental data. *Indoor Air* 2003;13:77–85.
- [321] Gao J, Zhao J, Li X, Gao F. A Zonal Model for Large Enclosures With Combined Stratification Cooling and Natural Ventilation: Part 1—Model Generation and its Procedure. *Journal of Solar Energy Engineering-Transactions of the ASME* 2006;128:367–75. doi:10.1115/1.2188958.
- [322] Wang X, Huang C, Cao W. Mathematical modeling and experimental study on vertical temperature distribution of hybrid ventilation in an atrium building. *Energy and Buildings* 2009;41:907–14. doi:10.1016/j.enbuild.2009.03.002.

- [323] Huang C, Song Y, Luo X. Application of the Gebhart-Block Model for Predicting Vertical Temperature Distribution in a Large Space Building with Natural Ventilation. ICEBO - International Conference for Enhanced Building Operations, Shenzhen, China: Energy Systems Laboratory (<http://esl.tamu.edu>); Texas A&M University (<http://www.tamu.edu>); 2006.
- [324] Miura K. The analysis of a thermal storage system utilizing building mass in a cold region. Proceedings of Building Simulation 2007, Beijing, China: 2007, p. 465–72.
- [325] Zhu Q, Yan D. Dynamic simulation of atrium thermal environment aiding building design. Proceedings of Building Simulation 2007, Beijing, China: 2007, p. 294–301.
- [326] Bordass W, Bemrose C. Heating Your Church. Church House Publishing; 1996.
- [327] Arai Y, Togari S, Miura K. Unsteady-state thermal analysis of a large space with vertical temperature distribution. ASHRAE Transactions 1994;100:396–411.
- [328] Takemasa Y, Togari S, Arai Y. Application of an unsteady-state model for predicting vertical temperature distributions to an existing atrium. ASHRAE Transaction 1996;102:239–47.
- [329] Wang Z, Zhang Y, Chen Z, Liu Y. The Multi-zonal Balance Model of Temperature Distribution in Data Center. Applied Sciences, Engineering and Technology 2013;5:1756–61.
- [330] Gao J, Li X, Zhao J, Gao F. Simplified model of temperature distribution in a large space with the stratificated air conditioning. In: Proceedings of the 4th International Symposium on Heating, ventilating and Air Conditioning, Oct 9-11, Beijing, China: 2003, p. 101–8.
- [331] Gao J, Zhang X, Zhao JN. Numerical Determination of Convection Coefficients for Internal Surfaces in Buildings Dominated by Thermally Stratified Flows. Journal of Building Physics 2008;31:213–23.
- [332] Gao J, Zhao J, Li X, Gao F. Evaluation of a Zonal Model for Large Enclosures Using Computational Fluid Dynamics. Journal of Asian Architecture and Building Engineering 2007;6:379–85. doi:10.3130/jaabe.6.379.
- [333] Beausoleil-Morrison I. An algorithm for calculating convection coefficients for internal building surfaces for the case of mixed flow in rooms. Energy and Buildings 2001;33:351–61. doi:10.1016/S0378-7788(00)00117-1.
- [334] Eckert ERG, Jacson TW. Analysis of turbulent free-convection boundary layer on flat plate. NACA; 1951.
- [335] Rong W, Huang C, Zhang X. Study on an Unsteady and Synchronous Solving Model for Low Sidewall Air Supply System in the Large-Space Building. Proceedings of the 8th International Symposium on Heating, Ventilation and Air Conditioning, Springer, Berlin, Heidelberg; 2014, p. 265–73. doi:10.1007/978-3-642-39584-0_29.
- [336] Heiselberg P, Murakami S, Rølet C-A. Annex 26: Ventilation of large spaces in buildings. Part 3. Analysis and Prediction Techniques. Denmark, Aalborg, Aalborg University: Physics International Energy Agency (IEA); 1998.
- [337] Etheridge DW, Sandberg M. Building ventilation: theory and measurement. John Wiley & Sons; 1996.
- [338] Awbi HB. Ventilation of Buildings. London: Spon Press Taylor & Francis; 2003.
- [339] Frean DH, Billington NS. The ventilation jet. The Ventilation Jet 1955;23:313–33.
- [340] Straub HE. Principles of room air distribution. Heating, Piping and Air Conditioning 1969;April:122–8.

- [341] Zhang Y. *Indoor Air Quality Engineering*. CRC Press; 2004.
- [342] ASHRAE. *ASHRAE Handbook: Fundamentals*. Chapter 33, American Society of Heating, Refrigerating and Air-Conditioning Engineers; 2005, p. 33.1-33.19.
- [343] Zou Y. *Air jets in ventilation applications*. PhD. Royal Institute of Technology, 2001.
- [344] Rajaratnam N. *Turbulent Jets*, Volume 5 - 1st Edition. Elsevier Science; 1976.
- [345] Goodfellow HD, Tahti E. *Industrial Ventilation Design Guidebook*. California San Diego: Academic Press; 2001.
- [346] Aschaber J, Hiller M, Weber R. TRNSYS 17: New Features of the Multi-zone Building Model. 11th International Building Performance Simulation Association Conference, vol. 11th International Building Performance Simulation Association Conference, Glasgow, Scotland: 2009.
- [347] Fisher DE, Pedersen CO. Modelling of natural convective heat transfer at an internal surface. *ASHRAE Transactions* 1997;103:137-48.
- [348] Goethals K, Breesch H, Janssens A. Sensitivity analysis of predicted night cooling performance to internal convective heat transfer modelling. *Energy and Buildings* 2011;43:2429-41. doi:10.1016/j.enbuild.2011.05.033.
- [349] Seem JE. *Modeling of heat transfer in buildings*. PhD dissertation. University of Wisconsin-Madison, 1987.
- [350] Maroy K, Steeman M, De Backer L, Janssens A, De Paepe M. Conservation Climate Analysis of a Church Containing Valuable Artworks. *Energy Procedia* 2015;78:1269-74. doi:10.1016/j.egypro.2015.11.286.
- [351] Geiger R. *Klassifikation der Klimate nach W. Köppen* [Classification of climates after W. Köppen]. *Landolt-Börnstein - Zahlenwerte und Funktionen aus Physik, Chemie, Astronomie, Geophysik und Technik, alte Serie*, vol. 3, Berlin: Springer; 1954, p. 603-7.
- [352] Departement Cultuur, Jeugd & Media. *Meeester van Frankfurt - Nood Gods*. Topstukken | Kunsten en Erfgoed 2009. <http://www.kunstenenerfgoed.be/nl/wat-doen-webeschermer-cultuurgoederen/topstukkenlijst/de-nood-gods> (accessed March 17, 2017).
- [353] Topstukkenlijst. Departement Cultuur, Jeugd en Media - Afdeling Cultureel Erfgoed; 2016.
- [354] Goetghebeur N, Lefève R, Philippot A, Thissen Je. *Het Nood-Godsdieluk van de kerk te Watervliet -Materiele Beschrijving, bewaringstoestand en behandeling*. *Bulletin van Het Koninklijk Instituut Voor Het Kunstpatrimonium* 1966;IX.
- [355] *Subsidie voor dringende conservatie van 16e-eeuws Nood Godsdieluk in Watervliet | Joke Schauvliege* 2013. <http://www.jokeschauvliege.be/content/subsidie-voor-dringende-conservatie-van-16e-eeuws-nood-godsdieluk-watervliet> (accessed January 1, 2017).
- [356] Fawcett J. *Historic floors: their history and conservation*. Butterworth-Heinemann; 2001.
- [357] Standardization IO for. *ISO 13370: 2007(E). Thermal Performance of Buildings — Heat Transfer via the Ground — Calculation Methods* 2007.
- [358] Krischer O, Kast W. *Zur Frage des Wärmebedarfes beim Anheizen selten beheizter Gebäude*. *Ges Ing n.d.*;78.
- [359] Heimsch R. *Planungsgrundsätze für den Erhalt und die Nutzung von historischen Gebäuden*. *IKZ-HAUSTECHNIK* 2003;15.
- [360] Raiß W, Roedler F. H. *Rietschels Lehrbuch der Heiz- und Lüftungstechnik*. Springer-Verlag; 2013.

- [361] Hayati A, Mattsson M, Sandberg M. Evaluation of the LBL and AIM-2 air infiltration models on large single zones: Three historical churches. *Building and Environment* 2014;81:365–79. doi:10.1016/j.buildenv.2014.07.013.
- [362] Ekelund S, Luimes R, Gauvin C, van duin P, Jorrison A, Ankersmit B, et al. The development of a methodology to understand climate induced damage in decorated oak wooden panels. *proceedings of ICOM-CC 18th Triennial Conference, Copenhagen, Denmark: 2017.*
- [363] Hayati A. Natural Ventilation and Air Infiltration in Large Single Zone Buildings. Measurements and Modelling with Reference to Historical Churches. PhD dissertation. University of Gävle, 2017.
- [364] Lower S. Activation energy, Arrhenius law. *General Chemistry* n.d. <http://www.chem1.com/acad/webtext/dynamics/dynamics-3.html> (accessed November 2, 2016).
- [365] JAIC. Arrhenius Equation Tutorial 2008. www.cool.conservation-us.org/jaic/.
- [366] Jagannadham V. How Do We Introduce the Arrhenius Pre-Exponential Factor (A) to Graduate Students? *Creative Education* 2010;2:128–9.
- [367] Sebera D. *Isoperms An Environmental Management Tool* 1994.
- [368] Strang T, Grattan D. TEMPERATURE AND HUMIDITY CONSIDERATIONS FOR THE PRESERVATION OF ORGANIC COLLECTIONS - THE ISOPERM REVISITED. *E-Preservation Science* 2009.
- [369] Reilly JM, Others A. *New Tools for Preservation: Assessing Long-Term Environmental Effects on Library and Archives Collections.* Commission on Preservation and Access, 1400 16th Street, N.W., Suite 740, Washington, DC 20036-2217 (\$10); 1995.
- [370] Padfield T. *The Preservation Index and the Time Weighted Preservation Index* 2004. <http://www.conservationphysics.org/> (accessed January 1, 2013).
- [371] Luxford N, Thickett D, Wyeth P. Applying Preventive Conservation Recommendations for Silk in Historic Houses - ICOM-CC. In: Janssen E, editor., Rome: ICOM-CC; 2010.
- [372] Michalski S. Double the life for each five-degree drop, more than double the life for each halving of relative humidity. In: Vontobel R, Conservation IC for, editors. 13th triennial meeting, vol. Preprints volume 1, London: James & James; 2002, p. 66–72.
- [373] Kubik ME. Preserving the Painted Image: The Art and Science of Conservation. *Colour: Design & Creativity* 2010;5:1–8.
- [374] Shaw K. *Display and Conservation: The Dilemma of lighting in Museums* 1996.
- [375] Michalski S. Agent of Deterioration: Light, Ultraviolet and Infrared. *Preventive Conservation and Risks* 2016. <http://canada.pch.gc.ca/eng/1444925073140#conc7> (accessed January 24, 2017).
- [376] Druzik J, Eshoj B. Museum lighting: its past and future development. *Museum microclimates: contributions to the Copenhagen conference, 19-23, Copenhagen, Denmark : National Museum of Denmark; 2007, p. 51–6.*
- [377] Michalski S. Towards specific lighting guidelines. In: Grimstad K, editor. *ICOM Committee for Conservation, 9th triennial meeting, Dresden, German Democratic Republic, ICOM Committee for Conservation; 1990.*
- [378] Padfield T. The lux is a poor predictor of photochemical damage. *Conservation Physics* n.d. <http://www.conservationphysics.org/lightmtr/luxerror.php> (accessed January 24, 2017).
- [379] Institute G of CCHCC. Light damage calculator 2016. <http://canada.pch.gc.ca/eng/1450464034106> (accessed January 24, 2017).

-
- [380] Sedlbauer K. Prediction of Mould Growth by Hygrothermal Calculation. *Journal of Thermal Envelope and Building Science* 2002;25:321–36. doi:10.1177/0075424202025004093.
- [381] Krus M, Sedlbauer K, Zillig W, Künzle HM. A new model for mould prediction and its application on a test roof. *Proceedings of the 2nd International Scientific Conference on the current problems of Building-Physics in the rural building, Krakow, Poland: 2001.*
- [382] Sedlbauer K, Krus M, Zillig W, Künzle HM. Mold Growth Prediction by Computational Simulation. *ASHRAE conference IAQ 2001, San Francisco, California, USA: 2001.*
- [383] Krus M, Seidler M, Sedlbauer K. Comparative evaluation of the predictions of two established mold growth models. In: *Buildings XI, Thermal Performance of the Exterior Envelopes of Whole Buildings XI 2010, Florida Atlanta: 2010.*
- [384] Warner CY, Arpacı VS. An experimental investigation of turbulent natural convection in air at low pressure along a vertical heated flat plate. *International Journal of Heat and Mass Transfer* 1968;11:397–406. doi:10.1016/0017-9310(68)90084-7.
- [385] Le Dréau J, Heiselberg P, Jensen RL. Experimental investigation of convective heat transfer during night cooling with different ventilation systems and surface emissivities. *Energy and Buildings* 2013;61:308–17. doi:10.1016/j.enbuild.2013.02.021.

ANNEXES

ANNEX H2

ANNEX 2.A: Standard EN16883:2017

Assessment scale				
High risk	Low risk	Neutral	Low Benefit	High Benefit
Assessment category	Assessment criteria	Measure 1	Measure n
Technical compatibility	hygrothermal risks			
	structural risks			
	corrosion risks			
	salt reaction risks			
	biological risks			
	reversibility			
Heritage significance	material impact			
	visual impact			
	spatial impact			
Economic viability	capital costs			
	operating costs, including maintenance costs			
	economic return			
	economic savings			
Energy	energy performance and operational energy demand: - primary energy rating (total)			
	primary energy rating (non-renewable)			
	primary energy rating (renewable)			
	energy saving			
	embodied energy, life cycle energy demand			
Indoor environment	indoor environmental conditions suitable for building content preservation			
	indoor environmental conditions suitable for building fabric preservation			
	indoor environmental conditions suitable for achieving good occupant comfort levels			
	emission of other harmful substances			
Outdoor environment	greenhouse gas emissions, from measures implemented and operation			
	emission of other harmful substances			
	water consumption			
	natural resources			
Aspects of use	influence on the use of the building			

Figure 0.1: Example of assessment table [96].

ANNEX 2.B: Chemical Degradation of Objects

Arrhenius Equation

The Arrhenius equation is commonly used to calculate the rate of decay dependent on the temperature. This equation was formulated in the 19th century by Swedish chemist Svante Arrhenius. He expressed the relation between the temperature and the decay rate by combining the concepts of activation energy and the Maxwell-Boltzmann distribution law [364]. The first concept, activation energy, is the critical energy necessary to cause a reaction. In this case the energy is supplied by thermal energy. The second concept, the Maxwell-Boltzmann distribution law defines the fraction of the molecules that possess enough kinetic energy to react at the given temperature T . Combining both concepts resulted in the following equation:

$$k = Ae^{-\frac{E_a}{RT}} \quad (0.1)$$

In this equation k is the decay rate. The exponential part of the Arrhenius equation expresses the fraction of reactant molecules that possess enough kinetic energy to react, as governed by the Maxwell-Boltzmann law. The exponent E_a/RT expresses the ratio between the activation energy [J/mol] and the average kinetic energy RT . R is the gas constant [8.314J/K.mol] and T the temperature at which the reaction takes place [K]. The activation energy E_a depends on the type of material and can be determined by experiments [365].

A is the pre-exponential factor and expresses the fraction of molecules that would react independent of the temperature and activation energy. As described in the first part, the concentration of water molecules in the air are responsible for the chemical degradation reaction. The dependency of the decay rate on the concentration of water molecules, expressed as relative humidity, is contained in this pre-exponential factor. The units of the pre-exponential factor are identical to those of the rate constant. If the reaction is first order, as is assumed in preservation science, it has the units s^{-1} [366].

Arrhenius Equation applied for Works of Arts

The first damage function in the table is the Isoperm method³⁷, which was introduced in 1994 by Sebera [367] to predict the relative lifetime of paper. The author used the Eyring equation, convertible into the Arrhenius equation, to estimate the decay rate. Further, he assumed a linear relationship between the degradation rate and the relative humidity. This assumption however, only holds in an intermediate zone of the relative humidity, as in this zone the relation between

³⁷ In many papers, the conversion from the original formula (temp in °F and ΔH in kcal) is not converted or not converted correctly (e.g. Costa et al. [37])

the relative humidity and the moisture content in the objects is quite linear. To overcome this problem, Strang and Grattan [368] revised the method by using the moisture sorption content of paper instead of the relative humidity. This is the second damage function.

The third damage function is developed by the Image Permanence Institute (IPI) in 1995 [369]. To evaluate the annual response, IPI defined an average value, which they named the Time Weighted Preservation Index (TWPI). This value is an average value of the Preservation Index (PI), which expresses, like the method of Sebera [367], the chemical decay rate for the combined effect of temperature and relative humidity. Although IPI states that their method goes further by allowing for life expectancy values expressed in years instead of relative factors, the principles of both methods are the same [370]. It means that the value of the life expectancy of an object must be interpreted in a relative sense and is meaningful when comparing to other conditions (improving, staying steady or getting worse). The reason is that the equation for the preservation index was based on the hydrolysis reaction of cellulose acetate, a common plastic which is used as base for photographic film. Even though, IPI uses the equation for organic materials in general, it must be kept in mind that the equation was fitted to specific data for cellulose acetate [370].

In 2000, Michalski [112] introduced the concept of Lifetime Multiplier (LM), which also calculates a relative lifetime similar to the method of Sebera [367]. Instead of comparing two conditions, one condition was compared with a temperature of 20°C and a relative humidity 50%, which is the standard museum set point. To account for the non-linear relation between the moisture content of the object and the relative humidity, the author applied a power law on the pre-exponential coefficient. When the value of LM becomes lower than one, the rate of deterioration is greater, and the lifetime shorter, than under standard conditions. A value of 0.5 for LM, indicating a doubling of rate and halving of lifetime, is defined as the threshold of risk [122]. To facilitate the analysis and to evaluate the annual response, Silva and Henriques [147] proposed to use on top an equivalent Lifetime Multiplier (eLM), a value representing the influence of all year. The equivalent Lifetime Multiplier is calculated by the average of the reciprocal values of the lifetime multiplier. To respect the response of the material, a response time of 24 hours for temperature and 30 days for relative humidity, according the IPI recommendations [230]. Further, a classification was defined around the mid value 1 (class 3 – some risks), with two classes for increased life expectancies (classes 4 and 5) and two for shorter life expectancies (classes 1 and 2). The definition of the intervals for each class was based on the classification of the Image Permanence Institute [122].

Table 0.1: Classification of the eLM-values [122].

Classification	eLM [-]
Ideal	>2.2
Good	[1.7;2.2]
Some Risk	[1;1.7]
Potential Risk	[0.75;1]
High Risk	<0.75

Padfield [370] criticized the method of IPI, because their method does not take into consideration the difference in activation energy of different materials. He also disapproved the concept of "lifetime" as indicator and suggested that using a relative parameter is more straightforward. As an answer, he proposed the decay index as an indicator of the relative damage to any object. The method is similar as this of Sebera and Michalski and the source code of his model is free for charge. As reference point, which equals with a decay rate 1, the condition 20°C/ 50% was used.

Table 0.2: Comparison of methods proposed in conservation science to estimate the decay rate of an object.

	Method	Author	Equation
1	Isoperm method	Sebera, 1994	$\frac{k_1}{k_2} = \left(\frac{RH_1}{RH_2}\right) \left(\frac{T_1}{T_2}\right) 10^{0.0523 (E_a - RT) \left(\frac{1}{T_2} - \frac{1}{T_1}\right)}$
2	Revised Isoperm method	Strang and Grattan, 2009	$\frac{k_1}{k_2} = \left(\frac{C_1}{C_2}\right) e^{\frac{E_a}{R} \left(\frac{1}{T_2} - \frac{1}{T_1}\right)}$
3	Preservation index	IPI,1995	$PI = \frac{e^{\frac{95220 - 134.9RH}{RT} + 0.0284RH - 28.023}}{360} (*)$
	TWPI	IPI,1995	$TWPI_n = \frac{n TWPI_{n-1} PI_n}{PI_n(n-1) + TWPI_{n-1}}$
4	Lifetime Multiplier	Michalski, 2000	$LM_x = \left(\frac{k_1}{k_2}\right) = \left(\frac{50\%}{RH_x}\right)^{1.3} e^{\frac{E_a}{R} \left(\frac{1}{T_x} - \frac{1}{293}\right)}$
	Equivalent Lifetime Multiplier	Silva and Henriques, 2015	$eLM = \frac{1}{\frac{1}{n} \sum_{i=1}^n LM_i}$
5	Isoburn	Padfield,2004	$\frac{k_1}{k_2} = RH_x \cdot 1,34 \cdot 10^{16} e^{\frac{E_a}{R} \left(\frac{1}{T_2} - \frac{1}{293}\right)}$

* The equation has been taken from Padfield [370] , because the full description of how the method was derived has not been published by IPI itself [368].

* Note: $\Delta H = E_a - R \cdot T$

* All equations are converted to have the same units:

- R gas constant, 8.314 J/(K. mole)
- E_a activation energy [J/(mole)] Table 0.3 displays the activation energy of some common objects.
- T temperature [K]
- RH relative humidity [%]

Table 0.3: Activation energy of some common objects present in a historical building or museum.

Material	E_a [kJ/mole]	Source
Silk	50	Luxford et al. [371]
Yellowing varnish	70	Michalski [372]
Cellulose	100	Michalski [372]

Light guidelines

For paintings, most common changes are yellowing and darkening of varnishes and fading of certain paint colours [373]. Sunlight naturally contains ultraviolet light (UV), so exposure of a painting with sensitive pigments to direct sunlight can cause those sensitive pigments to fade. UV is by far the most damaging portion of the electromagnetic spectrum and it adds little or nothing to our visual perception of objects. Therefore in the context of preservation, UV should be completely excluded from light in museums and galleries [374]. The traditional rule on UV was as follows not exceed $75\mu\text{W}/\text{lm}$ [375].

As for temperature and humidity, Garry Thomson [80] published in *The Museum Environment* 'magical numbers' for diffuse light. For items that are moderately sensitive such as oil and tempera paintings, lacquerware, plastics, wood, furniture, horn, bone, ivory, undyed leather and minerals, the maximum recommended level advised is 200lux. However, the "lux laws" supplemented with prohibitions on ultraviolet and infrared radiation is an over-simplification [376]. The past decades, research on risk assessment showed that the simple rules can be stretched, or violated [376–378]. To help make such decisions using a risk management strategy, CCI has developed a light damage calculator for the web [379].

ANNEX 2.C: The Sedlbauer model - A possible model to predict mould growth

One of the more sophisticated models based on isopleth system is the bio-hygrothermal model developed by Sedlbauer [5,109]. Figure 0.2 shows the isopleth model developed by Sedlbauer [380]. He subdivided the substrate materials into different classes. Furthermore the model consists out of a dual system [116]: isopleths indicating the time until spore germination occurs and isopleths indicating the mycelial growth rate [380]. For each class and system, he defined the lowest isopleth of mould (LIM), equalling the lowest boundary lines of possible fungus activity.

Figure 0.2 shows the different classes. These are:

- Class 0 optimal culture medium;
- Class I biologically recyclable building materials;
- Class II biologically adverse building materials;
- Class III building materials that are neither degradable nor contain any nutrients.
For Class III, there isn't any mould risk and therefore these materials aren't evaluated.

Furthermore, he defined a separate class K, which represents an isopleth system for the so called critical fungus species concerning health risk.

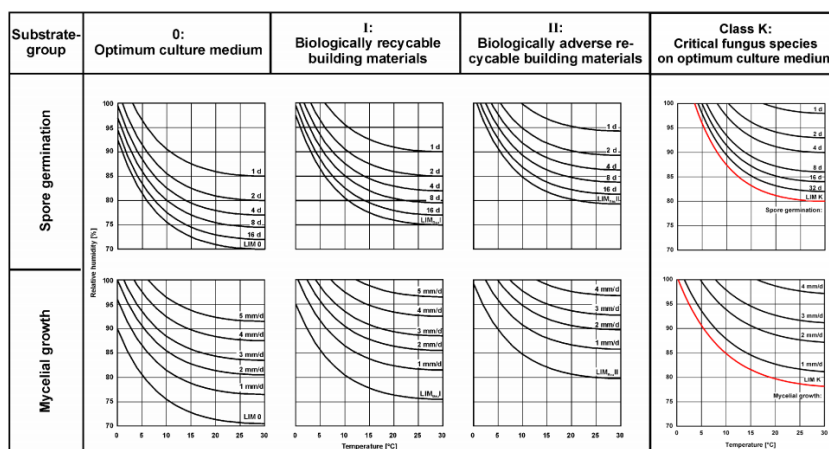


Figure 0.2: Isopleth systems for 3 categories of substrates and the isopleth system for the so called critical fungus species, called class K, given by Sedlbauer. [5,380].

The isopleth system, however, can only be used if steady-state conditions occur [116,380]. Consequently, moisture absorption and drying out of the fungi spores occurring under transient boundary conditions, is not taken into account [381]. To overcome this problem and to be able to predict more realistically the mould growth, Sedlbauer extended his isopleth model with a transient model. This model is called the bio-hygrothermal model [148,380,381] and is

implemented in the freeware WUFI Bio [149], which will be used in this work to analyse mould risk.

Figure 0.3 shows the principle of this bio-hygrothermal model: a wall with a mould spore. In this model the moisture balance of a spore is calculated. The moisture content in the spore will be used to calculate the spore germination, metabolic processes and mould growth [290].

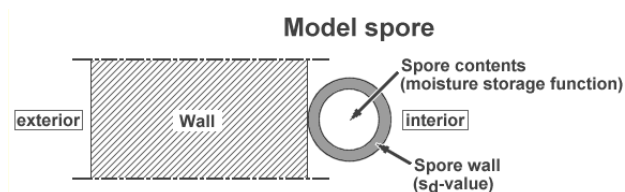


Figure 0.3: Schematic drawing of a spore model close to reality. A spore is present on the wall surface (highly enlarged).

Figure 0.4 shows how the moisture balance in the spore is calculated. In the Bio-hygrothermal Model the spore itself is presented as a 'biological' layer in which the one-dimensional moisture transport will be calculated. Implementing the spore element directly as a separate layer on the wall and then calculating the moisture balance, would introduce an unrealistically high diffusion resistance by the spore layer. Therefore, in a first step the moisture balance in the wall is calculated. In a second step, the resulting data for the wall surface are then used as boundary conditions for the bio-hygrothermal computation of the model spore [382].

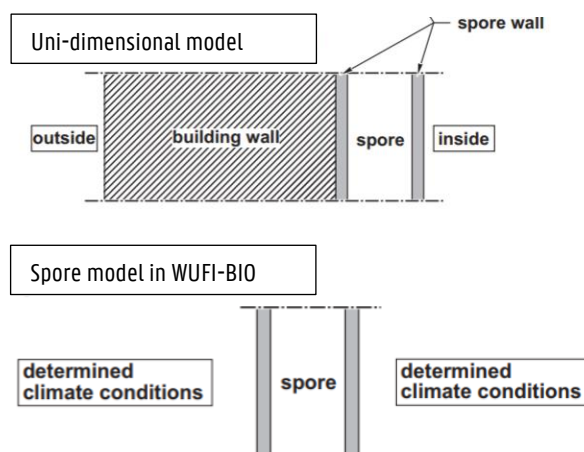


Figure 0.4: Unidimensional model: Spore treated as a separate 'biological' layer yield to a non-realistic additional diffusion resistance for the wall. For this reason, first the moisture balance in the wall is calculated. The inner surface temperature and humidity of the wall serve as boundary conditions on both sides of the spore [382].

Using these boundary conditions, this model allows the calculation of the moisture content in a spore. If the critical water content is achieved inside the spore, germination can be regarded as completed and mould growth will begin [383]. The critical water content is as stated earlier dependent on the substrate class and the time and is shown in Figure 0.2. The starting point of the germination is defined by the first visible growth, depending on the quality of the substrate. This influence is taken into account by shifting the LIM upwards. In WUFI Bio one of the classes shown in Figure 0.2 have to be selected before the risk on mould growth is calculated.

ANNEX 2.D: Rainflow Counting Method & Palmgren-Miner Rule

Rainflow Counting Method

Figure A.1 shows a stress range history. This time history is reduced to a manageable format that still contains the necessary characteristics of the fatigue cycle. To obtain a stress history following steps were used:

1. Calculate RH-cycles by comparing daily average with the yearly average.
2. Recalculate the daily average course and keep only the reversal points. These are where the load-time history changes in sign.
3. Apply the rain flow counting by the method described in ASTM 1049-85 [128].

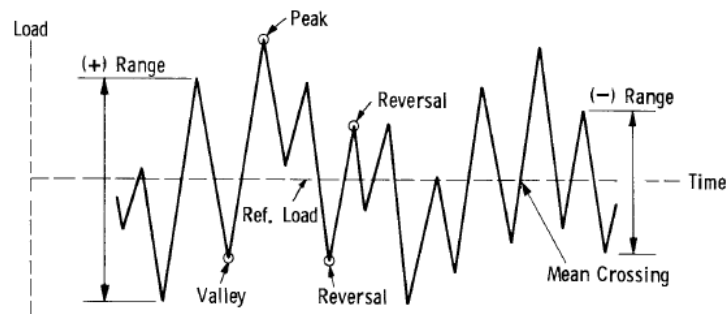


Figure A.1 Basic fatigue loading parameters [128].

Some sources rearrange stress history as:

1. Find in the history range the reversal point with highest absolute stress magnitude,
2. The part of the stress history before the absolute maximum have to be attach to the end of the history range,
3. Perform the rain flow counting on the re-arranged stress history

As stated in the ASTM rearranging the stress history can give a slightly different result. Therefore, the rearranging of the stress history is not used in this work.

Palmgren-Miner Rule

To estimate damage, one often uses a linear damage accumulation hypothesis according to the Palmgren-Miner rule. The damage fraction at a stress level S_i is linearly proportional to the ratio of number of cycles of operation to the total number of cycles that produces failure at that stress level. The ratio, D_i , is:

$$D_i = \frac{n_i}{N_i}$$

The cycle life N_i is obtained from S-N data tests, where the material is stressed by using cycles with a constant amplitude.

After calculating the fractional damage D_i for every stress level, a total damage can be calculated, defined as the sum of all the fractional damages over a total of k blocks:

$$D_{\text{tot}} = \sum_{i=1}^k D_i$$

The sum is extended over all cycles completed at time t . Fatigue failure occurs when $D(T)$ exceeds one.

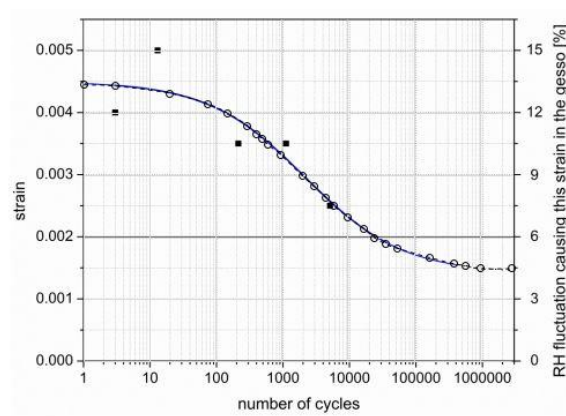


Figure A.2 Strain (S) leading to fracture versus number of cycles (N) to cause fracture at that strain level for a wooden panel covered with a gesso layer³⁸.

³⁸ Bratasz Ł, Kozłowski R, Lasyk Ł, Łukowski M, Rachwał B. Allowable microclimatic variations for painted wood: numerical modelling and direct tracing of the fatigue damage. In: Conservation IC for, editor., Bridgeland, J.; 2011.

ANNEX 3A. Additional Data Case Study Mystic Lamb

Chemical Decay

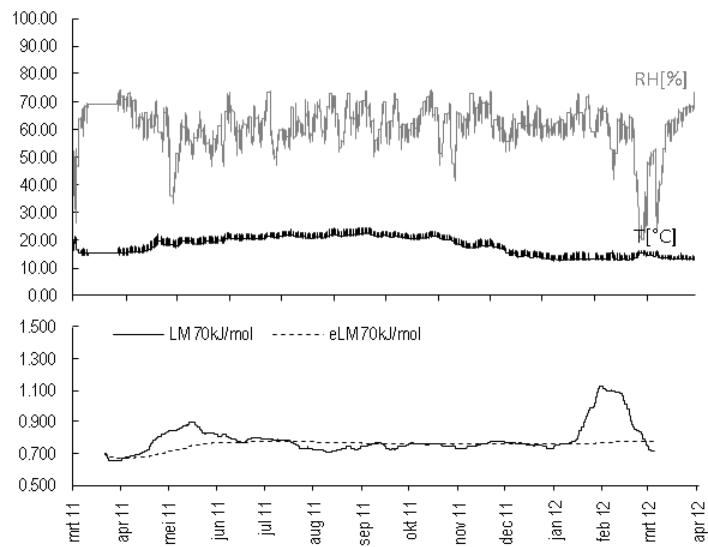


Figure: (a) Chemical decay for the measured climate.

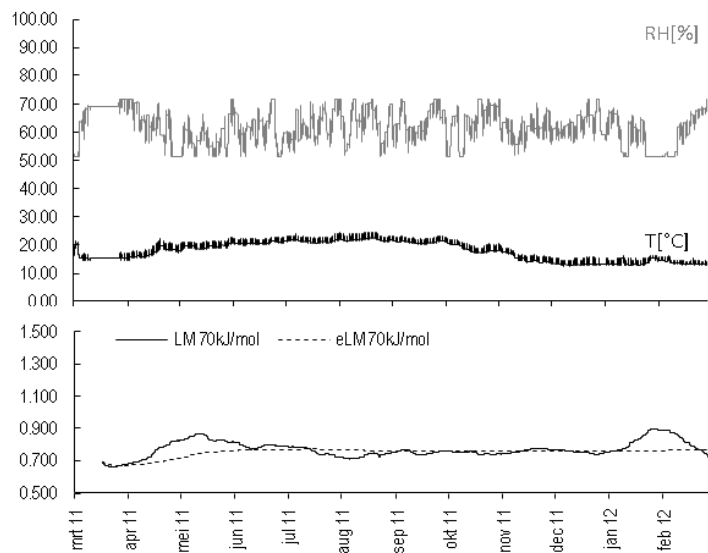
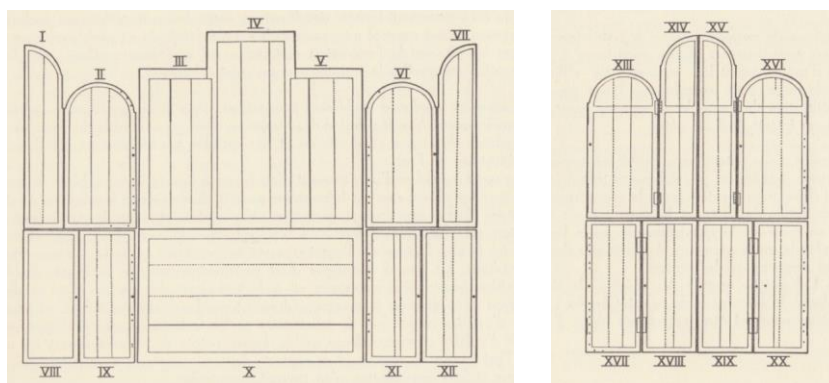


Figure: (a) Chemical decay for the measured climate.

Dimensions of all Panel of the Mystic Lamb

The following figure shows the composition of the polyptich [74]. Table 1 tabulates for every panel the thickness and the used species of wood.



Numbering of the different parts of the Ghent altarpiece [74].

Panel	Thickness panel [mm]	Type of Wood panel	Sawn cut
I /XIV	7-8 (edges) 8-15 (centre)	Baltic oak Baltic oak	radial cut
II	1-6	Baltic oak	radial cut
III	9-30	Baltic oak	radial cut
IV	10-16 (edge) 22 (centre)	Baltic oak	radial cut
V	22-30	Baltic oak	radial cut
VI	2-5	Baltic oak	radial cut
VII/XV	7-8(edges) 8-13(edges)	Baltic oak Baltic oak	radial cut radial cut
IX	3-5	Baltic oak	radial cut
X	10-34	Baltic oak	radial cut
XI	4-6	Baltic oak	radial cut
XII	2-4	Baltic oak	radial cut
XIII	1-6	Baltic oak	radial cut
XVI	2-6	Baltic oak	radial cut
XVII	4-6	Baltic oak	radial cut
XVIII	3-5	Baltic oak	radial cut
XIV	4-5	Baltic oak	radial cut
XX	3-5	Baltic oak	radial cut

ANNEX 4.A: Non-Isothermal Simplified Moisture Model (EMPD)

The EMPD model is implemented in the Simulation Studio as a new type (type 217). TRNSYS uses a so-called proforma file to define parameters, inputs and output values to the model. Required parameters, input and output values are listed in Table C.1.

Table C.1 Parameters, input and output values for Type 217.

Parameter Values		
area	Surface area	m ²
D[n]	Thickness of each layer	m
h _c	Convective vapour transfer coefficient	kg/(Pa.m ² .s)
S _d	Representing the thickness of an air layer with the same vapour resistance as the coating	m
T	Initial temperature of the wall	°C
RH	Initial relative humidity of the wall	%
Ro[n]	Dry density of the layer	kg/m ³
c _p [n]	Specific heat capacity of the material	J/kgK
lambda[n]	Heat conductivity of the layer	J/mK
lambda_corr[n]	Correction factor for lambda in case of a wet material	%
a[n]	Parameters for the equation of the vapour permeability, calculated as following:	kg/(Pa.m.s)
b[n]		
c[n]	$\Delta = a + b \cdot \exp(c \cdot \varphi)$	
w _{max} / A _{HH} [n]	Parameters for the equation of the sorption curve	kg/m ³
a / B _{HH} [n]		-
b / C _{HH} [n]		-
type of sorption curve	(1): theoretical (GAB) model [183] (2): empirical equation given by Hansen [201] (Chapter 3)	
Input Values		
n	Number of layers	°C
T _{zone}	Temperature of the zone	°C
RH _{zone}	Relative humidity of the zone	%
T _{S,wall}	Temperature of the wall	°C
h _{wall}	Convective heat transfer coefficient	W/m ² K
Output Values		
m _{vap}	Moisture gain	kg/h
Q _{cur}	Convective heat gain related to the thermal-zonal model	kJ/h

ANNEX 5.A: Temperature of Boundary Layer

This annex is largely based on the description in the paper of Togari et al. [66]

The average temperature of a boundary layer T_D is approximated by the following equation:

$$T_D = \frac{\int_0^\delta u(y)T(y)dy}{\int_0^\delta u(y)dy}$$

Where y vertical distance from the wall within the boundary layer
 $u(y)$ air velocity at distance y from the wall within the boundary layer [m/s]
 $T(y)$ air temperature at distance y from the wall within the boundary layer [°C]
 δ boundary layer thickness

According to the analytical solution described by Eckert and Jackson [334], the air velocity and temperature profiles in the boundary layer for a vertical flat plate can be estimated as following:

$$u(y) = \left(\frac{y}{\delta}\right)^7 \left(1 - \frac{y}{\delta}\right)^4$$

$$\frac{T(y) - T_\infty}{T_w - T_\infty} = 1 - \left(\frac{y}{\delta}\right)^7$$

This equation holds for fluids or gases with a Prandtl number equal to 1, where the temperature profile is similar to the velocity profile.

Combining the three equations described above, the following relation is obtained:

$$T_{D(i,K)} = 0.75T_{(i)} + 0.25T_{w(i,K)}$$

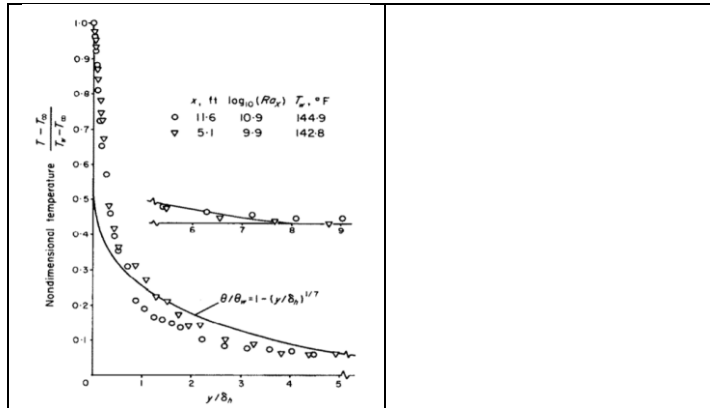


Figure: (a) Results of temperature measurements within the fully turbulent range and the power-law concept for turbulent natural convection data [384].

ANNEX 5.B: Infiltration equations in the thermal-zonal model

The mass conservation equations becomes:

$$0 = m_{\text{source}} + \sum_{k=1}^m (m_{\text{in},i,K} - m_{\text{out},i,K}) + m_{i-1} - m_i + m_{\text{inf},i-1} - m_{\text{inf},i} + m_{\text{inf_in}} + m_{\text{inf_out}}$$

Where $m_{\text{inf},i}$ the air flow between layer i and $i+1$
 $m_{\text{inf_in}} + m_{\text{inf_out}}$ mass added when there is an inlet opening, so the ambient air of the natural ventilation is added the layer i . The last term is the mass leaving when there is an outlet opening, so the air is subtracted from layer i .

Similar the equations for heat conservation and vapour flow are:

$$\begin{aligned} V_i \frac{(\rho C)^{t+\Delta t, m} T_i^{t+\Delta t, m+1} - (\rho C)^{t, T_i^t}}{\Delta t} &= q_{\text{source}} \\ &+ C_{b,i} A_{b,i} (T_{i-1} - T_i) + C_{b,i+1} A_{b,i+1} (T_{i+1} - T_i) \\ &+ \sum_{k=1}^m C_{m,i,K} (T_{m,i,K}) - \sum_{k=1}^m C_{m,out,i,K} T_i \\ &+ C_{\text{max}}(0, m_{i-1})(T_{i-1}) + C_{\text{min}}(0, m_{i-1})(T_i) \\ &- [C_{\text{max}}(0, m_i)(T_i) + C_{\text{min}}(0, m_i)(T_{i+1})] \\ &+ C_{\text{max}}(0, m_{\text{inf},i-1})(T_{i-1}) + C_{\text{min}}(0, m_{\text{inf},i-1})(T_i) \\ &- [C_{\text{max}}(0, m_{\text{inf},i})(T_i) + C_{\text{min}}(0, m_{\text{inf},i})(T_{i+1})] \\ &+ C_{m_{\text{inf_in}}} T_{\text{inf}} - C_{m_{\text{inf_out}}} T_i \end{aligned}$$

$$\begin{aligned} \frac{\rho_a V_i}{\Delta t} Y_i^{t+\Delta t, m} - \frac{\rho_a V_i}{\Delta t} Y_i^t &= \sum_{k=1}^m m_{\text{in}(i,K)} Y_{m(i,K)} - m_{\text{out}(i,K)} Y_i \\ &\max(m_{i-1}, 0) Y_{i-1} + \min(m_{i-1}, 0) Y_i \\ &- [\max(m_i, 0) Y_i + Y_{i+1} [\min(m_i, 0)]] \\ &\max(m_{\text{inf},i-1}, 0) Y_{i-1} + \min(m_{\text{inf},i-1}, 0) Y_i \\ &- [\max(m_{\text{inf},i}, 0) Y_i + Y_{i+1} [\min(m_{\text{inf},i}, 0)]] \\ &+ m_{\text{inf_in}} Y_{\text{inf}} + m_{\text{inf_out}} Y_i \end{aligned}$$

ANNEX 5.C: Radiation

This annex is largely based on the work of Holman³⁹

Radiation Properties

The enclosure is divided into N isothermal surfaces. Each surface, characterized by area A_k and temperature $T_{w,k}$, is considered a thermodynamic closed subsystem with energy balance $C_i dT_i/dt = Q_i$. Where C_i is the node thermal capacity, T_i its temperature and Q_i the net heat rate received due to temperature difference, split up in conductive, convective and radiative parts $Q_{i,rad}$.

To calculate the radiation energy exchange between opaque diffuse, grey temperature-uniform surfaces, Holman defined the following terms; irradiation (G) and Radiosity (J).

- Irradiation (G) is the total radiation incident upon a surface per unit time and per unit area and
- Radiosity (J) is the total radiation which leaves a surface per unit time and per unit area, and is the sum of energy emitted and energy reflected when no energy is transmitted.

The emitted power, called emittance and marked with E, was described by Holman as "the energy emitted by the body per unit area and per unit time". For black bodies, all radiant energy that strikes the body is absorbed and the radiosity is equal to the emittance $E_b = \sigma T^4$.

In a more general case, where grey bodies are involved, radiosity accounts for three different effects: the own emission by being hot $\epsilon \sigma T^4 = \epsilon J_{black\ body}$, the part reflected from irradiance falling on it ρG , and the transmitted radiation, which is not the case for opaque bodies. As a result, the radiosity J on a surface can be calculated by the following formula:

$$J_i = \epsilon J_{i,black\ body} + \rho G = \epsilon \sigma T^4 + \rho G$$

Where:

- ϵ Emissivity
- ρ Reflectivity: the fraction of incident radiation reflected. $\rho = (1 - \alpha)$
- α Absorptivity: the fraction of incident radiation absorbed
- (τ *Transmissivity: the fraction of incident radiation transmitted*)

Heat exchange between bodies

The net energy $Q_{i,rad}$ leaving surface i, is the difference between the radiosity and the irradiation and is expressed as:

$$Q_{i,rad} = [J_i - G]A_i$$

If we assume that the absorptivity α is equal to the emissivity ϵ then the equation reduces to:

³⁹ Holman. J.P.2008. Heat Transfer , 9th Edn., Tata McGraw Hill Book Co., New Delhi, 2008.

$$J_i = \epsilon J_{i,\text{black body}} + \rho G \Rightarrow G = \frac{J_i - \epsilon J_{i,\text{black body}}}{\rho}$$

$$\rho = 1 - \alpha = 1 - \epsilon$$

$$\Rightarrow Q_{i,\text{rad}} = \frac{(E_b - J_i)}{\left[\frac{\epsilon A_i}{1 - \epsilon} \right]}$$

This can be written in electrical analogy to Ohm's law, where the resistance is:

$$R = 1 / \left[\frac{\epsilon A_i}{1 - \epsilon} \right]$$

Let consider now the interaction among surfaces. The net radiation heat received by surface i from surface j is:

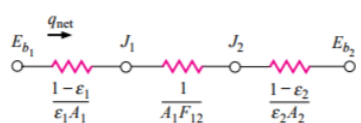
$$Q_{i,j} = Q_{i \rightarrow j} - Q_{j \rightarrow i} = \sum (J_i A_i F_{i,j} - J_j A_j F_{j,i}) = \sum \left(\frac{J_i - J_j}{1/A_i F_{i,j}} \right)$$

Where $F_{i,j}$ the radiation shape factor which expresses the fraction of energy leaving surface i and reaching surface j

This can be written in electrical analogy to Ohm's law, where the resistance is:

$$R_{i,j} = \frac{1}{A_i F_{i,j}} = \text{space resistance}$$

Combining the two equations of the heat transfer, two surfaces that exchange heat with each other and nothing else can be represented by the network shown in the figure below and written as:

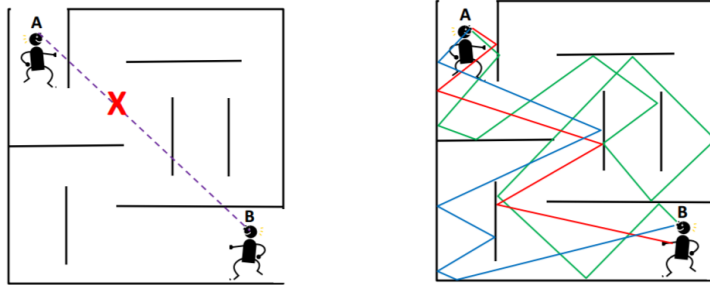


$$Q_{i,j} = \frac{5.67E^{-8}(T_j^4 - T_i^4)}{\left(\frac{1 - \epsilon_i}{\epsilon_i A_{w,i}} + \frac{1}{F_{i,k} A_{w,i}} + \frac{1 - \epsilon_k}{\epsilon_k A_{w,k}} \right)}$$

Using Gebharts absorption coefficients

A shape factor, as used above, describes how well one object sees another object via direct view; In other words, a shape factor quantifies the fraction of energy emitted from one surface that arrives at another surface directly. Elsewise, the grey body factor quantifies the fraction of energy leaving one surface that is absorbed another surface through all possible paths, thus direct and indirect. Grey body factor factors may be calculated by methods like the Gebhart⁴⁰ method.

⁴⁰ Gebhart, B. 1971. Heat Transfer. New York: McGraw-Hill



TRNSYS

The standard models in TRNSYS to calculate shortwave diffuse radiation distribution and longwave radiation exchange of surfaces in a zone are based on absorption-transmission weighted area ratios for all surfaces of a zone and on a starnode approach. Since TRNSYS 17, there is the possibility to calculate both radiation types more into detail by using Gebhart factors. Although it provides a more detailed calculation, the detailed radiation mode increases the calculation time by a factor of 2 – 3. Besides the zone (not airnode!) has to be a convex and closed volume.

ANNEX 5.D: Convective Heat Transfer Coefficients

Both equations were programmed in one new type in TRNSYS. In case there was a jet flow equations for mixed convection were used. Otherwise, the equations for natural convection were used.

Natural Convection

For vertical surfaces and for horizontal surfaces for which the convective heat flow is upward, the Alamdari and Hammond expression is:

$$h_c = \left[\left\{ a \left(\frac{T_{\text{air}} - T_{\text{surf}}}{L} \right)^{1/4} \right\}^6 + \left\{ b (T_{\text{air}} - T_{\text{surf}})^{1/3} \right\}^6 \right]^{1/6}$$

Where L the characteristic length of the surface and
a and b Coefficients set to 1,5 and 1,23 for vertical surfaces. For horizontal surfaces these are 1,4 and 1,63 in case of upward heat flow. In case the convective heat flow is downward, the expression becomes:

$$\alpha = 0,6 \left(\frac{T_{\text{surf}} - T_{\text{air}}}{L^2} \right)^{1/5}$$

All values of h_c were subject to a minimum of 1.0 W/m²K.

Mixed Convection

Mixed convection occurs when buoyancy and forced flow are both important. A technique commonly used to derive the convective heat transfer coefficient in such a case is the Churchill and Usagi method, which interpolates two independent variables between limiting solutions with a blending coefficient n [385]:

$$h_c^n = h_{c,\text{nat}}^n + h_{c,\text{forced}}^n$$

Different suggestions were made for this equation. The equation used in this work is the one suggested by Beausoleil-Morrison [333].

For vertical surfaces for which the buoyancy flow forces are assisting jet flow driving forces, the expression is:

$$h_c = \sqrt[3]{h_{c,A\&H}^3 + h_{c,F\&P}^3}$$

For vertical surfaces for which the jet flow driving forces are opposed to buoyancy flow forces, the expression is:

$$h_c = \max \begin{cases} \sqrt[3]{h_{c,A\&H}^3 - h_{c,F\&P}^3} \\ 0.8h_{c,A\&H} \\ 0.8h_{c,F\&P} \end{cases}$$

Where $h_{c,A\&H}$ convective heat transfer coefficient calculated following Alambdari and Hammond.

$h_{c,F\&P}$ convective heat transfer coefficient calculated following Fisher and Pedersen calculated by:

$$\left(\frac{T_{\text{surf}} - T_{\text{jet}}}{|T_{\text{air}} - T_{\text{surf}}|} \right) (-0.199 + 0.190 \cdot \text{ach}^{0.8}) \quad (0.2)$$

For floors for which the buoyancy flow forces are unstable.

$$h_c = \sqrt[3]{h_{c,A\&H}^3 + h_{c,F\&P}^3} \quad (0.3)$$

Where $h_{c,A\&H}$ convective heat transfer coefficient calculated following Alambdari and Hammond for horizontal surfaces for which the convective heat flow is upward

$h_{c,F\&P}$ convective heat transfer coefficient calculated following Fisher and Pedersen calculated by:

$$\left(\frac{T_{\text{surf}} - T_{\text{jet}}}{|T_{\text{air}} - T_{\text{surf}}|} \right) (0.159 + 0.116 \text{ach}^{0.8}) \quad (0.4)$$

For floors for which the buoyancy flow forces are stable.

$$h_c = \sqrt[3]{h_{c,A\&H}^3 + h_{c,F\&P}^3} \quad (0.5)$$

Where $h_{c,A\&H}$ convective heat transfer coefficient calculated following Alambdari and Hammond for horizontal surfaces for which the convective heat flow is downward.

$h_{c,F\&P}$ convective heat transfer coefficient calculated following Fisher and Pedersen calculated by:

$$\left(\frac{T_{\text{surf}} - T_{\text{jet}}}{T_{\text{air}} - T_{\text{surf}}} \right) g(0.159 + 0.116 \text{ach}^{0.8}) \quad (0.6)$$

For ceilings for which the buoyancy flow forces are unstable.

$$h_c = \sqrt[3]{h_{c,A\&H}^3 + h_{c,F\&P}^3} \quad (0.7)$$

Where $h_{c,A\&H}$ convective heat transfer coefficient calculated following Alambdari and Hammond for horizontal surfaces for which the convective heat flow is downward

$h_{c,F\&P}$ convective heat transfer coefficient calculated following Fisher and Pedersen calculated by:

$$\left(\frac{T_{\text{surf}} - T_{\text{jet}}}{T_{\text{air}} - T_{\text{surf}}} \right) g(-0.166 + 0.484ach^{0.8}) \quad (0.8)$$

For ceilings for which the buoyancy flow forces are stable.

$$h_c = \sqrt[3]{h_{c,A\&H}^3 + h_{c,F\&P}^3} \quad (0.9)$$

Where $h_{c,A\&H}$ convective heat transfer coefficient calculated following Alambdari and Hammond for horizontal surfaces for which the convective heat flow is upward.

$h_{c,F\&P}$ convective heat transfer coefficient calculated following Fisher and Pedersen calculated by:

$$\left| \frac{T_{\text{surf}} - T_{\text{jet}}}{T_{\text{air}} - T_{\text{surf}}} \right| (-0.166 + 0.484ach^{0.8}) \quad (0.10)$$

